



University  
of Glasgow

Moossen, Heiko Michael (2012) Palaeoclimate reconstructions from Arctic and Nordic Shelf seas: development and application of multiple proxies. PhD thesis

<http://theses.gla.ac.uk/3491/>

Copyright and moral rights for this thesis are retained by the author

A copy can be downloaded for personal non-commercial research or study, without prior permission or charge

This thesis cannot be reproduced or quoted extensively from without first obtaining permission in writing from the Author

The content must not be changed in any way or sold commercially in any format or medium without the formal permission of the Author

When referring to this work, full bibliographic details including the author, title, awarding institution and date of the thesis must be given.

Palaeoclimate reconstructions from Arctic and  
Nordic Shelf seas: development and application  
of multiple proxies.

Heiko Michael Moossen

Dipl. Chem.; Carl von Ossietzky University Oldenburg, Germany

Submitted in fulfilment of the requirements for the degree of  
Philosophiae doctor, PhD.

University of Glasgow  
School of Geographical and Earth Sciences  
College of Science and Engineering  
Glasgow  
United Kingdom

March 2012

© Heiko Michael Moossen, March 2012

Vielleicht werden Menschen späterer Jahrhunderte in die Arktis gehen, so wie Menschen in biblischen Zeiten in die Wüste zogen, um zur Wahrheit zurückzufinden.\*

Maybe people of future centuries will go into the Arctic, as people journeyed into the desert during biblical times, to rediscover truth.\*

(Translation by Heiko Moossen)

\* Christiane Ritter; Eine Frau Erlebt die Polarnacht; p. 83; 23rd ed. 2010: Ullstein Buchverlag

This PhD is dedicated to my mother

*Heiderose Friederike Moossen*

# Acknowledgements

The completion of this PhD would not have been possible without the input and support from a number of people to whom I am extremely grateful.

First and foremost I would like to thank Dr. James Bendle for investing his faith in me to tackle this project. I would also like to thank him for his support and the many hours he spent with me in discussion about various aspects of the project, and for the valuable help he offered during the course of the PhD. Furthermore, I would like to thank him for giving me the opportunity to take part in two research cruises in the course of the PhD. I would also like to thank Dr. James Bendle for running isotopic analyses on a number of my samples during his stay in Japan.

Secondly, I would like to thank Dr. Jaime Toney, a post-doctoral research associate in the Glasgow Molecular Organic Geochemistry Laboratory for the very valuable and interesting discussion and feedback on my research.

My thanks also go to my secondary and tertiary supervisors Dr. Finlo Cottier and Dr. William Austin, respectively, for their support.

The sediment core MD99-2266 was sub sampled at the Institute of Arctic and Alpine Research (INSTAAR) at the University of Colorado, Boulder. I would like to thank Prof. John T. Andrews and Ursula Quillmann. Ursula and John welcomed me in Boulder and helped me to sub sample the sediment core. Furthermore, throughout my PhD, they have been more than helpful in answering any questions I have had. Here I would also like to thank Dr. Ellen Roosen from the Woods Hole Oceanographic Institution who sent u-channels of the top most 3.5 meters of the archive half of the sediment core to Glasgow for me to analyse.

The bulk geochemical proxy measurements (Chapter 4) were done at the Scottish Association of Marine Science (SAMS) by Dr. Richard Abell and Dr. John Howe. Thank you for analysing my samples for me.

The GDGT analyses were conducted in the Organic Geochemistry Unit at the University of Bristol. I would like to thank Dr. Richard Pancost and his staff for analysing the samples for me. Furthermore, I would like to thank Dr. Pancost for valuable discussions on the GDGT results.

Prof. Osamu Seki from the Institute of Low Temperature Science, Hokkaido University, is thanked for conducting carbon isotopic analyses on a number of my samples.

I would like to thank the crew and scientists of the ICE CHASER 2010 cruise aboard the *RRS James Clark Ross*. Special thanks go to the principal scientific officer Dr. Raymond Leakey for granting me a berth on the cruise and for giving me the opportunity to dive in the Fram Strait to collect my own samples. Here I would also like to thank the dive team led by Hugh Brown. The two dives in the Fram Strait are among the greatest dives I have done and will ever do!

My thanks also go to Dr. Juliane Müller at the Alfred Wegener Institute for Polar and Marine Research, who supplied me with a sediment sample containing the IP<sub>25</sub> molecule.

Throughout my PhD, from setting up the laboratory, to logistical organisation for the cruises, to the use of the freeze dryer, Kenny Roberts has always been more than helpful. Thank you Kenny, for all your technical support.

Special thanks go out to Dr. Nick Kamenos and Heidi Burdett for letting me dive with them to help collect samples for various projects. Even though Loch Sween isn't one of the most exciting diving spots, it is always good to get ones head under water and to get away from the lab and office. Furthermore, I would like to thank Dr. Kamenos for his help with statistics on a number of occasions.

I have shared the PhD office with a number of people throughout the period of my PhD. I know that it has not always been easy to share an office with me (especially when I am stressed). So thanks to Heidi, Penny, Eric, Gill, Susan, Clare, Joanne,

Laura, Rachel, Mark, Ram, Neil, and all the rest for enduring my rants, sharing the office with me and for making my time here as enjoyable as it was.

I'd like to thank Dr. Fiona Meade. Fiona, you've been a great friend throughout my time in Glasgow. Thank you for what must have been 1000 cups of coffee (the usual) and short walks. Without these coffee breaks I would have gone insane! Thanks for two great conferences and sharing hostel rooms with me. Thanks for driving me halfway through England to Grimsby. Thanks you also for showing me the virtues of gin. There is so much more to say here, but words really can't express how grateful I am to you. Thank you Fiona, for everything!

I would like to thank my mother, Heiderose Moossen. She encouraged and enabled me to go to University and to pursue my dreams. Without her continued support, encouragement and love, I would not be where I am today.

I would also like to thank Elmarie who has accompanied me for part of my PhD. I am happiest with you.

Finally I thank the Scottish Alliance for Geoscience, Environment and Society (SAGES) who have funded this PhD.

## Declaration of Originality

The material presented in this thesis is the result of three years independent research carried out at the School of Geographical and Earth Sciences at the University of Glasgow. The research was supervised by Dr. James Bendle, Dr. Finlo Cottier and Dr. William Austin. This thesis represents my own research and any published or unpublished work by other authors has been given full acknowledgement in the text.

Heiko Michael Moossen

# Table of Contents

<b>Table of Contents</b> .....	<b>I</b>
<b>Table of Figures</b> .....	<b>VIII</b>
<b>Table of equations</b> .....	<b>XI</b>
<b>List of Tables</b> .....	<b>XIII</b>
<b>List of Abbreviations</b> .....	<b>XIV</b>
<b>Abstract</b> .....	<b>XVII</b>
<b>1 Introduction</b> .....	<b>1</b>
1.1 Aims of this PhD .....	3
1.2 Biomarker concept.....	6
1.2.1 <i>n</i> -Alkanes.....	7
1.2.2 Alkenones.....	9
1.2.3 Diglycerol tetraether lipids.....	13
1.2.3.1 Archaeal tetraether lipids.....	13
1.2.3.1 Bacterial tetraether lipids .....	18
1.2.4 Highly Branched Isoprenoids .....	23
1.2.5 Fatty acids in marine environments .....	24
1.3 Using contemporary observations to reconstruct changing climates .....	25
<b>2 Materials and Methods</b> .....	<b>29</b>

2.1	Elemental analysis .....	30
2.2	Biomarker extraction and purification.....	31
2.2.1	Extraction.....	31
2.2.2	Sulphur removal.....	31
2.2.3	Standardisation.....	32
2.2.4	Column chromatography.....	32
2.3	Quantitative and qualitative analysis of MD99-2266 sediment samples ..	33
2.3.1	Gas chromatography and mass spectroscopy.....	33
2.3.2	High performance liquid chromatography .....	35
2.3.3	Hydrogen isotopic analysis of the <i>n</i> -alkanes in core MD99-2266 .....	36
<b>3</b>	<b>Location, Oceanographic setting and sampling strategy of core MD99-2266 .....</b>	<b>38</b>
3.1	Core Location and Oceanography .....	38
3.2	Sampling Strategy .....	41
<b>4</b>	<b>Assessing Holocene changes in marine productivity and terrestrial organic carbon inputs into an Icelandic fjord: Application of molecular and bulk organic proxies.....</b>	<b>46</b>
4.1	Introduction .....	46
4.2	Methods.....	48
4.2.1	Mass accumulation rates .....	48
4.2.2	Bulk Parameters .....	48
4.2.3	Biomarkers.....	49
4.2.4	Modelling OC <sub>terr</sub> contributions .....	50
4.2.5	Marine sourced organic carbon .....	50
4.3	Results.....	51

4.3.1	Bulk parameters.....	51
4.3.1.1	Total organic carbon.....	52
4.3.1.2	Carbon/Nitrogen ratio.....	52
4.3.2	Biomarkers.....	53
4.3.2.1	BIT-Index.....	53
4.3.2.2	<i>n</i> -Alkanes.....	54
4.3.2.3	Alkenones.....	56
4.3.2.4	<i>n</i> -alkane/alkenone-index.....	57
4.3.3	Modelling the terrestrial organic carbon contribution to the sediments of Ísafjarðardjúp fjord.....	57
4.3.3.1	<i>n</i> -alkane/alkenone index.....	59
4.3.3.2	BIT-Index.....	59
4.3.3.3	C/N Ratio.....	59
4.3.4	Sedimentary OC <sub>mar</sub> content and modelling of Palaeoproductivity.....	59
4.4	Discussion.....	64
4.4.1	Terrestrial organic carbon contribution to the fjordic sediment.....	64
4.4.1.1	<i>n</i> -Alkane/Alkenone index.....	67
4.4.1.2	BIT-Index.....	68
4.4.1.3	C/N Ratio.....	69
4.4.2	Variations of OC <sub>terr</sub> in response to environmental and/or anthropogenic influences.....	69
4.4.3	Mass accumulation rates of marine and terrestrial OC.....	74
4.4.4	Marine paleoproductivity.....	75
4.5	Conclusion.....	77
<b>5</b>	<b>New insights into Holocene climate evolution from high-resolution terrestrial and marine biomarker records from Northwest Iceland.....</b>	<b>79</b>

5.1	Introduction .....	79
5.2	Methods .....	81
5.2.1	U <sup>K</sup> <sub>37</sub> -sea surface temperature proxy.....	81
5.2.2	Average chain length variability of long chained <i>n</i> -alkanes.....	81
5.2.3	Air temperature and soil pH reconstruction using branched GDGTs .....	81
5.2.4	Error analysis and data normalisation.....	82
5.3	Results.....	82
5.3.1	Alkenone derived sea surface temperatures.....	82
5.3.2	<i>n</i> -Alkanes.....	83
5.3.2.1	Hydrogen isotopes of <i>n</i> -alkanes .....	85
5.3.3	Bacterial Glycerol Dialkyl Glycerol Tetraethers (GDGTs) .....	86
5.4	Discussion .....	88
5.4.1	Sea surface temperatures.....	88
5.4.2	Air temperature and soil pH reconstruction.....	91
5.4.3	Precipitation change inferred from <i>n</i> -alkane average chain length variability.....	93
5.4.4	Palaeoclimate reconstruction.....	98
5.4.4.1	Early Holocene (10,800 - 7700 cal. a BP) .....	100
5.4.4.2	Middle Holocene (7700 - 2900 cal. a BP).....	102
5.4.4.3	Late Holocene (2900 - 300 cal. a BP).....	104
5.4.5	Climatic variability linked to the North Atlantic Oscillation .....	106
5.4.6	Late Holocene climate variability on Iceland - Influence on settlers.....	111
5.5	Conclusion .....	112
<b>6</b>	<b>Using the TEX<sub>86</sub> palaeothermometer in a fjordic environment: Unreasonable reconstructed sea surface temperatures indicate anaerobic oxidation of methane.....</b>	<b>114</b>

6.1	Introduction .....	114
6.2	Methods .....	115
6.3	Results.....	116
6.3.1	GDGT inferred SSTs.....	116
6.3.2	Methane Index.....	118
6.4	Discussion .....	119
6.4.1	Comparison between TEX <sub>86</sub> <sup>-</sup> and U <sup>K</sup> <sub>37</sub> -SSTs.....	119
6.4.2	Anoxic methane oxidation affects TEX <sub>86</sub> -SSTs.....	123
6.4.3	Temporal variability of AOM intensity in Ísafjarðardjúp fjord .....	126
6.5	Conclusion .....	130

## **7 Can the carbon isotopic signature of sedimentary fatty acids reconstruct palaeo-sea-ice cover? A case study for the north-western Fram Strait..... 133**

7.1	Introduction .....	133
7.1.1	Aim and hypothesis .....	135
7.2	Materials and Methods.....	135
7.2.1	Sampling strategy .....	137
7.2.2	Lipid extraction and analysis.....	139
7.2.2.1	Quantification of IP <sub>25</sub> .....	139
7.2.2.2	Clean-up of the acid fraction of ICE CHASER 2010 samples.....	143
7.3	Results.....	144
7.3.1	IP <sub>25</sub> .....	144
7.3.2	Fatty acid composition of ice algae, ice core, particulate organic matter and sediment samples .....	145
7.3.3	Amount of sea ice cover over the coring sites .....	150
7.4	Discussion .....	151

7.4.1	IP25 .....	151
7.4.2	Fatty acid composition of ice algae, ice core, particulate organic matter and sediment samples .....	152
7.4.2.1	Carbon isotopic composition of C <sub>16</sub> FA of POM.....	153
7.4.2.2	Carbon isotopic composition of C <sub>16</sub> FA of sediments.....	157
7.5	Conclusion .....	161
<b>8</b>	<b>Summary and Outlook .....</b>	<b>164</b>
8.1	Chapter 4: Assessing Holocene changes in marine productivity and terrestrial organic carbon inputs into Iceland fjords.....	164
8.2	Chapter 5: New insights into Holocene climate evolution from high-resolution terrestrial and marine biomarker records from Northwest Iceland .....	167
8.3	Chapter 6: Using the TEX <sub>86</sub> palaeothermometer in a fjordic environment: Unreasonable reconstructed sea surface temperatures indicate anaerobic oxidation of methane.....	169
8.4	Chapter 7: Can the stable carbon isotopic signature of sedimentary fatty acids reconstruct palaeo-sea-ice cover? a case study for the north-western Fram Strait .....	170
8.5	Concluding remarks .....	171
<b>9</b>	<b>Literature.....</b>	<b>173</b>

## **Appendix (provided by the author on request)**

### Appendix A: Raw data used in chapter 4

Appendix A1: Raw biomarker data

Appendix A2: Raw bulk proxy data

Appendix A3: Raw BIT-Index data

Appendix B: Raw data used in chapter 5

Appendix B1: Raw  $U^{K}_{37}$  data

Appendix B2: Raw  $ACL_{25-35}$  and  $CPI_{25-33}$  data

Appendix B3: Raw branched GDGT data

Appendix B4: Raw hydrogen isotope data

Appendix C: Raw data used in chapter 6

Appendix C1: Raw GDGT data

## Table of Figures

Figure 1.1: Oxygen isotope record of the GISP 2 (Greenland) and Taylor Dome (Antarctica) ice cores and the corresponding associated temperature variability ...	2
Figure 1.2: Chromatogram of sedimentary n-alkanes in core MD99-2266.....	8
Figure 1.3: Gas chromatogram of sedimentary alkenones in core MD99-2266 ....	10
Figure 1.4: Molecular structures of archaeal GDGTs.....	14
Figure 1.5: Molecular structures of branched GDGTs.....	18
Figure 1.6: Stereochemistry of archaeal and bacterial GDGTs.....	19
Figure 1.7: Sea ice proxy IP <sub>25</sub> .....	23
Figure 1.8: Considering different error sources when interpreting palaeoclimatic records.....	28
Figure 2.1: Sample extraction and purification process .....	29
Figure 2.2: Trimethylsilyl derivatisation of alcohols and acids using BSTFA.....	34
Figure 2.3: External standard mix .....	35
Figure 3.1: Main surface water masses in the eastern North Atlantic .....	39
Figure 3.2: Age model of core MD99-2266. ....	43
Figure 4.1: Sedimentation and mass accumulation rates of core MD99-2266.....	51
Figure 4.2: Biomarker and bulk parameter variability of core MD99-2266. ....	53
Figure 4.3: Variations of the ACL <sub>25-35</sub> , CPI <sub>25-33</sub> and the concentration of n-alkanes .....	55
Figure 4.4: Estimates of the OC <sub>terr</sub> contribution to the sedimentary TOC pool .....	58
Figure 4.5: Mass accumulation rates of total, marine- and terrestrial organic carbon.....	60

Figure 4.6: Palaeoproductivity of Ísafjarðardjúp fjord .....	63
Figure 4.7: Mean estimated OC <sub>terr</sub> input into the fjordic sediments .....	71
Figure 5.1: Holocene U <sup>K</sup> <sub>37</sub> -SST variations .....	83
Figure 5.2: <i>n</i> -Alkane average chain length (ACL <sub>25-35</sub> ) Holocene variability .....	84
Figure 5.3: Hydrogen isotopic signature of the C <sub>29</sub> and C <sub>31</sub> <i>n</i> -alkanes plotted against ACL <sub>25-35</sub> values .....	86
Figure 5.4: GDGT inferred Holocene mean air temperature variability .....	87
Figure 5.5: GDGT inferred Holocene soil pH variability .....	88
Figure 5.6: SST variations of Icelandic surface waters in 1999 .....	90
Figure 5.7: MBT/CBT mean air temperature reconstruction vs. ACL <sub>25-35</sub> variability throughout the Holocene.....	95
Figure 5.8: Holocene precipitation variability .....	97
Figure 5.9: Holocene terrestrial and marine palaeoclimate series .....	100
Figure 5.10: Present day NAO influenced precipitation and current patterns .....	107
Figure 5.11: Late Holocene terrestrial and marine palaeoclimate records .....	108
Figure 6.1: Reconstructed palaeo-SST variations using the TEX <sub>86</sub> and the TEX <sub>86</sub> <sup>L</sup> calibration equations .....	117
Figure 6.2: Variations of the Methane Index throughout the Holocene in Ísafjarðardjúp fjord. ....	118
Figure 6.3: TEX <sub>86</sub> -SST variability vs. U <sup>K</sup> <sub>37</sub> - and MI variability .....	121
Figure 6.4: Relative concentration of GDGT-0, -1, -2, -3 and Crenarchaeol .....	124
Figure 6.5: Gas chromatogram of the polar fraction of a sample correlating with very high MI values at 5400 cal. a BP .....	125

Figure 7.1 ICE CHASER 2010 sampling locations.....	137
Figure 7.2: Ice core collected at the ice station .....	138
Figure 7.3: Collection of sea-ice algae.....	138
Figure 7.4: Qualitative analysis of IP <sub>25</sub> ice-proxy .....	140
Figure 7.5: SIM-GC-MS analysis of the IP <sub>25</sub> -Standard and an ice algae sample	142
Figure 7.6: Response of the total ion current to the concentration of IP <sub>25</sub> .....	142
Figure 7.7: Chromatogram of the sedimentary fatty acid methyl esters from the pelagic station (10 cm bsf) .....	145
Figure 7.8: Free fatty acids in ice algae (a), ice core (b) and POM samples(c) ..	146
Figure 7.9: Carbon isotopic composition of the C <sub>16</sub> FA in the POM samples. ....	148
Figure 7.10: Concentrations and isotopic signatures of the C <sub>16</sub> FA of the PS and IE sediments .....	150
Figure 7.11: Summary of C <sub>16</sub> -FA producers and the oceanographic and biological processes .....	161

## Table of equations

Equation 1: Carbon preference index (CPI) .....	8
Equation 2: Average chain length (ACL) .....	9
Equation 3: Alkenone unsaturation index ( $U_{37}^K$ ) .....	11
Equation 4: Modified alkenone unsaturation index ( $U_{37}^{K'}$ ) .....	11
Equation 5: $U_{37}^{K'}$ calibration equation .....	12
Equation 6: Tetraether index ( $TEX_{86}$ ) .....	15
Equation 7: $TEX_{86}$ calibration equation after Kim <i>et al.</i> (2008) .....	16
Equation 8: Conversion of relative GDGT abundance into $TEX_{86}^L$ proxy .....	17
Equation 9: $TEX_{86}^L$ calibration equation after Kim <i>et al.</i> (2010) .....	17
Equation 10: Methane Index (MI) .....	17
Equation 11: Methylation index of branched tetraethers (MBT) .....	20
Equation 12: Cyclisation ratio of branched tetraethers (CBT) .....	20
Equation 13: Calibration equation of CBT with soil pH .....	21
Equation 14: MBT/CBT mean air temperature proxy .....	21
Equation 15: Branched and isoprenoid tetraether index (BIT-Index) .....	21
Equation 16: Calculation of the $\delta$ value of isotopic values. ....	36
Equation 17: Mass accumulation rate (MAR) .....	48
Equation 18: <i>n</i> -alkane/alkenone index .....	49
Equation 19: Binary mixing model .....	50
Equation 20: calculation of marine organic carbon ( $OC_{mar}$ ) .....	50

Equation 21: Marine primary production after Müller & Suess (1979).....	60
Equation 22: Palaeoproductivity after Stein (1986).....	61
Equation 23: Palaeoproductivity after Knies & Mann (2002).....	61
Equation 24: Correction of the FA isotopic value .....	144
Equation 25: Two end-member model to calculate the contribution of ice algal C <sub>16</sub> FA to marine sediments .....	150

## List of Tables

Table 1: $^{14}\text{C}$ Accelerated MS dates for MD99-2266 and corresponding calibrated ages used in the age model, as published by Quillmann et al. (2010). .....	45
Table 2: C/N values of different samples from terrestrial sources in northwest Iceland. ....	66
Table 3: Concentrations and carbon isotopic signatures of the $\text{C}_{16}$ FA in the analysed POM from water column, ice algae and ice core samples. ....	147
Table 4: Concentration and carbon isotopic signature of the $\text{C}_{16}$ FA found in sediments at the PS and IE .....	149

## List of Abbreviations

ACL <sub>(25-35)</sub>	Average chain length (using the odd-chained <i>n</i> -alkanes with chain lengths from 25 - 35 carbon atoms)
A.E.	Analytical error
AMS	Accelerated mass spectrometry
AMOC	Atlantic meridional overturning circulation
ANME	Methanotrophic archaea
AOM	Anaerobic oxidation of methane
BAME	Behenic acid methyl ester
BSTFA	N, O-Bis-(trimethylsilyl)-trifluoroacetamide
BIT-Index	Branched vs. isoprenoid tetraether index
cal. (k)a BP	calibrated (1000) years before present (present (0 BP) = 1950 AD)
CBT	cyclisation ratio of branched tetraethers
C.E	Calibration error
CPI <sub>(25-33)</sub>	carbon preference index (using the odd-chained <i>n</i> -alkanes with chain lengths from 25 - 33 carbon atoms)
D	water depth
DBD	Dry bulk density
DCM	Dichloromethane
DS	dry sample
EIC	East Icelandic Current
EGC	East Greenland Current
FC	Faroe Current
FA	Fatty acid
FAME	Fatty acid methyl ester
FATM	Fatty acid trophic marker
GC-FID	Gas chromatograph - Flame ionisation detector
GDGT (bacterial; branched)	glycerol dialkyl glycerol tetraether
GDGT	Glycerol dibiphytanyl glycerol tetraether
GISS	Goddard Institute for Space Studies

HBI	Highly branched isoprenoid
HPLC-APCI-MS	High pressure liquid chromatography - atmospheric pressure chemical ionisation - mass spectrometer
IC	Irminger Current
IE	Ice edge
InjSTD	Injection standard
IntSTD	Internal standard
IS	Ice station
IP <sub>25</sub>	Ice proxy with 25 carbon atoms
IRD	ice rafted debris
ISOW	Iceland-Scotland-Overflow-Water
LGM	Last glacial maximum
LIA	Little ice age
LSR	Linear sedimentation rate
MAT	Mean air temperature
MAR	Mass accumulation rate
MBT	Methylation index of branched tetraethers
MCA	Medieval climate anomaly
MeOH	Methanol
MHTM	Marine Holocene Thermal Maximum
MI	Methane index
MIZ	Marginal ice zone
MNAW	Modified North Atlantic Water
MS	Mass spectrometer
m/z	mass/charge ratio
NAC	North Atlantic Current
NAO	North Atlantic Oscillation
NAW	North Atlantic Water
NIIC	North Icelandic Irminger current
OC	Organic carbon
OC <sub>mar</sub>	Marine organic carbon
OC <sub>terr</sub>	Terrestrial organic carbon
OM	Organic matter

P.E	Propagated error
PF	Polar front
POM	Particulate organic matter
PP	Palaeoproductivity
PS	Pelagic station
PW	Polar waters
RT	Retention time
SAR	Sediment accumulation rate
(M)SLP	(Mean) sea level pressure
SIM	Single ion mode
SMOW	Standard mean ocean water
SST	sea surface temperature
TEX <sub>86</sub> <sup>(L)</sup>	tetraether index of tetraethers consisting of 86 carbon atoms (L = low temperature equation)
THTM	Terrestrial Holocene Thermal Maximum
TIC	Total ion current
TLE	Total lipid extract
TN	Total nitrogen
TOC	Total organic carbon
U <sup>K(1)</sup> <sub>37</sub>	(Modified) Alkenone unsaturation index

## Abstract

Although Holocene climate changes are significantly smaller in amplitude than the Pleistocene Glacial-Interglacial cycles (Dansgaard *et al.*, 1993), they have affected human civilisations over at least the last 4000 years (Buntgen *et al.*, 2011; Lamb, 1995; Mayewski & White, 2002). The study of Holocene climate variations is increasingly important to disentangle climate change caused by anthropogenic influences from natural climate change. Furthermore, Holocene climate change provides the geological context in which to place contemporary climatic observations.

Studying sedimentary records stemming from marine biotopes located close to land, such as fjords, affords the opportunity to study marine and terrestrial paleoclimatic variability, and therein linking the two together. Additionally, fjordic environments typically have a higher sediment accumulation rate than deeper ocean sites, facilitating resolution of rapid climate change events. The fjords of Northwest Iceland are ideal for studying Holocene climate change as they receive warm water from the Irminger current, an end member of the Atlantic current, but are also influenced by the east Greenland current, which brings cold polar waters to the region (Jennings *et al.*, 2011). Furthermore, the coring site is located beneath one of the dipoles of the North Atlantic Oscillation (Hurrell, 1995). Therefore, oceanic and atmospheric Holocene variability should be recorded in the sediments studied.

Alkenones, terrestrial leaf wax *n*-alkanes, branched and archaeal glycerol tetraethers and C/N ratios from a sediment core from the mouth of the Ísafjarðardjúp fjord (MD99-2266; location: 66° 13' 77" N, 23° 15' 93" W; 106 m water depth) were analysed. These terrestrial and marine biomarkers were used to produce biomarker based palaeoclimatic records with the highest resolution to date (one sample every ~ 32 years), covering the Holocene from ~ 10,700 calibrated years before present (cal. a BP) to ~ 300 cal. a BP.

The terrestrial and marine organic carbon contributions to the sediment and the palaeoproductivity of the fjord vary throughout the Holocene forced by changing

climate. While the amount of terrestrial organic carbon is primarily controlled by the development of vegetation as glaciers retreat, the primary productivity is controlled by varying influxes of nutrient rich water masses.

By combining the reconstructed sea surface temperature, air temperature and precipitation records, climatic changes that affect the terrestrial and marine realm are uncovered. Two periods in the Holocene where major climatic shifts in the North Atlantic region occur, one at ~ 7700 cal. a BP, and one at ~ 2900 cal. a BP, are observed. Meltwater events and decreasing summer insolation drive climatic change throughout the early Holocene. The middle Holocene climate, from 7700 to 2900 cal. a BP is driven by decreasing summer insolation, and meridional overturning circulation. The climate variability is decoupled from insolation change in the late Holocene, and the sea surface temperature and air temperature, and precipitation changes are driven by NAO-type fluctuations and variations in the heat transport via the meridional overturning circulation.

The TEX<sub>86</sub> palaeo-SST thermometer does not work in Ísafjarðardjúp fjord. The TEX<sub>86</sub>-SSTs are adversely affected by GDGTs associated with archaea mediating anaerobic oxidation of methane, as indicated by the methane index. Methane indices as low as 0.1 indicate anaerobic oxidation of methane at the site studied.

The palaeo-sea-ice proxy IP<sub>25</sub> was not detected in the sediments of MD99-2266 even though the northwest Icelandic coast has been affected by drift ice, particularly in the late Holocene. Therefore, the use of carbon isotopic signatures from sedimentary fatty acids, derived from ice and pelagic algae was investigated as a sea-ice proxy. Ice algae, ice core, water column particulate organic matter and sediment samples were collected on the ICE CHASER 2010 research cruise. The carbon isotopic signature of the ice algal C<sub>16</sub> fatty acid is significantly heavier than that of the pelagic derived organic matter. Furthermore, the carbon isotopic signature of the fatty acid in the samples from the sediment core located at the ice edge is isotopically heavier, compared to the fatty acid isotopic signature from the sediment core from a pelagic site. It appears that the isotopic signature of algal fatty acids can be used to elucidate sea-ice cover, however, more research is needed.

## 1 Introduction

Northern and southern hemisphere ice core records show that the 250,000 years preceding the Holocene (the last 11,500 years; Mayewski *et al.*, 2004) were characterised by climatic instability (Dansgaard *et al.*, 1993; Grootes & Stuiver, 1997; Steig *et al.*, 2000; Figure 1.1). In comparison, the Holocene climate was thought to be remarkably stable (Dansgaard *et al.*, 1993). We now know, that the last 11,500 years show significant climatic fluctuations (see review by Mayewski *et al.*, 2004 and references therein). Melting ice sheets, remnants of the last glacial maximum (LGM), caused meltwater events throughout the early Holocene, the most prominent being the 8.2 event, which caused a short term climatic deterioration (Alley & Ágústsdóttir, 2005). Throughout the Holocene, ice rafted debris found in North Atlantic sediments, implies climatic variability at ~ 1500 year cycles (Bond *et al.*, 2001). The medieval climate anomaly (MCA) lasting from ~ 1050 to ~ 600 cal. a BP (calibrated years before present; 0 BP = 1950; Graham *et al.*, 2011), and the little ice age (~ 450 to ~150 cal. a BP; Ogilvie & Jonsson, 2001) represent periods of climatic fluctuations during the late Holocene, which are not only evident from palaeo-geological, but also from historical records (Lamb, 1995; Ogilvie & Jonsson, 2001).

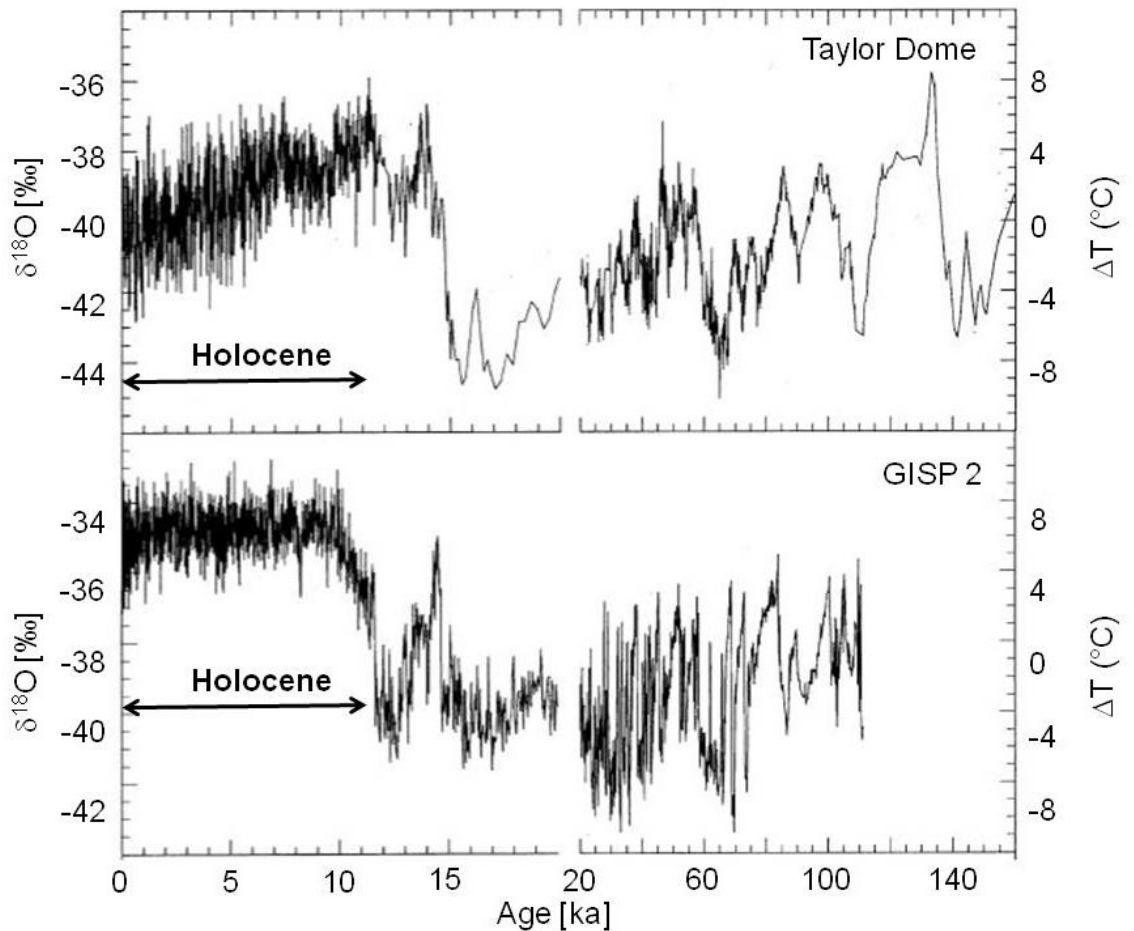


Figure 1.1: Oxygen isotope record of the GISP 2 (Greenland) and Taylor Dome (Antarctica) ice cores and the corresponding associated temperature variability (modified after Steig *et al.*, 2000).

Even though Holocene climate fluctuations are evidently smaller than those in the Pleistocene, changes in climate have profoundly affected human societies for at least the last 4500 years. The Saqqaq people colonised Greenland ca. 4500 years ago, but left, and were replaced by the Dorset culture when temperatures on Greenland abruptly cooled (D'Andrea *et al.*, 2011). 4200 years ago the Akkadian empire, located between the Tigris and Euphrates rivers, collapsed in response to increased regional aridity (deMenocal, 2001). The increase in aridity is synchronous with low sea-ice extent in the North Atlantic, indicating that changes in atmospheric circulation affected precipitation patterns over large areas of the northern hemisphere (Mayewski & White, 2002). Severe drought conditions starting ca. 2000 years ago led to the termination of trade between Europe and China via the Great Silk Road (Lamb, 1995). Ca. 300 years later, severe aridity

across Asia and eastern Europe lead to political and economic turmoil in the West Roman Empire and ultimately contributed to its downfall (Buntgen *et al.*, 2011; Lamb, 1995). The demise of the Mayan high culture ca. 1200 years ago is associated with a reduction of annual precipitation by 25 - 40 % (deMenocal, 2001; Medina-Elizalde & Rohling, 2012). Norse settlements were established at the onset of the MCA in Iceland and Greenland at ca. 1080 and 956 cal. a BP, respectively (Ogilvie *et al.*, 2005; references therein; Patterson *et al.*, 2010). Between the end of the MCA and the beginning of the LIA, the settlements of Greenland were abandoned due to the severity of the climate which prevented the supply of the Greenland settlements (Patterson *et al.*, 2010; references therein). Even today, at what may be termed the technological climax of human society, climate change impacts humanity. For example, the food security of Inuit communities in the Canadian Arctic has been compromised due to the retreat of sea-ice (Ford, 2009). Changes in temperature and precipitation in Northern Europe, caused by changing atmospheric circulation patterns, have a direct effect on the yield of agricultural produce, the growing season of plants, and the spatial distribution and breeding habit of animals in Europe and North America (Gimeno *et al.*, 2002; Ottersen *et al.*, 2001; references therein). Furthermore, sea surface temperature variability in the North Atlantic directly affects stock sizes of cod (Stenseth *et al.*, 2002), thereby affecting the fishing industry. Continually rising human population (Smith, 2011), coupled with decreasing natural resources such as crude oil (Murray & King, 2012), will adversely impact the ability of societies to deal with, and respond to changing environmental conditions caused by climate change.

### **1.1 Aims of this PhD**

To understand exactly how changing climate, natural or caused by anthropogenic activities, will affect future generations, it is imperative to better understand the climatic system, and to place recent climatic changes into the context of climatic history. Today, atmosphere-ocean general circulation models are used to predict the impact of future climate change (IPCC, 2007). The framework conditions used in these models are based on data derived from instrumental measurements (e.g. Hanna *et al.*, 2004; Hanna *et al.*, 2006), and palaeogeochemical climate proxies

(see Jansen *et al.*, 2007 for an overview). These palaeogeochemical proxies have much scope for improvement. By applying these proxies in diverse environments, and comparing them to existing climate records, the uncertainties associated with analytical measurements, the interpretation, and calibration of these proxies, can be reduced, making proxy data more useful to climate modellers.

Furthermore, the models that are used to predict climatic change also need to be improved. For example, Hansen *et al.* (2007) have highlighted model deficiencies of the Goddard Institute for Space Studies (GISS) atmospheric modelE. The production of deep water in the North Atlantic Ocean does not extend to sufficient depths, some deep water production is modelled for areas where it is not observed, and even though the global sea-ice cover extent is plausible, too much sea-ice is modelled for the Northern Hemisphere and too little for the Southern Hemisphere (Hansen *et al.*, 2007 and references therein).

The development and application of organic geochemical proxies and palaeoclimate records is imperative to: a) improve our understanding of the mechanisms driving Holocene climate change and to further study its impact, and b) to improve the interpretation of geochemical palaeoclimate proxies.

The aims of this PhD are:

- the application of organic geochemical proxies to understand the deposition dynamics of terrestrial and marine organic matter in Ísafjarðardjúp fjord in the Denmark Strait off of the coast of Northwest Iceland (chapter 4). The study site is described in detail in chapter 3. The studied site is very sensitive to climatic variability (Liu *et al.*, 2003), and geochemical proxies are likely to record changing climates when deposited in the sediments of the fjord. Depositional dynamics of terrestrial and marine organic carbon may have been influenced by changing climate regimes. Generally high sedimentation rates of fjordic environments cause an abundance of organic geochemical markers to be found in the sediment making Ísafjarðardjúp fjord an ideal study site for this PhD.

- The assembly of high resolution sea surface temperature, air temperature and precipitation records (chapter 5). Fjords are transition zones which are closely linked to marine and terrestrial environments. Thus, the host of biomarkers found in Ísafjarðardjúp fjord are likely to record the terrestrial and marine environmental response to changing climates throughout the Holocene. The assessment of the combined terrestrial and marine palaeoclimate records will lead to a better understanding of the interplay between terrestrial and marine environments throughout changing climates. The study site is again ideal for this project due to its location in the central North Atlantic. The site is located over one of the two dipoles of the North Atlantic Oscillation, an atmospheric phenomenon which affects precipitation, sea surface temperature and air temperature patterns throughout the North Atlantic region and Europe. Furthermore, cold and warm water currents meet in the vicinity of Iceland, and the biomarkers deposited at the studied site are likely to record changes in the atmospheric and oceanic systems.
- To use different organic geochemical biomarkers to reconstruct palaeo sea surface temperatures (chapter 6). Different proxy records are controlled by a host of variables, such as the biology of the organisms producing the geochemical marker, the depositional environment and the response of the biomarker to the environmental change it records. The Icelandic region has already received some scientific attention making it ideal for the study of inter-proxy relationships, as the framework climatic conditions are understood.
- The development of a sea ice proxy (chapter 7). The sea ice extent throughout the Holocene has been very variable, and the Arctic Ocean sea ice is currently retreating. Sea ice mediates climatic feedback affecting climate and biological processes at high latitudes. The effects of sea ice fluctuation on the environment and climate are discussed in detail in chapter 7.

Ultimately the data and insights obtained during this PhD should help to improve the climatic predictions made by climate models today, and in the future, these

improved climate models should help palaeoclimatologists to better interpret their palaeogeochemical proxy records.

## **1.2 Biomarker concept**

Organic geochemistry studies the distribution, composition and fate of organic matter in the geosphere, combining different disciplines like geology, chemistry and biology. The goal is to document and understand environmental changes which have shaped our planet.

Chemical fossils, so called biomarkers, are employed to achieve this goal. Biomarkers are organic molecules found in a variety of Earth's archives such as sediments (e.g. this study; Bendle & Rosell-Melé, 2007; Weijers *et al.*, 2009), oil (Peters *et al.*, 2005), ice (e.g. this study; Brown *et al.*, 2011; Budge *et al.*, 2008) and soils (Hedges & Oades, 1997; Peterse *et al.*, 2009b). Ideally, they have an unambiguous link to precursor molecule found in living organisms today (Killops & Killops, 2005). When these organisms die, most of their molecules are broken down and reutilised by other organisms. Some molecules however, survive biodegradation with little or no alteration to their molecular skeleton and are deposited in sediments, where they are susceptible to further degradation processes. The degradation of molecules during diagenesis (degradational processes under mild conditions; Killops & Killops, 2005) and catagenesis (thermal degradation at temperatures > 60 °C, Killops & Killops, 2005) varies greatly. The time it takes for different molecules to degrade, alter and break down, varies depending on the amount and the nature of functional groups they carry, and thus on the stability of these molecules. Generally the stability of molecules decreases with increasing polarity from less polar molecules such as alkanes to more polar molecules such as acids or alcohols (Cranwell, 1981). Besides the molecular structure itself, the depositional environment also plays a key role in the speed at which molecules break down. For example, molecules which are deposited in anoxic environments are less susceptible to alteration than those deposited in oxic environments (Paetzel & Schrader, 1992; Stein, 1986; Zonneveld *et al.*, 2010). The biomarkers studied in this thesis throughout the Holocene have previously been found in much older sediments. Alkenones have been detected in 160 million

year old sediments in the Pacific Ocean (Brassell & Dumitrescu, 2004). *n*-Alkanes, bacterial and archaeal tetraether lipids have been detected in Palaeocene/Eocene Arctic sediments (Pagani *et al.*, 2006; Sluijs *et al.*, 2006; Weijers *et al.*, 2007b), and fatty acids have been detected in the Fram Strait between Svalbard and Greenland in sediment horizons as old as 17,000 years (Birgel & Hass, 2004).

The distribution and occurrence of the biomarkers which survive the biological and geological degradation processes, offer insights into past environmental variability, by serving as proxies for sea surface temperature, precipitation, primary production etc. (Castañeda & Schouten, 2011; Eglinton & Eglinton, 2008; Pancost & Boot, 2004).

An increasing amount of biomarkers is emerging providing the tools with which to reconstruct palaeoclimate. The ubiquitous nature of many of these biomarkers, the host of different climatic variables that can be reconstructed with them, their geochemical longevity, and last, but not least, the ease with which these biomarkers can be analysed, makes them an ideal tool, suited specifically to the aims of this PhD. The following section provides an introductory overview of the biomarkers utilised in this study.

### 1.2.1 *n*-Alkanes

Long chain (24 to 36 carbon atoms in the chain) *n*-alkanes form part of a wax layer which covers the leaves of almost all terrestrial higher plants (Eglinton *et al.*, 1962; Eglinton & Hamilton, 1967). Besides protecting the plants from water loss (Cameron *et al.*, 2006; Daly, 1964), the wax layer also protects the leaf from mechanically, fungal, bacterial and insect induced damage (Eglinton & Hamilton, 1967). Leaf wax *n*-alkanes are transported into marine sediments by either aeolian (Bendle *et al.*, 2007; Poynter *et al.*, 1989; Schefuss *et al.*, 2003b), or fluvial mechanisms (Pancost & Boot, 2004; Weijers *et al.*, 2009).

## 1. Introduction

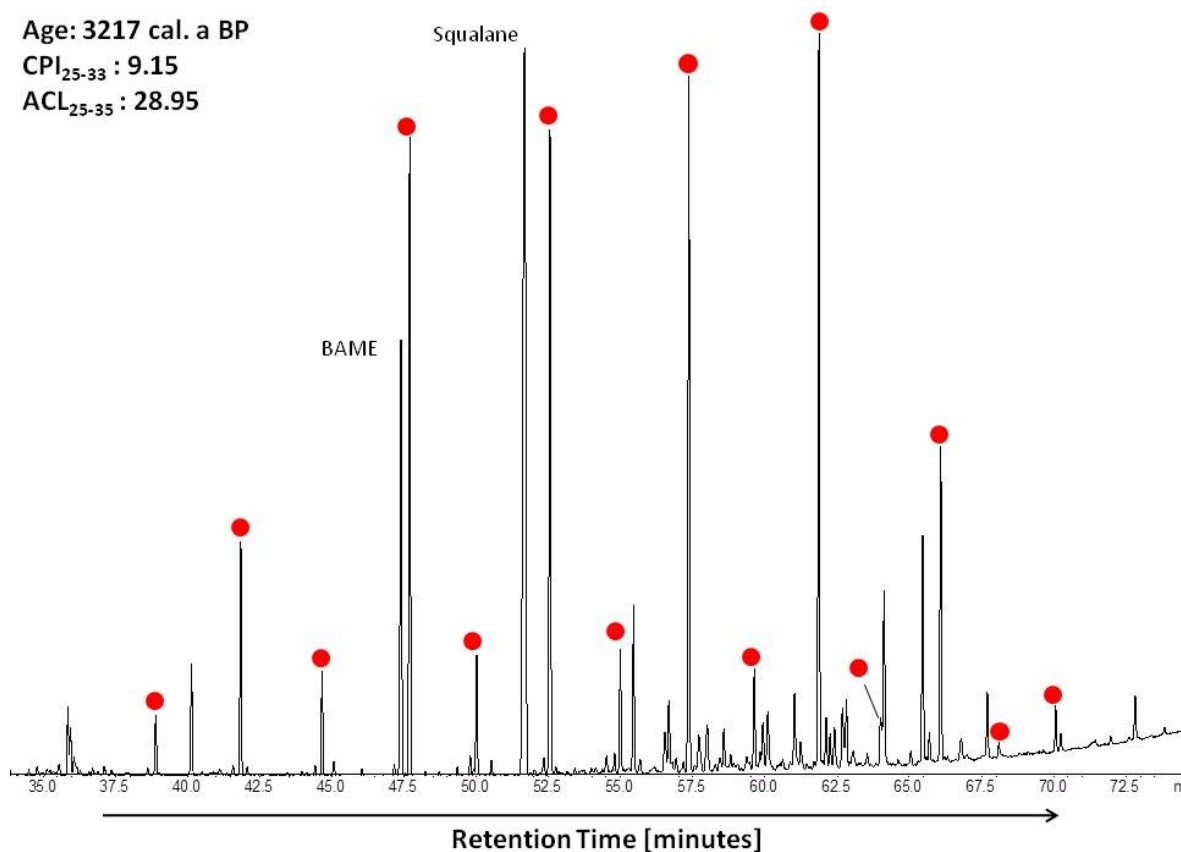


Figure 1.2: Chromatogram of sedimentary *n*-alkanes in core MD99-2266; red dots indicate the *n*-alkanes with chain lengths of 22 - 35 carbon atoms. Behenic acid methyl ester (BAME) and Squalane are the injection and internal standards, respectively.

The homologous series of *n*-alkanes in sediments (Figure 1.2) can be described using the carbon preference index (CPI) and the average chain length (ACL) values. The CPI indicates the relative dominance of *n*-alkanes with an odd number of carbon atoms over even-chained *n*-alkanes within a sample. It is calculated using the following equation developed by Bray and Evans (1961; Equation 1):

$$\text{CPI} = \frac{1}{2} \left( \left( \frac{C_{25} + C_{27} + C_{29} + C_{31} + C_{33}}{C_{24} + C_{26} + C_{28} + C_{30} + C_{32}} \right) + \left( \frac{C_{25} + C_{27} + C_{29} + C_{31} + C_{33}}{C_{26} + C_{28} + C_{30} + C_{32} + C_{34}} \right) \right)$$

Equation 1: Carbon preference index (CPI).  $C_x$  represents the abundance of an *n*-alkane with a particular number of carbons in its chain.

## 1. Introduction

Average chain length values indicate which odd-chained *n*-alkane tends to dominate in any given sample. The ACL value of a sample is calculated for the most abundant odd chained *n*-alkanes of a homologous series using the following equation (Equation 2; Schefuss *et al.*, 2003b).

$$ACL = \frac{\sum(x_i \cdot C_i)_n}{(C_i)_n}$$

Equation 2: Average chain length (ACL);  $x_i$  represents the *n*-alkane and  $C_i$  the concentration of the *n*-alkane.

Variations in the ACL of *n*-alkanes of terrestrial higher plants occur in response to temperature (Kawamura & Ishimura, 2003; Vogts *et al.*, 2009) and precipitation variability (Calvo *et al.*, 2004; Zhou *et al.*, 2005). Furthermore, terrestrial higher plants utilising different carbon assimilation mechanisms (e.g.  $C_3$  and  $C_4$  plants) exhibit different ACL values (Cranwell, 1973; Rommerskirchen *et al.*, 2006). By studying the *n*-alkane distribution in marine sediments, palaeotemperature and palaeoaridity conditions can be inferred, as well as vegetation changes.

### 1.2.2 Alkenones

Alkenones are long chained, unsaturated ketones which are produced by members of the genera *Haptophyceae*, for example the coccolithophorides *Emiliana huxleyi* and *Gephyrocapsa oceanica* (Volkman *et al.*, 1995; Volkman *et al.*, 1998; Volkman *et al.*, 1980). The most abundant alkenones produced, are those with chain lengths of 37 and 38 carbon atoms with two, three or four double bonds (Figure 1.3). The carbonyl functional group is either located at the second or third carbon in the chain.

## 1. Introduction

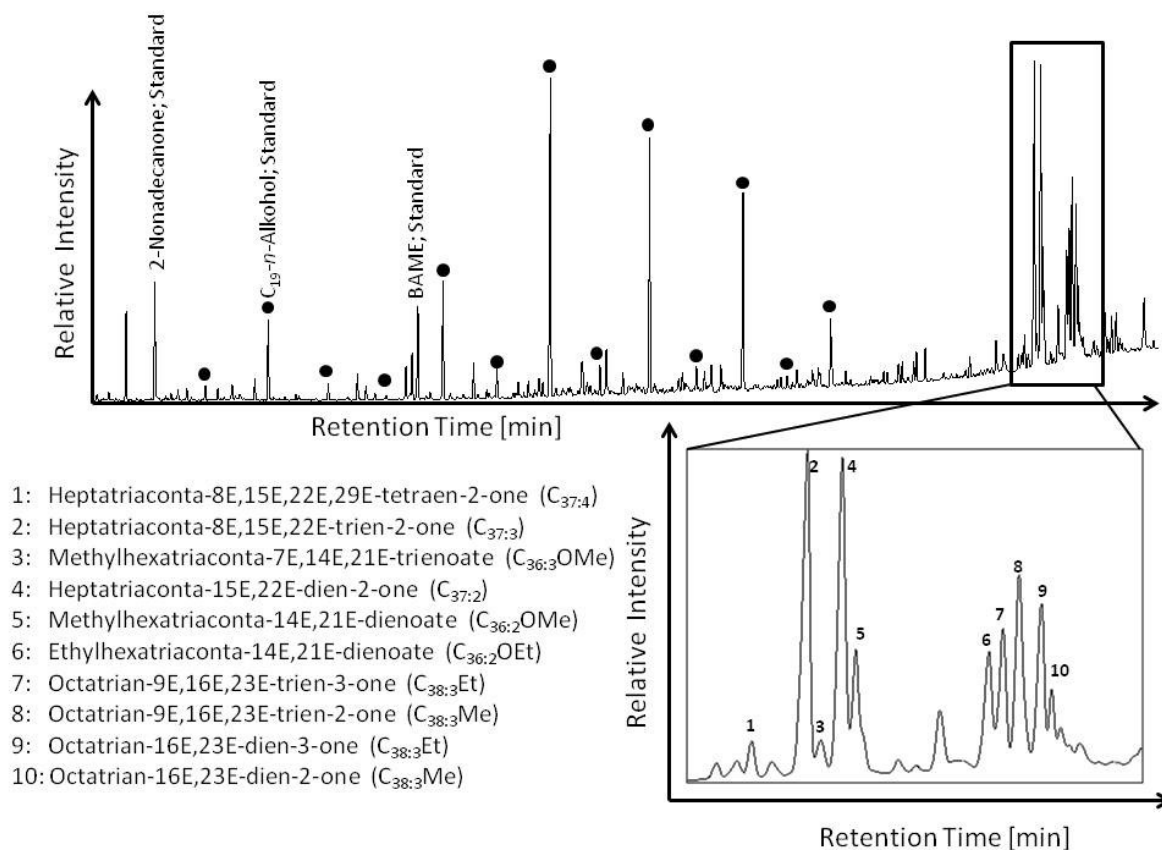


Figure 1.3: Gas chromatogram of sedimentary alkenones in core MD99-2266. Black dots denote  $n$ -alcohols ( $C_{18}$ - $C_{30}$ ); 2-Nonadecanone and the  $C_{19}$ - $n$ -alcohol are internal standards, and Behenic acid methyl ester (BAME) is the injection standard. The zoomed in section shows the  $C_{37}$  and  $C_{38}$  alkenones, and the  $C_{36}$  methyl esters.

The relative abundances of the  $C_{37:2}$ ,  $C_{37:3}$  and  $C_{37:4}$  (Shorthand nomenclature:  $C_{x:y}$ , where  $x$  indicates the number of carbon atoms in the molecule, and  $y$  the number of double bonds) alkenones within the synthesising organisms change with growth temperature (Prahl & Wakeham, 1987). Since the producing coccolithophores are ubiquitous in the euphotic zone of the world's oceans, the change of relative abundances of these two compounds reflects change in the sea surface temperature (SST). This relationship has led to the formulation of the alkenone unsaturation index ( $U^K_{37}$ ; Equation 3) by Brassel et al. (1986).

## 1. Introduction

$$U_{37}^K = \frac{(C_{37:2} - C_{37:4})}{C_{37:2} + C_{37:3} + C_{37:4}}$$

Equation 3: Alkenone unsaturation index ( $U_{37}^K$ ); The concentrations of the different alkenones are used to calculate the index.

The relative abundance of more unsaturated alkenones decreases with the increasing growth temperature of *Emiliana huxleyi* leading to high  $U_{37}^K$  values and therefore, inferring increasing SSTs. Prahl and Wakeham (1987) analysed cultures of *Emiliana huxleyi* grown under different temperatures and found the relationship between  $U_{37}^K$  and temperature to be:  $U_{37}^K = 0.033T + 0.043$ ;  $r^2 = 0.997$ ). Because the tetra unsaturated  $C_{37}$ -alkenone is usually not very abundant outside polar and sub-polar regions, its concentration is often omitted when calculating SSTs from alkenone concentrations (Prahl & Wakeham, 1987). It has also been noted, that the inclusion of the  $C_{37:4}$  concentrations in the  $U_{37}^K$  increases the error of inferred temperatures calculated in cultures grown below 15 °C (Prahl & Wakeham, 1987). Thus a modified alkenone unsaturation index ( $U_{37}^{K'}$ ; Equation 4) is often used.

$$U_{37}^{K'} = \frac{C_{37:2}}{C_{37:2} + C_{37:3}}$$

Equation 4: Modified alkenone unsaturation index ( $U_{37}^{K'}$ ) after Prahl & Wakeham (1987). The concentrations of the different alkenones are used to calculate the index.

Since the first calibration equations produced by Brassell *et al.* (1986) and Prahl and Wakeham (1987), a host of different calibration equations have been produced (see Rosell-Melé *et al.*, 1995 for a collection of calibration equations produced before 1995). Müller *et al.* (1998) and Conte *et al.* (2006) have produced the most comprehensive calibration equations, correlating the  $U_{37}^{K'}$  data from core top sediments with sea surface temperatures throughout the worlds oceans. In this study, the calibration equation produced by Conte *et al.* (2006) is used to convert  $U_{37}^{K'}$  values into SSTs (Equation 5).

## 1. Introduction

$$U_{37}^{K'} = 0.0709 + 0.0322 \cdot \text{SST}$$

Equation 5:  $U_{37}^{K'}$  calibration equation after Conte *et al.* (2006).

Alkenone producing phytoplankton are photosynthetic organisms, therefore their habitat is restricted to the euphotic zone. *Emiliana huxleyi* is globally distributed throughout the top 200 m of the water column (Okada & Honjo, 1973). Usually the water depth at which most of the alkenone producing microalgae are found coincides with the deep chlorophyll maximum (Lee & Schneider, 2005). In addition to variations of spatial distribution patterns, the location of micro plankton is also influenced by seasonality. In the North Pacific Central Gyre in the warm season, *E. huxleyi* is found between 100 and 120 m whereas its location is evenly distributed throughout the euphotic zone in the colder season (Reid, 1980).

Despite the occurrence of *E. huxleyi* within the top 200 m of the water column, Müller *et al.* (1998) and Rosell-Melé *et al.* (1995) found that the best correlation between the  $U_{37}^{K'}$  and  $U_{37}^K$ , respectively, and SSTs, was obtained when using SSTs from the mixed layer, the water body above the shallowest thermocline. Their results suggest that alkenone production below the mixed layer is not extensive enough to have an effect on the  $U_{37}^{K^{(c)}}$  signal recorded in sediments.

Müller *et al.* (1998) compared their core top  $U_{37}^{K'}$  signal to seasonal and annual SSTs and found that the  $U_{37}^{K'}$  best reflects the annual SSTs in the eastern South Atlantic. They attribute this result mainly to the fact that sedimentary alkenones produce signals which integrate long time periods, thus diminishing the effect of seasonality. Another reason for their result is that primary production of *E. huxleyi* occurs throughout the year in that area. This is unlikely to be true for sub-polar and polar regions, where the main season of primary production of coccolithophores is during late spring and summer (Prah *et al.*, 2010; Sikes *et al.*, 1997; Ternois *et al.*, 1998). Thus,  $U_{37}^{K'}$  signals from these regions may reflect warm season temperatures, rather than winter, spring, or indeed mean annual temperatures.

## 1. Introduction

The global  $U_{37}^K$  core top calibration equation produced by Müller *et al.* (1998) encompasses samples taken from five different biogeographical coccolithophore zones. Thus, the analysed alkenones were probably produced by different species of coccolithophores. Despite the species variation, the relationship between the alkenone unsaturation index and SST is linear, suggesting that different species react similarly to temperature changes. The most comprehensive global calibration of  $U_{37}^K$ , encompassing 742 samples, also shows a linear correlation (except for the North Atlantic and Nordic seas), which suggests that inter-species variations in the alkenone production are within the calibration error of the  $U_{37}^K$  (Equation 5; Conte *et al.*, 2006). Bendle and Rosell-Melé (2004) suggest that the breakdown of the relationship between the  $U_{37}^K$  and SSTs in the Nordic seas is due to mixing of allochthonous and autochthonous alkenones due to lateral advection of sediments and coccolithophores in the water column. Furthermore, unknown algal species unique to polar regions, contributing high amounts of the  $C_{37:4}$  alkenone, may also lead to a distortion of the relationship between the  $U_{37}^K$  and SSTs (Bendle & Rosell-Melé, 2004).

It is still unclear why the relative distribution of alkenones with different numbers of double bonds, correlate with growth temperature. Since alkenones are not part of the cytoplasm membrane of alkenone producing organisms, but reside within the cell itself, they do not play any part in membrane stability (Eltgroth *et al.*, 2005). There is some evidence that alkenones may serve as an energy source for the organisms producing them (Eltgroth *et al.*, 2005).

### 1.2.3 Diglycerol tetraether lipids

#### 1.2.3.1 Archaeal tetraether lipids

A second SST proxy derived from biomarkers has emerged over the last decade, based on the relative distribution of different glycerol dibiphytanyl glycerol tetraethers (GDGTs, Figure 1.4) in sediments (Kim *et al.*, 2008; Schouten *et al.*, 2007; Schouten *et al.*, 2002). These GDGTs are produced by mesophilic archaea called Thaumarchaeota (previously known as Crenarchaeota group I; Brochier-

## 1. Introduction

Armanet *et al.*, 2008), which are ubiquitous in marine environments (DeLong, 1992; DeLong, 1998; Massana *et al.*, 2000)

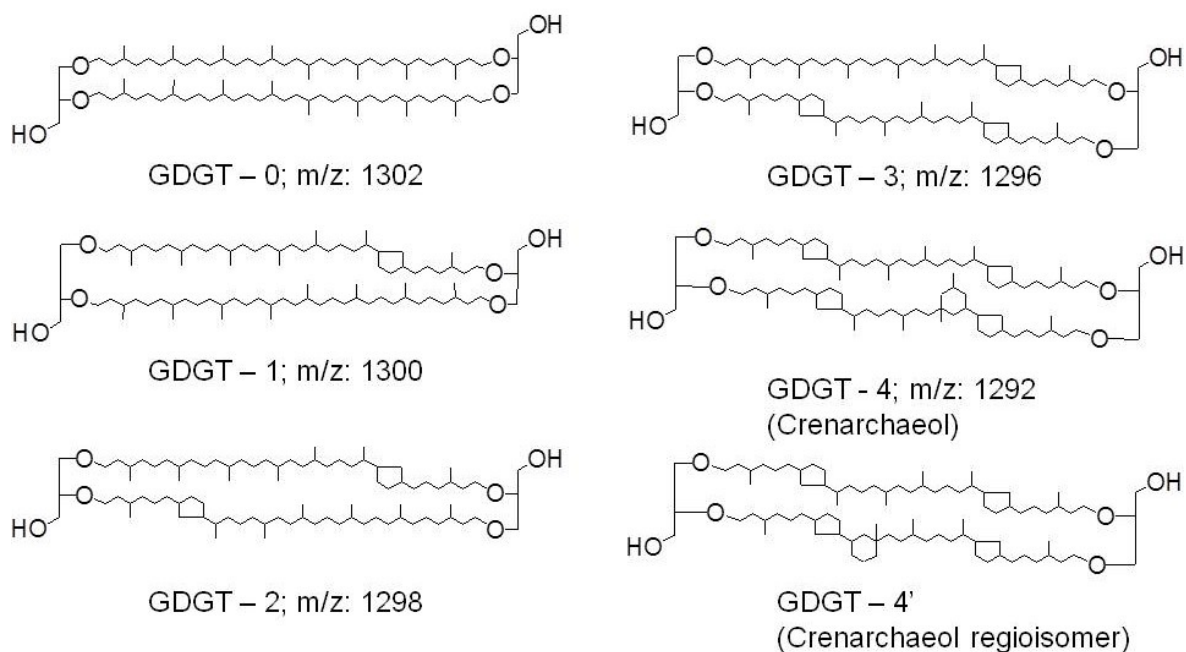


Figure 1.4: Molecular structures of archaeal GDGTs and the mass/charge (m/z) ratio of the molecular ion (Schouten *et al.*, 2007).

Archaea are the only known organisms that use isoprenoidal GDGTs as building blocks for their cytoplasm membrane (Madigan *et al.*, 2009). The cytoplasm membrane is a semi permeable hull separating the cell from the surrounding environment. With changing environments archaea alter the structure of their membrane to ensure its structural integrity and fluidity. It is thought that the use of GDGTs as membrane components evolved as a reaction to challenging environments in which archaea can be found, such as methane seeps (Pancost *et al.*, 2001; Zhang *et al.*, 2011), and hydrothermal vents (Huang *et al.*, 2011; Kan *et al.*, 2011). GDGTs are more stable compared to phospholipids which are used by most bacteria and prokaryotes as membrane constituents. The glycerol backbone of the GDGT is linked by an ether bond to the biphytanyl chain (Sinninghe Damsté *et al.*, 2002b; Figure 1.3), while the glycerol backbone of phospholipids is linked by an ester bond to the hydrophobic fatty acids. Since ether bonds are chemically more stable than ester bonds, GDGTs are more stable than phospholipids. The second reason why GDGT containing membranes are more stable than cytoplasm

## 1. Introduction

membranes made up of phospholipids is that GDGTs form mono layered membranes. These membranes cannot peel apart as bilayered ones can under adverse conditions (Madigan *et al.*, 2009).

In order to adapt to high temperatures, thermophilic archaea synthesise cyclic structures within the dibiphytanyl chains. Increasing the number of rings in the GDGTs leads to these molecules having higher melting points (Gliozzi *et al.*, 1983). Furthermore, membranes containing GDGTs with incorporated ring structures are more densely packed, which increases their thermal stability (Gabriel & Lee Gau Chong, 2000).

Culture studies have shown that archaea related to marine Thaumarchaeota increase the number of rings in the GDGTs they produce as the temperature at which the cells are grown rises (Uda *et al.*, 2001). Schouten *et al.* (2002) analysed 40 surface sediment samples from 15 different sites of the world's oceans, and found a correlation between the relative distribution of GDGTs and SST. From this relationship Schouten *et al.* (2002) deduced the Tetraether index of tetraethers consisting of 86 carbon atoms, the TEX<sub>86</sub>, linking the relative distribution of GDGTs to the annual mean sea surface temperature (Equation 6).

$$\text{TEX}_{86} = \frac{[\text{GDGT} - 2] + [\text{GDGT} - 3] + [\text{GDGT} - 4']}{[\text{GDGT} - 1] + [\text{GDGT} - 2] + [\text{GDGT} - 3] + [\text{GDGT} - 4']}$$

Equation 6: Tetraether index (TEX<sub>86</sub>). The structures of the different GDGTs are shown in Figure 1.4.

Incubation experiments have shown that the TEX<sub>86</sub> is independent of nutrient conditions and salinity (Wuchter *et al.*, 2004). By incubating seawater from the North Sea at different temperatures and salinities, Wuchter *et al.* (2004) showed that the overall concentration of GDGTs in the mesocosm tanks used for the incubation did not have an effect on the relative distribution of GDGTs, and therefore no effect on the TEX<sub>86</sub>. This result also indicates that the production of GDGTs is independent of nutrient levels because the relative distribution of

## 1. Introduction

GDGTs stayed constant during different growth stages and varying nutrient levels. The same study showed that different salinity levels also had no substantial effect on GDGT distribution.

While incubating water from the Indian Ocean, different types of Crenarchaeota with different optimal growth temperatures were detected (Schouten *et al.*, 2007). Even though different strains of Crenarchaeota were detected at different incubation temperatures, the TEX<sub>86</sub> values obtained in that study showed a linear relationship with temperature. Schouten *et al.* (2007) also showed, that when combining the TEX<sub>86</sub> data sets from Wuchter *et al.* (2004) and Schouten *et al.* (2007), both data sets formed a linear correlation with temperature, even though phylogenetically different species were detected in both studies. This result suggests that the TEX<sub>86</sub> palaeotemperature proxy is not affected by different species of Crenarchaeota.

Since the introduction of the TEX<sub>86</sub> proxy by Schouten *et al.* (2002) a number of calibration equations have been developed. In their global sediment calibration of the TEX<sub>86</sub> Kim *et al.* (2008) used the same equation (Equation 6) that Schouten *et al.* (2002) used to convert relative GDGT concentrations into the TEX<sub>86</sub> proxy. Based on the global sediment sample set, Kim *et al.* (2008) developed the following calibration equation (Equation 7) to convert TEX<sub>86</sub> values into SSTs:

$$\text{SST} = -10.78 + 56.2 \cdot \text{TEX}_{86}$$

Equation 7: TEX<sub>86</sub> calibration equation after Kim *et al.* (2008).

The correlation between TEX<sub>86</sub> and SST is not linear where SSTs are below 5 °C. Therefore, Kim *et al.* (2010) developed another calibration equation to convert GDGT concentrations into the TEX<sub>86</sub><sup>L</sup> (TEX<sub>86</sub> for low temperature regions) proxy (Equation 8) and subsequently into SSTs (Equation 9):

## 1. Introduction

$$\text{TEX}_{86}^{\text{L}} = \log \frac{[\text{GDGT} - 2]}{[\text{GDGT} - 1] + [\text{GDGT} - 2] + [\text{GDGT} - 3]}$$

Equation 8: Conversion of relative GDGT abundance into  $\text{TEX}_{86}^{\text{L}}$  proxy.

$$\text{SST} = 67.5 \cdot \text{TEX}_{86}^{\text{L}} + 46.9$$

Equation 9:  $\text{TEX}_{86}^{\text{L}}$  calibration equation after Kim *et al.* (2010).

The relative concentration of GDGT-4' does not correlate strongly with SST variations at low temperatures which is why it is not included in the  $\text{TEX}_{86}^{\text{L}}$  calibration equation (Kim *et al.*, 2010).

Archaeal GDGTs are not only produced in the water column, but also in the underlying sediments which are anoxic. Biomarker (Blumenberg *et al.*, 2004; Hinrichs *et al.*, 1999; Hinrichs *et al.*, 2000), and microbiological screening studies (Knittel *et al.*, 2005; Nauhaus *et al.*, 2002) have shown that methanotrophic archaea (ANME) are responsible for the anaerobic oxidation of methane (AOM) in sediments. AOM is mediated in symbiosis with sulphate-reducing bacteria (Boetius *et al.*, 2000; Nauhaus *et al.*, 2002). Distinctive isoprenoidal GDGT patterns have been found in sediments characterised by high AOM activity and populated by methanotrophs of the ANME-1 and ANME-2 cluster (Blumenberg *et al.*, 2004; Elvert *et al.*, 2005; Pancost *et al.*, 2001). Zhang *et al.* (2011) have introduced the Methane-Index (MI, Equation 10) to differentiate between marine settings where AOM is an important mechanism in sediments, and where it is not. The MI is defined as follows, where GDGTs-1, -2 and -3 represent the AOM mediating archaea, while GDGTs-4 and -4' represent Thaumarchaeota:

$$\text{MI} = \frac{[\text{GDGT} - 1] + [\text{GDGT} - 2] + [\text{GDGT} - 3]}{[\text{GDGT} - 1] + [\text{GDGT} - 2] + [\text{GDGT} - 3] + [\text{GDGT} - 4] + [\text{GDGT} - 4']}$$

Equation 10: Methane Index (MI). The structures of the different GDGTs are shown in Figure 1.4.

## 1. Introduction

Zhang *et al.* (2011) show that a MI of 0.5 or greater indicates marine settings where AOM is an important mechanisms, while an MI lower than 0.5 is indicative of normal marine conditions.

### 1.2.3.1 Bacterial tetraether lipids

A group of molecules have been detected which are structurally similar to GDGTs produced by Thaumarchaeota (Sinninghe Damsté *et al.*, 2000). These molecules are branched glycerol-dialkyl-glycerol-tetraethers, generally termed branched or bacterial GDGTs (Figure 1.5).

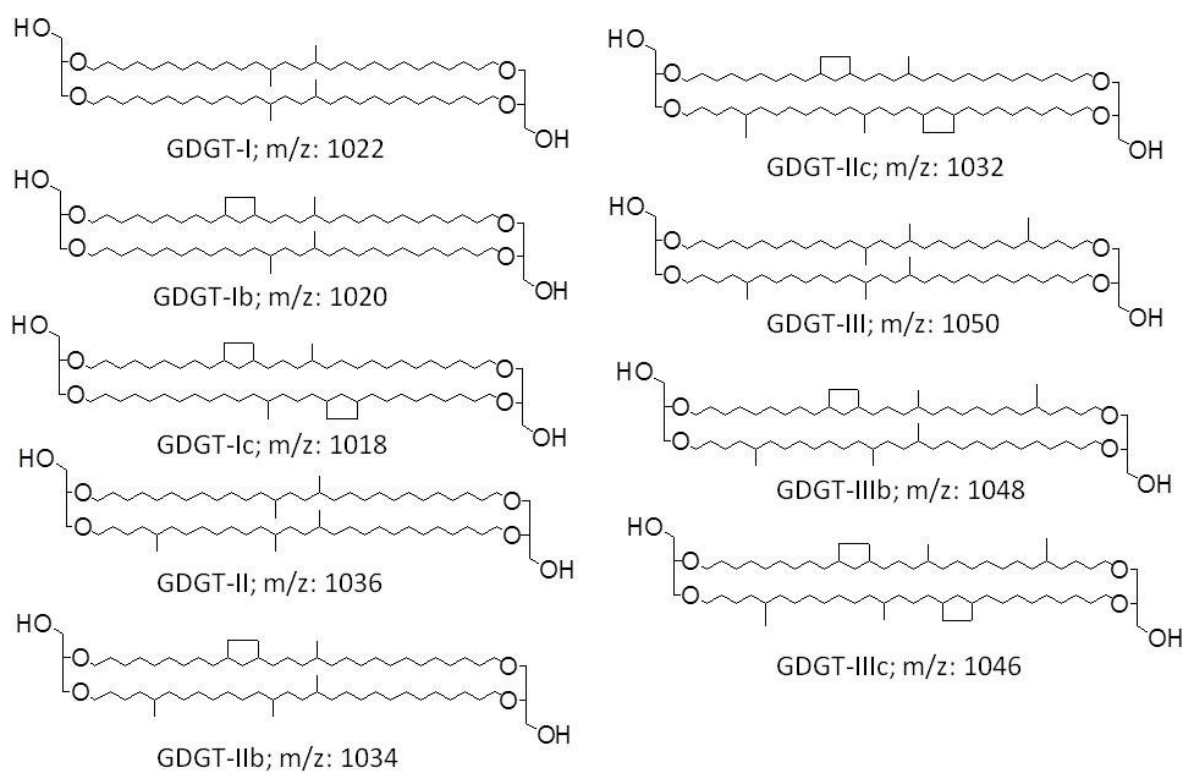


Figure 1.5: Molecular structures of branched GDGTs and the mass/charge ratio of their molecular ion (Weijers *et al.*, 2007c).

Branched GDGTs are synthesised by bacteria rather than archaea (Hopmans *et al.*, 2004; Weijers *et al.*, 2007c). GDGT-I has been detected in subdivisions of *Acidobacteria* that are ubiquitous in soils (Sinninghe Damsté *et al.*, 2011). GDGTs produced by archaea have a 2,3-di-O-alkyl-sn-glycerol backbone, whereas

## 1. Introduction

branched GDGTs have a 1,2-di-O-alkyl-sn-glycerol backbone which is the stereochemistry found in bacterial membranes (Figure 1.5; Kates, 1978; Weijers *et al.*, 2006a). Two distinct proteins are responsible for synthesising these stereo-specific glycerol backbones.

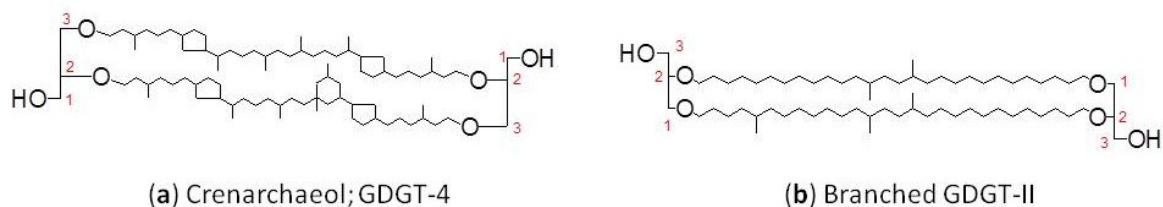


Figure 1.6: Stereochemistry of archaeal and bacterial GDGTs. The carbon atoms of the glycerol backbones are stereo specifically numbered according to the sn-system. (a) The chiral carbon atoms (2) of Crenarchaeol are **R** configured; (b) the chiral carbon atoms (2) of the branched GDGT-II are **S** configured.

The second distinct difference between GDGTs produced by archaea, and branched GDGTs produced by bacteria lies in the carbon chains connecting the glycerol backbones. Instead of having two isoprenoid chains which link the glycerol backbones of the molecules, branched GDGTs consist of two aryl chains with different numbers of methyl branches (Sinninghe Damsté *et al.*, 2000). To date bacteria with isoprenoid chains within their membrane lipids have not been reported.

The distribution of branched GDGTs in soils can be used to reconstruct palaeo air temperatures and soil pH changes. The relative abundance of branched GDGTs with different amounts of methyl branches and cyclic structures extracted from soils vary depending on the mean air temperature (MAT) and soil pH (Weijers *et al.*, 2007c). In order to quantify the degree of methylation in the branched tetraethers of the soil samples the methylation index of branched tetraethers (MBT) was defined (Equation 11).

## 1. Introduction

$$\text{MBT} = \frac{[\text{I} + \text{Ib} + \text{Ic}]}{[\text{I} + \text{Ib} + \text{Ic}] + [\text{II} + \text{IIb} + \text{IIc}] + [\text{III} + \text{IIIb} + \text{IIIc}]}$$

Equation 11: Methylation index of branched tetraethers (MBT). The roman numerals correspond to the structures shown in Figure 1.5.

Weijers *et al.* (2007c) found that the MBT decreased with decreasing MAT. In order to maintain the fluidity of the cytoplasm membrane, bacteria producing branched GDGTs likely change the relative amount of methyl functions with these molecules (Weijers *et al.*, 2007c).

In addition to being affected by MAT, bacterial GDGT structures are also affected by soil pH. Living cells create energy by pumping cations such as  $\text{Na}^+$ , or protons ( $\text{H}^+$ ), through the cytoplasm membrane into the cell. Because more protons are present in soils with high pH values the membrane needs to have lower proton permeability in order to keep the flow of ions and the internal pH at its optimal level (van de Vossenberg *et al.*, 1998a; van de Vossenberg *et al.*, 1998b). Weijers *et al.* (2007c) found that the relative amounts of GDGTs with cyclic structures increases in samples derived from soils with a high pH, which is thought to be a homo-proton permeability adaption. The cyclisation ratio of branched tetraethers (CBT; Equation 12) indicates the relative amount of branched GDGTs with cyclic moieties vs. branched GDGTs without cyclic structures.

$$\text{CBT} = -\log\left(\frac{[\text{Ib} + \text{IIb}]}{[\text{I} + \text{II}]}\right)$$

Equation 12: Cyclisation ratio of branched tetraethers (CBT). The roman numerals correspond to structures in Figure 1.5.

The CBT correlates with pH according to the following calibration equation (Equation 13) published by Weijers *et al.* (2007c):

## 1. Introduction

$$\text{CBT} = 3.33 - 0.38 \cdot \text{pH}$$

Equation 13: Calibration equation of CBT with soil pH.

Since the molecular structure of branched GDGTs is influenced by air temperature fluctuations and soil pH changes, Weijers *et al.* (2007c) proposed the MBT/CBT-palaeothermometer to reconstruct mean air temperature changes (Equation 14).

$$\text{MAT} = \frac{\text{MBT} - 0.122 - 0.187 \cdot \text{CBT}}{0.020}$$

Equation 14: MBT/CBT mean air temperature proxy

The large standard error of 5.5 °C which is associated with the MAT calibration equation may be due to an offset between soil and air temperatures (Weijers *et al.*, 2011a). Bacterial communities living in soils are likely more affected by soil, rather than air temperatures.

Branched GDGTs have been thought to originate from continental sources only (Hopmans *et al.*, 2004; Weijers *et al.*, 2007c). Based on this assumption, Hopmans *et al.* (2004) have proposed the branched and isoprenoid tetraether index (BIT; Equation 15) which compares the relative amounts of marine GDGTs and terrestrial GDGTs to elucidate the input of terrestrial organic carbon ( $\text{OC}_{\text{terr}}$ ) into marine sediments.

$$\text{BIT} = \frac{(\text{I} + \text{II} + \text{III})}{(\text{I} + \text{II} + \text{III}) + (\text{GDGT} - 4)}$$

Equation 15: Branched and isoprenoid tetraether index (BIT-Index). Roman numerals correspond to the structures shown in Figure 1.5. The structure of GDGT-4 (Crenarchaeol) is shown in Figure 1.4.

The BIT-Index uses Crenarchaeol to represent marine organic carbon ( $\text{OC}_{\text{mar}}$ ) because the other GDGTs associated with Thaumarchaeota are also produced by

anaerobic methane oxidizing archaea (Zhang *et al.*, 2011). Recent work has shown that the BIT-Index may be largely controlled by the abundance of Crenarchaeol (Fietz *et al.*, 2011; Walsh *et al.*, 2008). Fietz *et al.* (2012; accepted for publication) have shown that the correlation between Crenarchaeol and branched GDGTs in marine sediments is a global occurrence. One possible explanation for this observation is that increasing amounts of terrestrial organic carbon, indicated by a high BIT-Index, lead to increased amounts of Thaumarchaeota, and therefore increased amounts of Crenarchaeol (Fietz *et al.*, 2012; accepted for publication), which in turn decreases the BIT-Index.

Furthermore, branched GDGTs may also have a marine source, thus affecting the reliability of the BIT-Index, but also other proxies that are based on the abundance of branched and isoprenoidal GDGT in marine sediments. For example, Peterse *et al.* (2009a) suggest that branched GDGTs may be produced in marine environments, based on the distribution with monocyclic branched GDGTs in fjordic sediments of Svalbard.

In addition to bacterial GDGTs possibly being produced in the water column, Weijers *et al.* (2006b) show that Crenarchaeol also occurs in soils. The average BIT-Index of soils is 0.91 whereas the BIT-Indices for marine sediments are usually close to zero. Weijers *et al.* (2006b) concluded that the BIT-Index can be used to elucidate  $OC_{terr}$  input into marine sediments despite the ubiquitous occurrence of crenarchaeol.

Fietz *et al.* (2012; accepted for publication) suggest that branched GDGTs and isoprenoidal GDGTs (specifically Crenarchaeol) are of marine and terrigenous origin, and that mixing of the GDGTs of the different source regions occurs. The hypothesis, that branched and isoprenoidal GDGTs in marine and terrestrial environments are of allochthonous and autochthonous origin affects all GDGT derived proxies. Therefore, the results derived from such proxies need to be interpreted with caution.

### 1.2.4 Highly Branched Isoprenoids

Marine sourced C<sub>25</sub> highly branched isoprenoids (HBIs) with as many as five double bonds, and cyclical structures have been reported since the mid 1970s (see review by Rowland & Robson, 1990 and references therein). Volkman *et al.* (1994) and Sinninghe Damsté *et al.* (1999) found C<sub>25</sub> HBIs in the diatoms *Haslea ostrearia* and *Rhizosolenia setigera*, and Belt *et al.* (2000; 2001) have identified C<sub>25</sub> HBIs in the benthic diatoms *Pleurosigma intermedium* and *planktonicum* from French coastal waters. Xu *et al.* (2006) found a number of C<sub>25</sub> HBIs in the sediments of Florida Bay. They suggest that C<sub>25</sub> HBIs can be used to trace diatom input in palaeoenvironments.

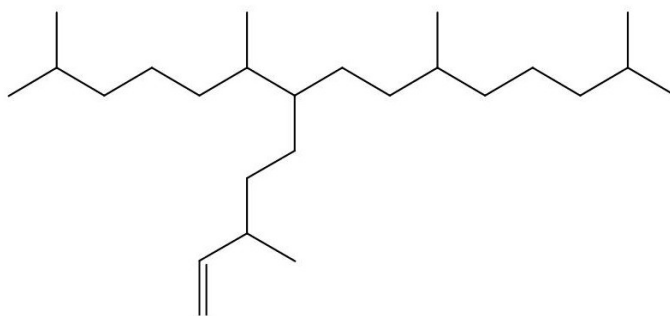


Figure 1.7: Sea ice proxy IP<sub>25</sub>

Rowland *et al.* (2001) have shown that cultures of *Haslea ostrearia* produce C<sub>25</sub> HBIs with a decreasing number of unsaturations with decreasing temperatures. Diatoms of the species *Haslea* have been found in Arctic and Antarctic sea-ice (Belt *et al.*, 2007; references therein). Based on the occurrence of a mono unsaturated C<sub>25</sub> HBI in sea-ice and sediments of the Canadian Arctic, Belt *et al.* (2007) have proposed a specific C<sub>25</sub> HBI with one unsaturation as a palaeo-sea-ice indicator, the Ice Proxy with 25 carbon atoms (IP<sub>25</sub>; Figure 1.7). Further evidence for an ice algal source of the IP<sub>25</sub> comes from the carbon isotopic signature of the molecule. Lipids produced by sea-ice algae are isotopically heavier than those produced by algae living in the open ocean (Belt *et al.*, 2008; Brown *et al.*, 2011; McMinn *et al.*, 1999). Isotopically light (<sup>12</sup>CO<sub>2</sub>) and heavy (<sup>13</sup>CO<sub>2</sub>) carbon dioxide is available to ice algae for photosynthesis. Photosynthetic

organisms discriminate against the isotopically heavy CO<sub>2</sub> during its uptake and subsequent processing (Schidlowski, 1987 and references therein). Culture experiments using algae have shown, that the isotopic fractionation between the two isotopically distinct CO<sub>2</sub> species increases with decreasing amounts of cells and increasing amounts of CO<sub>2</sub> (Pardue *et al.*, 1976). Consequently, in environments, where CO<sub>2</sub> availability is restricted and cell density is high, such as brine channels in sea-ice, the isotopic fractionation during photosynthesis decreases (Brown *et al.*, 2011; McMinn *et al.*, 1999). In other words, as the light, preferentially used CO<sub>2</sub> is used during photosynthesis, and subsequently depleted, more of the heavy carbon isotope containing CO<sub>2</sub> gets used, causing ice algal lipids with relatively heavy carbon isotopic signatures to be produced.

Brown *et al.* (2011) have shown that the highest concentration of IP<sub>25</sub> can be found in sea-ice during spring blooms, correlating with high diatom abundances. These spring blooms which occur along almost all of the marginal ice zone (MIZ; Perrette *et al.*, 2011), form the basis of the Arctic food web (Leu *et al.*, 2011). Further evidence for the importance of sea-ice algae as a food source was provided by Brown *et al.* (2012), who have detected IP<sub>25</sub> in benthic macro fauna.

### **1.2.5 Fatty acids in marine environments**

Fatty acids (FAs) are ubiquitous in the marine realm. They occur as triacylglycerols, wax esters and phospholipids (Dalsgaard *et al.*, 2003). FAs constitute an integral part of the cell membrane, but are also used in energy storage. *Calanus sp.* copepods for example synthesise wax esters which they use to store energy (Falk-Petersen *et al.*, 2009). The FAs in this thesis are named using the IUPAC nomenclature C<sub>x:y(n-x)</sub>, where x indicates the number of carbons in the carbon chain, y indicates the number of double bonds and (n-x) indicates the position of the double bonds when counting from the terminal carbon atom in the chain. FAs without double bonds will be described as C<sub>x</sub> instead of C<sub>x:0</sub>.

FAs are ubiquitous in living organisms, and different organisms produce different FAs. Diatoms and dinoflagellates are among the most important phytoplankton groups in polar waters (Falk-Petersen *et al.*, 2009). Diatoms produce specific FAs

such as C<sub>20:5(n-3)</sub>, C<sub>16:1(n-7)</sub>, while Dinoflagellates are rich in C<sub>18:4(n-3)</sub> and C<sub>18:5(n-3)</sub> (Dalsgaard *et al.*, 2003; references therein; Falk-Petersen *et al.*, 2009; Falk-Petersen *et al.*, 1998; Graeve *et al.*, 1994). Iso and anteiso C<sub>15</sub> and C<sub>17</sub> FAs are produced by bacteria (Hinrichs *et al.*, 2000; Viso & Marty, 1993). Long chained (C<sub>24</sub> - C<sub>30</sub>) saturated FAs found in marine sediments (Birgel *et al.*, 2004; Drenzek *et al.*, 2007) originate from terrestrial sources. Such acids are for example found in waxes of terrestrial higher plants (Bianchi, 1995; Eglinton *et al.*, 1962).

Fatty acids can be used to elucidate trophic relationships and food sources in marine food chains. Fatty acid trophic markers (FATMs) are fatty acids which are produced by specific organisms (Dalsgaard *et al.*, 2003). A number of authors have shown that the FA distribution of higher trophic levels corresponds to their food source. The FA composition of *Calanus* zooplankton for example resembles that of its diatomaceous prey (Lee *et al.*, 1971). In controlled feeding experiments Graeve *et al.* (1994) have shown that *Calanus finmarchicus* copepods that were fed with either diatoms or Dinoflagellates, displayed a FA composition resembling that of their food source. Fraser *et al.* (1989) and St. John and Lund (1996) have shown that the trophic marker concept can be extended to higher trophic levels.

The analysis of the isotopic composition of FAs specific to certain organisms, i.e. C<sub>16:1(n-7)</sub> for Diatoms, allows the differentiation between diatoms from different habitats. As discussed previously, specific ice algal produced molecules have significantly heavier carbon isotopic signatures compared to the molecules produced by pelagic algae (Belt *et al.*, 2008; Budge *et al.*, 2008). Furthermore ice algal particulate organic matter (POM) is enriched compared to pelagic POM (France *et al.*, 1998; Tamelander *et al.*, 2008; Tamelander *et al.*, 2006). By studying the carbon isotopic composition of FAs specific to diatoms at different trophic levels, Budge *et al.* (2008) have shown, that ice algal FAs may contribute up to 71 % of the total FAs of Arctic species.

### **1.3 Using contemporary observations to reconstruct changing climates**

Many organisms regulate the biosynthetic production of certain molecules in response to changing climates. Relationships between biomarker distributions, the

occurrence or absence of certain biomarkers, and environmental parameters, as observed today, are used to reconstruct past climate change. For example, haptophyte algae produce differing relative abundances of the  $C_{37:2}$  and  $C_{37:3}$  alkenones (Brassell *et al.*, 1986), and archaea produce different relative abundances of GDGTs (Schouten *et al.*, 2002) in response to different sea surface temperatures. The relationship between biomarker abundances and sea surface temperature has been shown through global calibration equations (Conte *et al.*, 2006; Kim *et al.*, 2008; Kim *et al.*, 2010; Müller *et al.*, 1998). These calibration equations are subject to a number of uncertainties (calibration errors; C.E.). In case of the relationship between the  $U_{37}^K$  core top values and the mean annual sea surface temperature (Conte *et al.*, 2006; Müller *et al.*, 1998), the calibration error arises for example from:

- different biological precursor organisms producing alkenones,
- different water depths, in which alkenones are produced,
- seasonal differences in the production of alkenones,
- the lateral transport of alkenones,
- post-depositional mixing of alkenones in the sediments.

Despite the various factors influencing the uncertainty of the  $U_{37}^K$ -SST palaeothermometer, the calibration error ( $1\sigma$ ) of the latest, most comprehensive core top calibration equation is  $\pm 1.1^\circ\text{C}$  (Equation 5; Conte *et al.*, 2006). All calibration equations describing relationships between biomarker abundances and climatic variables are subject to such uncertainties as described above. Additional factors influence the calibration error when terrestrial biomarkers in marine sediments are considered for palaeoclimate reconstructions because different transport pathways from land to sea can add to the source of error.

The key assumption that is made, when using modern analogues to reconstruct past climate change is, that the relationship between the studied biomarker and the climate variable is constant through time. This consideration has an important effect on how the error associated with a calibration equation is treated and interpreted in palaeoclimatic studies.

Figure 1.8 shows the  $U^{K}_{37}$ -SST reconstruction from 600 to 310 cal. a BP in Ísafjarðardjúp fjord, Iceland (the main study site in this thesis). The calibration equation published by Conte *et al.* (2006) was used to reconstruct SST variations. Under the assumption, that the uncertainty associated with the calibration equation is constant though time only one of the three (a, b or c) temperature reconstructions shown in Figure 1.8 is valid. This means that the temperature shift from  $11.8 \pm 0.44$  °C to  $9.0 \pm 0.44$  °C (line a; Figure 1.8) between  $\sim 540$  and  $\sim 516$  cal. a BP does in fact represent a genuine change in sea surface temperature. However, due to the uncertainty associated with the calibration equation, sea surface temperature may also have changed from  $12.8 \pm 0.44$  °C to  $10.0 \pm 0.44$  °C (line b; Figure 1.8) or  $10.8 \pm 0.44$  °C to  $8.0 \pm 0.44$  °C (line c; Figure 1.8).

The above example shows, that relatively small temperature changes can be considered as genuine. However, the calibration error adds another degree of uncertainty which is taken into account by propagating the analytical error through the variability of the calibration equation used. The propagated error is larger than the calibration and analytical errors, and it is important to note that when it is considered, the propagated error may be an overestimation of the true error, because the calibration equations used, and subsequently the associated uncertainties, are based on global rather than local datasets.

Throughout this thesis, palaeoclimate reconstructions are interpreted under the assumption that the “biomarker proxy-climate variable”-relationships are constant through time. However, since this assumption cannot be verified, the propagated error will be shown on all graphs where possible and applicable.

## 1. Introduction

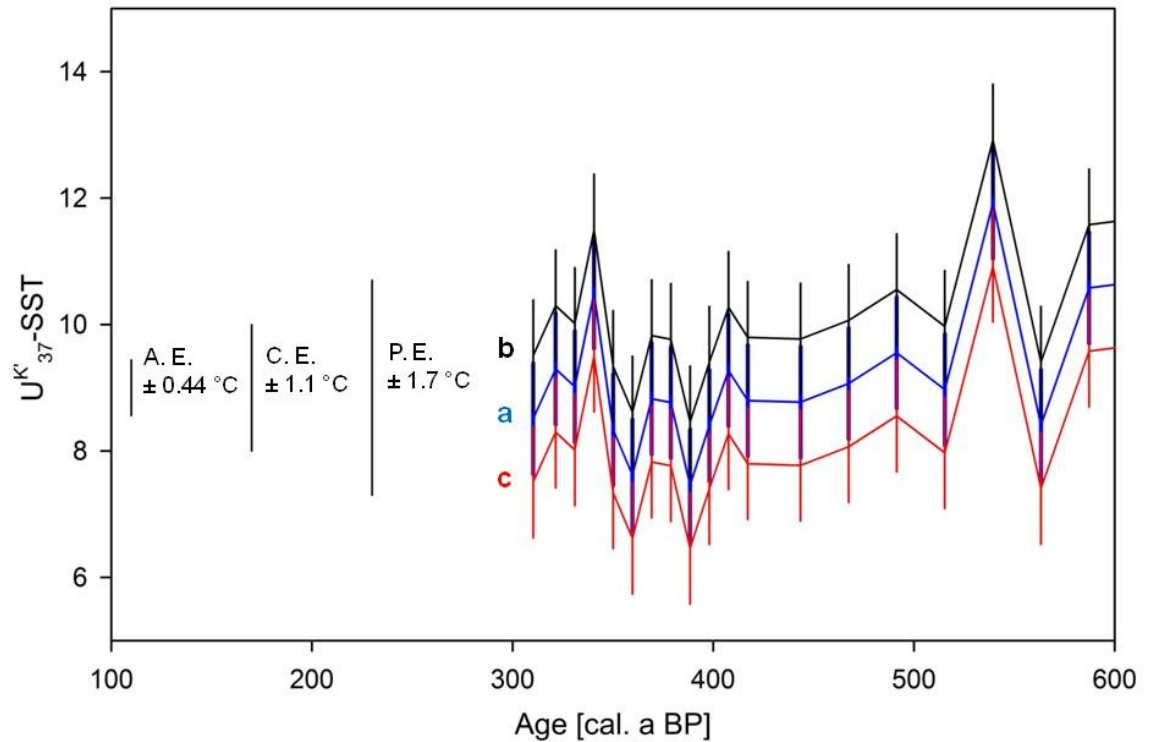


Figure 1.8: Considering different error sources when interpreting palaeoclimatic records. Three different  $U^K_{37}$ -SST reconstructions (within the calibration error from 600 to 310 cal a BP in Ísafjarðardjúp fjord, Iceland), is shown. The calibration equation published by Conte *et al.* (2006) was used to convert  $U^K_{37}$  values into temperatures. (a) mean SST reconstruction; (b) SST reconstruction with temperatures amended by + 1.1 °C due to calibration uncertainties; (c) SST reconstruction with temperatures amended by - 1.1 °C due to calibration uncertainties. The constant temperature interval between b and c indicates the calibration error ( $1\sigma$ ; ± 1.1 °C; C.E.). The black, blue and red vertical error bars indicate the analytical error (± 0.44 °C; A.E.) associated with each sample. The black vertical lines to the left of the temperature reconstruction show the A.E., the C.E. and the propagated error (± 1.7 °C; P.E.) Error propagation was conducted by propagating the analytical error through the scatter associated with the calibration equation.

## 2 Materials and Methods

The following section gives an overview of the methods used to extract, purify and analyse the biomarkers studied during this PhD (Figure 2.1). All 326 sediment samples of the Iceland core MD99-2266 were treated using the materials and methods introduced in this chapter (Figure 2.1). The qualitative and quantitative analysis of the IP<sub>25</sub>, and the carbon isotopic measurements of the C<sub>16</sub> fatty acid in chapter 7 required further sample workup, and specially adapted analysis methods. These methods are introduced and discussed in detail in chapter 7.

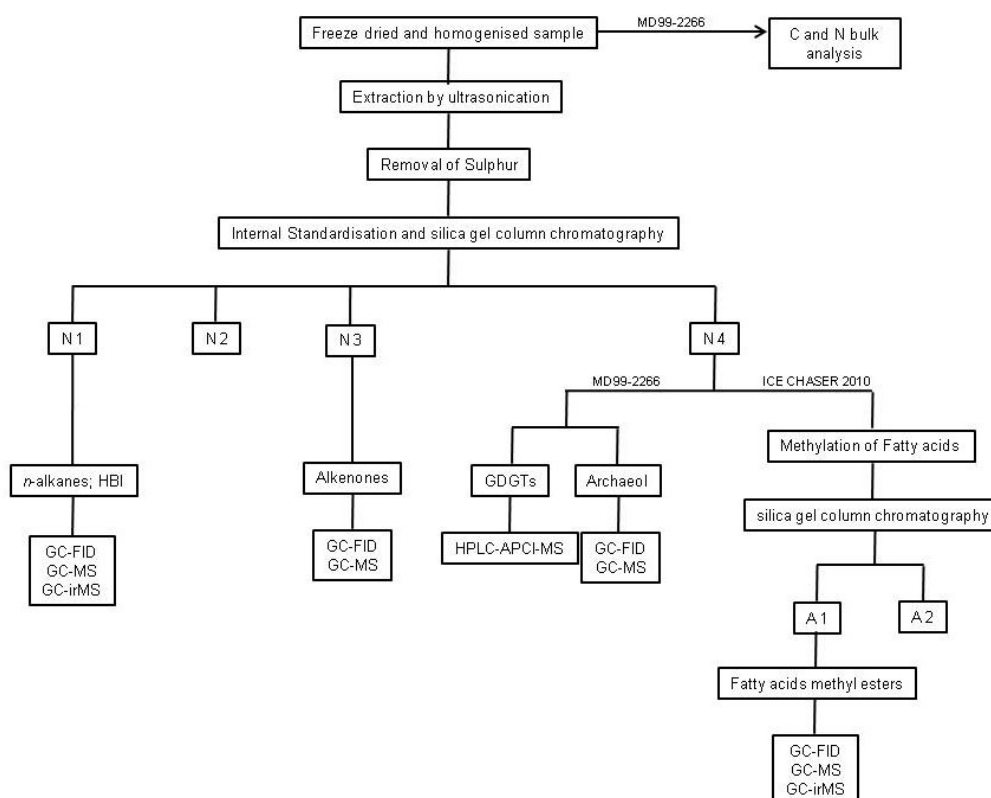


Figure 2.1: Sample extraction and purification process used for all samples in the course of this PhD. The sample analysis specific to the ICE CHASER 2010 samples is explained in chapter 7.

### 2.1 Elemental analysis

The sample preparation for the elemental analysis of MD99-2266 sediment samples was done at the G-MOL laboratory at the University of Glasgow. The sample measurements were done at the Scottish Association of Marine Science (SAMS) institute by Dr. Richard Abell.

The total organic carbon (TOC) and total nitrogen (TN) content of 156 MD99-2266 samples were measured using the following method. A 20 mg ( $\pm$  1 mg) aliquot of sediment was taken from the dried and ground core slice and placed into a 5 ml glass vial. To remove carbonate material, 1 ml of sulphurous acid was added to the vial, and the vial was gently tapped to remove bubbles from the sediment. The samples were then left overnight to react in a fume cupboard. Samples were initially dried on a hot plate at 40 °C and then transferred to a vacuum desiccator and held under vacuum for 2-3 hours to degas, before being freeze dried for 24 hours. The dry residue was placed into a 5x9 mm tin capsule and sealed. All carbon and nitrogen analyses were performed on a Costech International Elemental Combustion System (ECS) 4010 using a pneumatic auto-sampler. Operational temperatures were set to 1000 °C in the left combustion furnace, 630 °C in the right reaction furnace and 50 °C in the gas chromatographic separation oven. The helium (>99.9 %) carrier gas pressure was set to 1.2 bar giving a flow rate ~ 100 ml/min. Oxygen (>99.9 %) used for combustion, was set at 1.9 bar and air (water and oil free) was set to 2.4 bar. Five standards of acetanilide (10.36 % nitrogen, 71.09 % carbon) were weighed into the same batch of 5x9mm tin capsules from a range from 0.1 mg to 1.0 mg.

The analysis was run for 30 minutes on the 'Semi- $\mu$ ' setting. Three empty tin capsules were folded and sealed and the TOC and TN content was measured to blank correct the standards and samples. In addition, 1 capsule of acetanilide per 15 unknown samples was also measured. These reference samples were measured as unknown samples to correct any instrument drift. Calibration drift over long analytical sessions is small, and typically < 5 %.

To assess the reproducibility of this methodology, 17 samples were run in triplicate and the relative standard deviation measured. The mean relative standard deviation from 17 triplicate analyses is  $\pm 3.87\%$  for Nitrogen and  $\pm 2.47\%$  for Carbon. The mean relative standard deviation of the C/N ratio is  $\pm 0.14$ .

### **2.2 Biomarker extraction and purification**

All samples were freeze dried for 48 hours prior to the sample work-up and all sediment samples were homogenised using an agate mortar and pestle. All samples were worked up as seen in figure 2.1. The glassware used in the process was cleaned using detergent and water and furnaceed at 450 °C for 8 hours.

#### **2.2.1 Extraction**

The extraction procedure was modified after Kornilova and Rosell-Melé (2003). Ca. 6 g of each sediment sample were placed in a pre-weighed 30 ml test tube. In case of the POM-, ice algae-, and ice core-samples, all the GFF filters which were used to filter a sample, were placed in a 30 ml test tube. 20 ml of a solvent mixture of dichloromethane:methanol (DCM:MeOH; 3:1) were added into the test tube and each sample was suspended using a vortex mixer. Then the samples were ultrasonicated for 20 minutes, after which they were placed on a hotplate and heated at 55 °C for one hour. Subsequently the samples were placed in a centrifuge at 3300 rounds per minute (rpm) for 3 minutes and the extract was transferred into a 100 ml round bottom flask using a pipette. The samples were extracted three more times using 10 ml of DCM:MeOH (3:1) each time, and employing the same procedure. All extracts of the samples were combined and the solvent was evaporated using a rotary evaporator. The total lipid extract (TLE) obtained from each sample was transferred into a pre-weighed 2.5 ml GC-vial, dried down under N<sub>2</sub>, and stored.

#### **2.2.2 Sulphur removal**

Sulphur was removed from the samples using a method modified after Mangelsdorf (2000). 500 µl of *n*-hexane:DCM (9:1) were added to the TLE of each sample. Copper turnings were placed in a 250 ml beaker and activated using HCL

(37 %). The activated copper turnings were washed with MeOH (3 x 20 ml), then DCM (3 x 20 ml), and finally *n*-hexane (3 x 20 ml). Then a spatula tip full of dry, activated and washed copper turnings was added to the TLE, and the TLE was stored for at least 24 hours before continuing the sample work-up.

### 2.2.3 Standardisation

An internal standard (IntSTD) was added to the aliquot of the TLE which was fractionated using column chromatography. The IntSTD was used to quantify losses of sample during the biomarker purification procedure. For the sediment samples of MD99-2266 a standard mixture was prepared containing 100 µg/ml Squalane, 100 µg/ml 2-Nonadecanone, 100µg/ml 1-Nonadecanol and 100µg/ml of Eruic acid. The standard mixture for the samples collected on the ICE CHASER 2010 cruise the IntSTD contained 100 µg/ml Squalane, 100 µg/ml 2-Nonadecanone and 100 µg/ml 1-Nonadecanol. No standard compound which elutes in the N4 fraction was added, because the concentrations of the carboxylic compounds in the polar fraction (N4; Figure 2.1) of the ICE CHASER 2010 samples vary substantially, so that the addition of a standard compound may lead to adverse chromatographic results. Therefore, an estimate as to how much of the carboxylic compounds was lost during the workup and derivatisation procedures cannot be undertaken. Kornilova and Rosell-Melé (2003) have shown that 60 % of alkenones can be lost during the extraction process. Fatty acids are less easily extracted than alkenones due to their more polar nature. Thus the concentrations of the acids from the ICE CHASER 2010 samples reported in this thesis are certainly underestimated.

### 2.2.4 Column chromatography

The TLE of all samples was separated into four fractions using silica gel column chromatography (Figure 2.1) using a method adapted from Bendle *et al.* (2007). No more than 20 mg of the TLE were used for the column chromatography. The silica gel (60 Å) was activated and cleaned by furnacing it for 8 hours at 450 °C. Then 1 m/m% of deionised water was added to deactivate the silica gel. A Pasteur pipette was filled with 1.2 g of deactivated silica gel (4 cm of silica gel in the

Pasteur pipette). A small amount (ca. 4 mm) of furnace sea sand was added on top of the silica gel. After that the column was conditioned using 2 ml of *n*-Hexane. Then 10 µl of IntSTD were added onto the column. The TLE with the copper turnings suspended in 500 µl of *n*-Hexane:Dichloromethane (9:1) was ultrasonicated for 5 minutes and then a portion of the 500 µl of TLE equivalent to a maximum of 20 mg of extract was added on top of the silica gel. In the first fraction (N1) aliphatic and alicyclic hydrocarbons were eluted using 4 ml of *n*-Hexane. Aromatic hydrocarbons were eluted in the second fraction (N2) using 2 ml of *n*-Hexane:DCM (2:1). Ketones, *n*-alcohols and aldehydes were eluted with 4 ml of DCM in the third fraction (N3) and acids, sterols, tetraether- and diether-lipids were eluted using 5 ml of MeOH:DCM (95:5) in the fourth fraction (N4). Each of the four fractions was transferred into a 2.5 ml GC-vials, dried down under N<sub>2</sub>, and stored.

### **2.3 Quantitative and qualitative analysis of MD99-2266 sediment samples**

#### **2.3.1 Gas chromatography and mass spectroscopy**

All relevant fractions of the MD99-2266 samples in this study were analysed using a gas chromatograph (Shimadzu 2010 GC) with a flame ionisation detector (GC-FID). The GC-FID was equipped with an AOC-20i hot injector held at 350 °C. Hydrogen was used as a carrier gas (constant pressure; 190 KPa). The separation of the different compounds was achieved using one of two identical columns, either a BP1 (SGE Analytical Science) or a TG-1MS (Thermo Scientific) column (60m, diameter: 0.25 mm, film thickness: 0.25 µm; coating: 100 % Dimethyl-polysiloxane). The following temperature program was used. Initially the GC oven was held at 60 °C for two minutes, then the temperature was ramped up to 120 °C at 30 °C min<sup>-1</sup> and then to 350 °C at 3 °C min<sup>-1</sup>, where the temperature was held for 20 minutes. In order to account for, and eliminate drift effects of the GC, an injection standard (InjSTD) consisting of Behenic acid methyl ester (BAME; 100 µg/ml) was added to each sample so that the actual concentration of BAME in each analysed sample was 10 µg/ml. Compounds with hydroxyl-functional groups and carboxyl-functional groups were derivatised using N,O-Bis-(trimethylsilyl)-trifluoroacetamide (BSTFA; Figure 2.2).

## 2. Materials and Methods

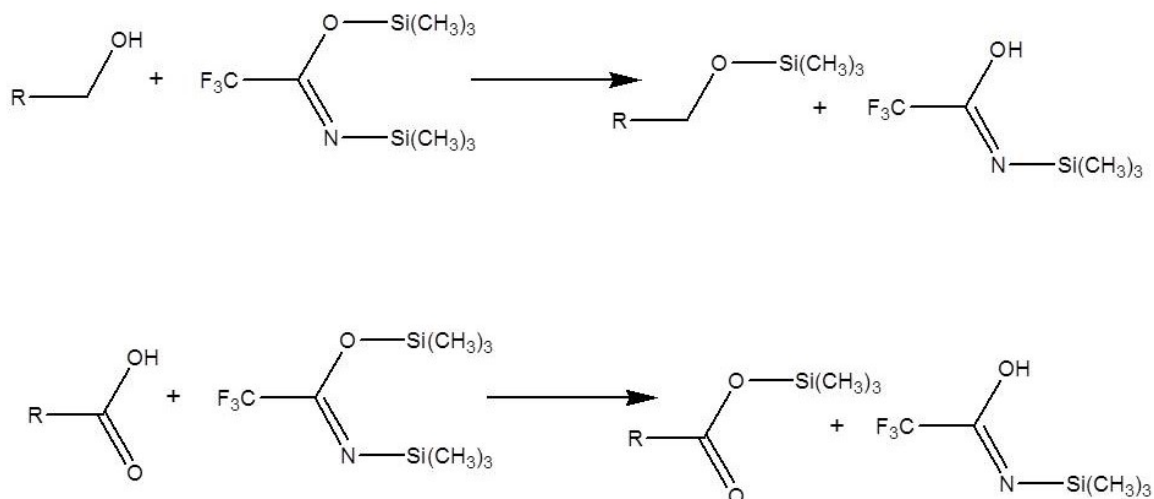


Figure 2.2: Trimethylsilyl derivatisation of alcohols and acids using BSTFA.

All analysed compounds were identified by comparing the retention time (RT) of the substances in the samples to the RT of standard substances and/or by using a Shimadzu OP2010-Plus Mass Spectrometer (MS) interfaced with a Shimadzu 2010 GC. Helium was used as a carrier gas (constant pressure; 230 KPa). The ion source temperature was 200 °C and the interface temperature was 300°C. The same GC columns and the same temperature program as for the GC-FID analysis were used. The ionisation energy was 70 eV and the scan width was 50 to 800 mass units.

Before, after and during the GC and GC-MS analysis of a batch of samples, an external standard mix (Figure 2.3) was analysed to ensure that the injectors, and the FID and MS detectors worked, but also to ensure that there was no contamination on the chromatography column and that the peak separation was adequate.

## 2. Materials and Methods

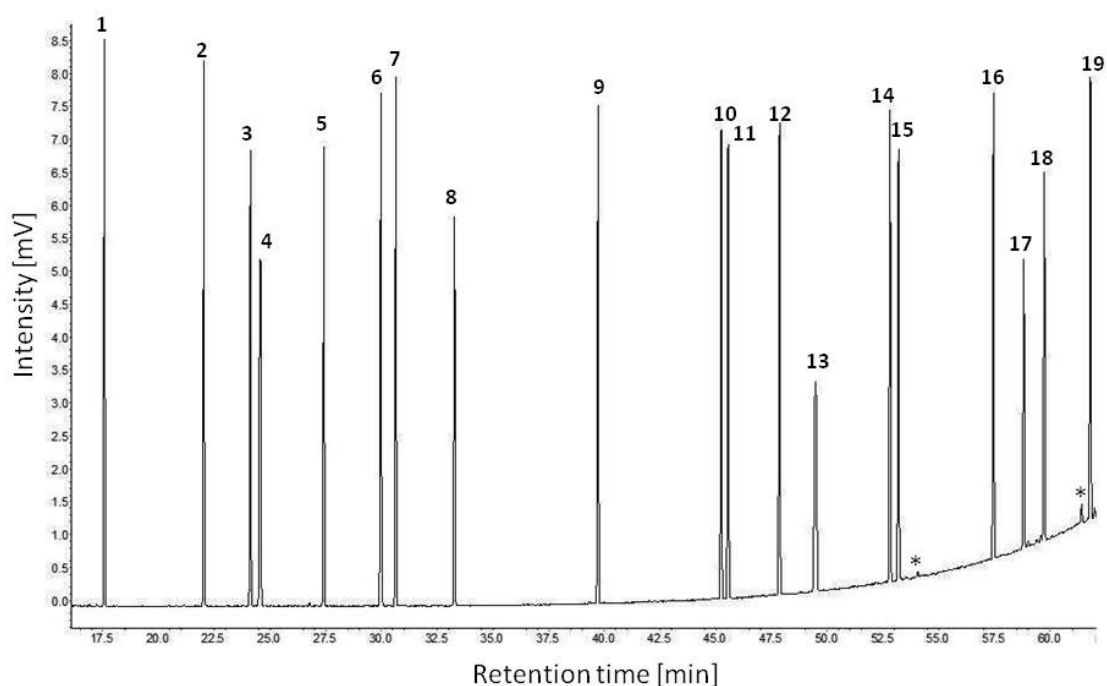


Figure 2.3: External standard mix Compound names of peaks 1-19 are: (1) *n*-Hexadecane ( $C_{16}$ -*n*-alkane), (2) Anthracene, (3) *n*-Octadecane ( $C_{18}$ -*n*-alkane), (4) Phytane, (5) Nonadecane ( $C_{19}$ -*n*-alkane), (6) Icosane ( $C_{20}$ -*n*-alkane), (7)  $5\alpha$ -Androstane, (8) Nonadecan-2-one ( $C_{19}$  Ketone), (9) Tricosane ( $C_{23}$ -*n*-alkane), (10) Pentacosane ( $C_{25}$ -*n*-alkane), (11) Behenic acid methyl ester (BAME), (12) Hexacosane ( $C_{26}$ -*n*-alkane), (13) Squalane, (14) Octacosane ( $C_{28}$ -*n*-alkane), (15) Cholestane, (16) Triacontane ( $C_{30}$ -*n*-alkane), (17) Cholesterol (Cholest-5-en- $3\beta$ -ol), (18) Cholestanone, (19) Docontane ( $C_{30}$ -*n*-alkane); Peaks marked with (\*) are contaminants.

Alkenones and *n*-alkanes were quantified by comparing their peak areas with that of the InjSTD. The mean standard deviation of the quantification error of 44 samples run in duplicate was less than 5.5 % for *n*-alkanes and alkenones.

### 2.3.2 High performance liquid chromatography

The relative abundances of archaeal and bacterial GDGTs of 299 MD99-2266 sediment samples were analysed using high performance liquid chromatography-atmospheric pressure chemical ionisation-mass spectrometry (HPLC-APCI-MS). The N4 fraction of each sample was redissolved in 200  $\mu$ l of *n*-Hexane:*i*-propanol (99:1) and filtered using a 0.45  $\mu$ m PTFE syringe filter. The GDGT analyses were performed at the Organic Geochemistry Unit (OGU) at the Bristol Biogeochemistry

Research Centre at the University of Bristol. The analyses were conducted on a Thermo Scientific TSQ Quantum Access equipped with an Acella Autosampler, Acella pump and Xcalibur software. The liquid chromatograph was equipped with an Alltech Prevail Cyano column (150 mm x 2.1 mm; film thickness: 3  $\mu\text{m}$ ) that was used to separate the GDGTs. Two mobile phases, *n*-hexane (A) and *i*-propanol (B) were used, and the flow rate was 0.2 ml min<sup>-1</sup>. Initially, 1 % of B v/v was held for 7 minutes. Then the concentration of B was increased on a linear gradient over 43 minutes to 1.6 % v/v B. Subsequently the concentration of B was increased to 10 % v/v at 51 min and held constant for 2 minutes. Finally the concentration of B was decreased to 1 % v/v within 2 minutes and held for 10 minutes. Single ion mode (SIM) was used to monitor the abundance of the [M+H]<sup>+</sup> (molecular ion + proton) ion. The peak areas produced by the molecular ions were used to calculate the relative abundance of each GDGT.

### **2.3.3 Hydrogen isotopic analysis of the *n*-alkanes in core MD99-2266**

The hydrogen isotopic measurements of the *n*-alkanes of the MD99-2266 core were measured by Dr. James Bendle and Dr. Osamu Seki at the Institute of Low Temperature Science at the Hokkaido University, Japan. The isotopic values are expressed as per mil (‰; Equation 16), vs. Standard Mean Ocean Water (SMOW) for the hydrogen isotopic measurements (Sharp, 2007). An external standard consisting of an *n*-alkane mix (C<sub>16</sub> - C<sub>30</sub>) with a known hydrogen isotopic composition was injected daily to evaluate the measurement drift of the instrument and ensure analytical precision.

$$\delta [\text{‰}] = \frac{R_{\text{sample}} - R_{\text{standard}}}{R_{\text{standard}}} \cdot 1000$$

Equation 16: Calculation of the  $\delta$  value of isotopic values.

The hydrogen isotopic signature of the *n*-alkanes was analysed using an HP 6890 GC interfaced with a Finnigan MAT Delta Plus XL MS. The ceramic tube of the Finnigan MAT combustion furnace was held at 1450 °C. The chromatographic separation of the *n*-alkanes was accomplished using a DB5-HT column (Agilent

## 2. Materials and Methods

J&W GC Columns; 30 m, 0.25 mm diameter; 0.1  $\mu\text{m}$  film thickness). The following GC oven temperature program was used: the temperature was ramped up from 50 to 120  $^{\circ}\text{C}$  at 10  $^{\circ}\text{C min}^{-1}$ , and then to 310  $^{\circ}\text{C}$  at 4  $^{\circ}\text{C min}^{-1}$ , where the temperature was held for 20 minutes. The isotopic composition of the *n*-alkanes was calculated relative to the isotopic composition of an external standard consisting of an *n*-alkane mix with known hydrogen isotopic values. The analytical error of all measurements as determined by an INTSTD (Squalane; 10  $\mu\text{g/ml}$ ) was within  $\pm 5 \text{ ‰}$ .

### **3 Location, Oceanographic setting and sampling strategy of core MD99-2266**

This section describes the oceanographic setting and sampling strategy of core MD99-2266. The results from the data of core MD99-2266 are discussed in chapters 4, 5 and 6, and these results are influenced by the core location, and the oceanographic conditions of the area.

#### **3.1 Core Location and Oceanography**

The location of the coring site of core MD99-2266, and the marine surface currents influencing the northeast Atlantic are shown in Figure 3.1. The location of the core site of MD99-2266 is  $66^{\circ} 13'77''$  N,  $23^{\circ} 15'93''$  W (Figure 3.1 inset, red dot). The giant Calypso piston core was retrieved from 106 m water depths and has a diameter of 10 cm, and a length of 3890 cm. The core was retrieved on Leg III of the 1999 IMAGES V cruise aboard the R/V *Marion Dufresne* (Quillmann *et al.*, 2010; and references therein). The coring site is located on the northwestern tip of Iceland, which is part of the Atlantic mid-ocean ridge and is located just south of the Arctic Circle. The core was taken from the mouth of Ísafjarðardjúp fjord on the eastern boundary of the Denmark Strait. Ísafjarðardjúp fjord is the largest fjord on the Vestfirðir Peninsula. The Drangajökull icecap is located in the north eastern highlands of Vestfirðir Peninsula and its melt waters flow into Ísafjarðardjúp fjord and into Jökullfirðir, which is the largest tributary fjord of Ísafjarðardjúp (Andrews *et al.*, 2008). Ísafjarðardjúp fjord is ~90 km long and 10 to 15 km wide. Together with its tributary fjords, it covers an area of ~1150 km<sup>2</sup> and drains ~2300 km<sup>2</sup> (Andrews *et al.*, 2008). A shallow sill just beyond the mouth of Ísafjarðardjúp separates the fjord itself from the continental Shelf (Quillmann *et al.*, 2010).

### 3. Location, Oceanographic setting and sampling strategy of core MD99-2266

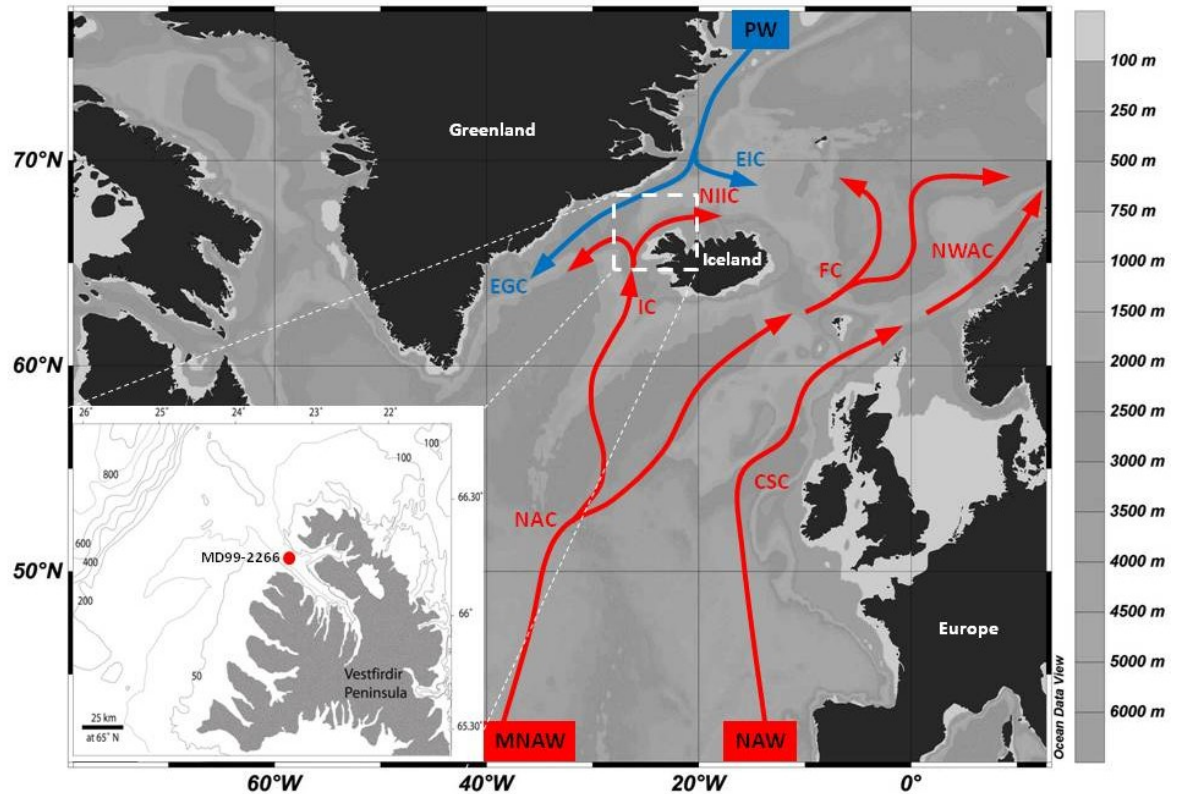


Figure 3.1: Main surface water masses in the eastern North Atlantic (modified after Hansen & Østerhus, 2000; Source of North Atlantic map: Schlitzer, 2010). Red arrows indicate warm, saline Modified North Atlantic Water (MNAW) and North Atlantic Water (NAW). The continental slope current (CSC), and the Norwegian Atlantic Current (NWAC) originate from the NAW. The North Atlantic Current (NAC) originating from the MNAW branches into the Faroe Current (FC) and the Irminger Current (IC). Part of the IC flows through the Denmark Strait and forms the North Icelandic Irminger Current (NIIC) on the North Icelandic Shelf, while another part turns southwards. Blue arrows indicate Polar Waters (PW). The East Greenland Current (EGC) originates from the PW. The east Icelandic Current (EIC), a branch of the EIC spits off north of Iceland and meets the NIIC. Inset: Vestfirðir Peninsula and Denmark Strait Bathymetry. The MD99-2266 core location is marked with a red dot in the mouth of Ísafjarðardjúp fjord (modified after Quillmann *et al.*, 2010).

The core site, located in the Denmark Strait, is affected by two surface currents. The Irminger Current (IC) is the most westerly water current of the North Atlantic bringing warm Atlantic Water into the Nordic Seas. Today, the volume flux of the IC is estimated to be one Sverdrup ( $1 \text{ SV} = 10^6 \text{ m}^3 \text{ s}^{-1}$ ) and its heat flux (relative to  $0^\circ \text{C}$ ) is estimated to be 25 Terra Watts (Hansen & Østerhus, 2000). The IC enters the Denmark Strait between Iceland and Greenland and divides into two branches (Figure 3.1). The North Icelandic Irminger Current (NIIC) branches off towards the

east where it flows onto the North Icelandic Shelf and meets the East Icelandic Current (EIC). The second branch flows southwest along the Greenland coast, parallel to the East Greenland Current (EGC; Hansen & Østerhus, 2000). The Polar Front (PF) divides the warm and saline waters carried north by the IC from the colder and fresher polar waters which are carried south by the EGC and the EIC (Jennings *et al.*, 2011), and the location of the PF is determined by the relative strengths of the IC and the EGC currents (Ólafsdóttir *et al.*, 2010).

Studying sediments of fjordic environments offers a number of advantages. Fjords are conducive to the deposition of large amounts of sediment within short periods of time due to high amounts of terrestrial materials being washed in. Fjords with a large supply of terrestrial mineral matter have been reported to have sedimentation rates between 2 cm and 13 m per year (see review by Howe *et al.*, 2010 and references therein). This land derived material provides essential nutrients that can stimulate marine bioproductivity. Silled fjords, such as Ísafjarðardjúp, are often characterised by inhibited deep water circulation. Coupled with high *in situ* marine productivity and high amounts of terrigenous material being washed into the fjord, this can cause a depletion of oxygen in the water column below the photic zone (Paetzel & Schrader, 1992). The biological degradation of organic material is inhibited by low amounts of oxygen in the water column, thus fjords with low oxygen content in their water column have high sedimentation rates of organic material. The average sediment accumulation rate (SAR) of the core MD99-2266 studied here is 363 cm/ka (calculated using the calibrated mean ages of the age model, Figure 3.2) over a core length of nearly 38 meters covering the last 10,338 cal. a BP (calibrated years before present; present (0 BP) = 1950 AD; Stuiver *et al.*, 1998).

The high sedimentation rates of Ísafjarðardjúp fjord make it a valuable target for palaeoclimatologists. Furthermore, due to its location in the Denmark Strait, it is predicted to be an especially sensitive archive of palaeoclimatic changes. The high sediment accumulation rate of the sediment core from Ísafjarðardjúp fjord along with its climatically sensitive location enables the production of high resolution records of the paleoclimatic variability of northwest Iceland covering the Holocene.

### **3.2 Sampling Strategy**

The sediment core MD99-2266 was sub-sampled in November 2009 at the Institute for Arctic and Alpine Research (INSTAAR) at the University of Colorado in Boulder Colorado, USA. The core consists of bioturbated silty clay containing shells (Labeyrie *et al.*, 2003) The age model published by Quillmann *et al.* (2010; Table 1 and Figure 3.2) is used in this thesis to calculate the calibrated age of each sample. The age model consists of 19  $^{14}\text{C}$ -AMS dates, as well as the Saksunarvatn tephra, which was located at a sediment depth of 3591 cm. The addition of the Saksunarvatn tephra into the age model makes the age model more robust. It also introduces a time constraint on the marine sediment which can be correlated with other terrestrial, lacustrine or marine sediment cores, in which the same tephra is found. Therefore, the inclusion of the Saksunarvatn tephra layer allows for a better comparison of palaeoclimatic records from different sources. Quillmann *et al.* (2010) omitted 5 of the  $^{14}\text{C}$ -AMS dates (not shown here) because the dates are older than the underlying dated horizons. Three of those dates are in the top 23 cm suggesting that the core top sediments were disturbed.

Using the age model published by Quillmann *et al.* (2010), sections of sediment representing discreet time intervals were sampled. Following Quillmann *et al.* (2010), a linear sedimentary deposition was assumed between each  $^{14}\text{C}$ -AMS dated horizon, and a sediment accumulation rate was determined. The sediment interval for a single sample representing a specific time interval was calculated using the sedimentary accumulation rate determined by the  $^{14}\text{C}$ -AMS dates bracketing that section of sediment. The ages of 7 samples below the youngest  $^{14}\text{C}$ -AMS dated sediment horizon were extrapolated, assuming that the sedimentation rate between the core top and the youngest  $^{14}\text{C}$ -AMS date is the same as that of the sediment interval bracketed by the two youngest  $^{14}\text{C}$ -AMS dates.

Other ways of constructing the age model and determining the ages of sediment samples exist. For example, instead of assuming linear sedimentation rates, a polynomial function can be applied to the dated horizons. A third order polynomial equation fits best to the age model of MD99-2266. However, this approach yields

ages around the deposition of the Saksunarvatn tephra ( $10,180 \pm 120$  cal. a BP; Gronvold *et al.*, 1995) which are outside the  $2\sigma$  error of the depositional date. Therefore this approach to age model construction was rejected. Bayesian statistics can also be used to construct the age model. This method does not assume that the measured  $^{14}\text{C}$ -AMS date lies in the middle (slope = 0) of a Gaussian distribution curve, but allows the date to vary within the boundaries of the Gaussian distribution. This allows for a certain degree of freedom within the construction of the age model. The three previously described ways of constructing an age model all assume, that the organic matter used for the  $^{14}\text{C}$ -AMS dating belongs into the sediment horizon in which it is found. A novel approach to the construction of age models does not assume that the organic matter which is dated has the same age as the surrounding sediment (Heegaard *et al.*, 2005). This approach also offers a degree of freedom to the allocation of ages within a dated sediment horizon.

Depending on how much sediment was available, a minimum of  $1 \text{ cm}^3$  and a maximum of  $6 \text{ cm}^3$  of sediment were sampled from each horizon. Where the piece of sediment representing one sample was longer than 6 cm, an equal amount of sediment was taken from the beginning, the middle and the end of the sediment package representing one sample interval. The top 259 cm of the core representing the first  $2145 \pm 155.5$  cal. a BP were sampled so that each sample interval represents no more than 25 calibrated years ( $\leq 3.5$  cm of sediment per sample). The sections from 259 cm to 1398.5 cm representing  $2145 \pm 155.5$  to  $7299 \pm 105$  cal. a BP ( $\leq 28.5$  cm of sediment per sample), and from 2238 cm to 3795 cm representing the time interval between  $8810 \pm 170$  and  $10,744 \pm 257$  cal. a BP ( $\leq 204$  cm of sediment per sample), were sampled so that each sample represents no more than 50 calibrated years. The sediment interval between 1398.5 and 2238 cm, representing the time interval from  $7299 \pm 105$  to  $8810 \pm 170$  cal. a BP, was sampled so that each sample represents no more than 15 cal. a BP ( $\leq 6.5$  cm sediment per sample). The reason for the higher sample density between  $7320 \pm 105$  and  $8810 \pm 170$  cal. a BP, is that short term meltwater events occurred during that period (e.g. Alley & Ágústsdóttir, 2005), which may not be observed in the biomarker record if the sampling is too coarse. The core section representing

the first  $2168 \pm 155.5$  cal. a BP was also sampled at small intervals in order to get the highest possible resolution during the period where human activity is influenced by climate change (see Introduction). A total of 326 sediment samples were collected.

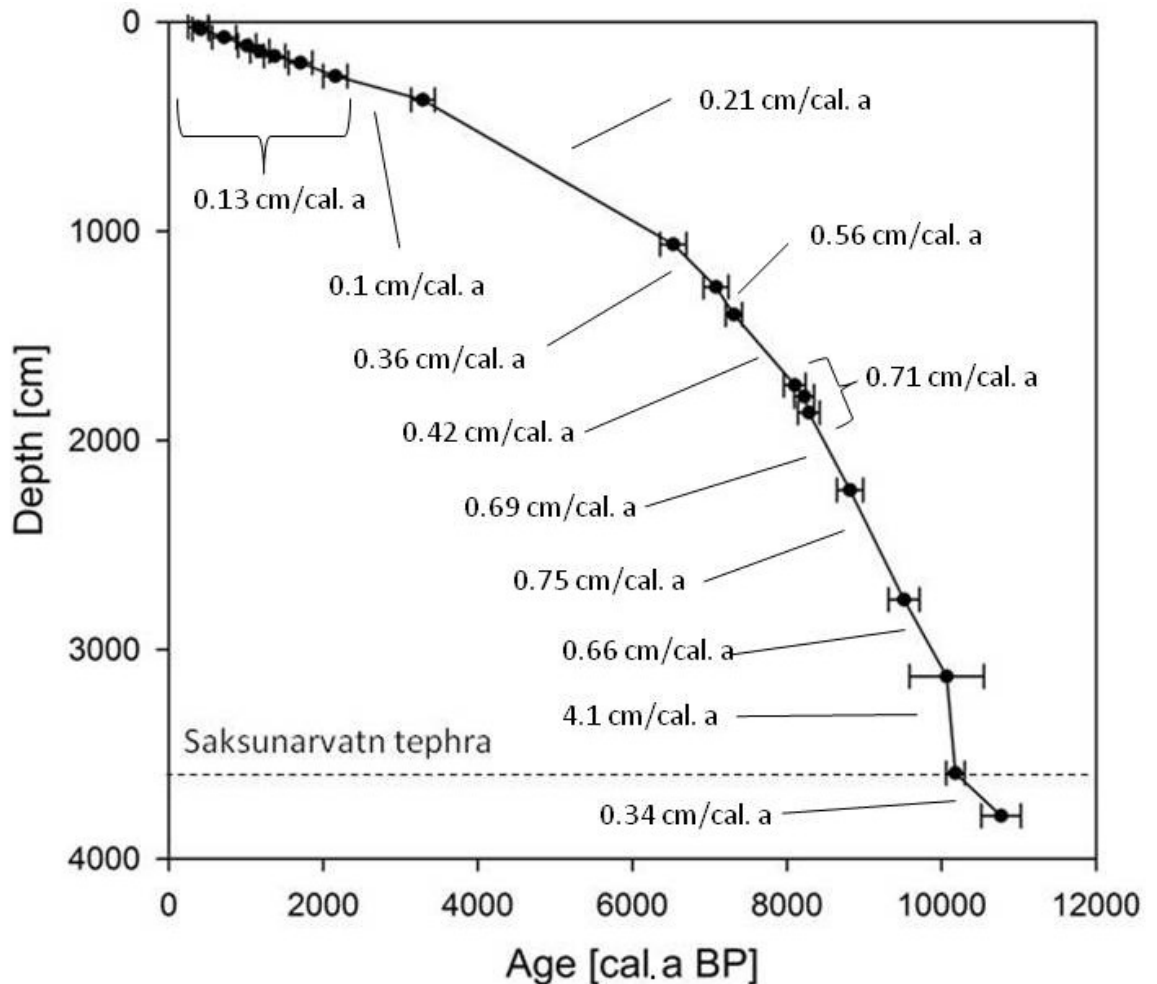


Figure 3.2: Age model of core MD99-2266. It is based on  $^{14}\text{C}$ -AMS dated sediment horizons and the depth horizon of the Saksunarvatn tephra (dashed line) which is dated at  $10,180 \pm 120$  cal. a BP (Gronvold *et al.*, 1995; Quillmann *et al.*, 2010). Sedimentation rates are calculated using the calibrated ages of the dated horizons.

The mean ( $2\sigma$  standard deviation) error associated with the  $^{14}\text{C}$ -dated sediment horizons and the Saksunarvatn tephra layer is  $\pm 165$  cal. years. The ages of all the samples and climatic events analysed and discussed from core MD99-2266 are subject to this error. This means that a climatic event such as the 8.2 ka event (Alley *et al.*, 1997) if detected in the biomarker record of core MD99-2266 may be

### 3. Location, Oceanographic setting and sampling strategy of core MD99-2266

found in a sediment horizons between ~ 8000 cal. a BP and ~ 8400 cal. a BP. Furthermore, since the sediment may have been bioturbated, further uncertainty is associated with the dating error. The author is aware of the uncertainties associated with age model constructions. Therefore, all ages given here are approximate (~), taking into account the dating error.

### 3. Location, Oceanographic setting and sampling strategy of core MD99-2266

Table 1:  $^{14}\text{C}$  Accelerated MS dates for MD99-2266 and corresponding calibrated ages used in the age model, as published by Quillmann et al. (2010).

Depth [cm]	Reported Age [ $^{14}\text{C}$ -AMS]	Error [ $1\sigma$ ]	Reservoir corrected age	Cal. range [ $\pm 2\sigma$ ]	Average age [cal. yr BP]	Material dated
24 - 25	746	61	346	251 - 514	382	<i>Thyasira flexuosa</i>
34 - 36	809	30	409	309 - 522	416	<i>Thyasira flexuosa</i>
72 - 74	1151	53	751	565 - 873	719	<i>Nuculana pernula</i>
112 - 114	1450	15	1050	897 - 1133	1015	<i>Yolida</i> sp.
139 - 141	1640	33	1240	1055 - 1302	1178	<i>Dentalium</i> sp.
162 - 164	1800	45	1400	1231 - 1508	1370	<i>Nuculana pernula</i>
194 - 196	2126	34	1726	1552 - 1858	1705	<i>Thyasira</i> sp.
258.5 - 259.5	2503	36	2103	2001 - 2312	2156	<i>Asarta</i> sp.
371 - 373	3424	35	3024	3136 - 3443	3290	<i>Thyasira</i> sp.
1062 - 1064	6098	50	5698	6359 - 6700	6530	<i>Nuculana buccata</i>
1266 - 1268	6570	45	6170	6921 - 7243	7082	<i>Nuculana buccata</i>
1398 - 1399	6790	20	6390	7209 - 7419	7314	Unidentified bivalve fragment
1736 - 1737	7640	30	7240	7961 - 8241	8101	<i>Nuculana</i> sp.
1789 - 1790	7755	20	7355	8096 - 8353	8224	Unidentified bivalve fragment
1867 - 1869	7826	49	7426	8144 - 8425	8284	<i>Nuculana pernula</i>
2237 - 2238	8285	15	7885	8646 - 8986	8816	Gastropod
2761 - 2763	8840	65	8440	9314 - 9714	9514	<i>Dentalium</i> sp.
3128 - 3130	9320	190	8920	9585 - 10,548	10066	<i>Nuculana pernula</i>
3794 - 3796	9804	70	9404	10,513 - 11,027	10,770	Unidentified bivalve

## **4 Assessing Holocene changes in marine productivity and terrestrial organic carbon inputs into an Icelandic fjord: Application of molecular and bulk organic proxies.**

### **4.1 Introduction**

Fjords play a major role in the global carbon cycle as a storage reservoir of organic carbon (OC). Fjordic sediments contain at least 12 % of the total OC which has been buried on the continental margin throughout the past 100,000 years (Nuwer & Keil, 2005). The generally high sedimentation rates prevalent in fjords are conducive to the preservation of OC (Smittenberg *et al.*, 2004). Seasonal, or even permanent anoxic conditions of fjordic water columns, particularly of silled fjords, further contribute to the preservation of OC (Howe *et al.*, 2010). Terrestrial ( $OC_{terr}$ ) and marine organic carbon ( $OC_{mar}$ ) is deposited in fjordic sediments, however, there is a general lack of data showing the relative abundance of  $OC_{terr}$  and  $OC_{mar}$  in fjord basins (Skei, 1983). Only in recent years have researchers started to elucidate the relative contributions of  $OC_{terr}$  and  $OC_{mar}$  to fjordic sediments (Nuwer & Keil, 2005; Smittenberg *et al.*, 2006; Walsh *et al.*, 2008). Elucidating relative inputs, transformation and fate of  $OC_{terr}$  and  $OC_{mar}$  is necessary for improved modelling of fluxes and carbon through sedimentary reservoirs, and also to better understand the importance of marine Shelf sediments as a sink for organic carbon.

Variations in the relative abundance of carbon from different carbon pools can offer insights into variable climatic conditions. Weijers *et al.* (2009) have shown that the relative amount of  $OC_{terr}$  content of sediments from the Angola Basin correlate with changes of Congo river discharge, which in turn is controlled by precipitation. A similar relationship has also been observed in a southwest Norwegian fjord (Smittenberg *et al.*, 2004). Higher mass accumulation rates

4. Assessing Holocene changes in marine productivity and terrestrial organic carbon inputs into an Icelandic fjord: Application of molecular and bulk organic proxies.

(MARs) of terrestrially sourced biomarkers between 1800 and 1850 AD are associated with an increasingly erosive climate due to cooling and rising precipitation in the studied area (Smittenberg *et al.*, 2004). Iceland is situated beneath one of the two dipoles of the North Atlantic Oscillation (NAO) that describes the fluctuation of the trajectory of westerlies traversing the North Atlantic (Hurrell, 1995). During positive phases of the NAO Iceland receives more precipitation than during negative NAO phases, and these precipitation shifts may influence the amount of terrestrial sediment washed into Ísafjarðardjúp fjord. Furthermore, along with precipitation, the NAO also influences the relative importance of warm and cold water currents in the Denmark Strait (Blindheim & Malmberg, 2005). Changes in the currents influencing the sampling site, as well as changes in terrestrial sediment runoff may influence the primary production in Ísafjarðardjúp fjord, and affect the deposition of  $OC_{terr}$  and  $OC_{mar}$ .

Varying  $OC_{terr}$  contributions to the sediment of core MD99-2266 throughout the Holocene are presented in this study. Recent studies have highlighted the need for a multi proxy approach to elucidate changing  $OC_{terr}$  contributions to fjordic sediments (Belicka & Harvey, 2009; Huguet *et al.*, 2007; Walsh *et al.*, 2008). Therefore, the *n*-alkane/alkenone-index (Marret *et al.*, 2001), the BIT-Index (Hopmans *et al.*, 2004), as well as C/N ratios (Meyers, 1997) are employed in three binary mixing models to reconstruct  $OC_{terr}$  contributions. The *n*-alkanes are derived from terrestrial leaf waxes that are transported into the sediments by fluvial and/or aeolian transport mechanisms (see *n*-alkane biomarker introduction, 1.2.1). Due to the vicinity of the sampling site to Iceland, it is assumed, that the majority of *n*-alkanes is sourced from the catchment area of Ísafjarðardjúp fjord and washed into the fjord with spring meltwater floods. The alkenones are derived from haptophyte algae (see alkenone biomarker introduction, 1.2.2) and constitute the marine component of the *n*-alkane/alkenone-index. The BIT-Index compares the relative amounts of branched GDGTs with the relative amount of Crenarchaeol. It is described in detail in section 1.2.3.1.

The aim of this chapter is to produce a continuous record of changing sedimentary  $OC_{terr}$  contributions throughout the Holocene by using the *n*-alkane/alkenone-

4. Assessing Holocene changes in marine productivity and terrestrial organic carbon inputs into an Icelandic fjord: Application of molecular and bulk organic proxies.

index, the BIT-Index and C/N ratios. Furthermore, changes in the  $OC_{mar}$  contribution are reconstructed, and using the  $OC_{mar}$  reconstruction, changes in the palaeoproductivity throughout the Holocene are modelled using three different models.

It is hypothesised, that the  $OC_{terr}$  and the  $OC_{mar}$  contribution to the fjordic sediments have varied throughout the Holocene in response to Holocene climate change, and that these changes are reflected in the primary production of Ísafjarðardjúp fjord.

## **4.2 Methods**

### **4.2.1 Mass accumulation rates**

Mass accumulation rates (MARs) for TOC ( $\text{mg cm}^{-2} \text{a}^{-1}$ ) and individual biomarkers ( $\text{ng cm}^{-2} \text{a}^{-1}$ ) were calculated using Equation 17 after Rommerskirchen *et al.* (2003; and references therein), where X is the TOC or specific biomarker concentration in  $\text{mg g}^{-1}$  dry sample ( $\text{mg g}^{-1}$  DS) or  $\text{ng g}^{-1}$  DS, respectively,  $\rho$  is dry bulk density ( $\text{g cm}^{-3}$ ) and LSR the linear sedimentation rate ( $\text{cm a}^{-1}$ ). The dry bulk density was obtained from the project collaborators Ursula Quillmann and Professor John T. Andrews.

$$\text{MAR} = X \cdot \rho \cdot \text{LSR}$$

Equation 17: Mass accumulation rate (MAR)

By comparing the concentration of the biomarkers (and TOC) to the MAR of the biomarkers (and TOC), dilution and concentration effects due to variable sedimentation rates can be accounted for.

### **4.2.2 Bulk Parameters**

The total organic carbon (TOC) content and the C/N ratios of 156 MD-99-2266 samples were measured according to the methods described in section 2.1. The

4. Assessing Holocene changes in marine productivity and terrestrial organic carbon inputs into an Icelandic fjord: Application of molecular and bulk organic proxies.

mean relative standard deviation from 17 triplicate analyses is  $\pm 2.47\%$  for the TOC measurements. The mean relative standard deviation of the C/N ratio is  $\pm 0.14$ .

### 4.2.3 Biomarkers

The concentration of the *n*-alkanes and alkenones was measured according to the methods described in the methods section. The analytical error associated with the quantification of the *n*-alkanes and alkenones was  $\pm 5\%$ . The concentration of the *n*-alkanes was used to calculate the ACL and the CPI values using equations 1 and 2. The ACL values in this study were calculated using the odd-chained *n*-alkanes with chain lengths of 25 to 35 carbon atoms, as these are the most abundant *n*-alkanes in all samples. The CPI values were calculated using the *n*-alkanes with chain lengths from 25 - 33 carbon atoms. 11 samples were analysed in triplicate and the mean error associated with the  $CPI_{25-33}$  and the  $ACL_{25-35}$  is  $\pm 0.5$  and  $\pm 0.06$ , respectively.

In order to assess the contribution of organic carbon from different sources to the TOC pool in the sediment, Marret *et al.* (2001) developed the *n*-alkane/alkenone index. This index can be used to assess the relative contribution of  $OC_{terr}$  vs.  $OC_{mar}$  into sediments. Here this index is employed, as modified by Weijers *et al.* (2009), and the concentrations of the *n*-alkanes and alkenones is used to calculate the index. The *n*-alkane/alkenone index is defined as:

$$n\text{-alkane/alkenone index} = \frac{\text{odd-chained } (C_{25}\text{-}C_{35}) \text{ } n\text{-alkanes}}{[\text{odd-chained } (C_{25}\text{-}C_{35}) \text{ } n\text{-alkanes}] + 3(C_{37} \text{ alkenones})}$$

Equation 18: *n*-alkane/alkenone index

The BIT-Index (branched vs. isoprenoidal tetraether index; Equation 15) compares the occurrence of branched GDGTs (glycerol-dialkyl-glycerol-tetraethers) with the occurrence of Crenarchaeol which belongs to the group of isoprenoidal GDGTs (Hopmans *et al.*, 2004). It was measured according to Equation 15 and the

4. Assessing Holocene changes in marine productivity and terrestrial organic carbon inputs into an Icelandic fjord: Application of molecular and bulk organic proxies.

relevant compounds were measured using the methods described in section 2.3.2. Nine samples were run in triplicate and two in duplicate in order to assess the analytical error. The mean analytical error associated with the BIT-Index is  $\pm 0.01$ .

#### **4.2.4 Modelling OC<sub>terr</sub> contributions**

The C/N ratio, *n*-alkane/alkenone-index, as well as the BIT-Index were employed in a binary mixing model to assess the contribution of terrestrial organic carbon to the total organic carbon pool of the sediment. The same binary mixing model that has previously been used by Weijers *et al.* (2009) is employed here to assess the terrestrial organic carbon contribution to Ísafjarðardjúp fjord. It is defined as follows:

$$f_{\text{terr}} = \frac{X_{\text{sample}} - X_{\text{Mar}}}{X_{\text{Terr}} - X_{\text{Mar}}} \cdot 100\%$$

Equation 19: Binary mixing model used to assess the relative contribution of OC<sub>terr</sub> to the sediment

X<sub>sample</sub>, X<sub>Mar</sub> and X<sub>Terr</sub> are the values of the sample, the marine end-member value and the terrestrial end-member value of the C/N ratio, the *n*-alkane/alkenone-index, and the BIT-Index.

#### **4.2.5 Marine sourced organic carbon**

The sedimentary TOC is comprised of two carbon pools, namely OC<sub>terr</sub> and organic carbon from marine sources (OC<sub>mar</sub>). The OC<sub>mar</sub> content of the fjordic sediment is calculated using the following equation:

$$\text{OC}_{\text{mar}} = \text{TOC} - \text{OC}_{\text{terr}}$$

Equation 20: calculation of marine organic carbon (OC<sub>mar</sub>)

4. Assessing Holocene changes in marine productivity and terrestrial organic carbon inputs into an Icelandic fjord: Application of molecular and bulk organic proxies.

### 4.3 Results

#### 4.3.1 Bulk parameters

The linear sedimentation rates (LSR;  $\text{cm}\cdot\text{a}^{-1}$ ) of core MD99-2266 were calculated based on the calibrated ages of twenty  $^{14}\text{C}$ -AMS and tephra dated horizons (Figure 4.1). The linear sedimentation rates vary from 0.09 to  $4.09\text{ cm}\cdot\text{a}^{-1}$ . The highest sedimentation rate coincides with the deposition of the Saksunarvatn tephra at  $10,180 \pm 120\text{ cal. a BP}$  (Gronvold *et al.*, 1995; Quillmann *et al.*, 2010). A second peak in sedimentation rate at  $\sim 8250\text{ cal. a BP}$  coincides with a turbidite or debris flow possibly caused by an earthquake (Andrews *et al.*, 2008). The sedimentation rates are highest in the early Holocene and decrease towards the late Holocene.

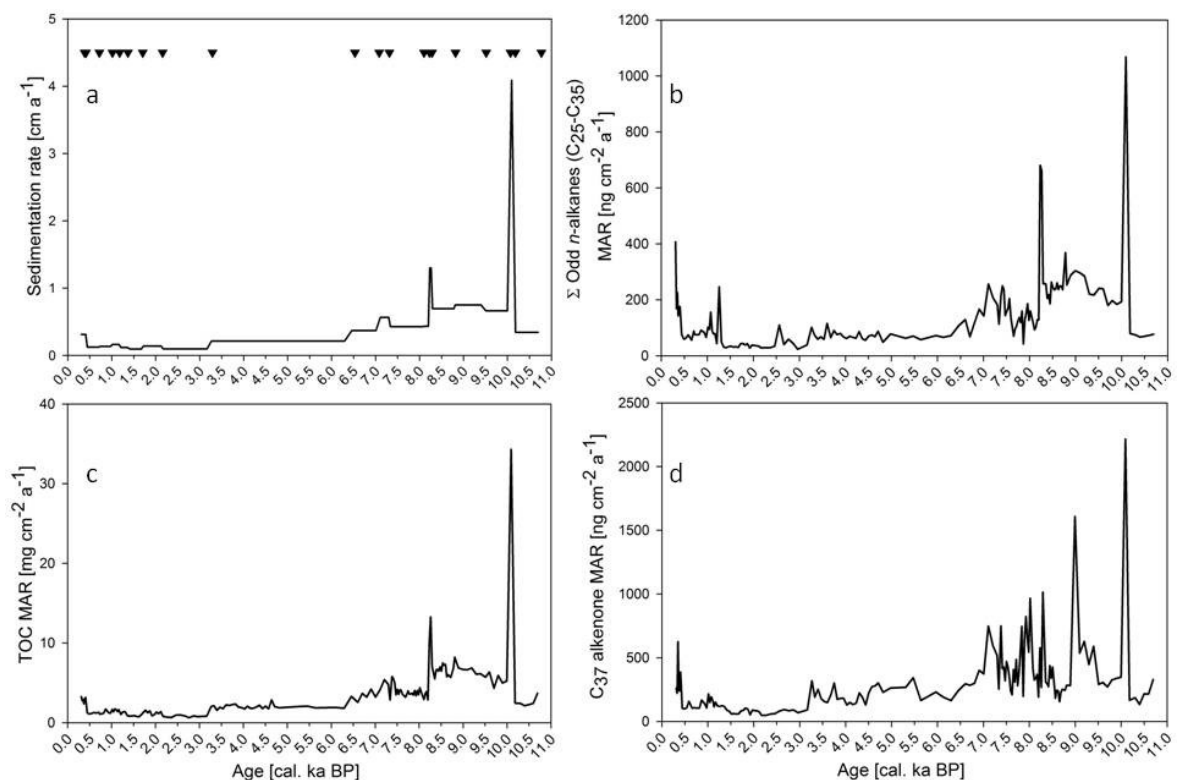


Figure 4.1: Sedimentation and mass accumulation rates of core MD99-2266. (a) LSR of core MD99-2266; black triangles indicate the  $^{14}\text{C}$ -AMS dated sediment horizons, (b) mass accumulation rate (MAR) of odd-chained ( $\text{C}_{25}\text{-C}_{35}$ ) *n*-alkanes, (c) MAR of TOC, (d) MAR of  $\text{C}_{37}$  alkenones.

4. Assessing Holocene changes in marine productivity and terrestrial organic carbon inputs into an Icelandic fjord: Application of molecular and bulk organic proxies.

#### 4.3.1.1 Total organic carbon

The MAR of TOC follow the sedimentation rate closely (Figure 4.1). The highest values are recorded during the early Holocene with the highest TOC MAR of  $34 \text{ mg}\cdot\text{cm}^{-2}\cdot\text{a}^{-1}$  at  $\sim 10,100$  cal. a BP. The total organic carbon content of the sediment core varies between 0.7 and 2.2 % throughout the Holocene (Figure 4.2). The mean TOC content is  $1.2 \pm 0.2$  %. Over the first 2400 years the organic carbon content slowly increases before decreasing sharply from  $\sim 8400$  to  $\sim 8100$  cal. a BP. The TOC content fluctuates between 1 and 1.5 % from  $\sim 8000$  and  $\sim 3000$  cal. a BP with the exception of a TOC spike at  $\sim 4600$  cal. a BP. The late Holocene shows a trend towards increasing TOC values.

#### 4.3.1.2 Carbon/Nitrogen ratio

The variability of the C/N values in core MD99-2266 is shown in Figure 4.2. The C/N ratio increases throughout the first  $\sim 7800$  years of the record from values of 3.6 to values of nearly 7. The variability of the C/N ratio increases throughout the last 4000 years of the record compared to the previous 6500 years, however, the clear tendency towards increasing C/N values is not observed. Excursions to C/N values of  $> 6.5$  occur at  $\sim 3300$  and from  $\sim 2700$  to  $\sim 2300$ , and at  $\sim 820$  cal. a BP.

4. Assessing Holocene changes in marine productivity and terrestrial organic carbon inputs into an Icelandic fjord: Application of molecular and bulk organic proxies.

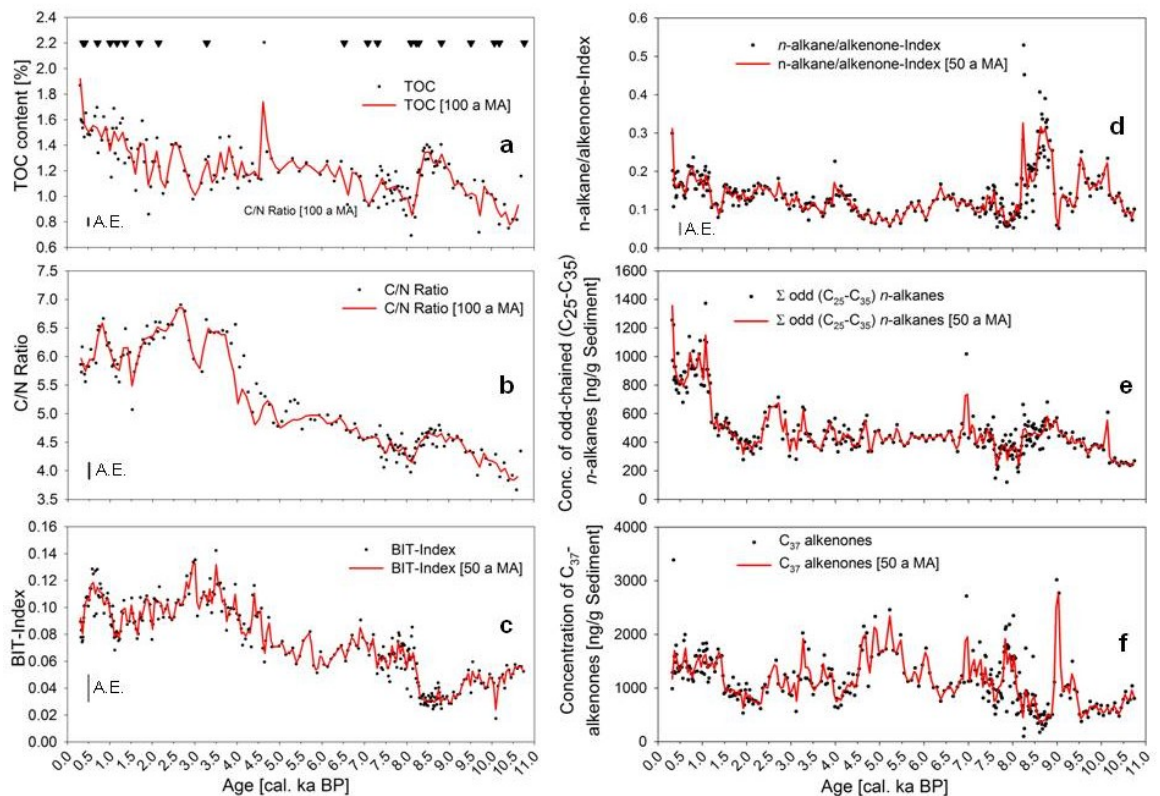


Figure 4.2: Biomarker and bulk parameter variability of core MD99-2266. (a) TOC content (A.E. ( $1\sigma$ ) =  $\pm 0.03$  %), black triangles indicate the  $^{14}\text{C}$ -AMS dated sediment horizons; (b) C/N ratio (A.E. ( $1\sigma$ ) =  $\pm 0.14$ ), (c) BIT-Index (A.E. ( $1\sigma$ ) =  $\pm 0.01$ ), (d) odd-chained ( $\text{C}_{25}\text{-C}_{35}$ ) *n*-alkane/alkenone index (A.E.  $\pm 0.016$ ); (e) concentration of odd-chained ( $\text{C}_{25}\text{-C}_{35}$ ) *n*-alkane (A.E. ( $1\sigma$ ) =  $\pm 5.5$  %); (f) concentration of  $\text{C}_{37}$  alkenones (A.E. ( $1\sigma$ ) =  $\pm 5.5$  %). Black dots signify values of individual samples; the red line indicates the moving average (MA).

### 4.3.2 Biomarkers

#### 4.3.2.1 BIT-Index

Throughout the record the BIT-Index does not rise above 0.14 (Figure 4.2). The consistently low BIT-Index values indicate that the contribution of OC from soils to the sediment is generally low. The lowest values are seen in the early Holocene (Figure 4.2). The mean value between  $\sim 10,800$  and  $\sim 8300$  cal. a BP is  $0.04 \pm 0.01$ . BIT-Index values increase from  $\sim 8300$  cal. a BP and the highest values of 0.13 and 0.14 are reached between  $\sim 4000$  and  $\sim 3000$  cal. a BP.

4. Assessing Holocene changes in marine productivity and terrestrial organic carbon inputs into an Icelandic fjord: Application of molecular and bulk organic proxies.

#### 4.3.2.2 *n*-Alkanes

The initial discussion of the *n*-alkane data will focus on the identification of outliers. Figure 4.3 shows average chain length ( $ACL_{25-35}$ , Equation 2) variations, the carbon preference index ( $CPI_{25-33}$ , Equation 1), and the concentration of the odd-chained ( $C_{25}-C_{35}$ ) *n*-alkanes derived from higher terrestrial plant leaf waxes.

*n*-Alkane distributions derived from terrestrial plant waxes typically have CPI values higher than 3.3 and as high as 40 (Chikaraishi & Naraoka, 2003; Collister *et al.*, 1994; Rommerskirchen *et al.*, 2006; Vogts *et al.*, 2009). CPI values of *n*-alkanes originating from higher terrestrial plants, derived from marine and lacustrine Holocene sediments exhibit CPI values greater than three (Cranwell, 1991; Fisher *et al.*, 2003; Rommerskirchen *et al.*, 2003; Smittenberg *et al.*, 2004). The  $CPI_{25-33}$  values reported in this study range from 1.2 to 13.9 (Figure 4.3). 16 samples exhibit a  $CPI_{25-33}$  of  $\leq 3.49$ , which tends to coincide with very high *n*-alkane concentrations as well as with very high (30.7) and very low (27.3)  $ACL_{25-35}$  values. Low CPI values can be a result of contamination by petrochemical products during laboratory workup of the samples or the drilling process itself (Pancost & Boot, 2004). Another source of *n*-alkane distributions with low CPI values are marine algae (Clark & Blumer, 1967). As the *n*-alkane distribution of terrestrial plant waxes usually exhibits CPI values higher than 3, samples with low ( $\leq 3.49$ )  $CPI_{25-33}$  values are regarded as outliers because these samples do not exclusively reflect a wax signal derived from terrestrial higher plants. Consequently, the 16 samples with low  $CPI_{25-33}$  values were not used in this, or in the following chapters.

4. Assessing Holocene changes in marine productivity and terrestrial organic carbon inputs into an Icelandic fjord: Application of molecular and bulk organic proxies.

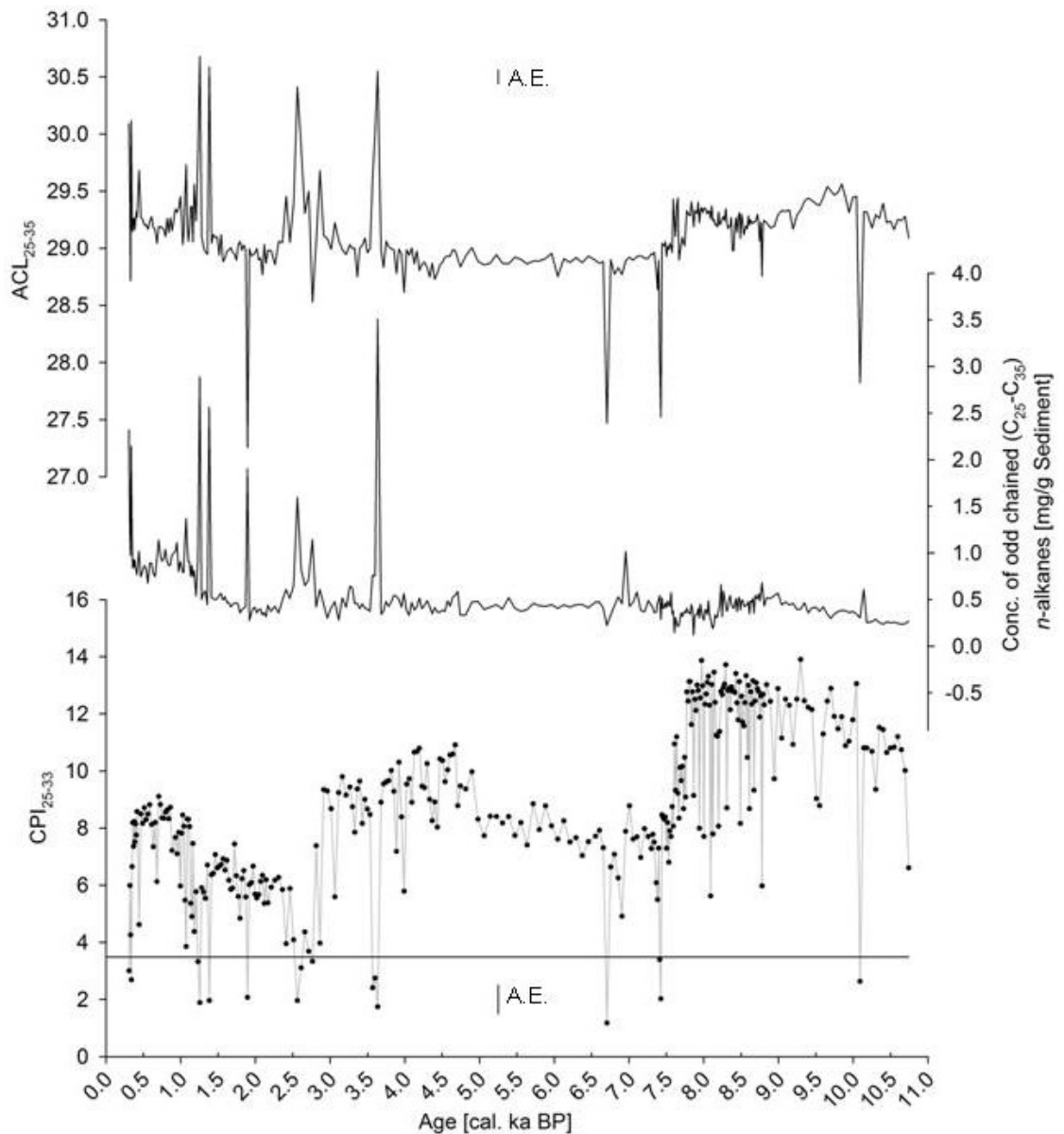


Figure 4.3: Variations of the  $ACL_{25-35}$ ,  $CPI_{25-33}$  and the concentration of  $n$ -alkanes. The horizontal black line indicates the threshold of the  $CPI_{25-33}$  (3.49). Samples falling below that threshold are considered as outliers. The analytical error ( $1\sigma$ ) associated with the  $ACL_{25-35}$ , the  $CPI_{25-33}$  and the  $n$ -alkane concentrations is  $\pm 0.5$ ,  $\pm 0.06$  and  $\pm 5.5$  %, respectively.

The average concentration of the odd-chained ( $C_{25}$ - $C_{35}$ )  $n$ -alkanes is  $537 \text{ ng}\cdot\text{g}^{-1}$  DS (Figure 4.2). The  $n$ -alkane concentration varies between 200 and  $800 \text{ ng}\cdot\text{g}^{-1}$  DS throughout most of the Holocene ( $\sim 10,800$  to  $\sim 1200$  cal. a BP) with one exception at  $\sim 6900$  cal. a BP, where the concentration increases to just over 1000

4. Assessing Holocene changes in marine productivity and terrestrial organic carbon inputs into an Icelandic fjord: Application of molecular and bulk organic proxies.

$\text{ng}\cdot\text{g}^{-1}$  DS, and three exceptions between  $\sim 7600$  and  $\sim 8100$  cal. a BP, where the concentration falls to  $\sim 150 \text{ ng}\cdot\text{g}^{-1}$  DS. The MAR of the odd-chained *n*-alkanes mirrors the sedimentation rate (Figure 4.1). The highest values of just over 1000 and 680  $\text{ng}\cdot\text{cm}^{-2}\cdot\text{a}^{-1}$  are recorded at  $\sim 10,100$  and  $\sim 8200$  cal. a BP respectively, correlating with the high sedimentation rates at those times.

#### 4.3.2.3 Alkenones

The mean combined concentration of the  $\text{C}_{37:2}$ - and  $\text{C}_{37:3}$ -alkenones is  $1134 \text{ ng}\cdot\text{g}^{-1}$  DS throughout the Holocene, and the alkenone concentration is 20 to 50 % higher than the *n*-alkane concentration indicating, that the contribution of marine organic carbon has continually been higher throughout the Holocene than the contribution of terrestrial organic carbon to the sediment. In contrast to the *n*-alkane concentration record, the record of the  $\text{C}_{37}$  alkenone concentration shows a higher variability (Figure 4.2). The highest concentration of alkenones of  $3000 \text{ ng}\cdot\text{g}^{-1}$  DS is recorded at  $\sim 9000$  cal. a BP, and the lowest concentration of  $120 \text{ ng}\cdot\text{g}^{-1}$  DS is recorded at 8200 cal. a BP.

The MAR of the sum of the  $\text{C}_{37:3}$  and  $\text{C}_{37:2}$  alkenones follows variations in the sedimentation rate in the similar way the MAR of the odd-chained *n*-alkanes does (Figure 4.1). The  $\text{C}_{37:4}$  alkenone was not detected in the majority of the sediment samples. Therefore its concentration was not used at all in this chapter. During the early Holocene, from  $\sim 10,800$  to  $\sim 7000$  cal. a BP, the variability of the alkenone MAR is higher than during the rest of the record. 2213 and 1600  $\text{ng}\cdot\text{cm}^{-2}\cdot\text{a}^{-1}$  are the highest alkenone MARs and they are recorded at  $\sim 10,100$  and  $\sim 9000$  cal. a BP respectively. The high MAR of alkenones at  $\sim 10,100$  cal. a BP is associated with the deposition of the Saksunarvatn tephra and does not reflect an increase in alkenone production. In contrast, the high MAR at 9000 cal. a BP coincides with high alkenone concentrations (Figure 4.2) and genuinely reflects a period of increased alkenone production.

4. Assessing Holocene changes in marine productivity and terrestrial organic carbon inputs into an Icelandic fjord: Application of molecular and bulk organic proxies.

#### 4.3.2.4 *n*-alkane/alkenone-index

The total concentrations of the odd-chained (C<sub>25</sub>-C<sub>35</sub>) *n*-alkanes and the C<sub>37</sub> alkenones were used to calculate the *n*-alkane/alkenone-index (Figure 4.2). High values indicate increased OC<sub>terr</sub> input, while lower values suggest a higher proportion of OC<sub>mar</sub> input. The average value of the index throughout the Holocene is 0.15. The highest fluctuation in the index is seen between ~ 10,800 and ~ 8000 cal. a BP owing to the high variability of the C<sub>37</sub> alkenone concentration during that interval. The highest *n*-alkane/alkenone-index values occur between 9000 and 8000 cal. a BP. Throughout most of the Holocene the *n*-alkane/alkenone index values are below 0.3 indicating that OC<sub>mar</sub> input dominates over OC<sub>terr</sub> input. The *n*-alkane/alkenone-index may underestimate the OC<sub>mar</sub> contribution if the reasonable assumption is made, that alkenones are preferentially degraded compared to *n*-alkanes (Hoefs *et al.*, 2002; Sinninghe Damsté *et al.*, 2002a).

#### 4.3.3 Modelling the terrestrial organic carbon contribution to the sediments of Ísafjarðardjúp fjord

The percentage of terrestrial organic carbon contributing to the sedimentary TOC pool as estimated by the binary mixing model (section 4.2.4), employing the three different proxies, is shown in Figure 4.4.

4. Assessing Holocene changes in marine productivity and terrestrial organic carbon inputs into an Icelandic fjord: Application of molecular and bulk organic proxies.

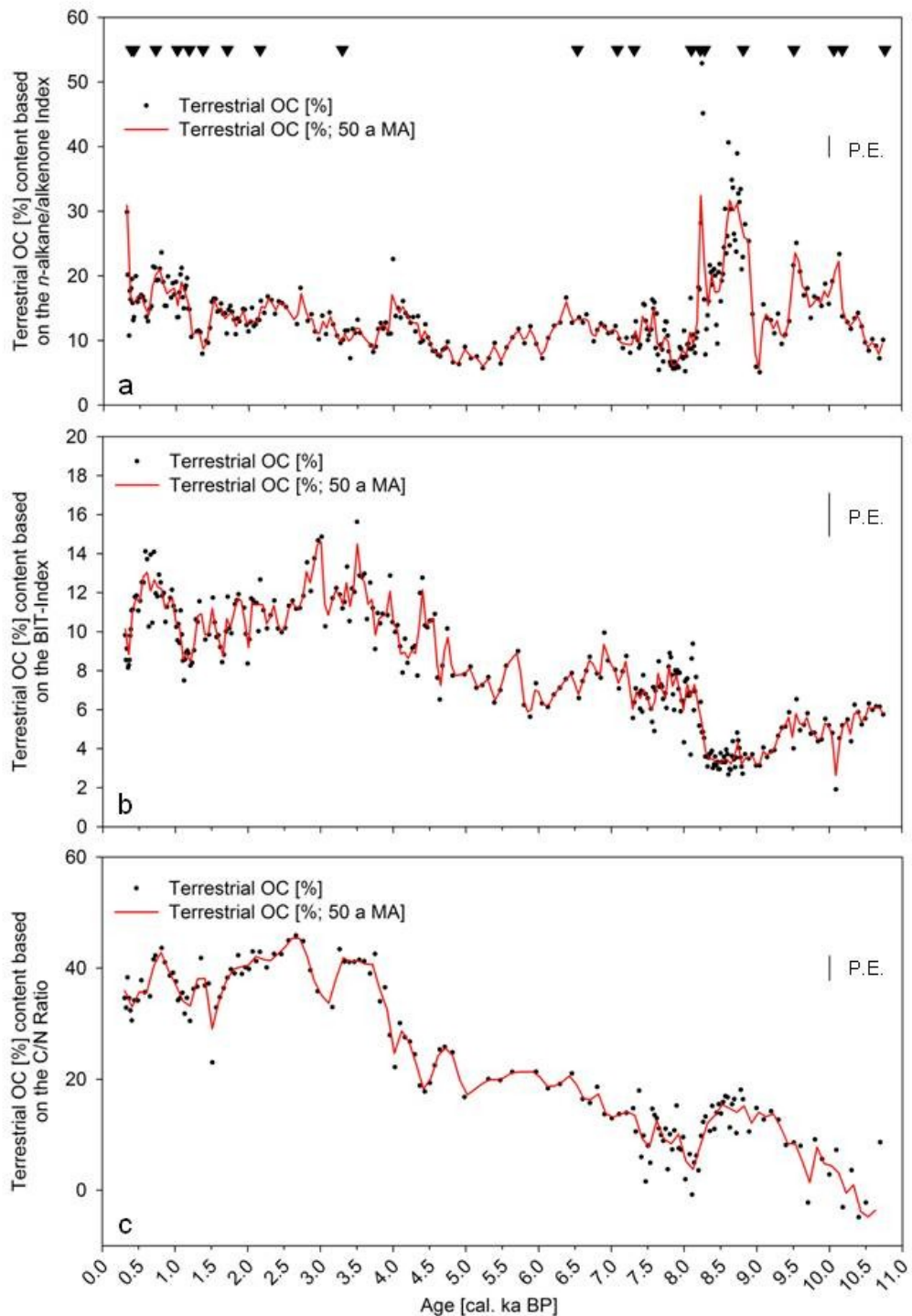


Figure 4.4: Estimates of the  $OC_{terr}$  contribution to the sedimentary TOC pool using a binary mixing model approach. Instrumental errors are propagated through the binary mixing model; (a)  $OC_{terr}$  estimate using the n-alkane/alkenone index ( $1\sigma = \pm 1.6\%$ ). Black triangles indicate the  $^{14}C$  dated sediment horizons; (b) the BIT-Index ( $1\sigma = \pm 1.1\%$ ) and (c) the C/N ratios ( $1\sigma = \pm 2.2\%$ ). Black dots are individual sample values; the red line indicates the moving average.

4. Assessing Holocene changes in marine productivity and terrestrial organic carbon inputs into an Icelandic fjord: Application of molecular and bulk organic proxies.

#### 4.3.3.1 n-alkane/alkenone index

The mean  $OC_{terr}$  contribution to the marine sediments, and its standard deviation estimated by the n-alkane/alkenone index is  $14 \pm 6$  % (Figure 4.4). The  $OC_{terr}$  contribution estimated by this proxy is highest in the oldest part of the record, from  $\sim 10,800$  to  $\sim 8000$  cal. a BP. This proxy is the only one showing  $OC_{terr}$  estimates higher than 30% in the early Holocene, between  $\sim 9000$  and  $\sim 8000$  cal. a BP.

#### 4.3.3.2 BIT-Index

The mean estimated  $OC_{terr}$  contribution to the fjordic sediment and its standard deviation is  $8 \pm 3$  % when using the BIT-Index in the binary mixing model (Figure 4.4). The  $OC_{terr}$  contributions remain low during the early Holocene until  $\sim 8500$  cal a BP at which point the  $OC_{terr}$  estimates sharply increase. The  $OC_{terr}$  contributions continually increase until  $\sim 3000$  cal a BP, before slowly decreasing again.

#### 4.3.3.3 C/N Ratio

$OC_{terr}$  estimates show the highest variability when using C/N ratios (Figure 4.4). The mean estimated  $OC_{terr}$  contribution to the sediment and the standard deviation is  $23 \pm 14$  %. In the early Holocene some of the estimated  $OC_{terr}$  values are negative. From  $\sim 8000$  to  $\sim 4000$  cal. a BP the C/N ratio estimated  $OC_{terr}$  increases from below 10 to above 40 %. In the latter part of the record the estimated  $OC_{terr}$  remains high.

#### 4.3.4 Sedimentary $OC_{mar}$ content and modelling of Palaeoproductivity

Using the estimated  $OC_{mar}$  content, the marine palaeoproductivity (PP) of Ísafjarðardjúp fjord was estimated. The mean estimated  $OC_{terr}$  values derived from the three binary mixing models were used to calculate the  $OC_{mar}$  content of MD99-2266 using equation Equation 20. The MARs of TOC,  $OC_{terr}$  and  $OC_{mar}$  are shown in Figure 4.5. Throughout the Holocene the MARs of TOC,  $OC_{mar}$  and  $OC_{terr}$  correlate with the sedimentation rate (Figure 4.1). The linear regression between

4. Assessing Holocene changes in marine productivity and terrestrial organic carbon inputs into an Icelandic fjord: Application of molecular and bulk organic proxies.

$OC_{mar}$  and sedimentation rate is very strong ( $r^2 = 0.95$ ), while the linear regression between  $OC_{terr}$  and sedimentation rate is much weaker ( $r^2 = 0.59$ ).

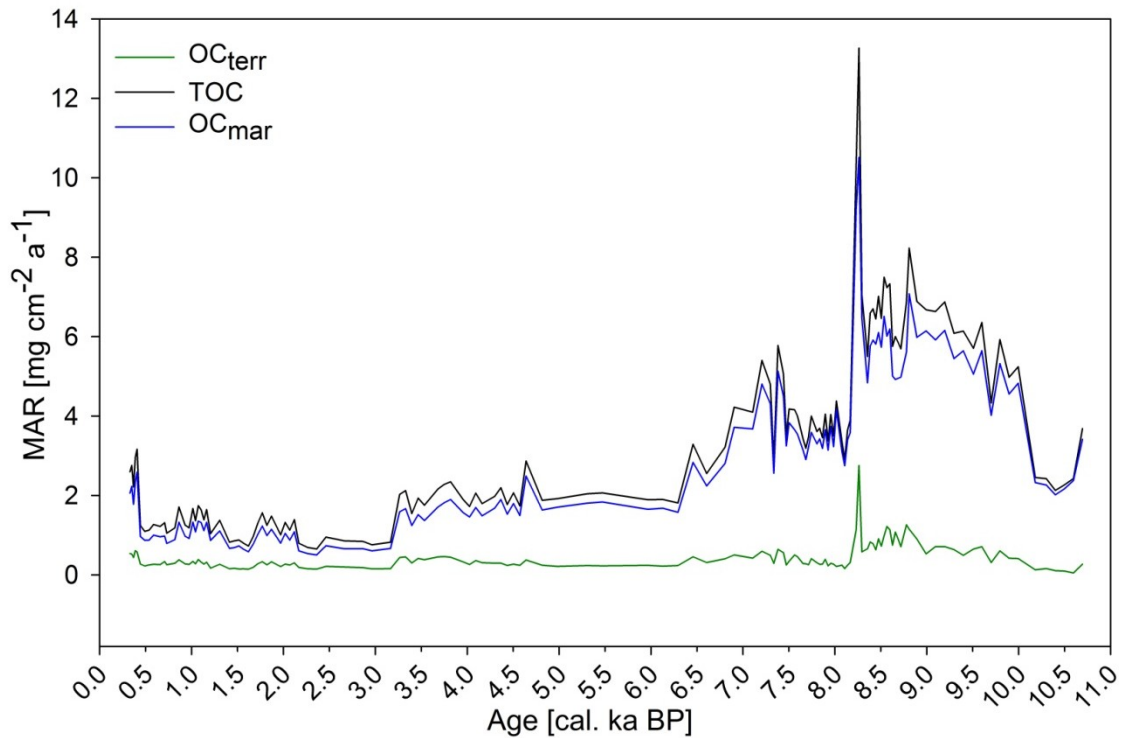


Figure 4.5: Mass accumulation rates of total, marine- and terrestrial organic carbon

Three different models were used to estimate palaeoproductivity. Based on 26 analysis of surface sediments, Müller & Suess (1979) found the following relationship between  $OC_{mar}$  and marine primary production [ $gC \cdot m^{-2} \cdot a^{-1}$ ]:

$$\text{marine primary production} = \frac{OC_{mar} \cdot DBD}{0.003 \cdot LSR^{0.3}}$$

Equation 21: Marine primary production after Müller & Suess (1979)

$OC_{mar}$  is the marine organic carbon content [%], DBD is dry bulk density [ $g \cdot cm^{-3}$ ] and LSR is the linear sedimentation rate [ $cm \cdot ka^{-1}$ ]. By combining the model of Müller & Suess (1979; Equation 21) with organic carbon flux variations depending on the water depth (Betzer *et al.*, 1984), Stein (1986) produced a model incorporating changing water depth, i.e. residence time of OC in the water column:

4. Assessing Holocene changes in marine productivity and terrestrial organic carbon inputs into an Icelandic fjord: Application of molecular and bulk organic proxies.

$$PP = 5.31 \cdot (OC_{\text{mar}} \cdot \text{DBD})^{0.71} \cdot \text{LSR}^{0.07} \cdot D^{0.45}$$

Equation 22: Palaeoproductivity after Stein (1986)

In this model, PP does not only depend on  $OC_{\text{mar}}$ , LSR and DBD (units identical to the ones in Equation 21: Marine primary production after Müller & Suess (1979)), but also on the water depth D [m]. Using this model, early Holocene sea level change in the Ísafjarðardjúp fjord as a response to final deglaciation as well as the isostatic rebound of Iceland (Quillmann *et al.*, 2010) is considered in the palaeoproductivity estimate (Figure 4.6). Quillmann *et al.* (2010) show that the relative sea level decreased by ~ 30 meters between ~10,700 cal. a BP and ~ 8900 cal. a BP. Subsequently relative sea level increased again and reached its contemporary level at ~ 5700 cal. a BP. Assuming a linear sea level decrease and subsequent increase, the relative sea level change was calculated using today's sea level as a reference point.

The final model used to estimate palaeoproductivity was developed by (Knies & Mann, 2002; Equation 23):

$$PP = \left\{ \frac{OC_{\text{mar}} \cdot 0.378 \cdot \text{DBD} \cdot \text{LSR} \cdot D^{0.63}}{\left[ 1 - \left( \frac{1}{0.037 \cdot \text{LSR}^{1.5} + 1} \right) \right]} \right\}^{0.71}$$

Equation 23: Palaeoproductivity after Knies & Mann (2002)

This is based on the two models previously described, but also on studies by Betts & Holland (1991) and Johnson-Ibach (1982). Besides the carbon flux, this model considers dilution effects depending on the amount of inorganic material in the water column, and the burial efficiency, which increases with increasing sedimentation rates.

4. Assessing Holocene changes in marine productivity and terrestrial organic carbon inputs into an Icelandic fjord: Application of molecular and bulk organic proxies.

Using the estimated  $OC_{\text{mar}}$  content, the marine palaeoproductivity (PP) of Ísafjarðardjúp fjord can be estimated. Using the model published by Müller & Suess (1979) the paleoproductivity in Ísafjarðardjúp fjord throughout the Holocene was estimated. The PP varies between 35 and 80  $\text{gC}\cdot\text{m}^{-2}\cdot\text{a}^{-1}$ . The model published by Stein (1986) considers water depth changes and suggests, that on average 3.4  $\text{gC}\cdot\text{m}^{-2}\cdot\text{a}^{-1}$  are lost due to degradation processes in the water column. During periods of very low sedimentation rates in the middle and late Holocene, the model predicts a lower palaeoproductivity than the model by Müller & Suess (1979). The model by Knies & Mann (2002) provides palaeoproductivity estimates which are on average nearly four times higher than those provided by the other two models. The modelled palaeoproductivity variability follows the mass accumulation rates of  $OC_{\text{mar}}$  and TOC (Figure 4.5). The model indicates that the early Holocene was characterised by high primary productivity followed by a decrease throughout the middle Holocene.

4. Assessing Holocene changes in marine productivity and terrestrial organic carbon inputs into an Icelandic fjord: Application of molecular and bulk organic proxies.

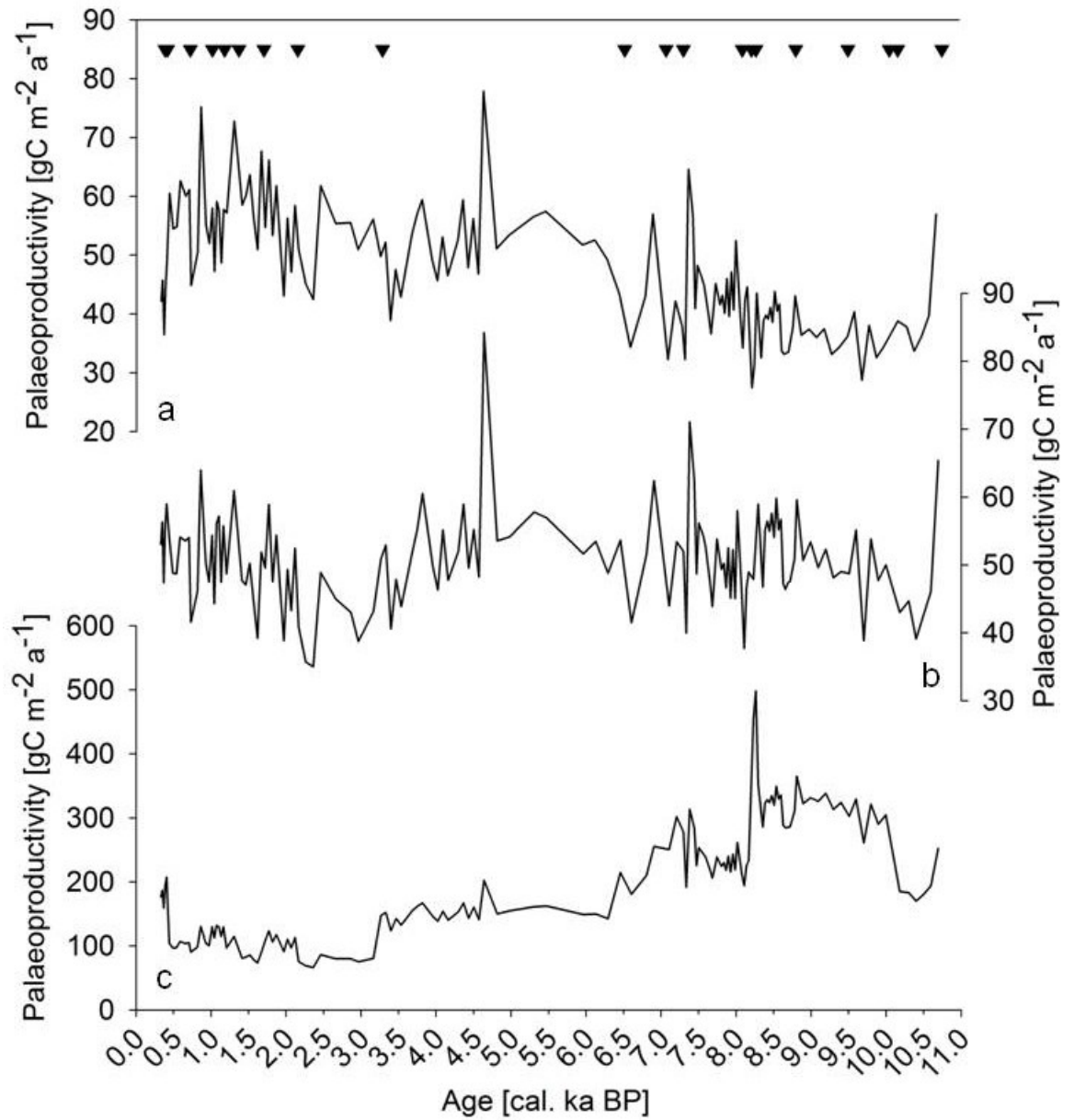


Figure 4.6: Palaeoproductivity of Ísafjarðardjúp fjord using three different models after (a) Müller & Suess (1979), (b) Stein (1986) and (c) Knies & Mann (2002). The modelled palaeoproductivity is subject to the errors associated with the estimated  $OC_{terr}$  content and the resultant  $OC_{mar}$  estimations.

4. Assessing Holocene changes in marine productivity and terrestrial organic carbon inputs into an Icelandic fjord: Application of molecular and bulk organic proxies.

#### 4.4 Discussion

##### 4.4.1 Terrestrial organic carbon contribution to the fjordic sediment

The estimated percentile terrestrial organic fraction ( $f_{\text{Terr}}$ ) depends on the end-member values employed in the binary mixing model. For the *n*-alkane/alkenone-index,  $X_{\text{Terr}}$  is 1 and  $X_{\text{Mar}}$  is 0. These end-member values are used under the assumptions that the odd-chained ( $C_{25}$ - $C_{35}$ ) *n*-alkanes do not have a marine source, alkenones are produced *in situ* by marine haptophytes, and that there is no, or negligible input of alkenones from lakes (Castañeda & Schouten, 2011). Furthermore, it is assumed that both *n*-alkanes and alkenones are a representative fraction of the terrestrial and marine OC contribution into the sediment and that the concentration of these compounds varies in step with changes of  $OC_{\text{terr}}$  and  $OC_{\text{mar}}$  contributions.

The  $X_{\text{Terr}}$  value used to evaluate the terrestrial OC input via the BIT-Index is 0.91 and not 1, as Crenarchaeol is not only found in marine environments, but also in soils (Weijers *et al.*, 2009; Weijers *et al.*, 2006b). 0 is used as the marine end-member value assuming that the vast majority of branched GDGTs are produced by organisms living on land. However, as discussed in the introduction, branched GDGTs likely have a marine source as well which means that the use of 0 as a marine end-member value may not be appropriate. Furthermore, Fietz *et al.* (2012; accepted for publication) have shown that the concentration of Crenarchaeol in marine sediments co varies with the concentration of the branched GDGTs used in the BIT-Index. The linear regression ( $r^2 = 0.75$ ) between the relative abundance of Crenarchaeol and the combined relative abundances of the branched GDGTs used in the calculation of the BIT-Index confirms the co variance of the concentrations of Crenarchaeol and branched GDGTs in the sediment core studied here. One explanation for the global relationship between the BIT-Index and the Crenarchaeol concentration is, that Thaumarchaeota may be more productive during periods where more terrestrial matter is washed into the water column, as indicated by high amounts of branched GDGTs (Fietz *et al.*, 2012 accepted for publication). In the fjord studied here, this constitutes a plausible

4. Assessing Holocene changes in marine productivity and terrestrial organic carbon inputs into an Icelandic fjord: Application of molecular and bulk organic proxies.

explanation, due to the proximity of land. Throughout the Holocene, the BIT-Index slowly increases. Under the assumption that most, if not all branched GDGTs are produced by terrestrial bacteria, a faster increase in the concentration of the branched GDGTs compared to the concentration increase of Crenarchaeol does however suggest an increasing  $OC_{terr}$  flux throughout the Holocene.

In the terrestrial realm the organisms producing the biomarkers used to calculate the BIT-Index are specific to soil and peat environments (Hopmans *et al.*, 2004). Therefore, if the BIT-Index indeed shows increased terrestrial input, then that contribution comes from soils and peats. Thus results of the binary mixing model employing the BIT-Index likely underestimate the amount of terrestrially derived OC contributing to the TOC pool.

The C/N ratio does not reflect the amount of OC in a system, but rather the amount of nitrogen (Perdue & Koprivnjak, 2007). It is the N/C ratio that reflects the amount of OC. Since the C/N ratio is more commonly used in the scientific literature, in this study Weijers *et al.* (2009) is followed in giving the C/N ratio in the text, but using the N/C ratio to calculate  $f_{Terr}$ . The C/N ratio has been used to distinguish between marine and terrestrially sourced OM (Meyers, 1997). Different OM pools have widely varying C/N ratios (Lamb *et al.*, 2006), with typical C/N values for algae between 4 and 10, while vascular land plants have C/N values of  $\geq 20$  (Meyers, 1994). No C/N ratios of marine organisms have been measured in the Denmark Strait. In order to be sure, that the marine end-member of the C/N ratio exclusively represents a marine source, 4 is used as the representative value of  $X_{Mar}$ . This value is used under the assumption, that algae are the sole or at least main contributor of marine sourced OC to the sediment.

4. Assessing Holocene changes in marine productivity and terrestrial organic carbon inputs into an Icelandic fjord: Application of molecular and bulk organic proxies.

Table 2: C/N values of different samples from terrestrial sources in northwest Iceland. The C/N value of the Sedge *Carex cf. rariflora* (\*) is used as a terrestrial end-member value.

Sample type	No. of samples	Location	C/N Ratio	Literature
Terrestrial Plants	6	64°32' N; 22°31' W	41.3 - 72.6	(Langdon <i>et al.</i> , 2010)
Moss <i>Warnstorfia exannulata</i>	1	66°06' N; 22°23' W	62	(Skrzypek <i>et al.</i> , 2008)
Sedge <i>Carex cf. rariflora</i> *	1	66°06' N; 22°23' W	48*	(Skrzypek <i>et al.</i> , 2008)
Peat (upper 10 cm)	1	64°32' N; 22°31' W	15.4	(Langdon <i>et al.</i> , 2010)
Soil	3	64°32' N; 22°31' W	16.5 - 22	(Langdon <i>et al.</i> , 2010)
<i>Carex</i> Peat	5	66°06' N; 22°23' W	33 - 44	(Skrzypek <i>et al.</i> , 2008)

The variability of possible  $X_{Terr}$  end-member values for use in the binary mixing model employing the C/N ratio is comparatively larger than the variability of  $X_{Mar}$  values. C/N values from two studies which took place in northwest Iceland and comprise a total of 18 samples are summarised in Table 2. C/N values of peat samples from the vicinity of Drangajökull glacier on Vestfirðir peninsular vary between 44 and 33 (Skrzypek *et al.*, 2008). The same study shows that the sedge *Carex cf. rariflora*, which dominates the wetland environment near Drangajökull, has a C/N value of 48, while the value of the dominant moss (*Warnstorfia exannulata*) is 62. C/N values of plants from western Iceland vary between 72.6 and 41.3, while peat has a C/N value of 15.4 and the C/N values of three soil samples vary between 22 and 16.5 (Langdon *et al.*, 2010). Most soils in Iceland have C/N ratios between 11 and 17 (Pitty, 1979). Due to the large variety of C/N values from different terrestrial carbon sources, the choice of a “true” C/N value,

#### 4. Assessing Holocene changes in marine productivity and terrestrial organic carbon inputs into an Icelandic fjord: Application of molecular and bulk organic proxies.

representing the total terrestrial organic carbon is difficult. In this study the C/N value of the sedge *Carex cf. rariflora* which today dominates the wetland environment north of Ísafjarðardjúp fjord is chosen (Skrzypek *et al.*, 2008). It is assumed that the vegetation of the catchment area of Ísafjarðardjúp fjord has not undergone major changes throughout the Holocene, and that sedge type vegetation has therefore been a constant source of terrestrial input into the fjordic sediments. This assumption is supported by pollen analysis by Caseldine *et al.* (2003) who show that 80 % of the vegetation on Vestfirðir Peninsular was made up of sedge and shrub type plants throughout most of the Holocene. If a C/N value typical for Icelandic soils (C/N = 15) is chosen as the terrestrial end-member for the binary mixing model, then  $f_{\text{Terr}}$  increases by 20 %. The varying results depending on the choice of different end-members show, that this model underestimates  $\text{OC}_{\text{terr}}$  by possibly as much as 20 % when using the C/N value of sedge. This is expected, as plants, as well as soils and peat bogs all represent terrestrial carbon sources for the fjordic sediment. Since the choice of different end-members for the binary mixing model has a profound effect on the result,  $\text{OC}_{\text{terr}}$  estimates using C/N ratios have to be interpreted with caution.

The results of the different biomarker proxies employed in the binary mixing model to produce  $\text{OC}_{\text{terr}}$  estimates throughout the Holocene are discussed in the following sections.

##### 4.4.1.1 n-Alkane/Alkenone index

The *n*-alkane/alkenone index indicates the highest  $\text{OC}_{\text{terr}}$  contribution in the early Holocene (Figure 4.4). With the exception of the period between ~ 9500 and ~ 9000 years ago, the lowest concentrations of  $\text{C}_{37}$ -alkenones in the sediment are recorded in the early Holocene. During the same time period the concentrations of the *n*-alkanes range very close to the mean concentration of *n*-alkanes of the whole Holocene. Thus, the estimated high  $\text{OC}_{\text{terr}}$  contribution in this part of the record is not caused by an actual high terrigenous input into sediments, but rather by low  $\text{C}_{37}$ -alkenone concentrations. The high  $\text{OC}_{\text{terr}}$  contribution estimated for the

#### 4. Assessing Holocene changes in marine productivity and terrestrial organic carbon inputs into an Icelandic fjord: Application of molecular and bulk organic proxies.

early part of the record may therefore be a result of adverse growing conditions for alkenone producing haptophytes. This explanation is supported by reduced salinity of Ísafjarðardjúp fjord waters caused by meltwater events, that had a strong influence on the fjordic environment before ~ 8000 cal. a BP (Quillmann *et al.*, 2010). The influx of meltwater may have adversely affected the growing conditions of alkenone-producing algae. The estimated  $OC_{terr}$  contribution between ~ 8000 and ~ 1200 cal. a BP fluctuates between ~10 and ~20 %. During the last ~ 1000 years of the record the concentration of the *n*-alkanes increases and this increase of terrestrially derived matter is reflected in a gradual increase of the  $OC_{terr}$  contribution which nearly reaches 30 % at ~ 300 cal. a BP. The two periods of relatively high estimated  $OC_{terr}$  values due to low alkenone concentration in the early Holocene and high *n*-alkane concentrations in the late Holocene highlight that the estimates of  $OC_{terr}$  into sediment must be assessed cautiously when using this approach.

##### 4.4.1.2 BIT-Index

Compared to the other two binary mixing model estimates of the fraction of  $OC_{terr}$ , the BIT-Index provides the lowest values over the length of the record (Figure 4.4). This is an expected result, as the BIT-Index reflects changing contributions of soil organic matter only (Walsh *et al.*, 2008; Weijers *et al.*, 2006b). The relationship between the concentrations of the Crenarchaeol and the branched GDGTs observed in this study, also causes lower BIT-Index values. The numerical value of Crenarchaeol is found in the denominator of the BIT-Index equation (Equation 15). An increase in the relative abundance of Crenarchaeol therefore causes lower BIT-Index values. Furthermore, it is not conclusively resolved whether a linear relationship exists between the concentration of branched GDGTs and the concentration of  $OC_{terr}$  (Weijers *et al.*, 2009). In other words it is not certain whether a 50 % decrease of  $OC_{terr}$  input leads to a 50 % decrease in the concentration of branched GDGTs. This constitutes another reason for why the BIT-Index might give lower  $OC_{terr}$  estimates.

4. Assessing Holocene changes in marine productivity and terrestrial organic carbon inputs into an Icelandic fjord: Application of molecular and bulk organic proxies.

#### 4.4.1.3 C/N Ratio

$OC_{terr}$  estimates show the highest variability when using C/N ratios (Figure 4.4). The C/N values of the samples which produce negative  $OC_{terr}$  values are lower than the  $X_{Mar}$  end member value used, explaining the negative  $OC_{terr}$  estimates in the early Holocene. An explanation for very low C/N values is that the contribution of bacterial organic matter to the total organic matter pool can, in conjunction with very low terrestrially derived organic matter, cause very low C/N values. Lamb et al. (2006) show that bacterial C/N values can be lower than 4.

The  $OC_{terr}$  increase between ~ 8000 to ~ 4000 cal. a BP based on changing C/N ratios may indicate a deteriorating climate. In a lacustrine environment C/N values have been shown to increase with decreasing temperatures (Axford et al., 2009). Axford et al. (2009) attribute the changing C/N values to either changes in primary production or changes in the flux of terrestrial material being transported into the lacustrine sediments. Thus, increasing C/N values throughout the Holocene are associated with deteriorating climatic conditions, as discussed in the following section.

#### 4.4.2 Variations of $OC_{terr}$ in response to environmental and/or anthropogenic influences.

The three model approaches used to estimate the amount of organic carbon derived from terrestrial sources show divergent results highlighting the strengths and weaknesses of the individual proxies applied to the problem of quantifying  $OC_{terr}$  input. By combining the three estimates for  $OC_{terr}$  into one record showing the mean estimate of  $OC_{terr}$  to the fjordic sediment, the closest approximation of the correct input of  $OC_{terr}$ , that the use of the molecular tools applied here can provide, is given (Figure 4.7). Only the samples (n=137) where all biomarker data and bulk parameters are available, were used to produce the combined record showing the  $OC_{terr}$  estimate.

#### 4. Assessing Holocene changes in marine productivity and terrestrial organic carbon inputs into an Icelandic fjord: Application of molecular and bulk organic proxies.

Different biomarker molecules are more or less susceptible to degradation in the water column and the topmost layers of sediments, particularly in oxic environments (Hoefs *et al.*, 2002; Sinninghe Damsté *et al.*, 2002a). This may well contribute to the uncertainty margin of the combined  $OC_{terr}$  estimate shown in Figure 4.7. However, the study site has a low water depth equating to short residence times of biomarker molecules in the water column, as well as high sedimentation rates which promote a quick burial of the molecules, removing them from the biologically active topmost layer of sediment (Zonneveld *et al.*, 2010). Therefore it is suggested, that the degradation of biomarker molecules does not lead to large errors, when estimating the  $OC_{terr}$  input. Transport times of the different molecules to the sediments are considered. Ísafjarðardjúp fjord is a silled fjord that drains most of the Vestfirðir Peninsular (Quillmann *et al.*, 2010). Most of the terrestrially derived biomarker molecules are thought to derive from the Peninsula itself. Furthermore, due to the sheltered nature of the fjord it is assumed, that most of the marine biomarkers are produced in the fjord itself and that only a negligible amount is laterally transported to the site. Due to the short transport distances it is assumed, that the differences in transport time of the different biomarkers to the site is years and decades, rather than centuries. The temporal resolution of the combined  $OC_{terr}$  variability is greater than 50 years, and therefore probably not high enough to be affected by the proposed short transport time of the different molecules. Furthermore, the temporal uncertainty associated with the age model (mean  $2\sigma$  error: 165 cal. a) is larger than the assumed transport times.

4. Assessing Holocene changes in marine productivity and terrestrial organic carbon inputs into an Icelandic fjord: Application of molecular and bulk organic proxies.

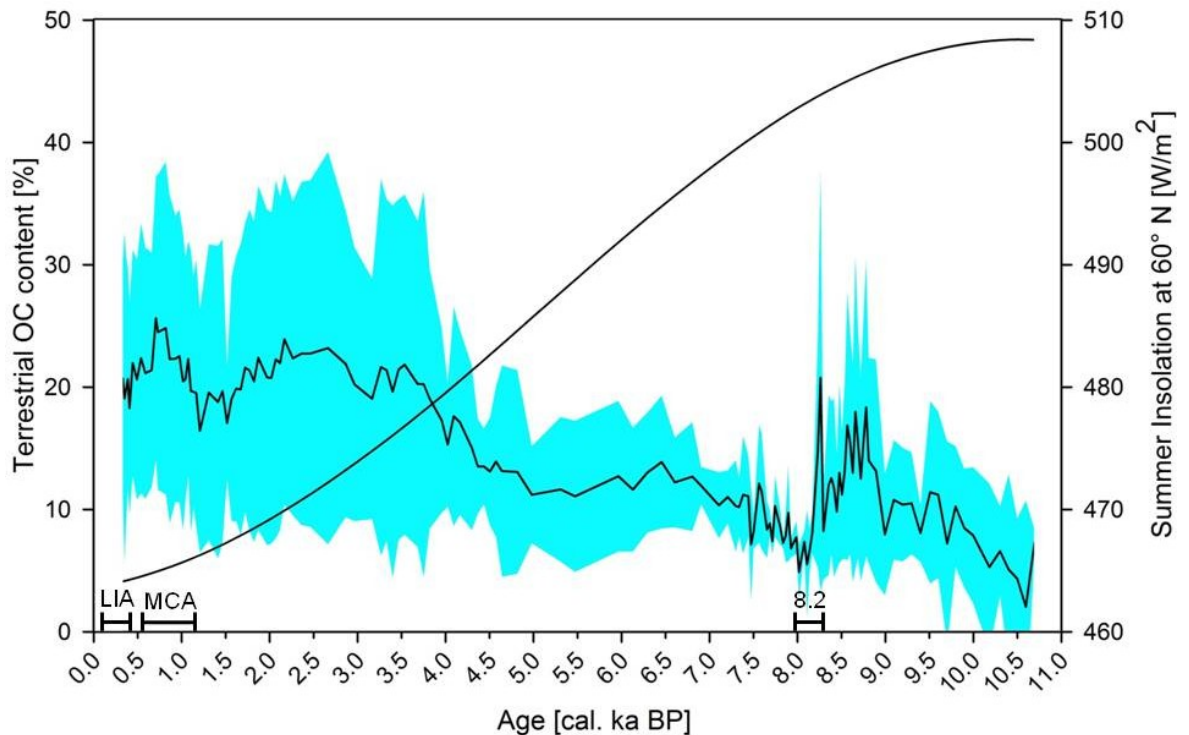


Figure 4.7: Mean estimated  $OC_{terr}$  input into the fjordic sediments plotted against the summer insolation change at  $60^\circ N$  (Laskar *et al.*, 2004). The shaded area indicates the uncertainty (standard deviation from the mean) that arises from combining the estimates of the three  $OC_{terr}$  proxies. The Little Ice Age, the Medieval Climate Anomaly and the 8.2 ka event are indicated.

The combined record of  $OC_{terr}$  estimates shows two periods where the  $OC_{terr}$  content in the sediment rises. Throughout the early Holocene, from  $\sim 10,700$  to  $\sim 8800$  cal. a BP, the  $OC_{terr}$  contribution to the TOC pool of the sediment increases from 2 to 18 %. The early Holocene was characterised by high Northern Hemisphere summer insolation and glaciers on Iceland were continually retreating (Geirsdottir *et al.*, 2009). The retreat of glaciers on Iceland freed up land area for soil formation and subsequent increase in vegetation cover. An increase in the pollen concentration from lacustrine sediments from Vestfirðir, beginning at  $\sim 9500$   $^{14}C$  years BP ( $\sim 11,000$  cal. a BP), as well as an increase in the concentration of *Betula sp.* pollen commencing at  $\sim 9800$  cal. a BP in central northern Iceland has previously been reported (Caseldine *et al.*, 2003; Langdon *et al.*, 2010). Increasing amounts of soil and plant material provide an explanation for the rising portion of  $OC_{terr}$  in the early Holocene.

4. Assessing Holocene changes in marine productivity and terrestrial organic carbon inputs into an Icelandic fjord: Application of molecular and bulk organic proxies.

From ~ 8600 to ~ 8000 cal. a BP the contribution of  $OC_{terr}$  decreases. Several marine archives from the Denmark Strait and the north Icelandic Shelf have recorded either one prolonged (~ 500 year long) cooling event centred around 8200 cal. a BP (Giraudeau *et al.*, 2000; Knudsen *et al.*, 2004; Ólafsdóttir *et al.*, 2010), or a number of shorter cooling events (Jennings *et al.*, 2011). Based on chironomidae assemblages, temperatures in northwest Iceland decreased slightly at ~ 8200 cal. a BP (Caseldine *et al.*, 2003), and at ~ 8500 cal. a BP (Langdon *et al.*, 2010). This downturn of climate could have caused the development of soil reservoirs and vegetation cover to halt, or even reverse, thus decreasing the amount of  $OC_{terr}$  contribution to the sediment. Indeed, Hallsdottir (1995) notes, that the development towards subalpine birch woodland suddenly halted ~ 7500  $^{14}C$  years (~ 8300 cal. a BP) ago. Ólafsdóttir *et al.* (2001) have modelled a dramatic decrease in vegetation cover at ~ 8000 cal. a BP. This explanation is supported by an increased soil organic matter contribution to the sediments as indicated by the BIT-Index (Figure 4.4) in this study. Decreased vegetation cover would have led to more soil erosion and thus to higher input of soil organic carbon into the sediments.

Despite the short, cold interval causing a decrease of the  $OC_{terr}$  contribution as previously discussed, the period from ~ 8600 to ~ 5400 cal. a BP was regarded as the warmest episode of the Holocene (Kaufman *et al.*, 2004; Knudsen *et al.*, 2008). This warm climate was conducive to extensive soil and vegetation development on Iceland (Caseldine *et al.*, 2003; Hallsdottir, 1995; Wastl *et al.*, 2001). This development would have stored up carbon in soil reservoirs, providing a source of  $OC_{terr}$ , and likely explains the continued increase in the fraction of estimated  $OC_{terr}$  to the fjordic sediments.

The marked increase of  $OC_{terr}$  input to the sediments after ~ 5000 cal. a BP is attributed to the climatic deterioration following the Holocene thermal maximum which is apparent in marine as well as terrestrial records (Jennings *et al.*, 2002; Justwan *et al.*, 2008; Principato, 2008; Wastl *et al.*, 2001). The deteriorating climate affected caused accelerated soil degradation during the neoglaciation. As

4. Assessing Holocene changes in marine productivity and terrestrial organic carbon inputs into an Icelandic fjord: Application of molecular and bulk organic proxies.

the climate deteriorated soils started to freeze and dry out periodically. This process made the soils and vegetation cover more susceptible to erosion by high velocity winds (Ólafsdóttir & Gudmundsson, 2002). The contribution of soil derived  $OC_{terr}$  as indicated by the BIT-Index increases steadily from  $\sim 6000$  to  $\sim 3000$  cal. a BP (Figure 4.2), confirming the process of soil erosion in contributing a significant amount of  $OC_{terr}$  to the fjordic sediment. A second explanation for the continued increase of  $OC_{terr}$  into the sediment is provided by changes in vegetation cover. Birch woodland was in retreat throughout the Neoglaciation shown by decreasing *Betula sp.* pollen concentrations (Hallsdóttir, 1995; Hallsdóttir *et al.*, 2005). In the latter half of the Holocene heathland and mires expanded and in the lowlands woods were replaced and buried by peat (Hallsdóttir *et al.*, 2005). Changing soil and vegetation types as well as increased amounts of peat could have caused increased amounts of  $OC_{terr}$  to be transported into the fjord, compounding the effects of increased soil erosion as discussed above.

The sharp increase in the estimated contribution of  $OC_{terr}$  to the fjordic sediments between  $\sim 1200$  and  $\sim 600$  cal. a BP was caused by anthropogenic actions and/or climatic fluctuations. The period from  $\sim 1100$  to  $\sim 550$  cal. a BP is known as the medieval climate anomaly (MCA; Hughes & Diaz, 1994), which was characterised by warm climate throughout Europe (Buntgen *et al.*, 2011; Graham *et al.*, 2011). The Norse established settlements on Iceland at around  $\sim$  AD 870 ( $\sim 1080$  cal a BP; Andrews *et al.*, 2001). Domestic land use on Iceland has been shown to cause increased soil erosion (Dugmore *et al.*, 2000). The first generation of settlers cleared woodland to make space for farmland (Hallsdóttir *et al.*, 2005). The sharp human driven vegetation change is probably reflected by a drastic rise in the odd chained *n*-alkane concentration at  $\sim 1200$  cal. a BP (Figure 4.2). The error ( $2\sigma$ , Table 1) of the two closest dated sediment horizons at 1370 and 1178 cal. a BP is  $\pm 138$  and  $\pm 124$  cal. a BP, respectively. Within the dating errors, the timing of the rise of the *n*-alkane concentration coincides with the first settlement of Iceland. Increased soil erosion, along with possible burning of woodland to make space for pastures and fields could therefore explain increased amounts of  $OC_{terr}$  in the sediments.

4. Assessing Holocene changes in marine productivity and terrestrial organic carbon inputs into an Icelandic fjord: Application of molecular and bulk organic proxies.

A second explanation is provided by the drastic change in climate itself. The ameliorated climate of the MCA has been associated with a prevailing positive North Atlantic oscillation (NAO) phase (Trouet *et al.*, 2009). Throughout the period of instrumental measurements of the NAO, positive NAO phases have been associated with increased precipitation in Iceland (Hurrell, 1995). If the prevailing positive NAO mode throughout the MCA caused increased precipitation, more terrestrial runoff would have resulted in a higher amount of OC<sub>terr</sub> to be washed into the fjord. This mechanism provides a second explanation for high amounts of sedimentary OC<sub>terr</sub> during the MCA.

#### **4.4.3 Mass accumulation rates of marine and terrestrial OC**

The mass accumulation rates of TOC, OC<sub>mar</sub> and OC<sub>terr</sub> are shown in Figure 4.5. The close correlation between the OC<sub>mar</sub> MAR and the sedimentation rate suggests that the sedimentation rate, i.e. the amount of material reaching the sediment is the main factor controlling the OC<sub>mar</sub> content in the fjordic sediment, rather than primary production itself.

The high sedimentation rate implies a large flux of inorganic terrestrial material being washed into the fjord, carrying with it nutrients which are essential for primary production. Thus, increased terrestrial runoff can cause increased primary production and subsequent increased sedimentation of OC<sub>mar</sub>. The link between the nutrient supply and high sedimentation rates has previously been suggested by Quillmann *et al.* (2010). They show that the benthic foraminifera species *F. fusiformis*, which is associated with an increased nutrient supply, is most abundant during the early Holocene while sedimentation rates are high.

In addition to the primary productivity, the preservation of TOC in sediments is also controlled by the oxygenation of the water column as well as sinking speed of OC, and by high flux and deposition rates of inorganic material (Knies *et al.*, 2003; Stein, 1990; Stein *et al.*, 1986). In an oxygenated water column more organic matter is decomposed compared to an anoxic or euxinic water column. Increased

4. Assessing Holocene changes in marine productivity and terrestrial organic carbon inputs into an Icelandic fjord: Application of molecular and bulk organic proxies.

flux speeds through the water column as well as increased burial rates increase the amount of OM being buried without being decomposed. Increased amounts of inorganic material favour this process as this material can form aggregates with the OM and increase sinking speeds, and burial rates (see review by Zonneveld *et al.*, 2010 and references therein). Thus high sedimentation rates favour the deposition of labile marine organic matter which explains the close correlation between the high sedimentation rates and the  $OC_{\text{mar}}$  MAR. The weak correlation between the MAR of  $OC_{\text{terr}}$  and the sedimentation rate indicates that the  $OC_{\text{terr}}$  content of the fjords sediment is not controlled by sedimentary processes but rather forced by climatic variations as discussed above.

#### **4.4.4 Marine paleoproductivity**

The three models employed to estimate palaeoproductivity assume that the water column is oxygenated (Figure 4.6). This may not be true for Ísafjarðardjúp fjord, as the water exchange of fjords, particularly silled fjords is restricted (Howe *et al.*, 2010). Furthermore, the water column within the fjord may be stratified for at least part of the year (Cottier *et al.*, 2010). Restricted water exchange, as well as a stratified water column can result in suboxic or even anoxic conditions which are conducive to the preservation of OM in sediments (Bralower & Thierstein, 1984; Zonneveld *et al.*, 2010). Thus all the models used in this study may overestimate the palaeoproductivity of Ísafjarðardjúp fjord. Furthermore, all models used here were conceived for open ocean environments rather than fjordic systems. Since open ocean environments are very different from fjordic environments, i.e. oceans tend to have lower sedimentation rates, lower primary production and less terrigenous input, the quantitative palaeoproductivity estimates must be interpreted with caution.

The model published by Knies & Mann (2002) has previously been used to estimate the palaeoproductivity in areas exhibiting very high sedimentation rates (Knies *et al.*, 2003), and may therefore be the most suited model to estimate palaeoproductivity in Ísafjarðardjúp fjord. The model by Knies & Mann (2002) provides palaeoproductivity estimates which are on average nearly four times

4. Assessing Holocene changes in marine productivity and terrestrial organic carbon inputs into an Icelandic fjord: Application of molecular and bulk organic proxies.

higher than those provided by the other two models (Figure 4.6). Satellite data shows that annual primary production in the waters surrounding Iceland is between  $\sim 200$  and  $\sim 300 \text{ gC m}^{-2} \text{ a}^{-1}$  today (Longhurst *et al.*, 1995; Sathyendranath *et al.*, 1995; Schlüter *et al.*, 2000). The Knies & Mann (2002) model produces average palaeoproductivity values of  $170 \text{ gC} \cdot \text{m}^{-2} \cdot \text{a}^{-1}$  in the first 100 years of the record. Based on the comparison of the modelled palaeoproductivities of the different models with today's primary production estimates it is suggested that the model provided by Knies & Mann (2002) is the most suitable model to estimate paleoproductivity in Ísafjarðardjúp fjord. All further discussion on primary productivity variations throughout the Holocene will be based the results of that model (Figure 4.6). Variations in palaeoproductivity correlate closely with changing MARs of  $\text{OC}_{\text{mar}}$  showing that the degradation of OM which affects the export of  $\text{OC}_{\text{mar}}$  from the surface to the sediments must have been more or less constant throughout the Holocene.

The primary production in Ísafjarðardjúp fjord may have been as high as  $300 \text{ gC} \cdot \text{m}^{-2} \cdot \text{a}^{-1}$  between  $\sim 10,000$  and  $\sim 8000$  cal. a BP. Similar high primary production values are found in the arctic today in areas with a high supply of nutrients due to for example upwelling or riverine input (Wollenburg *et al.*, 2004; references therein). The peak in primary production at  $\sim 8250$  cal. a BP coincides with a debris flow as discussed by Andrews *et al.* (2008) and is probably an artefact. However, this is superimposed on a period of high productivity between  $\sim 10,000$  and  $\sim 8000$  ca a BP. The production of marine organic carbon is linked to the amount of nutrients being washed into the fjord. Thus the PP is high in the early Holocene due to the high amounts of terrigenous material being washed into the fjord as shown by the close correlation between  $\text{OC}_{\text{mar}}$  and the sedimentation rate.

Besides the autochthonous supply of nutrients, an allochthonous supply of nutrients may also have played a major role in affecting palaeoproductivity throughout the Holocene. A maximum in primary production from 8000 to 6000 cal. a BP in the Andfjord on the northwest Norwegian coast has been attributed to a strong inflow of nutrient rich Atlantic water (Knies, 2005). Further north in the Fram Strait times of high primary productivity have also been associated with an

4. Assessing Holocene changes in marine productivity and terrestrial organic carbon inputs into an Icelandic fjord: Application of molecular and bulk organic proxies.

increased nutrient supply (Wollenburg *et al.*, 2004). The primary production at the studied site rises dramatically from below 200 to 300 gC m<sup>-2</sup>a<sup>-1</sup> at 10,200 cal. a BP. At the same time the Irminger Current, that supplies Atlantic water to the Denmark Strait fully penetrated the area (Ólafsdóttir *et al.*, 2010). After ~ 8000 cal. a BP the primary production decreases and reaches values varying around 100 gC m<sup>-2</sup>a<sup>-1</sup> at ~ 3000 cal. a BP, coinciding with a diminishing influence of the Irminger current in the waters surrounding northwest Iceland (Giraudeau *et al.*, 2004; Koc *et al.*, 1993; Ólafsdóttir *et al.*, 2010). Today Atlantic water is the main source of nutrients to the north of Iceland (Giraudeau *et al.*, 2004; references therein). This is compelling evidence that the long-term changes in primary production at the site studied here have been forced by variations in the nutrient supply brought about by either Arctic or Atlantic water masses dominating the area. Furthermore, this interpretation correlates with contemporary observations, whereby the primary production on the North Icelandic Shelf is greater in years, when warm Atlantic waters dominate it (Jónsson & Valdimarsson, 2010; reference therein). The strength of Atlantic water masses has been influenced by changing climate forcing factors such as changes in northern Hemisphere insolation (Koc & Jansen, 1994), and changes in the strength of the Meridional overturning circulation (Bianchi & McCave, 1999; Hoogakker *et al.*, 2011), but also by variations in atmospheric circulation patterns in the Denmark Strait (Blindheim & Malmberg, 2005). Therefore, changes in the amount of primary production throughout the Holocene may have at least indirectly been forced by climatic change.

#### **4.5 Conclusion**

In this study the contributions of organic carbon derived from terrestrial, as well as from marine sources to Ísafjarðardjúp fjord sediments have been estimated. Three biomarker and bulk proxy datasets in binary mixing models were used to calculate the contribution of OC<sub>terr</sub> to the TOC pool. Subsequently the results of the three models were combined to produce the most accurate OC<sub>terr</sub> estimate possible.

The estimated OC<sub>terr</sub> contribution to the sediment increases throughout the Holocene to a maximum of 25 %. Furthermore, the OC<sub>terr</sub> influx into the sediments

4. Assessing Holocene changes in marine productivity and terrestrial organic carbon inputs into an Icelandic fjord: Application of molecular and bulk organic proxies.

is not strongly correlated with sedimentation rate but rather controlled by climatic changes. Retreating glaciers and an ameliorated climate led to increased soil and vegetation cover which provided a large, proximal  $OC_{terr}$  pool for erosion and sedimentary deposition. A brief cold period centred on the 8.2 ka event caused less  $OC_{terr}$  to be introduced into the sediments as the expansion of vegetation halted. The increased  $OC_{terr}$  contribution throughout the middle Holocene was driven by a continual expansion and shift of soil and vegetation cover, and also by increased soil erosion due to deteriorating climate conditions. The sharp rise of sedimentary  $OC_{terr}$  during the medieval warm period is attributed to the activities of the Norse settlers, but also to increased runoff into the fjord mediated by high precipitation due to the prevailing positive NAO mode.

The  $OC_{mar}$  contribution to the fjordic sediments was also estimated. The palaeoproductivity was calculated based on the variation of the  $OC_{mar}$  content throughout the Holocene using three different models. The model produced by Knies and Mann (2002) provides the most realistic numerical values of primary production around Iceland and is thus considered to be the most applicable model for the studied site. The MAR of  $OC_{mar}$  correlates well with changes in marine palaeoproductivity indicating that processes affecting the  $OC_{mar}$  export from surface waters to the sediment must have been relatively stable throughout the Holocene.

It appears that changes in the palaeoproductivity throughout the Holocene were forced by changing amounts of allochthonous and autochthonous nutrient supplies. Northern Hemisphere insolation change and changes in the strength of the Meridional overturning circulation have caused different current systems to dominate throughout the Holocene and have thus affected the allochthonous nutrient supply at the coring site.

## **5 New insights into Holocene climate evolution from high-resolution terrestrial and marine biomarker records from Northwest Iceland**

### **5.1 Introduction**

The last 11,500 years of earth's history are known as the Holocene and are characterised by a more stable climate compared to the climatic variability of the Pleistocene, the last 2.6 Million years (Dansgaard *et al.*, 1993). Since the first major work on Holocene climate change (Denton & Karlén, 1973), the idea that the Holocene is characterised by a stable climate has been revised (see review by Mayewski *et al.*, 2004 and references therein). Prominent climatic events, such as the Holocene thermal maximum (Kaufman *et al.*, 2004) the 8.2 ka event (Alley & Ágústsdóttir, 2005), the neoglacial period (Jennings *et al.*, 2002), the medieval climate anomaly (Graham *et al.*, 2011) and the Little Ice Age (Ogilvie & Jonsson, 2001) have been identified, indicating a highly variable climate throughout the Holocene.

The mechanisms and processes driving, and affected by climate change throughout the Holocene, are an active field of research, and they are still not fully understood. For example, the North Atlantic Oscillation (NAO) has major effects on northern hemisphere temperature and precipitation (Hurrell, 1995). The NAO describes strength and directional changes of the westerlies traversing the North Atlantic. These changes are caused by changing sea level pressure (SLP) differences between the Icelandic Low and the Azores high pressure systems. When the NAO is in its positive mode, the westerlies bring moist and warm air massed to Northern Europe. When the NAO is in its negative mode, the westerlies take a more southerly direction causing a drier and colder climate in Northern Europe. Contemporary observations of the NAO show that its short term fluctuations operate over annual and decadal time scales (Dickson *et al.*, 2000; Hurrell, 1995; Hurrell *et al.*, 2003). Palaeoclimatic studies of recent years show

that atmospheric fluctuations similar to the NAO have operated on centennial and even millennial time scales. For example, the MCA was characterised by the NAO predominantly in its positive mode (Trouet *et al.*, 2009). Whether NAO-type fluctuations have controlled climate further in the past is still under debate.

Northern hemisphere high latitudes are the ideal place to study Holocene climate change as these areas are very climate sensitive. Using two coupled ocean-atmosphere models, Liu *et al.* (2003) have shown that the ocean response to changing insolation throughout the Holocene is greatest in the northern hemisphere around 60°N. Iceland, situated southeast of Greenland at 60°N (Figure 3.1), is of particular interest for paleoclimatic research as it straddles atmospheric and oceanic boundary zones in the central North Atlantic (Axford *et al.*, 2011; Jennings *et al.*, 2011). These boundary zones are susceptible to variations produced by climate forcing factors, and such variations can be captured by studying terrestrial and marine sedimentary records. Therefore Iceland, and its surrounding waters have received a lot of scientific attention, especially in the last decade (Andrews *et al.*, 2005; Axford *et al.*, 2011; Calvo *et al.*, 2002; Giraudeau *et al.*, 2000; Sicre *et al.*, 2008a).

The aim of this section is to produce high resolution terrestrial and marine palaeoproxy records to reconstruct Holocene climate change. The alkenone derived  $U^{K}_{37}$ -SST proxy is used to reconstruct SST variability. The CBT/MBT, and the CBT proxies, which are based on branched GDGT abundances, are used to reconstruct air temperature and soil pH changes, respectively. The average chain length (ACL) variability of long chained *n*-alkanes derived from terrestrial higher plants is hypothesised to indicate precipitation changes. This hypothesis is tested by comparing the ACL variability with the change of the hydrogen isotopic variability of the  $C_{29}$  *n*-alkane, and changes in soil pH throughout the Holocene. Furthermore, it is hypothesised that the combined palaeoproxy records of precipitation, sea surface and air temperature will reveal land/ocean interactions and provide a clearer picture of the drivers which force Holocene climate change.

## 5.2 **Methods**

### 5.2.1 **U<sup>K'</sup><sub>37</sub>-sea surface temperature proxy**

The Sea surface temperatures (SSTs) presented here (Figure 5.1) were calculated using the alkenone derived U<sup>K'</sup><sub>37</sub> index (Equation 4; Prahl & Wakeham, 1987). The calibration equation provided by Conte *et al.*(2006; Equation 5) was used to convert U<sup>K'</sup><sub>37</sub> values into sea surface temperatures, as it is the most comprehensive calibration equation to date. 34 samples were analysed in triplicate and the mean analytical error (1 $\sigma$ ) associated with the U<sup>K'</sup><sub>37</sub>-SSTs (alkenone derived palaeo-SSTs) is  $\pm 0.01$  ( $\pm 0.44$  °C).

### 5.2.2 **Average chain length variability of long chained *n*-alkanes**

The ACL values (Equation 2) in this study were calculated using the concentration of the leaf wax derived odd-chained *n*-alkanes with chain lengths of 25 to 35 carbon atoms, as these are the most abundant *n*-alkanes in all samples. 11 samples were analysed in triplicate and the mean analytical error (1 $\sigma$ ) associated with the ACL<sub>25-35</sub> values is  $\pm 0.06$ .

The hydrogen isotopic values of the C<sub>29</sub> and C<sub>31</sub> *n*-alkanes were calculated according to the methods described in the methods section.

### 5.2.3 **Air temperature and soil pH reconstruction using branched GDGTs**

The Holocene mean air temperature (MAT, Equation 14, Figure 5.4) and soil pH variability (Equation 13, Figure 5.5) in northwest Iceland were reconstructed using bacterial membrane GDGTs. Nine samples were analysed in triplicate and two in duplicate. The analytical error (1 $\sigma$ ) associated with the MBT and CBT indices are  $\pm 0.013$  and  $\pm 0.033$  respectively, resulting in an analytical error of  $\pm 0.6$  °C for the MAT reconstruction, and an analytical error of  $\pm 0.044$  pH units for the soil pH reconstruction.

#### **5.2.4 Error analysis and data normalisation**

Where proxy records are converted into climate proxies via a calibration equation (eg.  $U^{K}_{37}$  to SST using the calibration equation provided by Conte *et al.*, (2006)), the analytical error is propagated through the variance of the calibration equation used. However, the resulting propagated error likely constitutes a considerable overestimation of the actual error. This is due to the fact, that the calibration equations are based on global calibration sets which have a considerable amount of scatter.

The  $ACL_{25-35}$  and the soil pH datasets were normalised by subtracting the mean of the total dataset from the value of a single data point, and then dividing by the standard deviation.

### **5.3 Results**

#### **5.3.1 Alkenone derived sea surface temperatures**

The sea surface temperatures show substantial variability throughout the Holocene (Figure 5.1). Using the  $U^{K}_{37}$ -SST palaeothermometer, SST changes as small as 1 °C have been recorded and interpreted (Sicre *et al.*, 2008a), indicating a high proxy sensitivity. From ~ 10,700 to ~ 10,150 cal. a BP the sea surface temperatures initially decrease. After that  $U^{K}_{37}$ -SSTs increase to 11.2 °C at ~ 8800 cal. a BP. Throughout the next 2500 years SSTs fluctuate over short periods of time. At ~ 7330 cal. a BP a SST of 14.9 °C is recorded which is the warmest temperature reconstructed in the record. After an initial sharp temperature drop starting at ~ 5800 cal. a BP and lasting for 200 years, temperatures gradually decrease until ~ 3200 cal. a BP, where the lowest recorded temperature of 6.7 °C is observed. Subsequently the sea surface temperatures increase again over approximately the next 1500 calibrated years. At ~ 910 and at ~ 640 cal. a BP SSTs of 12.8 and 13.1 °C are recorded, respectively, which are only slightly lower than the highest temperatures seen in the early Holocene. As well as a return to higher sea surface temperatures, the late Holocene also sees a return to high frequency/high amplitude fluctuations in the sea surface temperature record.

5. New insights into Holocene climate evolution from high-resolution terrestrial and marine biomarker records from Northwest Iceland

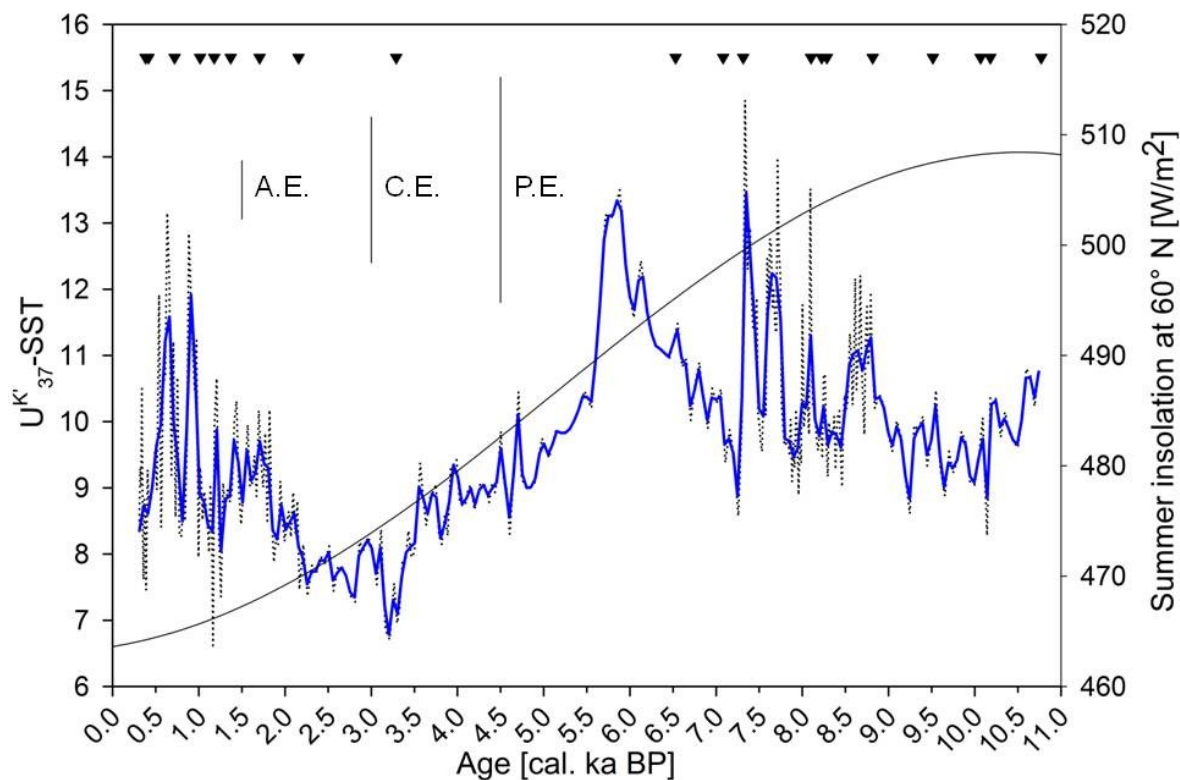


Figure 5.1: Holocene  $U_{37}^K$ -SST variations plotted against northern hemisphere summer insolation variability (black line; Laskar *et al.*, 2004). The black dotted line represents the raw  $U_{37}^K$ -SST data overlaid by the 50 year moving average (blue line). The black triangles represent the  $^{14}\text{C}$ -AMS dated sediment horizons of core MD99-2266. The vertical black lines indicate the analytical error (A.E.), the  $1\sigma$  calibration error (C.E.) and the propagated error (P.E.).

### 5.3.2 *n*-Alkanes

The *n*-alkane average chain length ( $ACL_{25-35}$ , Equation 2) variability throughout the Holocene is shown in Figure 5.2. Average chain length values indicate which odd-chained *n*-alkane dominates in a sample. Changing  $ACL_{25-25}$  values are hypothesised to reflect changing precipitation regimes. In the central Atlantic Ocean  $ACL$  changes of 0.1 units have been interpreted to indicate changing precipitation regimes suggesting a very high proxy sensitivity (Schefuss *et al.*, 2003a).

5. New insights into Holocene climate evolution from high-resolution terrestrial and marine biomarker records from Northwest Iceland

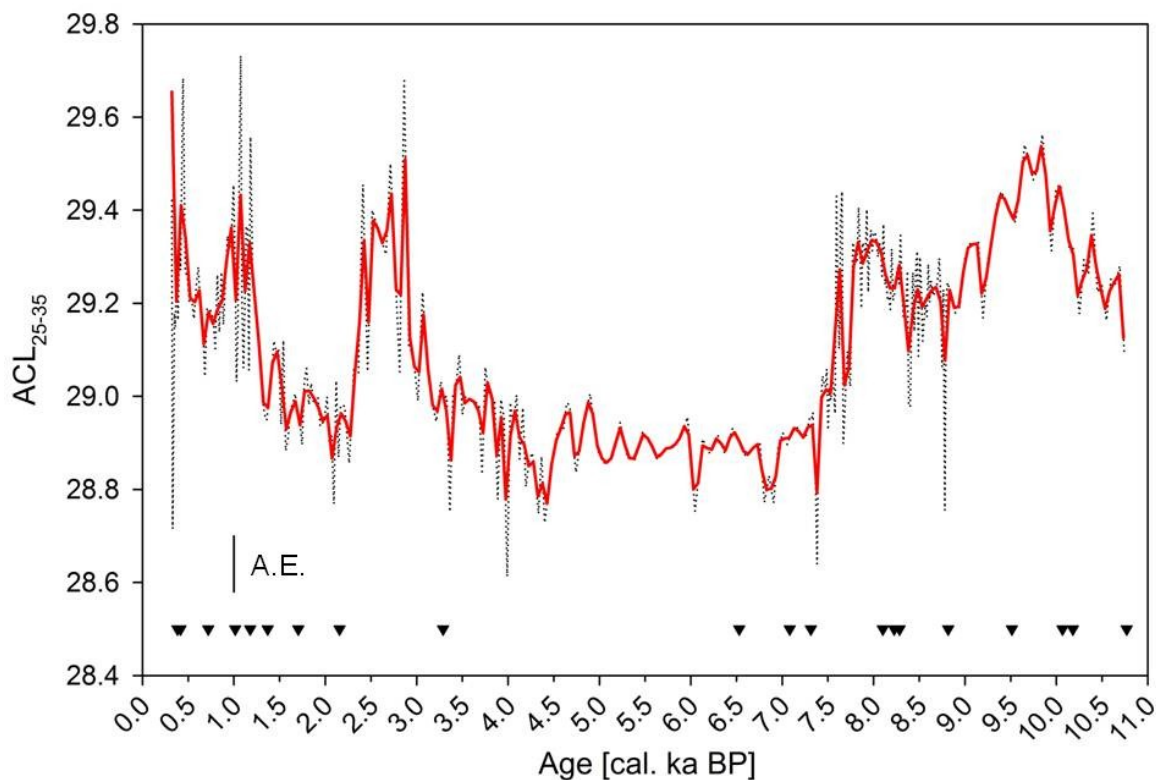


Figure 5.2: *n*-Alkane average chain length ( $ACL_{25-35}$ ) Holocene variability. The dotted line represents the raw  $ACL_{25-35}$  data (less the outliers as discussed in chapter 4) and the red line shows the 50 year moving average. The black triangles show the  $^{14}\text{C}$ -AMS dated sediment horizons of core MD99-2266. The  $1\sigma$  analytical error associated with the  $ACL_{25-33}$  values is  $\pm 0.06$  (black vertical bar).

The  $ACL_{25-35}$  values show significant variations over the period of the Holocene. The oldest sample at 10,750 cal. a BP has an  $ACL_{25-35}$  value of 29.08. The  $ACL_{25-35}$  values initially rise to 29.56 at  $\sim 9850$  cal. a BP before falling to a minimum of 28.75 at  $\sim 8800$  cal. a BP. From then on  $ACL_{25-35}$  values rise again until they sharply fall within  $\sim 200$  years from 29.4 to 28.6. The amplitude of change of the  $ACL_{25-35}$  values between  $\sim 7400$  and  $\sim 3400$  cal. a BP remains relatively low with a mean  $ACL_{25-35}$  value of 28.91. The  $ACL_{25-35}$  values rise again sharply after 3400 cal. a BP to a maximum of 29.68 and stay high until  $\sim 2410$  cal. a BP. Within the next 140 years  $ACL_{25-35}$  values fall again sharply and stay low until  $\sim 1340$  cal. a BP. At that time  $ACL_{25-35}$  values rise and the maximum  $ACL_{25-35}$

value is reached at  $\sim 1070$  cal. a BP with 29.73. There is another slight dip within the  $ACL_{25-35}$  values between  $\sim 970$  and  $\sim 500$  cal. a BP, before a final rise in  $ACL_{25-35}$  values leads up to the youngest part of the record.

#### 5.3.2.1 Hydrogen isotopes of *n*-alkanes

The hydrogen isotopic signatures of the  $C_{29}$ - and  $C_{31}$ -*n*-alkanes of 18 samples were analysed and are shown in Figure 5.3. Variations of hydrogen isotopic values of terrestrial leaf wax *n*-alkanes have been linked to changing precipitation regimes (Sachse *et al.*, 2004; Sachse *et al.*, 2006) Due to the time constraints of the PhD only 18 pilot samples covering the first 3000 years of the record were analysed.

The  $\delta D$  values of both *n*-alkanes vary between  $-180$  and  $-155$  ‰. The  $\delta D$  isotopic signature of the  $C_{31}$  *n*-alkane is on average 19 ‰ heavier (enriched in Deuterium) than the isotopic signature of the  $C_{29}$  *n*-alkane. The isotopic signatures of the  $C_{29}$  *n*-alkanes between  $\sim 1350$  and  $\sim 800$  cal. a BP are significantly heavier ( $-164 \pm 7$  ‰), suggesting more precipitation, compared to the periods before ( $-178 \pm 4$  ‰) or after ( $-182 \pm 3$  ‰). The isotopic signatures of the  $C_{31}$  *n*-alkanes do not reflect this trend as clearly, however, the two most positive  $\delta D$  values are also found in that period.

5. New insights into Holocene climate evolution from high-resolution terrestrial and marine biomarker records from Northwest Iceland

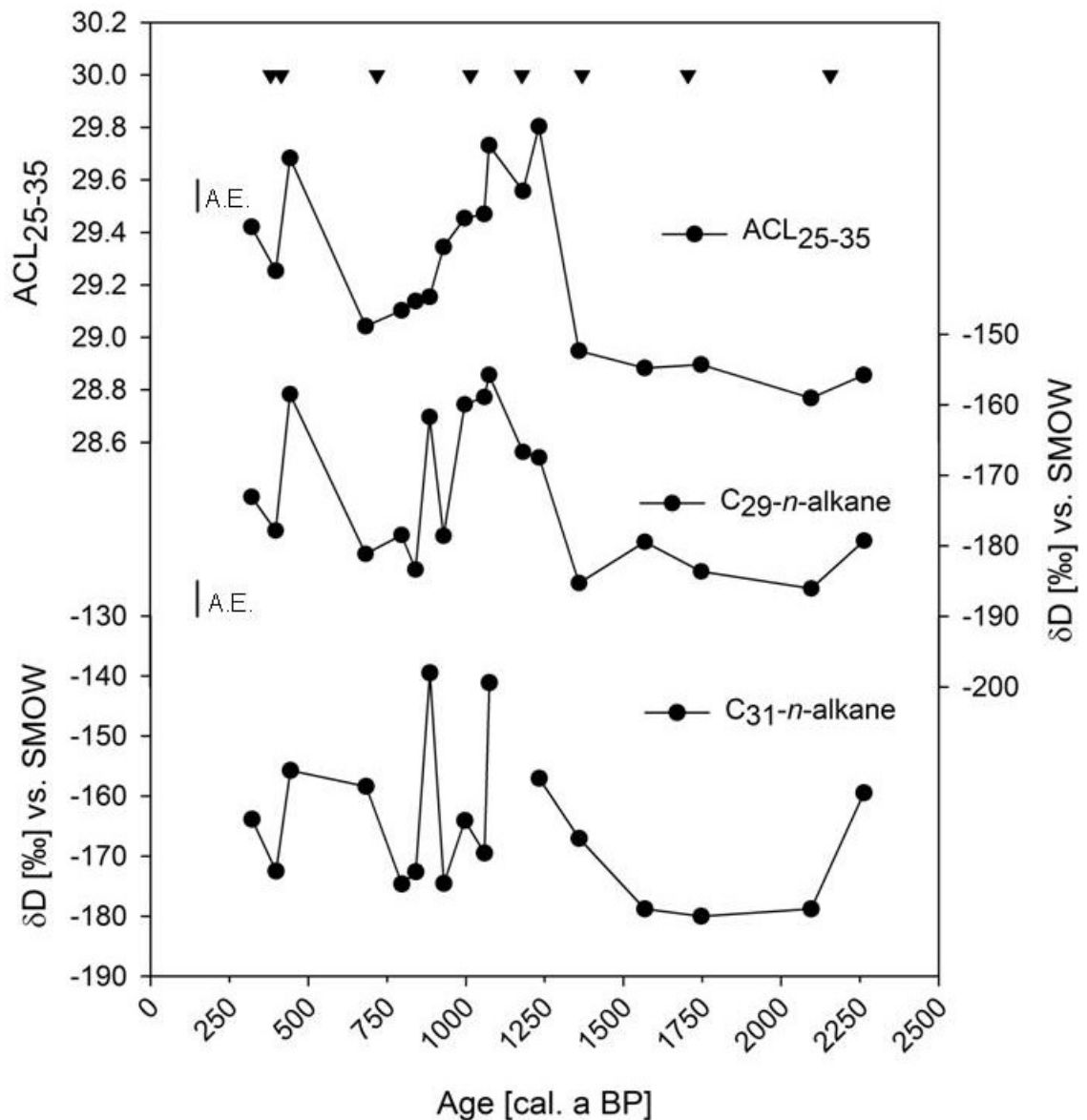


Figure 5.3: Hydrogen isotopic signature of the C<sub>29</sub> and C<sub>31</sub> n-alkanes plotted against ACL<sub>25-35</sub> values. The analytical error (1 $\sigma$ ) associated with the ACL<sub>25-35</sub> values is  $\pm 0.06$  (black vertical bar) and the analytical error (1 $\sigma$ ) associated with the  $\delta D$  measurements is within 5 ‰ (black vertical bar).

### 5.3.3 Bacterial Glycerol Dialkyl Glycerol Tetraethers (GDGTs)

The Holocene CBT/MBT MAT variability in Iceland plotted against summer insolation changes is shown in Figure 5.4. Previously, 2 °C mean air temperature changes have been interpreted using the CBT/MBT palaeothermometer (Weijers *et al.*, 2007b). The mean reconstructed Holocene air temperature throughout the

5. New insights into Holocene climate evolution from high-resolution terrestrial and marine biomarker records from Northwest Iceland

Holocene is 10.8 °C. The warmest MATs of around 18 °C are observed at ~ 9750 and ~ 9100 cal. a BP respectively, after an initial temperature rise. From 9100 cal. a BP temperatures continually decrease to just above 5°C at ~ 3000 ca. a BP. In the last 3000 years of the record the decreasing temperature trend stops, and temperatures vary around  $7.3 \pm 1.5$  °C.

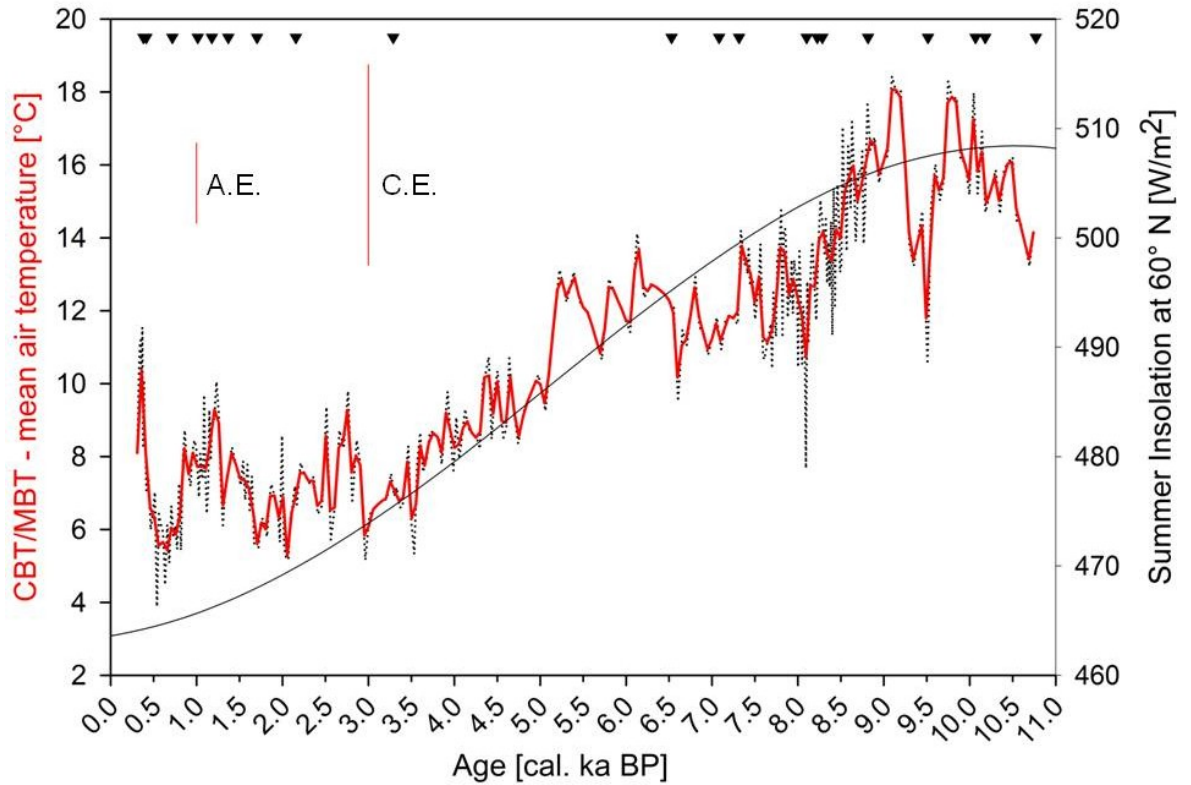


Figure 5.4: GDGT inferred Holocene mean air temperature variability plotted against summer insolation change at 60° N (black line; Laskar *et al.*, 2004). The dotted black line represents the raw data; the red line represents the 50 year moving average. The <sup>14</sup>C-AMS dated horizons of the sediment core are indicated by black triangles. The red vertical bars indicate the analytical error and the calibration error (+ or -) after Weijers *et al.* (2011a) associated with the CBT/MBT temperature calibration. The propagated error was not calculated because the raw dataset of the calibration equation published by Weijers *et al.* (2007c) was not available.

The reconstructed soil pH variability is shown in Figure 5.5. The observed pH changes are interpreted to indicate changing precipitation patterns. The reconstructed soil pH mean is  $8.6 \pm 0.2$  throughout the Holocene. The highest values are observed in the early Holocene until ~ 8000 cal. a BP. From ~ 8000 cal.

## 5. New insights into Holocene climate evolution from high-resolution terrestrial and marine biomarker records from Northwest Iceland

a BP until ~ 3900 ca. a BP the soil pH decreases. After ~ 3900 cal. a BP the soil pH values increase again.

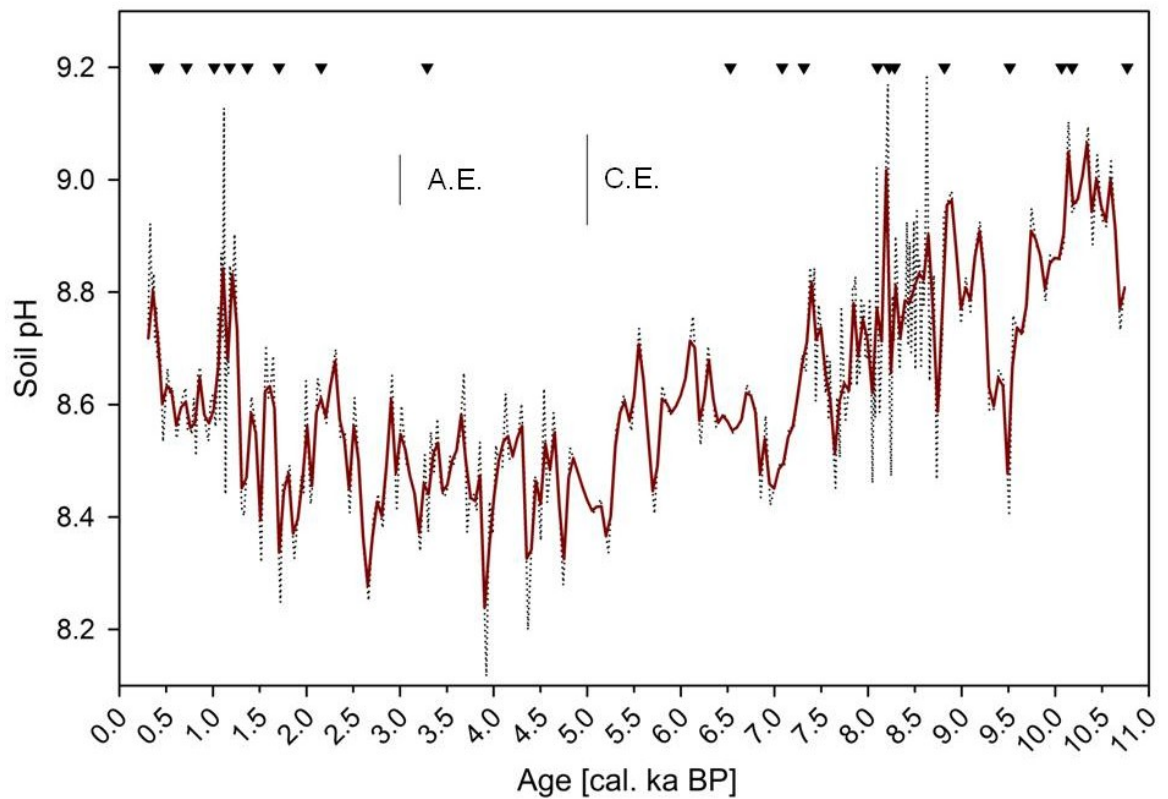


Figure 5.5: GDGT inferred Holocene soil pH variability. The dotted black line represents the raw data; the dark red line represents the 50 year moving average. The <sup>14</sup>C-AMS dated horizons of the sediment core are indicated by black triangles. The analytical error and the calibration error( + or -) are indicated by vertical black bars. The analytical error propagated through the calibration equation amounts to  $\pm 1.8$  pH units. The propagated error is not shown on the graph as it likely is an overestimated error because the calibration equation of the pH reconstruction is based on a global, rather than a local soil pH data set.

### 5.4 Discussion

#### 5.4.1 Sea surface temperatures

Analysis of alkenones from water column derived particulate organic matter (POM) show good correlation between the SST and  $U^{K'}_{37}$  in the area surrounding Iceland (Bendle & Rosell-Melé, 2004). Recent studies of alkenones in sediments of the North Icelandic Shelf have shown that the  $U^{K'}_{37}$  is a valid tool for palaeo-SST

studies in the area (Bendle & Rosell-Melé, 2007; Sicre *et al.*, 2008a). The  $U^{K'}_{37}$ -SSTs reported here tend to be higher compared to those reported previously (Bendle & Rosell-Melé, 2007; Sicre *et al.*, 2008a). Ísafjarðardjúp fjord is located on the northwest tip of Iceland and is more strongly influenced by the warm waters of the Irminger Current than the sites studied by Sicre *et al.* (2008a) and Bendle & Rosell-Melé (2007), which are situated on the North Icelandic Shelf. Another explanation for the higher SSTs is the proximity of the coring site to the land. A warm, radiation induced thermocline, reinforced by meltwater input into coastal waters in spring, prevails during the summer near the Icelandic coast (Hanna *et al.*, 2006). Alkenone producers may record the SST of this warm water layer, rather than the temperatures of the deeper water layers. Besides the oceanographic setting of the core having a possible effect on the alkenone derived SSTs, so does the timing of the alkenone production. As discussed by Sicre *et al.* (2008a), alkenone production in the area surrounding Iceland may be most prominent during the summer, analogous to the alkenone production of the Southern Ocean (Sikes *et al.*, 1997; Ternois *et al.*, 1998) and that of the Gulf of Alaska (Prahl *et al.*, 2010). Such a seasonal bias in the alkenone production would lead to the recording of warmer SSTs.

Furthermore, the  $U^{K'}_{37}$  palaeothermometer gives different temperatures, depending on which calibration equation is used. When using the global core top calibration equation published by Müller *et al.* (1998), the  $U^{K'}_{37}$ -SSTs are on average  $0.2 \pm 0.02$  °C warmer than those produced by the use of the calibration equation published by Conte *et al.* (2006).  $U^{K'}_{37}$ -SSTs obtained by using the calibration equation published by Rosell-Melé *et al.* (1995) are on average  $0.44 \pm 0.15$  °C cooler than those obtained by the use of the calibration equation of Conte *et al.* (2006). The standard error of the Conte *et al.* (2006) core top calibration is  $\pm 1.1$  °C and the standard error of the Müller *et al.* (1998) calibration equation is  $\pm 1.2$  °C. Thus the standard error of these calibrations is bigger than the difference in temperature when different calibration equations are used. Therefore, the physical differences between different coring sites, as discussed above, appear to be mainly responsible for the temperature differences of different coring

5. New insights into Holocene climate evolution from high-resolution terrestrial and marine biomarker records from Northwest Iceland

sites, and the use of different calibration equations does not affect the reported temperatures significantly.

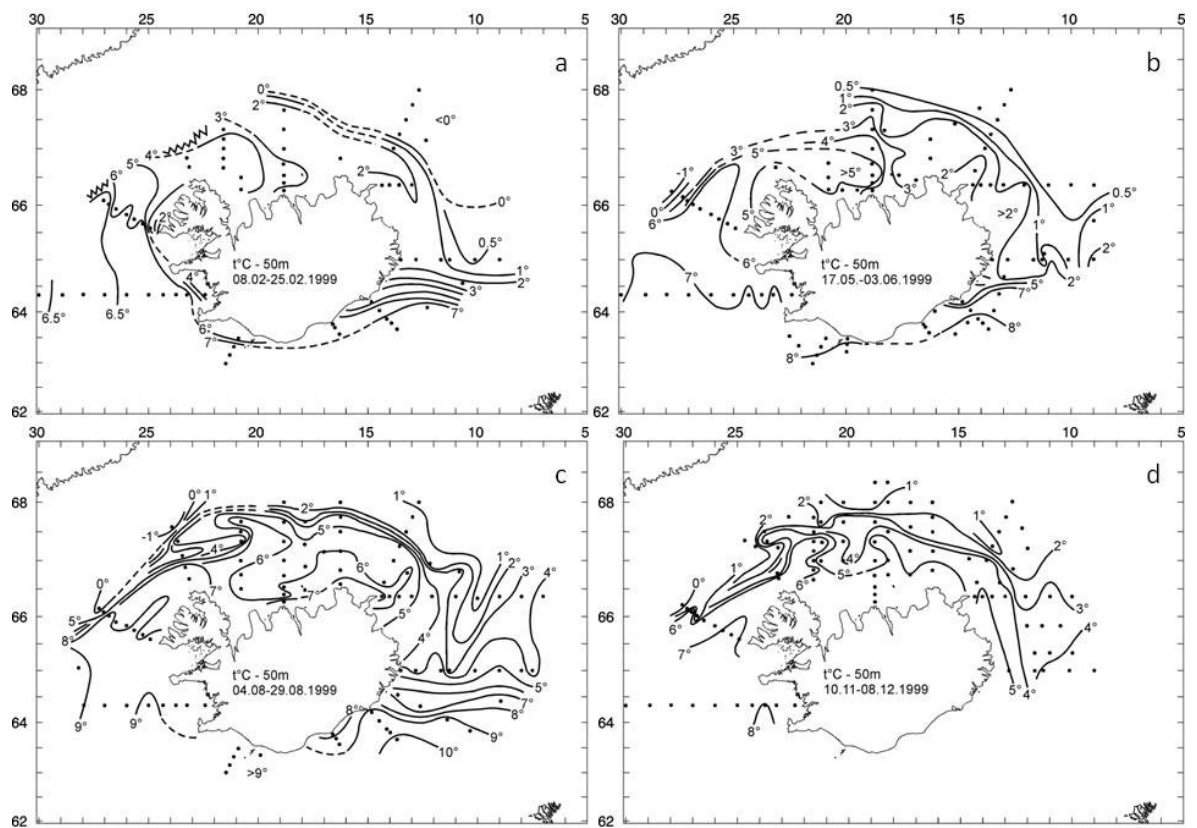


Figure 5.6: SST variations of Icelandic surface waters in 1999 in (a) February, (b) May-June, (c) August and (d) November-December. Source: <http://www.hafro.is/Sjora>

It is hypothesised, that the  $U^{K'}_{37}$ -SSTs shown in Figure 5.1 represent summer, rather than mean annual SSTs. Contemporary mean annual SSTs since 1869 have varied between 3 and 7 °C on the west coast of Iceland (Hanna *et al.*, 2006). The mean reconstructed SSTs of the youngest 100 years of the record (~ 400 - ~ 300 cal. a BP; n = 10) is 9.3 °C with a standard deviation of  $\pm 0.9$  °C. Figure 5.6 shows the seasonal SST variations around Iceland in 1999. SSTs varied near Vestfirðir Peninsular between 2°C in February and 9 °C in August. June to September SSTs between 1867 and 1985 have varied between 7.5 and 10.6 °C on the Icelandic west coast (Hanna *et al.*, 2006). Even though there is a hiatus of ~ 230 years between the end of the  $U^{K'}_{37}$ -SST record and the beginning of the instrumental record, the west coast Icelandic summer SSTs fit the youngest

reconstructed  $U^{K'}_{37}$ -SSTs better, than the mean annual SSTs do. Therefore it is suggested that the  $U^{K'}_{37}$ -SSTs reflects summer, rather than mean annual SSTs in this case.

#### **5.4.2 Air temperature and soil pH reconstruction**

The production of GDGT membrane lipids is linked to the metabolic activity of soil bacteria. It is, however, unclear whether temperature or another environmental variable such as nutrient transport controls the activity of soil bacteria. Weijers *et al.* (2011a) speculate, that long periods of darkness at high latitudes may control microbial activity indirectly via seasonal vegetation and nutrient variability. It is hypothesised that more branched GDGTs are produced on Vestfirðir Peninsula during the summer, when the soil is not frozen. Therefore, CBT/MBT reconstructed air temperatures should reflect summer temperatures.

Rueda *et al.* (2009) have shown that an air temperature reconstruction in the Skagerrak based on GDGTs, correlates with summer air temperatures throughout the last 200 years. A 2000 year temperature record reconstructing August air temperatures from east Iceland, based on chironomids, shows that temperatures have varied between 7 and 11 °C over that period (Axford *et al.*, 2009). The temperatures reconstructed in this study, covering the last 2000 years, show more variability, but are similar to those reconstructed by Axford *et al.* (2009). Mean June temperatures in Stykkisholmur (~ 50 km south of Vestfirðir Peninsula) have varied around  $8.2 \pm 0.9$  °C since 1878 (Hanna *et al.*, 2004). Even though there is a gap of ~ 230 years between the instrumental record and the youngest samples of the MAT record, which show temperature fluctuating between 8 and 11 °C, the similarity between the reconstructed temperatures and those of the instrumental record adds support to the statement that GDGT inferred air temperatures reflect summer rather than mean temperatures. Finally, a linear regression between summer insolation change at 60° North (Laskar *et al.*, 2004), and changing air temperatures throughout the Holocene is observed ( $n = 106$ ;  $r^2 = 0.79$ ; Figure 5.4). The regression suggests that GDGT inferred air temperature may have mainly been forced by changes in summer insolation throughout the Holocene. That,

along with the other evidence discussed above, indicates that GDGT inferred air temperatures represent summer rather than mean air temperatures.

Soil pH changes throughout the Holocene are shown in Figure 5.5. The main soil types found on Vestfirðir Peninsula today are andosols and to a lesser degree vitrisols (Arnalds & Gretarsson, 2001). There is some scattering of histosols around the coastline of the Peninsula. The soil pH of andosols ranges between 5.5 and 6.5, while that of vitrisols varies between 7 and 7.5 pH units (Arnalds, 2008). The lowest soil pH values are found in areas which are the furthest away from active volcanic zones such as the Vestfirðir Peninsula (Arnalds, 2008; references therein). The two Icelandic soil samples that were analysed by Weijers *et al.* (2007c), and form part of the global soil data set used to calibrate the CBT and MBT proxies, exhibit soil pH values varying between 6.5 and 3.4. The soil pH change reconstructed for the first 100 years (~ 400 to ~ 300 yr BP; n = 10) of the record varies around 8.8. This value is much higher than the values of Icelandic soils today. If the soil pH of today's soils is similar to the soil pH 300 years ago, then the pH reconstruction overestimates the absolute pH values of Icelandic soils throughout the Holocene. Results published by Peterse *et al.* (2010) support the hypothesis, as they have recently shown that soil pH reconstructions using the CBT ratio overestimate soil pH in soils with a pH lower than 5. The discrepancy between observed and reconstructed soil pH is as much as 1 pH unit where the measured soil pH is below 4.5 (Peterse *et al.*, 2010). A second reason for the overestimated soil pH values may be the possible contribution of branched GDGTs from a marine source (Fietz *et al.*, 2012, accepted for publication; Peterse *et al.*, 2009a). If marine bacteria produce different branched GDGTs in response to the oceanic pH in a similar way that soil bacteria respond to soil pH, then the contribution of marine sourced, branched GDGTs could cause soil pH estimates to be more basic. If such an offset exists, it is expected to be relatively constant and minor throughout the Holocene, because Hönisch and Hemming (2005) have shown that the surface ocean pH during the last four interglacial periods (including the current one) has varied less than ~ 0.1 pH units. Throughout the pre-industrial Holocene period, an ocean sourced GDGT induced offset in the soil pH estimates would therefore constitute a systematic error.

The absolute soil pH values are not interpreted here, because as previously discussed, the reconstructed soil pH is likely too alkaline. Furthermore, soil pH changes of at least 1 pH unit have previously been interpreted to show changing precipitation regimes (Fawcett *et al.*, 2011). The interpreted soil pH changes cover the last 560,000 years (Fawcett *et al.*, 2011), and it is likely that smaller precipitation changes observed throughout the Holocene elicit smaller responses in soil pH. In this study, coherent fluctuations in the soil pH estimates throughout the Holocene are observed and interpreted to indicate changes in precipitation. Alkaline reconstructed pH units are interpreted to coincide with drier periods, while more acidic reconstructed pH units are interpreted to indicate more precipitation.

#### **5.4.3 Precipitation change inferred from *n*-alkane average chain length variability**

The ACL<sub>25-35</sub> values reported in this study lie between 29.7 and 28.6. Similar ACL values to those reported in this study have previously been reported from dust samples along the West African coast and over the Pacific Ocean (Kawamura *et al.*, 2003; Schefuss *et al.*, 2003a), in plants from different biomes of west Africa (Vogts *et al.*, 2009), and in peat in southeast China (Zhou *et al.*, 2005). A lacustrine sediment core in England spanning the last 3500 years (Fisher *et al.*, 2003) and marine sediments from western Africa and from the Tasman Sea (Boot *et al.*, 2006; Calvo *et al.*, 2004) also exhibit ACL values similar to the values shown here. Variations of the *n*-alkane ACL<sub>25-35</sub> values throughout the Holocene are hypothesised to reflect changes in precipitation rather than temperature and/or vegetation change. Variations of ACL values have been attributed to temperature changes (Kawamura *et al.*, 2003; Simoneit *et al.*, 1991; Vogts *et al.*, 2009), different plants types (Cranwell, 1973; Fisher *et al.*, 2003; Rommerskirchen *et al.*, 2006), as well as precipitation variability (Calvo *et al.*, 2004; Schefuss *et al.*, 2003b; Zhou *et al.*, 2005).

A detailed pollen study encompassing the early and middle Holocene has been conducted on a sediment core from Lake Efstadalsvatn, which is located 10 km

south of Ísafjarðardjúp fjord (Caseldine *et al.*, 2003). The pollen record from 11,000 cal. a BP to 3700 cal. a BP shows that ~ 80% of the pollen are derived from land plants belonging to the families of Cyperaceae (sedges) and Poaceae (grasses) and some from the genera *Juniperus*, *Salix* and *Betula*. As there are no major shifts in the pollen distribution at Efstadalsvatn between 10,000 and 3700 cal. a BP, the leaf wax derived *n*-alkanes in the Ísafjarðardjúp sediments are assumed to derive mainly from Cyperaceae and Poaceae growing on Vestfirðir Peninsula. Therefore, the shift of the ACL<sub>25-35</sub> values between ~ 9800 and ~ 3900 cal. a BP (Figure 5.2) cannot be attributed solely to vegetation change, although it may have some influence on ACL<sub>25-35</sub> values. To the author's knowledge, no pollen data exists for the Vestfirðir Peninsula covering the last 3700 years BP. The pollen record of Efstadalsvatn is the only record of this type on the Vestfirðir Peninsula. Since it does not cover the late part of the Holocene (present - 3700 cal. a BP) the variations of *n*-alkane chain length during that period are not compared with pollen data. Variations of ACL<sub>25-35</sub> values with pollen records from other parts of Iceland are not compared, as there are significant differences in the pollen records. For example, pollen records from the Troellaskagi Peninsula, west of Vestfirðir Peninsula show, that *Betula* pollen make up more than 30 % of the total pollen concentration from ~ 9500 cal. a BP (Caseldine *et al.*, 2006; Langdon *et al.*, 2010), whereas *Betula* pollen are not a major component of the pollen signature of Efstadalsvatn, barely reaching abundances higher than 20 % from ~ 7000 cal. a BP. Caseldine *et al.* (2003) report that the dwarf-shrub dominated vegetation on the northwest Peninsula of Iceland seems to be very robust and resistant to changes in climate. A possible mechanism explaining the robustness of the vegetation may then be the constitutional changes of the leaf waxes in order to adapt to changes in temperature or aridity. Therefore, Holocene *n*-alkane ACL<sub>25-35</sub> variability is interpreted as a signal for paleoclimate variations rather than vegetation dynamics.

Another environmental driver that is thought to have an influence on *n*-alkane ACL<sub>25-35</sub> values is ambient growing season temperature. However, no significant linear regression between the reconstructed MAT (Figure 5.4), and the ACL<sub>25-35</sub> record (Figure 5.2) is observed in this study. This suggests that ACL<sub>25-35</sub> variability

5. New insights into Holocene climate evolution from high-resolution terrestrial and marine biomarker records from Northwest Iceland

is not controlled by air temperature. Furthermore, where ACL values have been interpreted as a proxy for temperature in the literature, high ACL values have been associated with high temperatures (Kawamura & Ishimura, 2003; Simoneit *et al.*, 1991; Vogts *et al.*, 2009). A visual comparison of the Icelandic MAT (Figure 5.4) and  $ACL_{25-35}$  (Figure 5.2) records reveals that in the last 3500 years of the Holocene,  $ACL_{25-35}$  values are as high as in the early Holocene, whereas MATs are nearly 10 °C lower (Figure 5.7). Therefore, the relationship between high ACL values and high air temperatures is not consistent throughout the record.

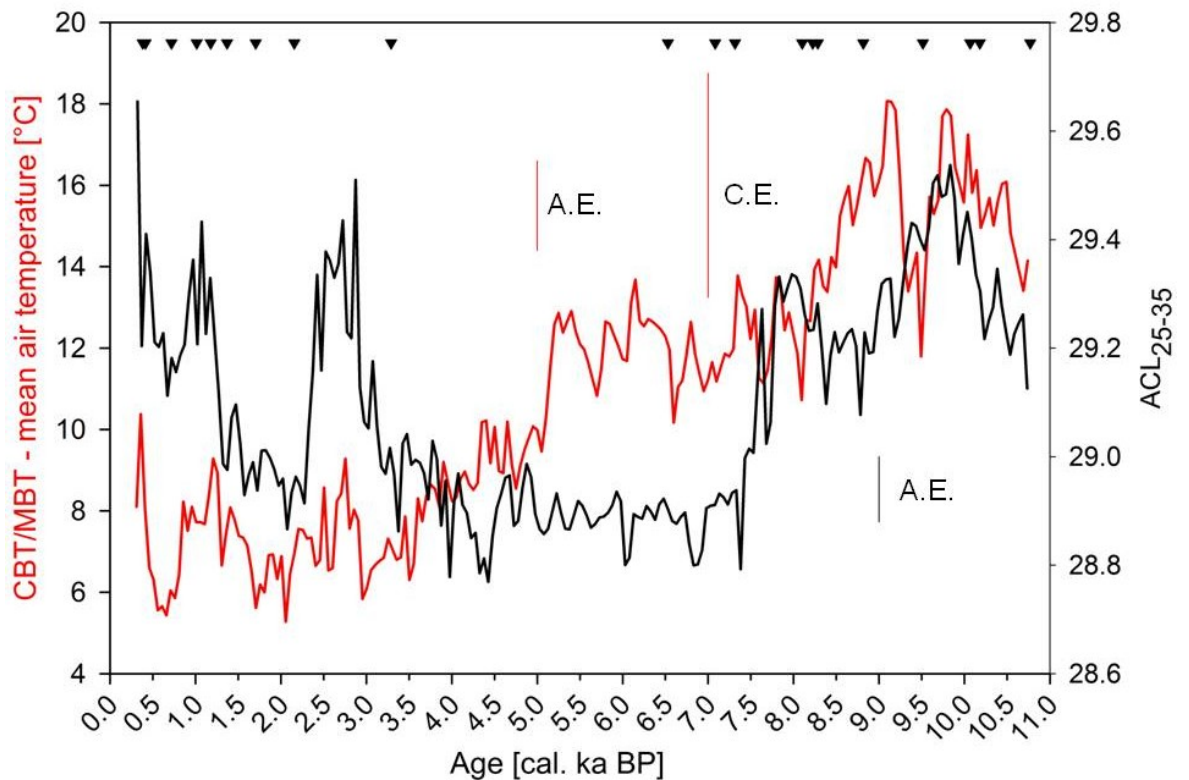


Figure 5.7: MBT/CBT mean air temperature reconstruction vs.  $ACL_{25-35}$  variability throughout the Holocene. The red vertical bars indicate the analytical error and the calibration error (+ or -) of the CBT/MBT calibration equation (Weijers *et al.*, 2011a). The propagated error associated with the CBT/MBT ratio was not calculated because the raw dataset of the calibration equation published by Weijers *et al.* (2007c) was not available. The black vertical bar indicates the analytical error associated with the  $ACL_{25-35}$  reconstructions. The black triangles indicate the  $^{14}\text{C}$ -AMS dated sediment horizons.

The previous discussion has shown that neither temperature nor vegetation change are the main factors forcing changes in  $ACL_{25-35}$  values, leaving precipitation change as the main factor driving  $ACL_{25-35}$  variability throughout the Holocene in the studied area. Decreasing  $ACL_{25-35}$  values have been associated with an increase in precipitation (Calvo *et al.*, 2004; Schefuss *et al.*, 2003b; Zhou *et al.*, 2005). Thus it is hypothesised that changes of *n*-alkane  $ACL_{25-35}$  values throughout the Holocene indicated precipitation change.

The hydrogen isotopic variability of the  $C_{29}$  *n*-alkane indicates precipitation variability throughout the late Holocene (Figure 5.3). Sauer *et al.* (2001) have shown that the  $\delta D$  signature of lipid biomarkers changes with the isotopic composition of source water of the organisms producing the biomarkers. More recently it has been shown that the isotopic signature of terrestrial leaf wax *n*-alkanes records precipitation changes (Sachse *et al.*, 2006; Smith & Freeman, 2006). The relationship between the hydrogen isotopic signature of lipid biomarkers, and changes in the supply of water to the plants has been used to reconstruct Holocene aridity changes in West Africa and in the North-eastern United States (Schefuss *et al.*, 2005; Shuman *et al.*, 2006). The linear regression ( $r^2 = 0.64$ ) between the  $\delta D$  values of the  $C_{29}$  *n*-alkane of 18 samples and the corresponding  $ACL_{25-35}$  values (Figure 5.3) implies that the Holocene  $ACL_{25-35}$  variability reflect precipitation change.

Further evidence for this hypothesis comes from the comparison of the  $ACL_{25-35}$  values (Figure 5.2) with the reconstructed changes in soil pH (Figure 5.5). Long-term changes in the aridity regime are thought to be reflected in soil pH changes, as higher precipitation causes increased soil acidification through soil leaching processes (Johnson *et al.*, 1998). Using GDGT inferred changes in soil pH, changes in the precipitation regime have been reconstructed for the past 550 ka in the southwestern United States (Fawcett *et al.*, 2011), and throughout the Holocene in West Africa (Weijers *et al.*, 2007a). In this study the  $ACL_{25-35}$  and the soil pH record show the same long-term trends throughout the Holocene, where high  $ACL_{25-35}$  values correspond to a more basic soil pH. To better illustrate the

5. New insights into Holocene climate evolution from high-resolution terrestrial and marine biomarker records from Northwest Iceland

relationship between  $ACL_{25-35}$  and soil pH, both datasets were normalised and the mean, as well as, the standard deviation of both datasets was calculated. Figure 5.8 shows the mean precipitation variability around the mean precipitation state of the Holocene and the resultant uncertainty (standard deviation) when combining the dataset. Both datasets show similar long-term trends throughout the Holocene. Figure 5.8 shows that the early Holocene is characterised by dryer conditions relative to the mean precipitation of the Holocene. The middle Holocene is characterised by more precipitation than the mean, while the precipitation regime of the late Holocene varies around the mean Holocene precipitation. The fact that the  $ACL_{25-35}$  and the soil pH records show similar long term trends further corroborates the hypothesis that  $ACL_{25-35}$  values in the studied area reflect precipitation change.

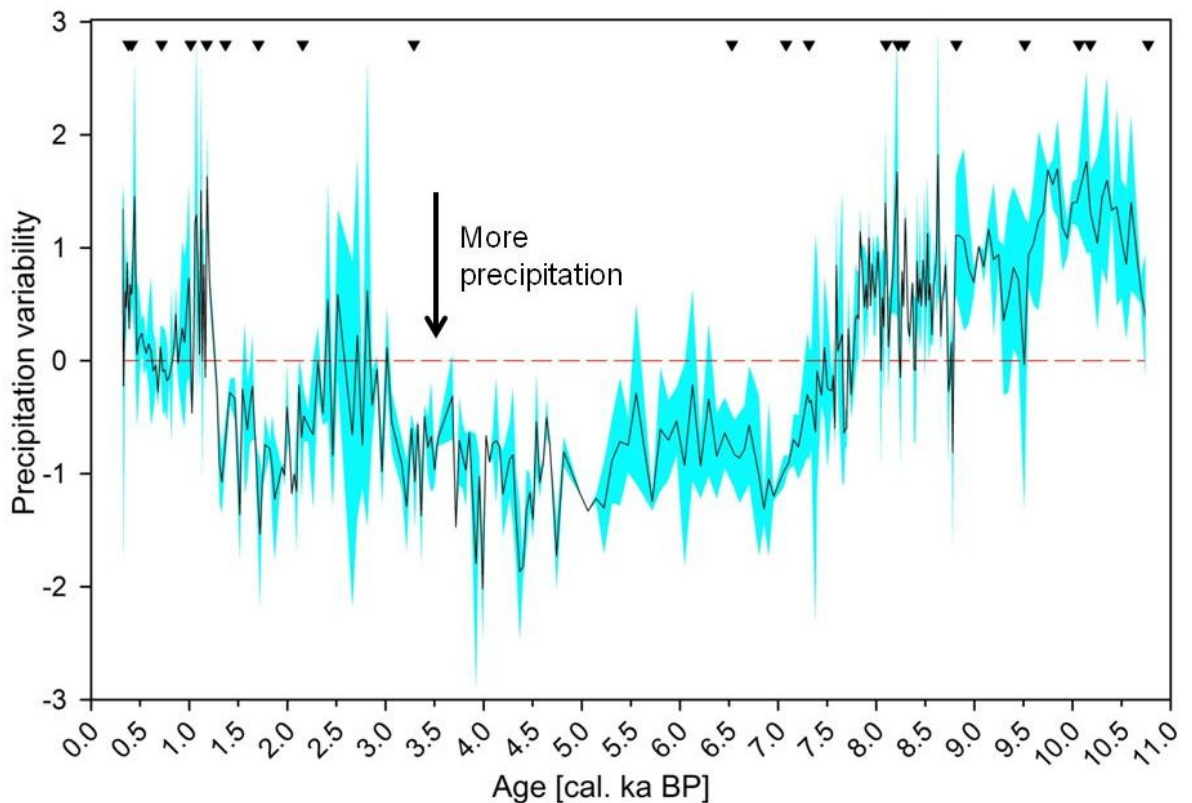
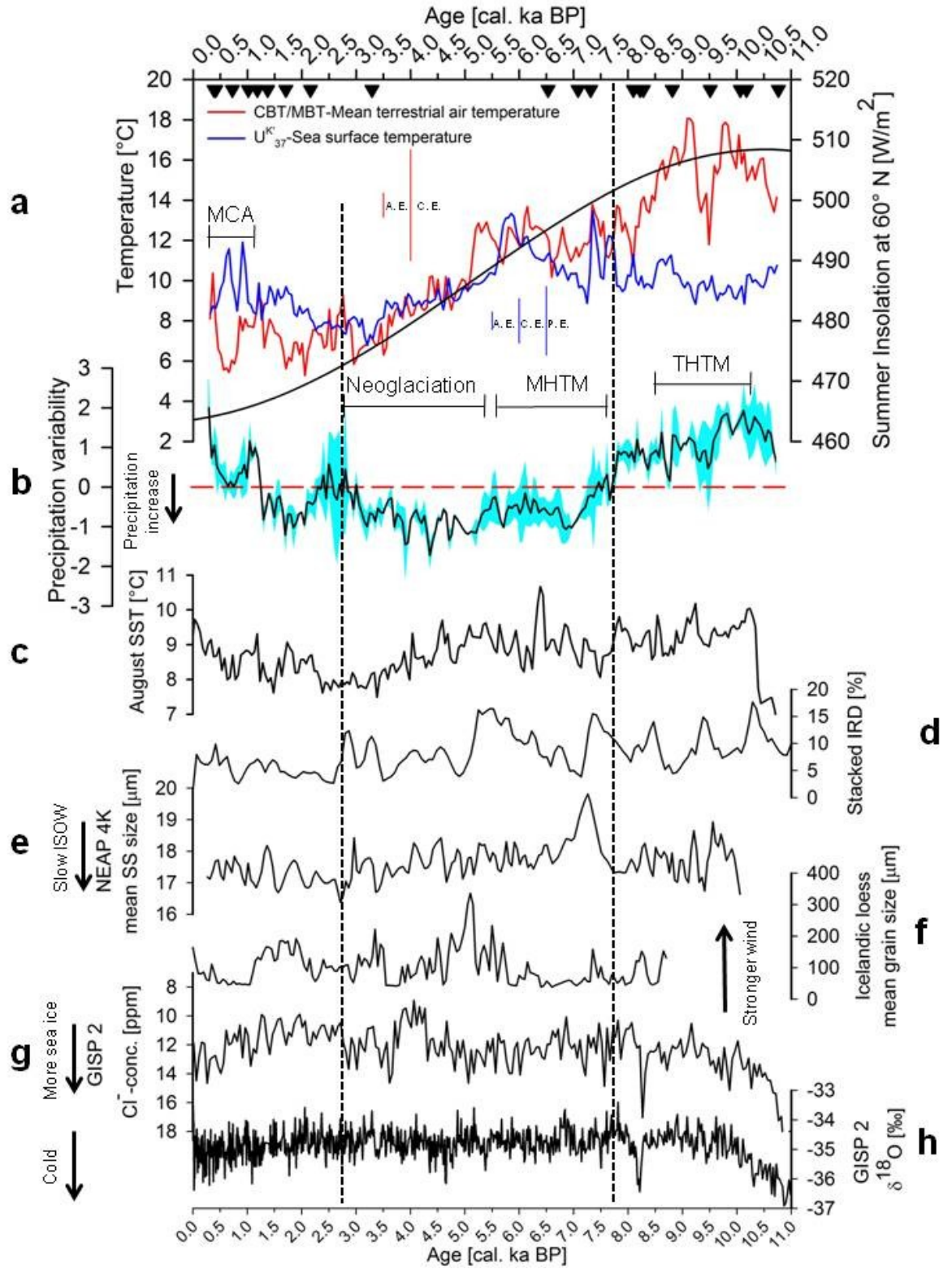


Figure 5.8: Holocene precipitation variability (black line) around the mean state (dashed red line) and the uncertainty (turquoise area) arising from combining the normalised  $ACL_{25-35}$  and soil pH datasets. The black triangles indicated the  $^{14}C$ -AMS dated sediment horizons of core MD99-2266.

#### **5.4.4 Palaeoclimate reconstruction**

Figure 5.9 shows the reconstructed SSTs and MATs plotted against summer insolation, and the precipitation variability throughout the Holocene. Furthermore, it compares the terrestrial and marine palaeoclimatic records with other North Atlantic palaeoclimate records. In the early Holocene, from ~ 10,800 to ~ 7700 cal. a BP, the MAT and SST records are divergent and precipitation is less than the mean Holocene precipitation. From ~ 7700 to ~ 2900 cal. a BP the MAT and SST records converge while precipitation increases and stays higher than the mean Holocene precipitation. During the late Holocene from ~ 2900 to ~ 300 cal. a BP, the MAT and SST records diverge again, while the precipitation regime becomes more variable and fluctuates around the mean. The combined dataset shows two major climatic shifts throughout the Holocene, one at ~ 7700 and one at ~ 2900 cal. a BP. Based on these shifts, the Holocene is divided into three periods, the early Holocene (10,800 - 7700 cal. a BP), the middle Holocene (7700 - 2900 cal. a BP) and the late Holocene (2900 - 300 cal. a BP).

5. New insights into Holocene climate evolution from high-resolution terrestrial and marine biomarker records from Northwest Iceland



## 5. New insights into Holocene climate evolution from high-resolution terrestrial and marine biomarker records from Northwest Iceland

Figure 5.9: Holocene terrestrial and marine palaeoclimate series (previous page). The horizontal dashed lines indicate major shifts in the Holocene climate pattern (as seen in the datasets analysed in this study (a and b)). (a) Mean terrestrial air (50 a moving average; red line) and sea surface temperatures (50 a moving average; blue line), plotted against summer insolation change at 60 °N (Laskar *et al.*, 2004). The blue vertical lines indicate the  $U_{37}^K$ -SST analytical, calibration (Conte *et al.*, 2006) and propagated errors. The red vertical lines indicate the analytical error and the calibration error (+ or -) of the CBT/MBT air temperature proxy (Weijers *et al.*, 2011a). The propagated error was not calculated because the raw dataset of the calibration equation published by Weijers *et al.* (2007c) was not available. Black triangles indicated  $^{14}\text{C}$ -AMS dated sediment horizons of core MD99-2266. (b) Holocene precipitation divergence (black line) from the mean state (dashed red line) and uncertainty (turquoise area) arising from the combination of the normalised  $\text{ACL}_{25-35}$  and soil pH datasets (this study). (c) August SSTs based on Diatom assemblages (50 a running average; Justwan *et al.*, 2008). (d) Record of ice rafted debris (IRD) indicating periods (1500 a cyclicity) of enhanced drift ice (Bond *et al.*, 2001). (e) Variations in the speed of the Iceland-Scotland-Overflow-Water (ISOW) south of Iceland linked to the speed of the Meridional overturning circulation (MOC; 50 a running average); the 2700 year event marks a dramatic slowdown of the ISOW (Hall *et al.*, 2004). (f) Mean grain size variations indicate periods of increased windiness in Iceland (50 a running average; Jackson *et al.*, 2005). (g) North Atlantic sea-ice extent inferred from the GISP 2  $\text{Cl}^-$  record (50 a running average; Mayewski & White, 2002). (h) GISP 2 oxygen isotope inferred temperature variations of the North Atlantic sector (Grootes & Stuiver, 1997). The medieval climate anomaly (MCA), neoglaciation, marine (MHTM) and terrestrial Holocene thermal maxima (THTM) are indicated as observed in the datasets a, b and c.

### 5.4.4.1 Early Holocene (10,800 - 7700 cal. a BP)

After initially decreasing, SSTs start to slowly increase from ~ 10,100 cal. a BP. The timing of the SST increase coincides with the establishment of the Irminger Current at 10,200 cal. a BP in the northern Denmark Strait, off of the coast of Vestfirðir Peninsular (Ólafsdóttir *et al.*, 2010). Eiriksson *et al.* (2000) report a strengthening of the palaeo Irminger Current just before the deposition of the Saksunarvatn tephra, that is deposited in core MD99-2266 at ~ 10,180 cal. a BP (Figure 3.2). The timing of its deposition coincides with a SST increase. The evidence points towards the initial temperature rise to be forced by the establishment and strengthening of the IC transporting warm Atlantic water into the Denmark Strait. Changes in coccolithophore assemblages from sediments south of Iceland record a temperature increase at this time, that has been

associated with a retreat of the polar front (Giraudeau *et al.*, 2000), supporting the hypothesis presented here.

The MAT initially increases and reaches a plateau between ~ 10,500 and ~ 8500 cal. a BP. Chironomide based temperature reconstructions from northern Iceland show that mean July temperatures continually increased from ~ 10,800 and the ~ 9400 cal. a BP (Caseldine *et al.*, 2003; Langdon *et al.*, 2010), which is in agreement with the data shown here. Studies of vegetation expanse indicate that the highest terrestrial temperatures occurred later compared to the MAT record. The highest elevation of the tree line was reached between ~ 7500 and ~ 6800 cal. a BP in central north Iceland (Wastl *et al.*, 2001). Pollen studies show that the expansion of vegetation on Iceland had reached its maximum during that same period (Caseldine *et al.*, 2003; Hallsdottir, 1995). The terrestrial Holocene thermal maximum (THTM) occurs earlier than the marine Holocene thermal maximum (MHTM) which takes place in the early middle Holocene as indicated by the SST record (Figure 5.9). Caseldine *et al.* (2003) point out that the expansion of vegetation was not uniform throughout Iceland. The arrival of tree birch for example, was very late in northwest Iceland. The time lag between the THTM indicated by the MAT record and the vegetation expansion studies may therefore be due to the time it takes for the expansion and succession of vegetation into certain areas.

GDGT reconstructed MATs are coherent with summer insolation throughout the early and middle Holocene. Furthermore, the MATs are continually higher than the SSTs during the early Holocene. This offset suggests that SSTs in the Denmark Strait were not only forced by summer insolation during the early Holocene. Indeed,  $\delta^{18}\text{O}$  isotopic data from Foraminifera assemblages show that meltwater events affected the waters of the Denmark Strait throughout the early Holocene until ~ 7900 cal. a BP (Ólafsdóttir *et al.*, 2010; Quillmann *et al.*, 2010). The occurrence of these meltwater events, causing lowered SSTs, coincides with the maximum retreat of the Laurentide ice sheet, but local glaciers on Iceland itself may also have contributed meltwater to Ísafjarðardjúp fjord (Dyke *et al.*, 2002; Geirsdóttir *et al.*, 2009). Cooler SSTs are recorded between ~ 8500 and ~ 7800

cal. a BP, and colder conditions have also been observed in other marine archives surrounding Iceland (Giraudeau *et al.*, 2000; Jennings *et al.*, 2011; Knudsen *et al.*, 2004). The MAT record shows a 3 °C temperature drop between ~ 8300 and ~ 8100 cal. a BP. These temperature excursions observed in the MAT and SST records may indicate the 8.2 ka event, a prominent meltwater event with widely felt consequences in the northern hemisphere surrounding the North Atlantic (Alley & Ágústsdóttir, 2005). Bendle and Rosell-Melé (2007) suggest that the influence of the north Icelandic Irminger Current dampened the impact of the 8.2 event on the north Icelandic Shelf, and therefore its palpability within palaeoclimate archives. According to this rationale, the 8.2 event would not exert a pronounced influence on the west coast of Iceland, where the warm Irminger current dominates, and therefore it does not leave a distinct imprint on the SST and the MAT records of Ísafjarðardjúp fjord, compared to the Greenland ice sheet records (Figure 5.9).

Another explanation for the SST variability during the early Holocene may be a lateral movement of the polar front (PF) across the Denmark Strait causing alternating currents, the warm Irminger Current and the cold East Greenland Current to affect the coring site. This scenario is supported by Ólafsdóttir *et al.* (2010) who have shown that the Denmark Strait just north of the MD99-2266 coring site was strongly affected by the polar front. Between 9500 and 6500 cal. a BP warm variable SSTs have been reported in the Denmark Strait close to Greenland, and have been attributed to the variable influence of the Irminger Current vs. the East Greenland Current (Andersen *et al.*, 2004) However, other studies show that the polar front retreated further northward from the North Icelandic Shelf coinciding with a strengthening of the Irminger current (Justwan *et al.*, 2008; Koc *et al.*, 1993), suggesting that the influence of cold polar waters may not have been very significant in the early Holocene in Ísafjarðardjúp fjord.

#### 5.4.4.2 Middle Holocene (7700 - 2900 cal. a BP)

The transition from the early to the middle Holocene is characterised by a major climatic shift which was caused by the cessation of meltwater events. The

warmest SSTs of the Holocene in this study are recorded between 7700 and 6000 cal. a BP indicating the MHTM. Diatom derived August SSTs on the North Icelandic Shelf peaked at ~ 6400 cal. a BP (Justwan *et al.*, 2008; Figure 5.8). High percentages of subarctic foraminifera species in the sediment core point to the HTM starting at 8000 cal. a BP and lasting until 5700 cal. a BP (Quillmann *et al.*, 2010). South of Iceland changes in coccolithophore assemblages occur at 6500 cal. a BP and infer high SSTs (Giraudeau *et al.*, 2000). Oxygen isotope records from sediment cores located on the North Icelandic Shelf place the start of the HTM at 7800 cal. a BP and its end at 6200 cal. a BP (Castañeda *et al.*, 2004). The timing of the MHTM coincides with the end of meltwater events influencing the marine environment in the area. The temporal divergence between the terrestrial and the marine Holocene thermal maximum is therefore explained by different response rates of the marine and terrestrial environments to insolation forcing as has been suggested previously (Imbrie *et al.*, 1992). Furthermore, the temporal divergence between the MHTM and the THTM may explain the large uncertainties associated with the onset ( $8.6 \pm 1.6$  ka) and the end ( $5.4 \pm 1.4$  ka) of the HTM in the region around Greenland and Iceland as reported by Kaufman *et al.* (2004).

As the meltwater influence on the SSTs ceases and the decreasing summer insolation forces the MATs to drop, the air- and sea temperature records converge at the onset of the middle Holocene. Subsequently, both records show decreasing temperatures in step with decreasing summer insolation from ~ 6000 cal. a BP until the onset of the late Holocene ~ 2900 cal. a BP ago. The decreasing sea surface temperatures after 6000 cal. a BP herald the neoglaciation period which is observed in a number of marine records. The timing of the onset of the Neoglaciation is confirmed by a transition towards colder bottom water temperatures in the Denmark Strait inferred from changes in foraminiferal assemblages just after 6000 cal. a BP (Ólafsdóttir *et al.*, 2010). Based on the  $U^{K}_{37}$  proxy, a SST drop between ca. 5500 to 2500 cal. a BP, has been reported 1350 km west of Ísafjarðardjúp fjord, in the Norwegian Sea (Calvo *et al.*, 2002; Moros *et al.*, 2004). Corresponding SST drops north of Iceland and in the Greenland basin, along with a return to more Arctic conditions off of northwest Iceland have been observed by studying changes in diatom assemblages and their  $\delta^{18}O$  record (Koc

& Jansen, 1994; Koc *et al.*, 1993). Jennings *et al.* (2002) infer an onset of cold conditions at 4.7 ka BP from carbonate flux peaks indicating IRD in sediments off of west Greenland. They observe an advancing of the polar front coinciding with a strengthening east Greenland current.

The neoglacial cooling is thought to have been forced by decreasing summer insolation in the northern hemisphere (Calvo *et al.*, 2002; Jennings *et al.*, 2002). The close correlation between the reconstructed MATs, the  $U^{K'}_{37}$ -SSTs, and summer insolation confirms that decreasing insolation drove the air and SST decrease throughout the middle Holocene. Changes in the strength of the Irminger Current offer a second explanation for the link between decreasing  $U^{K'}_{37}$ -SSTs and summer insolation change. The decrease in northern hemisphere insolation may have caused the flux of cold bottom water from the polar North Atlantic towards the equator to slow down, due to increasing sea-ice cover in the Arctic (Hoogakker *et al.*, 2011, and references therein). The slowdown of deep water formation is associated with a slowing down of the Atlantic meridional overturning circulation (AMOC; Bianchi & McCave, 1999; Hall *et al.*, 2004; Hoogakker *et al.*, 2011). The Irminger Current constitutes an end member branch of the AMOC. A slowdown of the AMOC could have been the cause for the influence of the IC to decrease in the Denmark Strait, giving way for the east Greenland current to penetrate further south, and causing SSTs to decrease further. This interpretation is supported by models showing decreasing AMOC from 9000 years BP to the present day (Renssen *et al.*, 2005).

#### 5.4.4.3 Late Holocene (2900 - 300 cal. a BP)

The lowest SSTs are observed at the end of the neoglacial period. The deteriorated climate conditions between ~ 2500 and ~ 3500 cal. a BP are evident in a number of different marine and terrestrial records. The last major glacial advance on the east Vestfirðir Peninsular before the Little Ice Age glacial advances is recorded at ~2600 cal. a BP (Principato, 2008). Further evidence for a downturn of climate comes from a pollen study. Wastl *et al.* (2001) observe the

smallest amount of *Betula pubescens* pollen in a sediment core from the Trollaskagi Peninsular in northern Iceland at 3300 <sup>14</sup>C years BP (~3550 cal. a BP). Marine paleoclimate records offer a more comprehensive host of evidence for the climatic low point in the Holocene ~ 3000 years ago. SSTs reconstructions from the north Icelandic Shelf (Bendle & Rosell-Melé, 2007; Justwan *et al.*, 2008; Figure 5.8) and from a core west of Norway (Calvo *et al.*, 2002) indicate cooling North Atlantic surface waters. Furthermore, increased sea-ice cover and increased amounts of drift ice have been observed in Greenland ice core records (Mayewski & White, 2002), and in North Atlantic sediment cores (Bond *et al.*, 2001), respectively (Figure 5.9). The low SSTs in the Denmark Strait and on the north Icelandic Shelf corroborate low Atlantic water inflow through the Denmark Strait into the Nordic Seas as observed from coccolithophore assemblages (Giraudeau *et al.*, 2010). The decreased penetration of warm Atlantic waters into the Denmark Strait correlates with the “2700 cal. a BP event” observed by Hall *et al.* (2004), indicating a dramatic slowdown of the Iceland-Scotland-Overflow-Water (ISOW). The velocity of the ISOW waters is associated with the speed of the Atlantic Meridional Overturning Circulation (AMOC), which transports warm water from the tropical Atlantic to the Nordic Seas (Bianchi & McCave, 1999; Bryden *et al.*, 2005; Hall *et al.*, 2004; Hoogakker *et al.*, 2011).

At the onset of the late Holocene (~ 2900 cal. a BP), both the MAT, and the SST record are decoupled from the summer insolation decrease indicating the second major climatic shift of the Holocene (Figure 5.9). As summer insolation continues to decrease, such a trend is not evident from the MAT record, and the SSTs show an increasing temperature trend. Bendle and Rosell-Melé (2007), and Justwan *et al.* (2008) also observe a SST increase from ~3000 cal. a BP. Therefore, insolation change cannot have been the major forcing factor affecting MATs and SSTs in the late Holocene. The decoupling of MAT and SST from the continued summer insolation decrease coincides with velocity increase of the ISOW waters following the 2700 cal. a BP event (Hall *et al.*, 2004). It is suggested, that the heat transport mediated by the AMOC (Bryden *et al.*, 2005), became more important for the Icelandic climate than summer insolation during the late Holocene, causing air and sea temperature to stay high, even though insolation continued to decrease.

#### **5.4.5 Climatic variability linked to the North Atlantic Oscillation**

The observed variability in precipitation in Iceland throughout the Holocene (Figure 5.9), may be related to fluctuations of the North Atlantic Oscillation (NAO). Figure 5.10 shows the influence of the NAO on the North Atlantic region and Iceland. Contemporary observations show, that in periods where the NAO is in its positive mode (NAO+), the strength of the westerlies is increased, and their trajectories acquire a more northerly direction, compared to periods when the NAO is in its negative mode (NAO-). These westerlies carry more precipitation towards Iceland (Hurrell, 1995; Hurrell & Deser, 2009; Hurrell *et al.*, 2003). The NAO also affects surface ocean currents around Iceland, and SSTs in the Denmark Strait (Blindheim *et al.*, 2000; Hurrell & Deser, 2009). Blindheim *et al.* (2002) have identified a link between different NAO modes and the mean sea level pressure (MSLP) gradient in the Denmark Strait. A high MSLP gradient between Iceland and Greenland is associated with prevailing northerly winds, which cause the influence of Atlantic water in the Denmark Strait to decrease (Blindheim & Malmberg, 2002). Furthermore, a high MSLP gradient coincides with cold conditions north of Iceland, and also with a low NAO index (Blindheim & Malmberg, 2002). Blindheim *et al.* (2002) have demonstrated that MSLP variations show an inverse correlation with sea surface temperature variations delayed by one year. Other studies have linked fluctuations of atmospheric conditions to fluctuations in SSTs with a three month-delay northeast of Iceland (Stefansson & Gudmundsson, 1969).

5. New insights into Holocene climate evolution from high-resolution terrestrial and marine biomarker records from Northwest Iceland

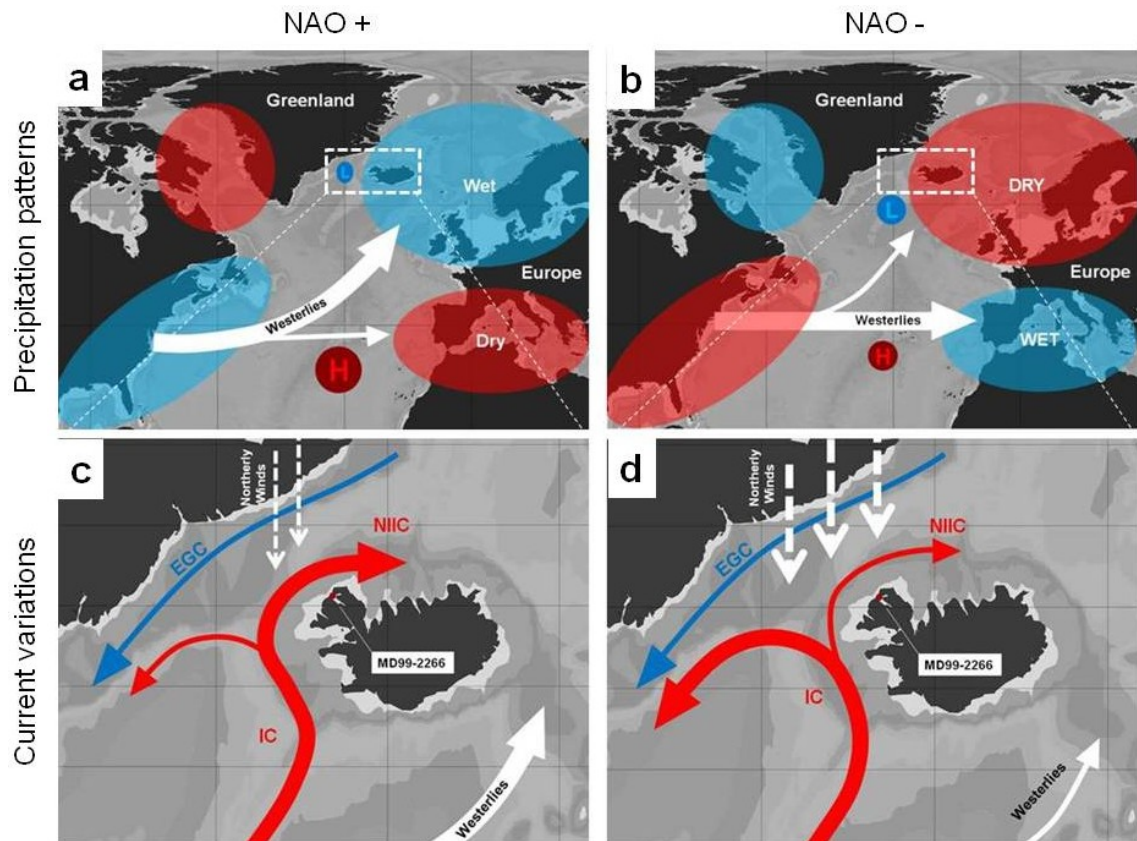


Figure 5.10: Present day NAO influenced precipitation and current patterns. Northern Europe and Iceland receive more precipitation during NAO+ phases (a), and less precipitation during NAO-phases (b; Hurrell, 1995; precipitation patterns after: <http://www.ideo.columbia.edu/res/pi/NAO>; Hurrell *et al.*, 2003). NAO+ phases coincide with an increased Atlantic water influence on the North Icelandic Shelf and in the Denmark Strait, and decreased prevalence of northerly winds (c); NAO-phases correlate with less Atlantic water influence in the Denmark Strait, and increased prevalence of northerly winds (Blindheim & Malmberg, 2005). Source of map: (Schlitzer, 2010).

If the interconnections between the NAO, precipitation variability and SST that have been observed in the instrumental record, have existed further back in time, high precipitation, brought by strong westerlies, and high SSTs, during periods where the NAO prevails in its positive mode, and lower precipitation and low SSTs during periods where the NAO prevails in its negative mode, are expected to be observed.

5. New insights into Holocene climate evolution from high-resolution terrestrial and marine biomarker records from Northwest Iceland

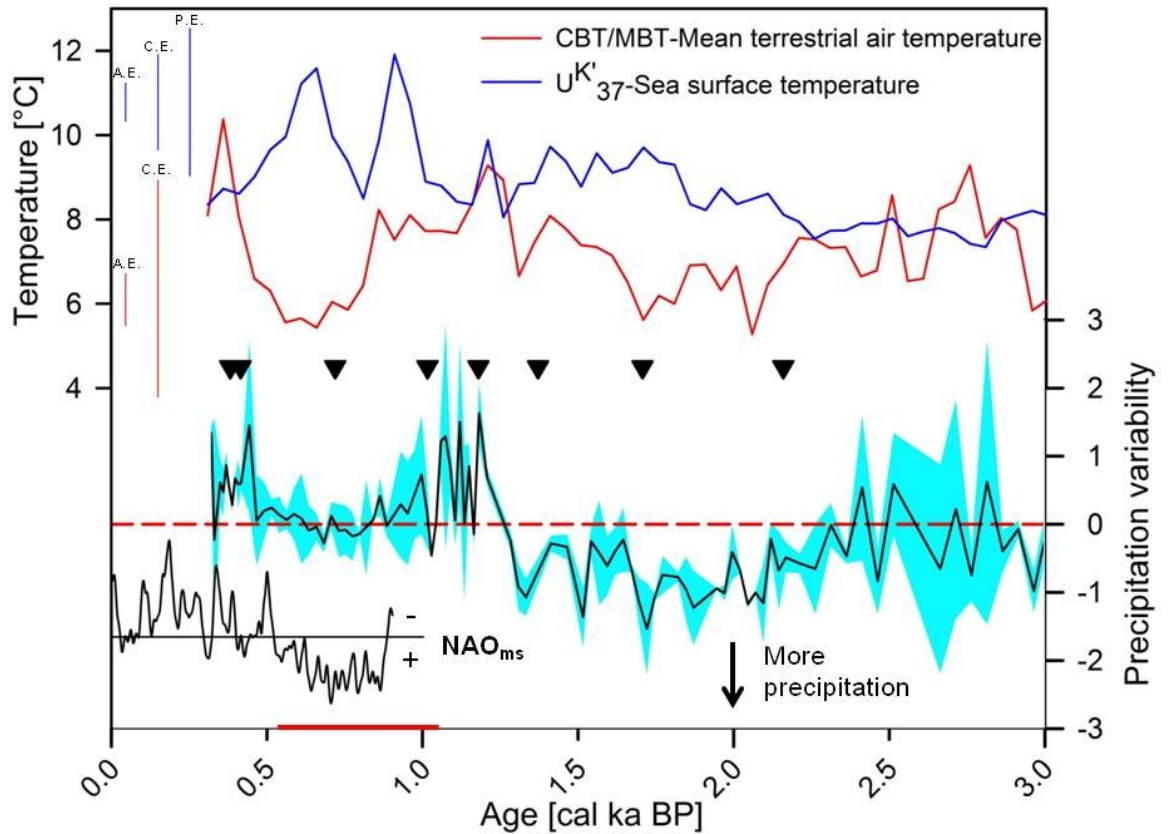


Figure 5.11: Late Holocene terrestrial and marine palaeoclimate records. The mean terrestrial air (50 year moving average; red line) and sea surface temperatures (50 year moving average; blue line) are plotted against summer insolation change at 60 °N (Laskar *et al.*, 2004). The blue vertical lines indicate the U<sup>K</sup><sub>37</sub>-SST analytical, calibration (Conte *et al.*, 2006) and propagated errors. The red vertical lines indicate the analytical and the calibration error (+ or -; Weijers *et al.*, 2011a). The propagated error was not calculated because the raw dataset of the calibration equation published by Weijers *et al.* (2007c) was not available. The black triangles indicated <sup>14</sup>C-AMS dated sediment horizons of core MD99-2266. The Holocene precipitation divergence (black line) from the mean state (dashed red line) and uncertainty (turquoise area) arising from the combination of the normalised ACL<sub>25-35</sub> and soil pH datasets is plotted against the reconstructed NAO<sub>ms</sub> variability of the last 950 years (Trouet *et al.*, 2009). The red line on the x-axis indicates the medieval climate anomaly (MCA).

Figure 5.11 shows MAT, SST, and precipitation variability of the last 3000 years plotted against the reconstructed NAO variability of the last 950 years (Trouet *et al.*, 2009). Trouet *et al.* (2009) have shown that the MCA was characterised by the NAO in its positive mode. Changes in the precipitation record presented here can

be visually compared with the reconstructed NAO fluctuations (within the dating error;  $2\sigma = 130$  years) for the time interval where the two records overlap. It is suggested, that the high precipitation observed during the MCA in Iceland was driven by strong westerlies induced by the NAO in its positive mode. Furthermore, high  $U^{K}_{37}$ -SSTs during the MCA co-occur with the high precipitation and NAO+ regime. The warmer SSTs during the MCA were likely driven the NAO in its positive mode.

The reconstructed air temperatures are lower throughout the last 3000 years in periods which are thought to be dominated by the NAO in its positive mode, compared to periods which are dominated by the NAO in its negative mode (Figure 5.11). Contemporary observations show that mild temperatures prevail in northern Europe when the NAO is in its positive mode (Bukantis & Bartkeviciene, 2005; Hurrell & VanLoon, 1997). This begs the question why the reconstructed air temperatures indicate the opposite relationship between NAO phases and air temperature. Wang *et al.* (2011) have shown that negative precipitation anomalies cause increased summer warmth and vice versa throughout Central Europe. This is explained by increased thermal conductivity of moist, compared to dry soils (Wu *et al.*, 2011). Thus wet soils give off heat energy quicker than dry soils. During positive NAO phases, Iceland receives more precipitation. Therefore, even though the air may have been warm, the soil itself was cold. Since the air temperature reconstruction is based on branched GDGTs produced by soil bacteria, this proxy likely records the lower soil temperature. Subsequently it is reasonable that the recorded terrestrial temperature is lower during positive NAO phases and higher during negative NAO phases.

The hypothesis that NAO type fluctuations controlled precipitation is further supported by the apparent precipitation see-saw between northern and southern Europe observed in the contemporary instrumental record (Trouet *et al.*, 2009; references therein). A comparison between the Icelandic precipitation and historical precipitation records of the Mediterranean area reveals a similar precipitation gradient across Europe, which reach further back in time than the MCA. Around the time Rome was founded (753 BC), the climate in the

Mediterranean region was colder and wetter than it is today (Lamb, 1995). During the same period, between ~ 3000 and ~ 2400 cal. a BP, the Icelandic precipitation record presented here indicates a dryer climate than that which followed, and that of the middle Holocene. During the time which encompasses the Roman Warm Period (RWP; Sicre *et al.*, 2008a), from ~2100 to ~1300 cal. a BP, precipitation markedly increased and reached levels, which were nearly as high as those observed during the middle Holocene (Figure 5.11). During the latter part of this period, the Mediterranean areas were characterised by droughts with maxima at ~1750 (300 - 400 AD) and ~ 1200 cal. a BP (800 AD; Lamb, 1995). The above examples indicating the existence of a precipitation gradient across Europe throughout the late Holocene corroborating the hypothesis that NAO type fluctuation have affected precipitation in Iceland for at least the last 3000 years.

During the late Holocene, high precipitation in Iceland is linked to prevalent, positive NAO-type fluctuations, but does this relationship extend to the middle and early Holocene? During the middle Holocene more precipitation than at any other time in the Holocene is observed (Figure 5.9). The precipitation was likely transported by prevailing westerlies which are stronger than those traversing the Atlantic today (Harrison *et al.*, 1992). The link between strong westerlies and high precipitation suggests that NAO-type fluctuations prevailed mainly in their positive mode throughout the middle Holocene. Further evidence for stronger winds comes from Icelandic loess deposits which indicate, that the middle Holocene was characterised by very strong winds (Jackson *et al.*, 2005; Figure 5.8). If the relative amount of precipitation is an indication for the strength of these NAO-type fluctuations, then the precipitation variability indicates that such fluctuations would have been more pronounced during the middle Holocene and that those fluctuations weakened throughout the latter half of the Holocene. Andersen *et al.* (2004) have made similar observations based on North Atlantic SST gradients, lending support to the evolution of the NAO from the middle to the late Holocene, as shown by the data presented here.

SSTs decrease during the middle Holocene which is not in accordance with observations between NAO and SST variability in Northwest Iceland today. NAO

induced effects on SSTs around Northwest Iceland were apparently overprinted by the effects of the changing influence of different water currents on SSTs during the middle Holocene at the coring site, and by decreasing summer insolation, as discussed earlier.

The observed low precipitation in Iceland throughout the early Holocene (Figure 5.9) suggests that NAO-type fluctuations prevailed in their negative mode. This result contrasts some model data and palaeoclimatic records. For example, Harrison *et al.* (1992) have modelled even stronger westerlies during the early Holocene than during the middle Holocene. Giraudeau *et al.* (2004) and Andersen *et al.* (2004) suggest that the NAO prevailed in its positive mode during the early Holocene. The prevailing strong westerlies and associated positive NAO mode stand in contrast to the continually low precipitation observed in the early Holocene. Model results confirm the result of lower precipitation in the early Holocene (Renssen *et al.*, 2005), despite strong westerlies. Thus a mechanism which could have switched off precipitation in the early Holocene in northwest Iceland needs to be discussed. Today, the precipitation distribution over Iceland is strongly influenced by the positions and intensities of the Greenland high and the Icelandic Low. A 4 - 5° shift of the Icelandic Low towards the east causes Iceland to be affected by winds from the north east, from Greenland, which bring less precipitation to the west of Iceland (Bromwich *et al.*, 2005; Hanna *et al.*, 2004). 9000 years ago, the Icelandic Low was located farther north than today causing the westerlies to traverse the North Atlantic farther north than they do today (Harrison *et al.*, 1992). If the Icelandic Low was also shifted further to the east, then the west of Iceland may have been influenced by dry air masses from Greenland, thus receiving less precipitation.

#### **5.4.6 Late Holocene climate variability on Iceland - Influence on settlers**

There are reports that Iceland may have been inhabited as early as 2300 cal. a BP, and that Irish monks lived on Iceland (Lamb, 1995), before the Norse settlers arrived on Iceland around 871 AD (~ 1080 cal a BP; Ogilvie *et al.*, 2005). With the onset of the MCA, which lasted from ~ 1100 to ~ 600 cal. a BP (Graham *et al.*,

2011), MATs decreased except for a temperature stagnation between 1000 and 900 cal. a BP. A similar temperature decrease has been observed in a  $\delta^{18}\text{O}$  record of mollusc shells recovered from marine sediment cores close to Vestfirðir peninsular (Patterson *et al.*, 2010). Shortly after the arrival of the Icelandic settlers, famines were reported (Patterson *et al.*, 2010), which were likely caused by deteriorating climatic conditions on Iceland leading up to the period known as the Little Ice Age (Ogilvie & Jonsson, 2001; Sicre *et al.*, 2008a). It has been shown that climatic variability affected human societies throughout the late Holocene in Europe (Buntgen *et al.*, 2011; Lamb, 1995), and also on Greenland (D'Andrea *et al.*, 2011). It seems that Icelandic settlers were no exception, and also at the mercies of abrupt climate change. Furthermore, climatic variations on Iceland and Greenland may have had much more adverse affects on the people living there than on societies in more temperate regions, because the Icelandic economy is and has been based on agriculture, fishing and farming (Ogilvie & Jonsdottir, 2000; Ogilvie & Jonsson, 2001). Therefore, even small temperature fluctuations could have caused crop failures causing famines.

## **5.5 Conclusion**

In this study biomarker proxies are employed to produce a high resolution reconstruction of Icelandic Holocene climate change from 10,700 - 300 cal. a BP. SST, MAT, soil pH and precipitation variability throughout the studied time period have been reconstructed. The high resolution palaeo proxy records from Northwest Iceland, which is known to be sensitive to climate change, show remarkable climatic variation over the studied time period. Therefore, such records are very valuable for studying climate change at very high resolution.

The absolute reconstructed air temperatures and  $U_{37}^K$ -SSTs in this study reflect summer rather than mean annual temperatures.  $ACL_{28-35}$  variations, along with changes in soil pH, are shown to reflect changing precipitation amounts throughout the Holocene.

## 5. New insights into Holocene climate evolution from high-resolution terrestrial and marine biomarker records from Northwest Iceland

Combining the MAT, SST and precipitation records reveals two periods, one at ~7700 cal. a BP, and the other at ~ 2900 cal. a BP, where major climatic shifts occur. In the early Holocene MATs are driven by changing summer insolation. SSTs are influenced by meltwater events which depress them and cause a divergence between the MAT and SST records. As a result of these meltwater events, the THTM and the MHTM are temporally divergent. The middle Holocene is characterised by cooling MATs and SSTs as they are driven by decreasing insolation. The cooling culminates at ~ 3000 cal. a BP which coincides with very slow ISOW water velocities. The latitudinal heat transport from the equator into the northern hemisphere mediated by the AMOC becomes more important in the late Holocene than insolation change as both, the MAT and the SST record are decoupled from insolation.

The Holocene precipitation and  $U_{37}^K$ -SST records produced in this study are coupled to NAO fluctuations throughout the late Holocene. Times where the NAO dominates in its positive mode are characterised by higher precipitation and SSTs over northwest Iceland and vice versa. High precipitation during the middle Holocene indicates that the NAO prevailed in its positive mode. In the early Holocene Icelandic precipitation is lower than expected which may be due to decreased moisture transport possibly caused by a more easterly position of the Iceland Low.

6. Using the TEX<sub>86</sub> palaeothermometer in a fjordic environment: Unreasonable reconstructed sea surface temperatures indicate anaerobic oxidation of methane.

## **6 Using the TEX<sub>86</sub> palaeothermometer in a fjordic environment: Unreasonable reconstructed sea surface temperatures indicate anaerobic oxidation of methane**

### **6.1 Introduction**

Thaumarchaeota (previously known as Crenarchaeota group I; Brochier-Armanet *et al.*, 2008), which are ubiquitous in the world's oceans (Sinninghe Damsté *et al.*, 2002b), produce glycerol dibiphytanyl glycerol tetraethers (GDGTs) with different amounts of cyclic structures within the GDGT molecules (Figure 1.4). This fact has been exploited to develop the TEX<sub>86</sub> palaeo SST thermometer (Schouten *et al.*, 2002). Since the establishment of the TEX<sub>86</sub>-SST proxy, it has been successfully employed to reconstruct palaeo-SST changes as far into the past as the mid-Cretaceous (Hofmann *et al.*, 2008), and in varying environments, from the Northwest Indian Ocean to high latitude regions (Huguet *et al.*, 2006; Weijers *et al.*, 2007b). However, compared to the organic geochemical SST palaeothermometer based on alkenones (Brassell *et al.*, 1986; Prahil & Wakeham, 1987), and even more so, compared to the palaeothermometer based on oxygen isotopic signatures of planktonic foraminifera (Emiliani, 1955), the TEX<sub>86</sub> is a young proxy, and in some marine areas, its application as a palaeo-SST proxy may not work. For example, terrigenous sources of GDGTs in coastal areas with a high organic matter input from land can impact the TEX<sub>86</sub> reconstructed palaeo-SSTs (Weijers *et al.*, 2006b). Other marine sediments, where the TEX<sub>86</sub> may not be applicable, are those affected by the anaerobic oxidation of methane (AOM), a microbial process mediated by archaea that also produce isoprenoidal GDGTs (Zhang *et al.*, 2011).

The aim of this chapter is to assess, whether the TEX<sub>86</sub> palaeothermometer is applicable in fjordic environments. To this end, the TEX<sub>86</sub> and the U<sup>K</sup><sub>37</sub> sea surface temperature proxies are compared. It is hypothesised, that the TEX<sub>86</sub>-SSTs will

6. Using the TEX<sub>86</sub> palaeothermometer in a fjordic environment: Unreasonable reconstructed sea surface temperatures indicate anaerobic oxidation of methane.

show similar long and short-term trends and absolute temperatures to the U<sup>K'</sup><sub>37</sub>-SSTs (Chapter 5).

## 6.2 Methods

A number of calibration equations have been developed to convert relative GDGT concentrations into SSTs. In their global sediment calibration of the TEX<sub>86</sub>, Kim *et al.* (2008) used the same equation (Equation 6) that Schouten *et al.* (2002) used to convert relative GDGT concentrations into the TEX<sub>86</sub> proxy. Based on a global sediment sample set, Kim *et al.* (2008) converted TEX<sub>86</sub> values into TEX<sub>86</sub>-SSTs using Equation 7. The correlation between TEX<sub>86</sub> and SST is not linear where SSTs are below 5°C. Therefore Kim *et al.* (2010) developed the TEX<sub>86</sub><sup>L</sup> proxy (Equation 8) and the corresponding calibration equation (Equation 9).

The palaeo-sea surface temperature reconstructions based on the archaeal GDGT abundances are calculated using the TEX<sub>86</sub> and the TEX<sub>86</sub><sup>L</sup> calibration equations. Nine samples were analysed in triplicate and two in duplicate. The analytical error (1σ) associated with the TEX<sub>86</sub> and the TEX<sub>86</sub><sup>L</sup> is ± 0.01 for both calculations corresponding to an error (1σ) in the estimated temperatures of ± 0.67 and ± 1.1 °C respectively. The TEX<sub>86</sub> palaeothermometer has previously been used to reconstruct SST changes as small as 1 °C (Sluijs *et al.*, 2006). It was not possible to include the relative abundance of GDGT - 4' in the TEX<sub>86</sub> calculation because the relative abundance of the crenarchaeol isomer in 256 samples was consistently below 1 % (mean and standard deviation: 0.6 ± 0.2 %) of the total GDGT concentration. Low GDGT - 4' concentrations increase the analytical error introduced by the integration of very small peaks.

The Methane Index was calculated using Equation 10. Nine samples were analysed in triplicate and two in duplicate. The analytical error associated with the methane index is ± 0.01. Similar to the TEX<sub>86</sub> calculation above, the crenarchaeol isomer is not included in the calculation of the MI index, because of its very low concentration. Therefore, the MI values presented here are slightly offset to higher values. However, the offset is not significant. To verify this statement, it was tested

6. Using the  $\text{TEX}_{86}$  palaeothermometer in a fjordic environment: Unreasonable reconstructed sea surface temperatures indicate anaerobic oxidation of methane.

on the sample with the highest relative amount of crenarchaeol isomer (3 %). When the value of the crenarchaeol isomer is included, the MI is 0.0275. Without the crenarchaeol isomer, the MI is 0.0288.

Where proxy records are converted into climate proxies via a calibration equation (eg.  $\text{TEX}_{86}$  to SST using the calibration equation provided by Kim *et al.*, (2008)), the analytical error is propagated through the variance of the calibration equation. However, the resulting propagated error likely constitutes a considerable overestimation of the actual error. This is due to the fact, that the calibration equations are based on global calibration sets which have a considerable amount of scatter.

### **6.3 Results**

Holocene  $\text{TEX}_{86}$ - and  $\text{U}^{\text{K}}_{37}$ -SST records from Ísafjarðardjúp fjord are presented. The  $\text{TEX}_{86}$  dataset is made up of 299 samples, while the  $\text{U}^{\text{K}}_{37}$  dataset is made up of 326 samples.

#### **6.3.1 GDGT inferred SSTs**

Figure 6.1 shows the assumed, reconstructed Holocene SST variability using the  $\text{TEX}_{86}$ , and the  $\text{TEX}_{86}^{\text{L}}$  proxy. The calibration equation developed by Kim *et al.* (2008; Equation 9) is used, because it is based on the most comprehensive sediment sample dataset to date. Additionally, the  $\text{TEX}_{86}^{\text{L}}$  calibration equation developed by Kim *et al.* (2010) is used, because of its proposed applicability to cold water (SST < 17°C) environments. Weijers *et al.* (2006b) have shown that in environments with high terrestrial organic carbon input (BIT-Index: 0.2-0.3), a +1 °C temperature deviation can affect the  $\text{TEX}_{86}$ -SSTs. The BIT-Index in Ísafjarðardjúp fjord does not exceed 0.14 (Figure 4.2) throughout the Holocene record. Therefore, no  $\text{TEX}_{86}$ - and  $\text{TEX}_{86}^{\text{L}}$ -SST measurements were excluded on the basis of the BIT-Index being too high.

The reconstructed SST fluctuations using the different calibration equations show the same long term trends, albeit with different absolute temperature estimates

6. Using the  $\text{TEX}_{86}$  palaeothermometer in a fjordic environment: Unreasonable reconstructed sea surface temperatures indicate anaerobic oxidation of methane.

(Figure 6.1). Throughout the early Holocene, until  $\sim 7550$  cal. a BP, the  $\text{TEX}_{86}$ -SSTs fluctuate between 15.2 and 4.9 °C (mean 10.9 °C), while the  $\text{TEX}_{86}^{\text{L}}$ -SSTs fluctuate between 9.6 and -7.4 °C (mean 3.2 °C). After  $\sim 7550$  cal. a BP both calibration approaches indicate an apparent SST increase. Between  $\sim 5500$  and  $\sim 1000$  cal. a BP the  $\text{TEX}_{86}$ - and the  $\text{TEX}_{86}^{\text{L}}$ -SSTs fluctuate around 23.4°C ( $\pm 3.7$  °C) and 28.9 °C ( $\pm 4.4$  °C), respectively. Throughout the youngest part of the record, from  $\sim 1300$  cal. a BP, the estimated SSTs decrease.

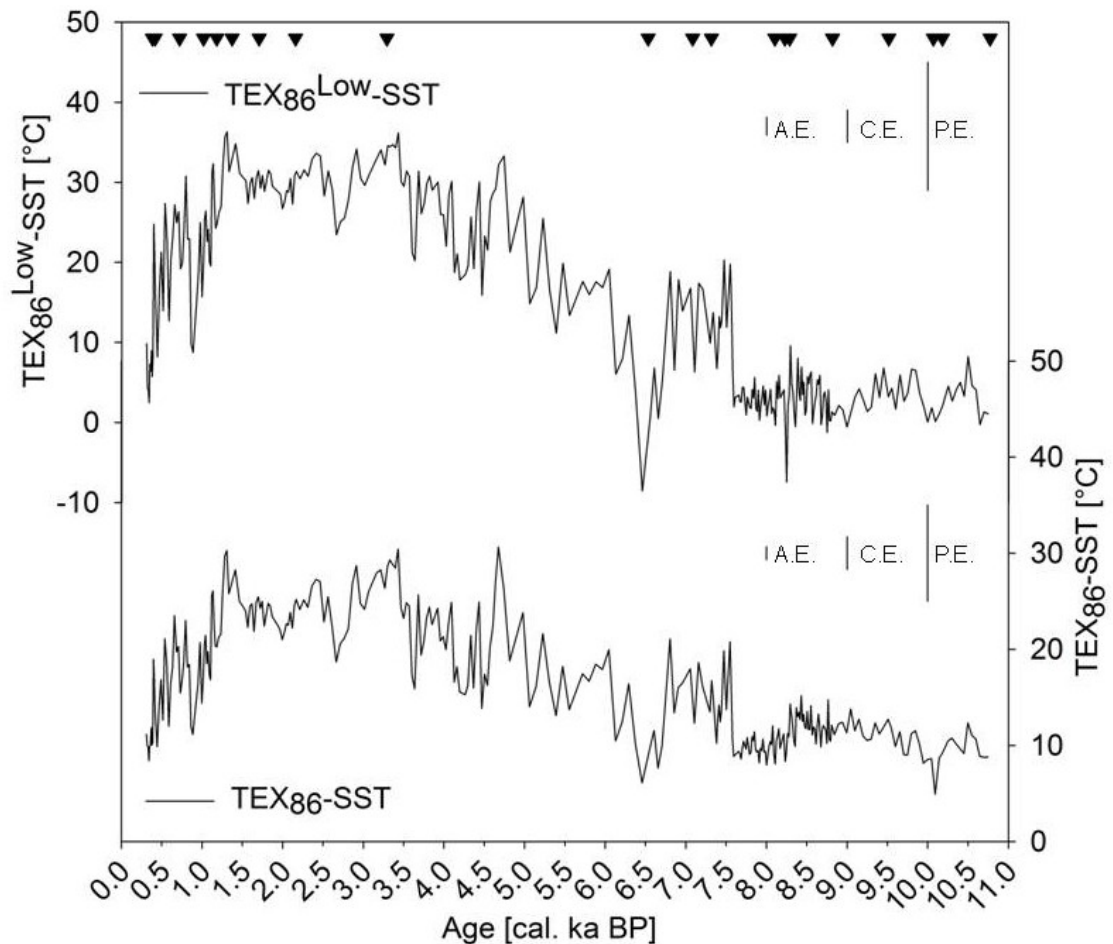


Figure 6.1: Reconstructed palaeo-SST variations using the  $\text{TEX}_{86}$  and the  $\text{TEX}_{86}^{\text{L}}$  calibration equations. The black triangles show the  $^{14}\text{C}$ -AMS dated sediment horizons of core MD99-2266. The vertical error bars represent the analytical error (A.E.), the  $1\sigma$  (+ or -) calibration error (C.E.), and the propagated error (P.E.).

6. Using the TEX<sub>86</sub> palaeothermometer in a fjordic environment: Unreasonable reconstructed sea surface temperatures indicate anaerobic oxidation of methane.

### 6.3.2 Methane Index

The Methane Index (MI) variability that is exhibited throughout the Holocene in Ísafjarðardjúp fjord is shown in Figure 6.2.

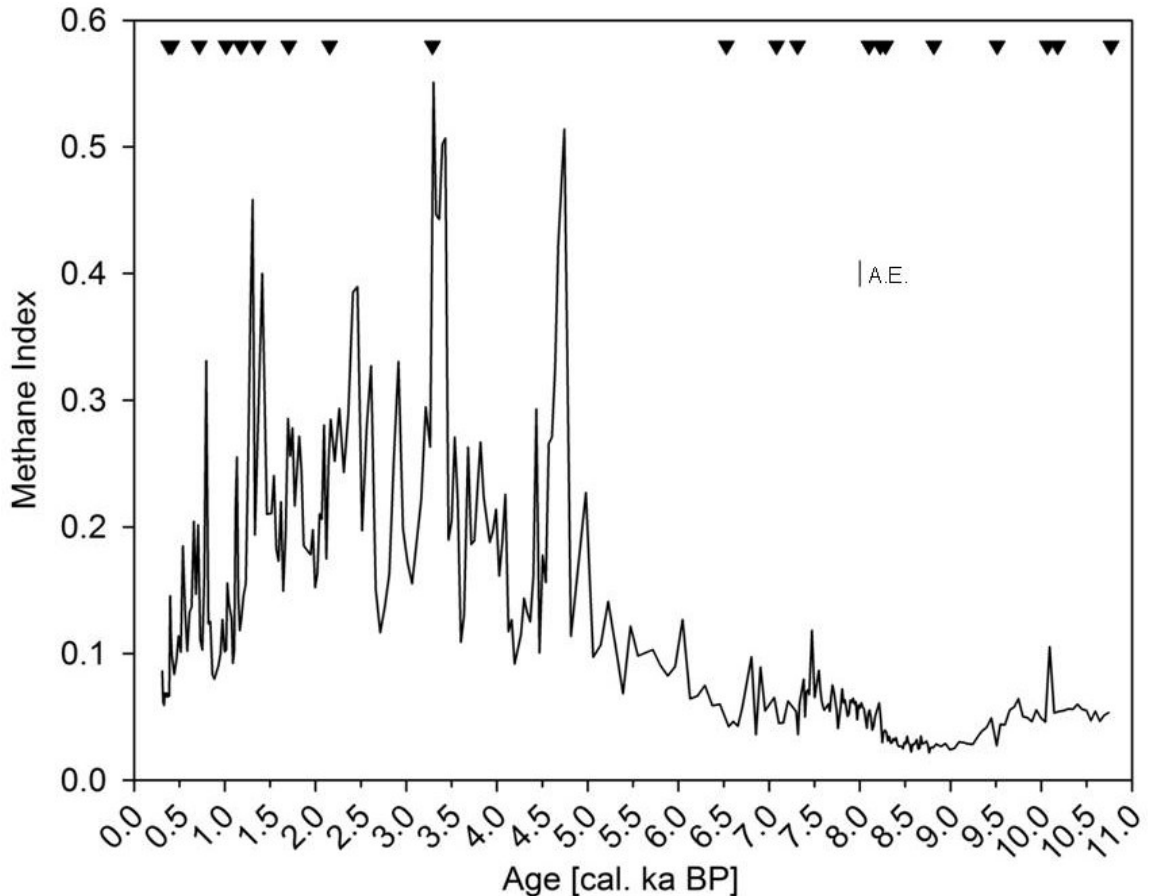


Figure 6.2: Variations of the Methane Index throughout the Holocene in Ísafjarðardjúp fjord. Black triangles represent the <sup>14</sup>C-AMS dated sediment horizons of core MD99-2266. The vertical bar indicates the analytical error associated with the MI Index.

Throughout the early Holocene, until ~ 6500 cal. a BP, the MI index is low, varying around  $0.05 \pm 0.02$ . From ~ 6500 cal. a BP the MI index starts to increase and quickly reaches values higher than 0.5 around ~ 4750 cal. a BP, and between ~ 3500 and ~ 3300 cal. a BP. Between ~ 1300 and ~ 6500 cal. a BP the MI index varies around  $0.2 \pm 0.1$ . The MI index exhibits a decreasing trend after 1300 cal. a BP returning to values below 0.1.

6. Using the TEX<sub>86</sub> palaeothermometer in a fjordic environment: Unreasonable reconstructed sea surface temperatures indicate anaerobic oxidation of methane.

## 6.4 Discussion

### 6.4.1 Comparison between TEX<sub>86</sub>- and U<sup>K</sup><sub>37</sub>-SSTs

The comparison of the TEX<sub>86</sub> and U<sup>K</sup><sub>37</sub> inferred palaeo-SSTs reveals that the respective palaeo-SST records show considerable differences (Figure 6.3a). Only samples where TEX<sub>86</sub><sup>L</sup> and U<sup>K</sup><sub>37</sub>-SST data was available, were used for this comparison. During the early Holocene the TEX<sub>86</sub><sup>L</sup> inferred SSTs are on average  $7.2 \pm 2.6$  °C lower than the U<sup>K</sup><sub>37</sub>-SSTs, and the TEX<sub>86</sub> derived SSTs. As the reconstructed SSTs using the calibration equation published by Kim *et al.* (2008) correlates better with the absolute SSTs reconstructed using the U<sup>K</sup><sub>37</sub>-SST proxy in the early Holocene, the further discussion of the GDGT inferred SSTs will exclusively focus on the apparent temperatures reconstructed using the TEX<sub>86</sub> calculation.

Figure 6.3 shows the variations of the TEX<sub>86</sub><sup>L</sup> and the U<sup>K</sup><sub>37</sub>-SSTs, the difference between the reconstructed absolute temperatures, and the methane index variability throughout the Holocene. The following discussion is based on the assumption, that the absolute U<sup>K</sup><sub>37</sub>-SSTs and their trends are correct. The U<sup>K</sup><sub>37</sub>-SST variability has been discussed in detail in the previous chapter (Chapter 5), and it has been compared to other Holocene SST records from the vicinity of Iceland. The temperature trend, and also the absolute temperatures reconstructed in the previous chapter, using the U<sup>K</sup><sub>37</sub>-SST proxy, show good agreement with these records. The general trend of high SSTs in the early Holocene and a subsequent cooling in the middle Holocene have been reported south and west of Iceland, as well as on the Icelandic Shelf (Bendle & Rosell-Melé, 2007; Calvo *et al.*, 2002; Koc *et al.*, 1993; Marchal *et al.*, 2002; Quillmann *et al.*, 2010). The absolute U<sup>K</sup><sub>37</sub>-SSTs reconstructed in this study (Figure 5.1) vary around  $9.7 \pm 1.4$  °C throughout the Holocene. Similar temperatures have been reported north (Bendle & Rosell-Melé, 2007; Justwan *et al.*, 2008), as well as south of Iceland (Marchal *et al.*, 2002). Throughout the last 4500 cal. a BP Jiang *et al.* (2002) and Sicre *et al.* (2008b) report temperatures between 6 and 8 °C, and 7 and 11 °C, respectively. These temperatures coincide with the reconstructed alkenone

6. Using the  $\text{TEX}_{86}$  palaeothermometer in a fjordic environment: Unreasonable reconstructed sea surface temperatures indicate anaerobic oxidation of methane.

derived SSTs in this study. The comparison with other studies supports the earlier statement that the alkenone derived SSTs show reasonable absolute SSTs and trends.

The absolute temperatures reconstructed using the  $\text{TEX}_{86}$  proxy (Figure 6.1), are similar to the alkenone derived SSTs throughout the early Holocene until  $\sim 7600$  cal. a BP. After an initial SST decrease both SST reconstructions show a SST increase from  $\sim 10,100$  cal. a BP. The temperature increase coincides with the establishment of the Irminger Current in the Denmark Strait which supplies warm Atlantic water to the area (Ólafsdóttir *et al.*, 2010). The alkenone derived SST record indicates a cold period between  $\sim 8500$  and  $\sim 7800$  cal. a BP where SSTs decrease by  $\sim 2$  °C. This cold spell is possibly recorded in the GDGT derived SST record, albeit with a time lag of  $\sim 200$  years. A period with colder SSTs between  $\sim 8500$  and  $\sim 8000$  cal. a BP has been reported previously (Giraudeau *et al.*, 2000; Jennings *et al.*, 2011; Knudsen *et al.*, 2004), and is associated with melt water events, possibly including to the 8.2 ka event (Alley & Ágústsdóttir, 2005). It is suggested, that the decreased SSTs which are recorded by the GDGTs are a direct response to the influence of meltwater in the area. Therefore the low  $\text{TEX}_{86}$ - and  $\text{U}^{\text{K}}_{37}$ -SSTs are likely forced by the same mechanisms in the time period between  $\sim 8500$  and  $\sim 7600$  cal. a BP.

6. Using the TEX<sub>86</sub> palaeothermometer in a fjordic environment: Unreasonable reconstructed sea surface temperatures indicate anaerobic oxidation of methane.

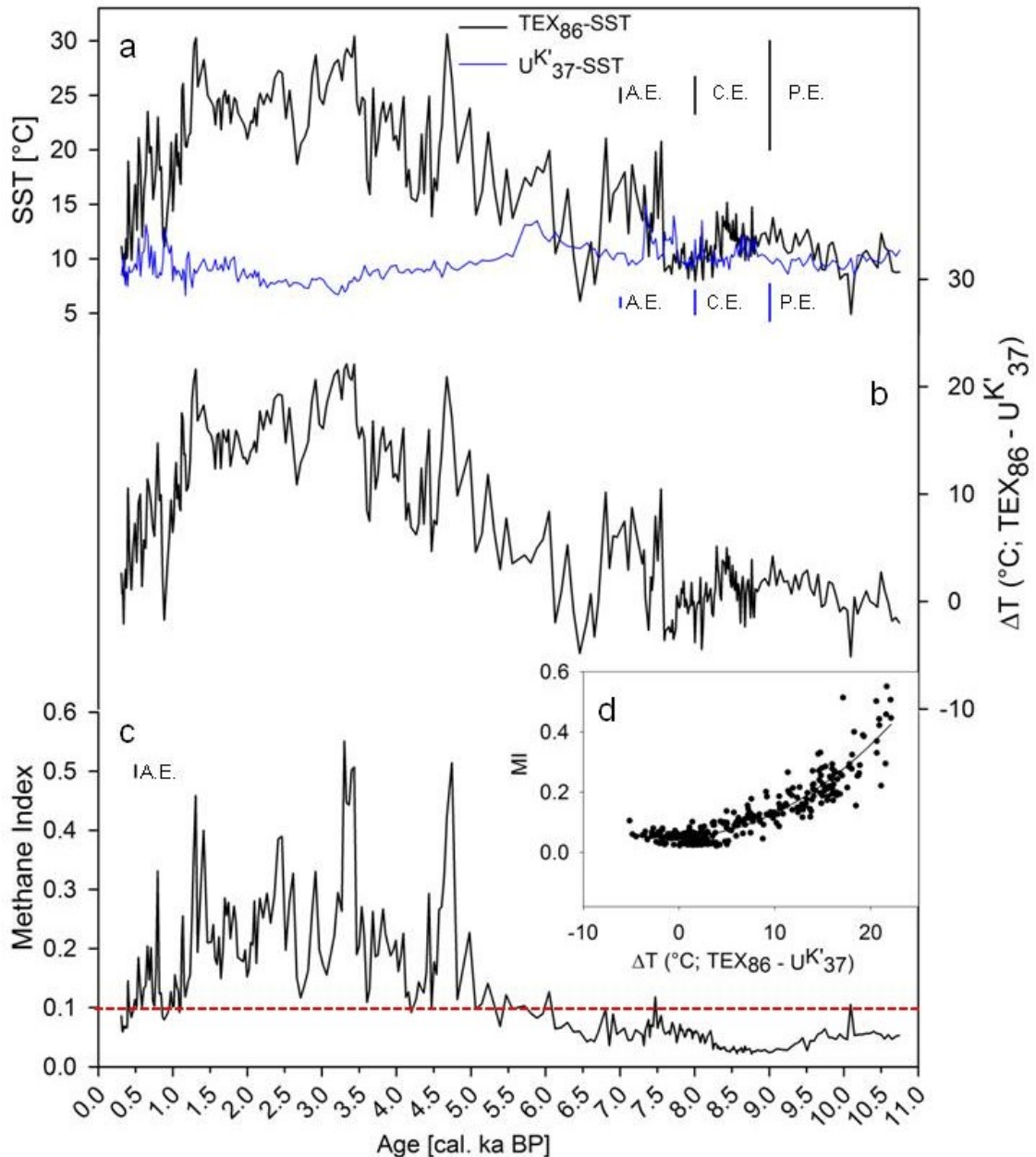


Figure 6.3: TEX<sub>86</sub>-SST variability vs. U<sup>K'</sup><sub>37</sub>- and MI variability. (a) Comparison between the U<sup>K'</sup><sub>37</sub>-SST variability (Figure 5.1) and the TEX<sub>86</sub>-SST variability (Figure 6.1) throughout the Holocene; The black vertical error bars represent the analytical, the calibration (+ or -) and the propagated errors associated with the TEX<sub>86</sub>-SST reconstruction. The blue vertical error bars indicate the analytical, calibration and propagated errors associated with the U<sup>K'</sup><sub>37</sub>-SST reconstruction; (b) difference between the reconstructed absolute TEX<sub>86</sub>- and U<sup>K'</sup><sub>37</sub>-SSTs; (c) variations of the Methane Index. The dashed red line indicates the MI Index threshold above which TEX<sub>86</sub>-SST results need to be viewed critically due to possible AOM-activity. The black vertical bar indicates the analytical error; (Inset; d) 2<sup>nd</sup> order polynomial regression between the Methane Index and ΔT (TEX<sub>86</sub>-SST - U<sup>K'</sup><sub>37</sub>-SST;  $y=0.0496+0.0001x+0.0007x^2$ ;  $r^2=0.85$ ).

6. Using the TEX<sub>86</sub> palaeothermometer in a fjordic environment: Unreasonable reconstructed sea surface temperatures indicate anaerobic oxidation of methane.

There is a major discrepancy between the GDGT inferred SSTs and the alkenone derived SSTs after ~ 7600 cal. a BP. The GDGT inferred SSTs increase until 1300 cal. a BP, and produce implausible palaeo-SSTs in excess of 30°C. During this period the trends and the absolute temperatures produced by the TEX<sub>86</sub>, and the TEX<sub>86</sub><sup>L</sup> proxies (Figure 6.1) clearly do not reflect known Holocene climatic variations in the North Atlantic. The SSTs produced by the TEX<sub>86</sub> proxies decrease after 1300 cal. a BP, and the gap between the SST records produced by the different biomarkers decreases. The TEX<sub>86</sub>-SSTs indicate a short, warmer period between ~ 900 and ~470 cal. a BP, which coincides with warm U<sup>K</sup><sub>37</sub>-SSTs between ~ 1000 and ~ 500 cal. a BP. The high U<sup>K</sup><sub>37</sub>-SSTs are associated with positive NAO type atmospheric fluctuations during that period (Chapter 5.3.3). The fact that both the TEX<sub>86</sub> and the U<sup>K</sup><sub>37</sub>-SSTs show this warm period suggests, that the TEX<sub>86</sub>-SSTs are influenced by the same drivers that force the U<sup>K</sup><sub>37</sub>-SSTs during the late Holocene. However, the reconstructed TEX<sub>86</sub>-SSTs are still warmer than the warmest summer month SSTs expected for northwest Iceland.

The large disagreements in trend and absolute temperature between the SST reconstructions using the TEX<sub>86</sub>- and the U<sup>K</sup><sub>37</sub>-proxy indicates, that the TEX<sub>86</sub> proxy and thus the archaeal GDGTs are not primarily influenced by SST changes throughout much of the Holocene. The temperature differences between the TEX<sub>86</sub> and the U<sup>K</sup><sub>37</sub>-SST records are small during the early Holocene, until 7500 cal. a BP (Figure 6.3b). Subsequently the temperature difference increases during the middle and late Holocene. The low MI values throughout the first 3200 years of the record coincide with the similar temperature ranges for the TEX<sub>86</sub>- and the U<sup>K</sup><sub>37</sub>-SSTs (Figure 6.3). As the TEX<sub>86</sub>-SSTs and the U<sup>K</sup><sub>37</sub>-SST deviate from each other, the MI values increase. There is a close correlation between the TEX<sub>86</sub> proxy SST deviation and the MI values (Figure 6.3d). The second order polynomial regression between the TEX<sub>86</sub>-SST values and the MI values ( $r^2=0.87$ ) is only marginally better than the regression between the TEX<sub>86</sub>-SST deviation from the UK<sup>K</sup><sub>37</sub>-SSTs and the MI ( $r^2=0.85$ ; Figure 6.3). Therefore, the TEX<sub>86</sub>-SSTs, and the deviations of the different temperature proxies are clearly correlated with MI.

6. Using the TEX<sub>86</sub> palaeothermometer in a fjordic environment: Unreasonable reconstructed sea surface temperatures indicate anaerobic oxidation of methane.

Low MI Index values coincide with low  $\Delta T$  (TEX<sub>86</sub> - U<sup>K'</sup><sub>37</sub>) values throughout most of the Holocene with the exception of the period between ~ 7600 and ~ 6500 cal a BP. The divergence of the TEX<sub>86</sub> inferred palaeo SSTs from the U<sup>K'</sup><sub>37</sub>-SSTs may be due to increased transport of terrestrial organic matter to the fjordic sediment. Precipitation in northwest Iceland increases sharply at ~7700 cal a BP (discussed in chapter 5). This precipitation increase likely increased the terrestrial OC transport to the fjordic sediments which is reflected in the Holocene terrestrial organic carbon input discussed in chapter 4. Schouten *et al.* (2002) have suggested that land derived GDGTs can adversely influence the TEX<sub>86</sub> palaeothermometer. Fietz *et al.*, (2012; accepted for publication) have previously indicated that archaeal GDGTs may also have a terrestrial source. Therefore, it is conceivable that a contribution of terrestrially derived archaeal GDGTs, transported by increased terrestrial run-off due to increased precipitation, caused the initial SST discrepancy shown by the TEX<sub>86</sub> and the U<sup>K'</sup><sub>37</sub> palaeothermometers.

#### **6.4.2 Anoxic methane oxidation affects TEX<sub>86</sub>-SSTs**

The MI index has been proposed by Zhang *et al.* (2011) to indicate increased anoxic methane oxidation (AOM) mediated by methane oxidising archaea, that live in a symbiotic relationship with sulphate reducing bacteria (Boetius *et al.*, 2000; Pancost *et al.*, 2000). These archaea, belonging to the kingdom of *Euryarchaeota*, are known to produce GDGTs-1, -2 and -3 (Pancost *et al.*, 2001; Figure 1.3). In marine environments where AOM is an important mechanism, *Euryarchaeota* can contribute a substantial amount of GDGTs to the total GDGT pool, and thus their occurrence can influence, or overprint the TEX<sub>86</sub> temperature proxy (Zhang *et al.*, 2011). In fact, Schouten *et al.* (2002) have indicated that SST estimates may be offset by GDGT contributions from methanogens which can be present in anoxic environments.

6. Using the  $\text{TEX}_{86}$  palaeothermometer in a fjordic environment: Unreasonable reconstructed sea surface temperatures indicate anaerobic oxidation of methane.

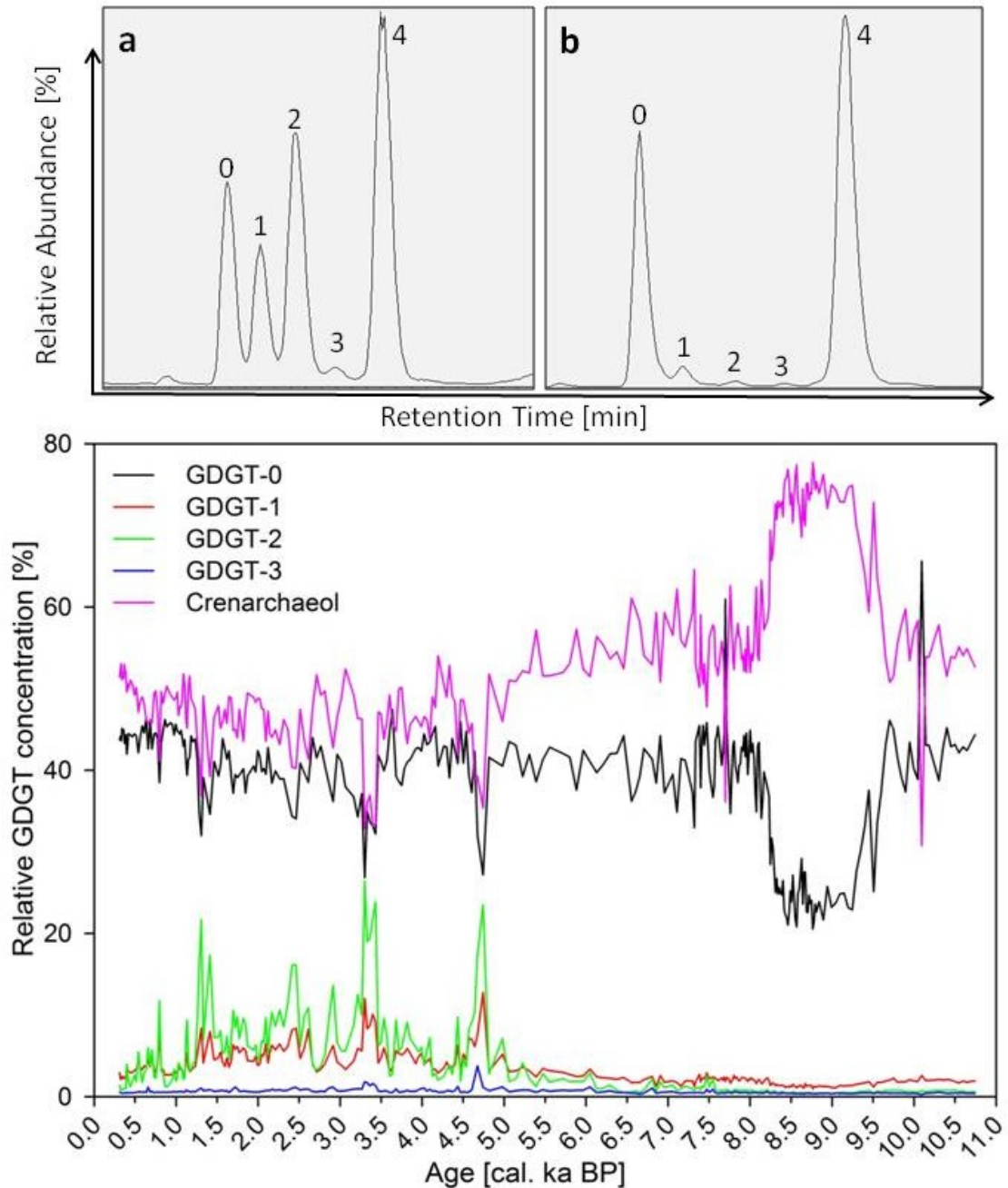


Figure 6.4: Relative concentration of GDGT-0, -1, -2, -3 and Crenarchaeol. The structure of the GDGTs are shown in Figure 1.4; (a) chromatogram of the GDGT concentration at ~ 5400 cal. a BP; (b) chromatogram of the GDGT concentration at ~ 7500 cal. a BP.

Figure 6.4 shows that the relative concentrations of GDGTs-1, -2 and -3 begin to increase between ~ 5500 and ~ 6000 cal. a BP coinciding with the increased deviation of  $\text{TEX}_{86}$  derived SST estimates from  $U^{K'}_{37}$  proxy SST estimates. Therefore, the unreasonable temperatures produced by the  $\text{TEX}_{86}$  proxy, along

6. Using the TEX<sub>86</sub> palaeothermometer in a fjordic environment: Unreasonable reconstructed sea surface temperatures indicate anaerobic oxidation of methane.

with elevated methane indices throughout most of the Holocene indicate an increasing contribution of GDGTs produced by AOM mediating archaea.

This result is supported by the identification of archaeol (Figure 6.5) in samples with an elevated MI. Archaeol has not only been found in methanogens, but also in thermophiles and halophiles (Koga *et al.*, 1998), and it is the most common and ubiquitous representative of the archaeal diethers (Pancost *et al.*, 2000). In this case it is believed to be indicative of methanogens that mediate AOM, as it has been associated with methane oxidising archaea in sediments (Hinrichs *et al.*, 1999; Hinrichs *et al.*, 2000; Niemann & Elvert, 2008).

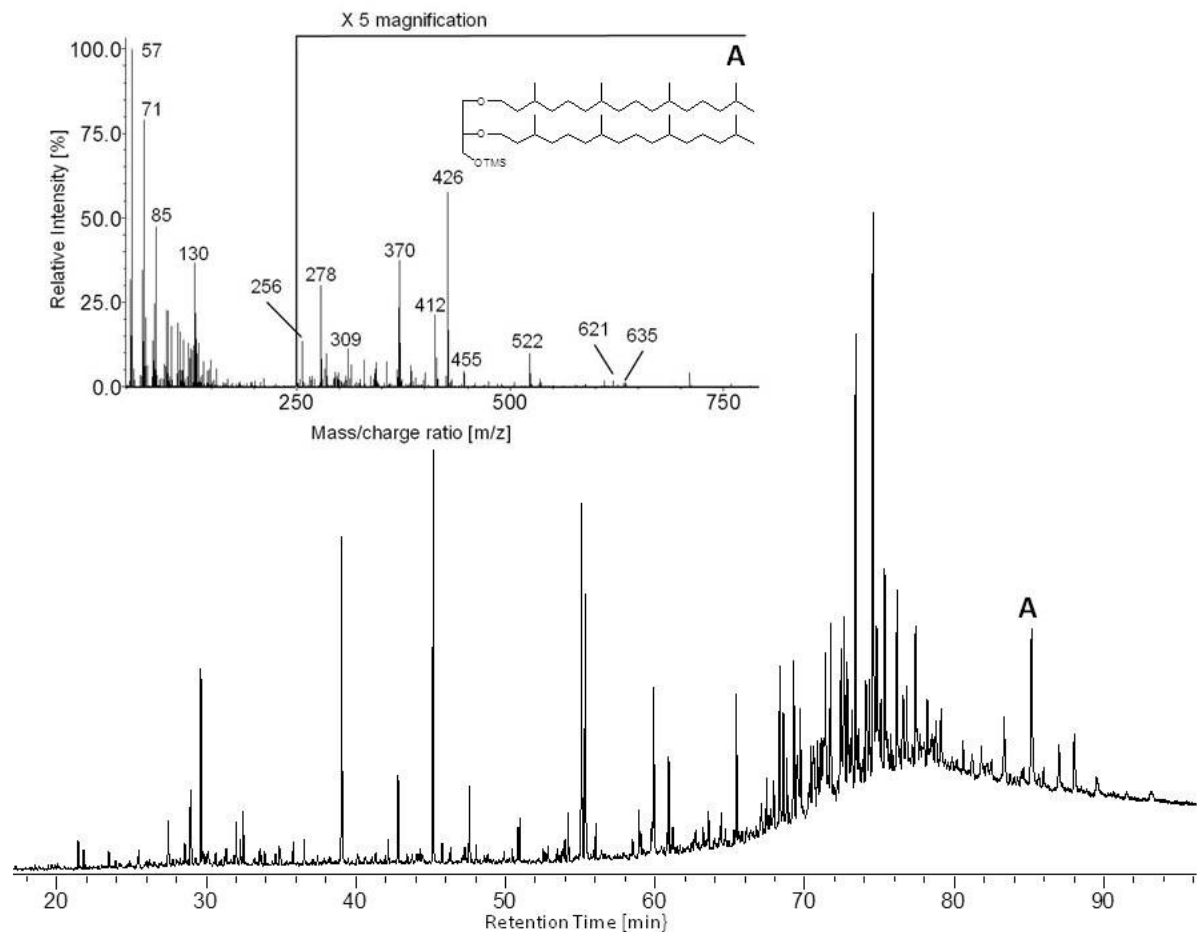


Figure 6.5: Gas chromatogram of the polar fraction of a sample correlating with very high MI values at 5400 cal. a BP. Inset is the mass spectrum of compound A which was identified as bis-O-phytanyltrimethylsilylglycerol, also known as Archaeol after Teixidor & Grimalt, (1992).

6. Using the TEX<sub>86</sub> palaeothermometer in a fjordic environment: Unreasonable reconstructed sea surface temperatures indicate anaerobic oxidation of methane.

The values of the MI which indicate AOM in this study are lower than the MI values indicating AOM activity at other studied sites (Zhang *et al.*, 2011). Zhang *et al.* (2011) suggest that a MI greater than 0.5 indicates AOM activity. However, methane was expected to have a large impact on the ecosystems of their studied sites, as they were located close to hydrothermal vents, cold seeps and mud volcanoes. One sample set is derived from the Black Sea which is known to have extreme anoxic conditions which are conducive to AOM activity. The extreme conditions at these sites likely foster higher AOM activity in comparison to areas where the influence of methane is lower (Valentine, 2002). It is suggested that this is the reason why the MI values published by Zhang *et al.* (2011) are higher than those observed in this study. The MI values presented in this study may be more representative of diffusive AOM activity in anoxic marine sediments, including partial or interstitial anoxia, which are not influenced by methane sources such as seeps and hydrothermal vents. Thus, the results of this study have wider implications for the application of TEX<sub>86</sub> in numerous palaeoceanographic studies. A second explanation for the lower MI values observed here lies in the relative concentration of the GDGTs. The MI is based the assumption that the GDGTs contributing to the GDGT pool come from two sources, pelagic *Thaumarchaeota*, and sedimentary, AOM mediating *Euryarchaeota*. Zhang *et al.* (2011) show that the relative concentration of GDGTs produced by *Thaumarchaeota* (GDGT-4 and -4') decreases relative to the contribution of GDGTs produced by *Euryarchaeota* (GDGTs-1, -2 and -3). However, both GDGT-4, and -4' also have terrestrial sources such as organisms living in peats and soils (Weijers *et al.*, 2006b; Weijers *et al.*, 2011b). A site located close to land with a noticeable terrigenous input of organic matter (OM) into the sediments, such as Ísafjarðardjúp fjord, can be affected by an influx of GDGT-4 from that terrestrial source. This influx would lead to lower MI values possibly causing AOM activity to be underestimated.

#### **6.4.3 Temporal variability of AOM intensity in Ísafjarðardjúp fjord**

Increased relative concentrations of GDGTs associated with AOM mediating *Euryarchaeota* after ~ 6000 cal. a BP indicate that the process of AOM was more important in the middle and late Holocene compared to the early Holocene at the

6. Using the TEX<sub>86</sub> palaeothermometer in a fjordic environment: Unreasonable reconstructed sea surface temperatures indicate anaerobic oxidation of methane.

studied site. This begs the question as to why AOM became an important microbial process during the middle and late Holocene in Ísafjarðardjúp fjord. The process of AOM in sediments is at least 300 Ma old (Birgel *et al.*, 2008), and changing AOM intensities in sediments have since been documented and associated with climate and ocean circulation change (Cook *et al.*, 2011), as well as with changing flow intensities of methane seeps (Peckmann *et al.*, 2009).

Since AOM only takes place under anoxic conditions in sediments and in the water column (Valentine, 2002 and references therein), one explanation for increased AOM activity could be changing redox conditions in the fjord. No inorganic analyses were conducted on core MD99-2266 that would verify changing redox conditions. Fjordic environments are conducive to anoxia due to their physical properties. Restricted water circulation, particularly in silled fjords such as Ísafjarðardjúp, can lead to a stratification of the water column (Cottier *et al.*, 2010). Due to the stratification, oxygen in the lower water layers, that is consumed during the biochemical digenesis of organic matter (OM) is not replenished, leading to anoxic conditions (Paetzel & Schrader, 1992). The stratification of the water column can be exacerbated by freshwater runoff during late winter and spring, which introduces a freshwater layer in Icelandic coastal waters, and further stabilises the radiation induced thermocline formed during summer (Hanna *et al.*, 2006; reference therein). The stratification of fjordic water is affected by changing seasons, wind strength and changing sea level, among other forcing factors (Cottier *et al.*, 2010; Inall & Gillibrand, 2010).

In open ocean environments the availability of OM is the limiting factor for microbial degradation in the water column and sediment. In fjordic systems, which typically have higher sedimentation rates and more OM input into the sediments, the availability of oxygen can become the limiting factor for the degradation of the OM. When the replenishment of oxygen is inhibited, or when the introduction of OM into the marine realm is very high, then all the oxygen can be consumed, creating anoxic conditions (Paetzel & Schrader, 1992).

6. Using the TEX<sub>86</sub> palaeothermometer in a fjordic environment: Unreasonable reconstructed sea surface temperatures indicate anaerobic oxidation of methane.

The water column of Ísafjarðardjúp fjord may not have been stratified during the early Holocene leading to an oxic environment despite high primary productivity rates and high sedimentation rates during that period (see chapter 4). One possible explanation is that the overturning of fjord waters was driven by changing seasons as observed in arctic fjords today (Cottier *et al.*, 2010). The early Holocene was characterised by strong seasonal differences, driven by high summer and low winter insolation (Laskar *et al.*, 2004), which would have exacerbated seasonal water column overturning. Even though no direct evidence for vertical water mixing has been found at the coring site, Quillmann *et al.* (2010) suggest that water masses started to overturning deeper inside Ísafjarðardjúp fjord ~ 8900 cal. a BP ago. The water mass overturning is indicated by increased amounts of arctic foraminiferal assemblages and heavier  $\delta^{18}\text{O}$  values (Quillmann *et al.*, 2010). If such vertical mixing took place at the fjord mouth, it would have re-oxygenated the complete water column and impaired the formation of anoxic sediments, and thus decreased favourable conditions for AOM.

Despite decreasing sedimentation rates and primary production, the MI values indicate an anoxic depositional and/or sedimentary environment from ~ 6000 cal. a BP. Coinciding with the end of the Holocene thermal maximum, the influence of cold, less saline Arctic waters increased between 6200 and 6500 years ago on the northwest Icelandic coast (Castañeda *et al.*, 2004; Giraudeau *et al.*, 2004). Along with this increased influence of arctic waters, the U<sup>K</sup><sub>37</sub>-SSTs (Figure 5.1) decreased and the frequency of drift ice reaching northwest Iceland increased (Andrews *et al.*, 2009b). Furthermore, the middle Holocene is characterised by increased precipitation (see chapter 5) which would have caused increasing amounts of freshwater runoff. Increased amounts of drift ice, along with increased freshwater runoff could have stabilised the stratification of the fjordic water column by introducing a freshwater lens on the surface. Therefore, increased stratification of the water column could have caused anoxic conditions despite decreased amounts of OM reaching reaching the sediments.

Changing environmental conditions affecting the activity of the AOM mediating archaeal communities may offer another explanation for an increase in the

6. Using the TEX<sub>86</sub> palaeothermometer in a fjordic environment: Unreasonable reconstructed sea surface temperatures indicate anaerobic oxidation of methane.

anaerobic oxidation of methane in the middle and late Holocene. Three archaeal groups associated with AOM, namely ANME-I, -II and -III are known (Niemann *et al.*, 2006; Orphan *et al.*, 2002). ANME-I and ANME-II are affected by environmental parameters such as temperature and partial pressure of methane (Nauhaus *et al.*, 2002; Nauhaus *et al.*, 2005). The ANME-I community is adapted to lower methane concentrations and its optimal temperature range is between 16 and 24 °C. The ANME-II community handles lower temperatures better, but needs higher methane partial pressure. The alkenone derived SST record shows that SSTs were continually lower than 16 °C throughout the Holocene (Figure 5.1). The highest bottom water temperature recorded in the Denmark Strait throughout the Holocene is ~ 8 °C (Ólafsdóttir *et al.*, 2010). The low recorded palaeo temperatures suggest, that the environment may have been too cold for ANME-I archaea. Archaea belonging to a subgroup of the ANME-II community, ANME-IIc, are associated with increased amounts of GDGTs associated with AOM (Elvert *et al.*, 2005). Therefore, under the assumption that the ANME-IIc community dominated in Ísafjarðardjúp fjord, possible methane partial pressure fluctuations throughout the Holocene could have affected its activity. Quillmann *et al.* (2010) have shown, that the relative sea level was as much as 40 m lower during the early Holocene than today. Assuming that the methane production was constant throughout the Holocene, it is possible that the decreased water pressure (~ 0.4 MPa) on the sediment would have caused less methane to be dissolved in the sedimentary pore water, thus inhibiting the activity of the ANME-IIc community. Nauhaus *et al.* (2005) have shown that an *in vitro* increase of the partial pressure of methane by 1 MPa can lead to a fivefold increase of the AOM activity in samples dominated by ANME-II communities. Today's relative sea level was reached just after 6000 cal. a BP, just as MI values indicating increased AOM activity began to increase. The activity of the ANME-IIc community was possibly enhanced by increasing methane partial pressure due to the sediments being submerged deeper in the middle and late, compared to the early Holocene.

However, the fact that no *sn*-2-hydroxyarchaeol has been detected in the sediments which exhibit high MI values suggests, that ANME-II, and subgroups of ANME-II type archaea may not have dominated the sediment (Blumenberg *et al.*,

6. Using the TEX<sub>86</sub> palaeothermometer in a fjordic environment: Unreasonable reconstructed sea surface temperatures indicate anaerobic oxidation of methane.

2004). Biomarker studies of AOM mediating archaea have to date only been conducted in marine sediments which are expected to exhibit exceptional AOM activity such as cold- and methane-seeps, hydrothermal vents and the black sea (Blumenberg *et al.*, 2004; Hinrichs *et al.*, 2000; Pancost *et al.*, 2001). Not detecting biomarkers such as *sn*-2-hydroxyarchaeol may therefore not indicate that a certain type of archaeal community is not present, but rather indicate lower AOM activities.

## 6.5 Conclusion

The initial aim of this study was to compare palaeo-SST reconstructions using GDGT and alkenone derived proxies in order to assess the applicability of the TEX<sub>86</sub> palaeo thermometer in fjordic environments. The hypothesis, that TEX<sub>86</sub>-SSTs should exhibit similar absolute temperatures and temperature trends to the U<sup>K</sup><sub>37</sub>-SSTs throughout the Holocene was shown not to be correct. The TEX<sub>86</sub><sup>L</sup> inferred SSTs do not agree with the U<sup>K</sup><sub>37</sub>-SSTs at all, while the TEX<sub>86</sub> inferred temperatures show some agreement with alkenone derived palaeo-SSTs in the early Holocene. As the TEX<sub>86</sub>- and U<sup>K</sup><sub>37</sub>-SSTs deviate from each other, the methane index rises. The good agreement between rising MI values and the marked deviation of the TEX<sub>86</sub> inferred SSTs from the U<sup>K</sup><sub>37</sub>-SSTs indicates, that changing redox conditions in the fjord cause the TEX<sub>86</sub> palaeo thermometer to fail.

It is suggested, that MI values as low as 0.1 indicate AOM in the studied fjord even though values lower than 0.5 have previously been interpreted as reflecting marine environments without measurable AOM taking place (Zhang *et al.*, 2011). Furthermore, the methane index threshold (MI ~ 0.5), indicating AOM influenced marine environments, may not be applicable for many marine environments such as fjords which are prone to anoxia, and where high concentrations of GDGT-1, -2 and -3 indicate AOM activity.

One possible explanation for increased AOM activity may be a shift from an oxic to an anoxic environment from ~ 6500 cal. a BP. Pronounced seasonality induced by high summer and low winter insolation could have caused seasonal overturning of

6. Using the TEX<sub>86</sub> palaeothermometer in a fjordic environment: Unreasonable reconstructed sea surface temperatures indicate anaerobic oxidation of methane.

fjordic waters, thus preventing anoxic conditions from unfolding in the early Holocene, despite high sedimentation rates and the introduction of high amounts of OM into the water column and sediments. It is suggested, that despite decreasing amounts of OM being deposited, anoxic conditions developed in the middle and late Holocene. These anoxic conditions, caused by a stratification of the water column which was brought about by increased precipitation and drift ice in the area, and decreasing seasonality, may have caused a freshwater layer to form on the surface. This freshwater layer would have stopped fjordic waters overturning, preventing the replenishment of oxygen and thus inducing conditions favourable to the anaerobic oxidation of methane.

Another explanation for changing AOM activities throughout the Holocene is that changing environmental conditions either favoured or prevented AOM mediating microbial communities from growing. ANME-II communities need higher amounts of dissolved methane than ANME-I communities. If ANME-II communities were responsible for the mediation of AOM in Ísafjarðardjúp fjord, then their activity may have been impaired by lower relative sea levels of the early Holocene, as these would have reduced the amount of methane dissolved in the pore water of the sediments. This explanation will have to be tested by studying biomarkers which are specific to different AOM mediating archaeal communities.

This study has shown that the TEX<sub>86</sub> proxy is not applicable in areas which are prone to anoxia. Thus, the results shown here have implications for the application of TEX<sub>86</sub> in numerous palaeoceanographic settings.

This study also has implications for reconstructed TEX<sub>86</sub>-palaeo SSTs. Warm SSTs during oceanic anoxic periods have been reconstructed using the TEX<sub>86</sub>-palaeotemperature proxy (Hofmann *et al.*, 2008; Mutterlose *et al.*, 2010). Mutterlose *et al.* (2010) show that the TEX<sub>86</sub> inferred SSTs are consistently 4 - 5 °C warmer than those reconstructed using the  $\delta^{18}\text{O}$  belemnite signal. They suggest that the temperature offset is due to the different organisms (archaea and belemnites) living at different depths in the water column, and that the belemnite  $\delta^{18}\text{O}$  signal is influenced by increased sub surface salinity. The data presented

6. Using the TEX<sub>86</sub> palaeothermometer in a fjordic environment: Unreasonable reconstructed sea surface temperatures indicate anaerobic oxidation of methane.

here suggests, that a temperature offset as observed by Mutterlose *et al.* (2010) can also be caused by the influence of GDGTs produced by AOM mediating archaea. It is suggested that the MI is measured, along with the TEX<sub>86</sub>, when reconstructing palaeo SSTs during periods of oceanic anoxia. Where the MI is higher than 0.1, the TEX<sub>86</sub> derived palaeo-SSTs need to be interpreted with caution.

## **7 Can the carbon isotopic signature of sedimentary fatty acids reconstruct palaeo-sea-ice cover? A case study for the north-western Fram Strait.**

The northwest of Iceland has experienced an increase in drift ice throughout the Holocene (Andrews, 2009; Andrews *et al.*, 2009b). Historical records show that periods of increased drift ice affected the area during the late Holocene (Ogilvie & Jonsdottir, 2000; Ogilvie & Jonsson, 2001), and its extent has been reconstructed over the last 2000 years using the novel sea-ice proxy IP<sub>25</sub> (Andrews *et al.*, 2009a; Massé *et al.*, 2008). However, the IP<sub>25</sub> was not detected in the sediments of MD99-2266. The fact that IP<sub>25</sub> was not detected in an area which is known to have been influenced by drift ice in the Holocene necessitates the development of further sea-ice proxies. The first step of developing a new sea-ice proxy is described in the following chapter.

### **7.1 Introduction**

The amount of September sea-ice covering the Arctic Ocean is rapidly declining, and some models predict, that the Arctic Ocean may be ice free during late summer by 2100 (Boe *et al.*, 2009; Stroeve *et al.*, 2007). Changes in the sea-ice extent exert feedback mechanisms on the climatic system (Bader *et al.*, 2011). For example, sea-ice has a 50 % higher surface albedo than ocean water (Bader *et al.*, 2011; references therein) and controls the amount of solar radiation absorbed in the Arctic. Furthermore, sea-ice offers a habitat for considerable amounts of micro faunal biomass that stands at the base of the food chain. Ice algae is estimated to contribute between 24 and 71 % of total fatty acids to higher trophic levels (Budge *et al.*, 2008). Due to the considerable importance of sea-ice to the climatic system, and to the Arctic food chain, it is imperative to reconstruct past sea-ice extent in order to understand its role as a climatic and environmental forcing factor.

7. Can the carbon isotopic signature of sedimentary fatty acids reconstruct palaeo-sea-ice cover? A case study for the north-western Fram Strait

Historical records provide information on the sea-ice extent reaching back ~ 250 years (Divine & Dick, 2006). In order to obtain estimates of sea-ice extent going further back in time, skeletal remains of diatomaceous ice algae (Gersonde & Zielinski, 2000), and dinoflagellate cysts (de Vernal *et al.*, 2000) have been used as proxies. More recently, an organic geochemical biomarker called IP<sub>25</sub> (Ice proxy with 25 carbon atoms; Figure 1.7) has been developed to offer insights into past sea-ice extent (Belt *et al.*, 2007). Diatoms of the Genera *Haslea* spp. found in sea-ice produce the mono-unsaturated highly branched isoprenoid (HBI) IP<sub>25</sub> (Massé *et al.*, 2004), however other diatoms may also produce the compound (Belt *et al.*, 2007). The IP<sub>25</sub> Proxy has been employed to reconstruct sea-ice conditions throughout the arctic and subarctic oceans (Massé *et al.*, 2008; Müller *et al.*, 2009; Vare *et al.*, 2010; Vare *et al.*, 2009). One limitation to the use of IP<sub>25</sub> is that fluxes into the sediments tend to be relatively low. Thus, IP<sub>25</sub> concentrations can be below the detection limit in some sediments and therefore sea-ice extent in space and time may be underestimated or even interpreted as being nonexistent.

Certain fatty acids are also indicative of diatoms living in sea-ice. The C<sub>14:0</sub>-, C<sub>16:0</sub>- and C<sub>16:1</sub>-fatty acids (FAs; see chapter 1.2.5 for an explanation of the nomenclature) have been shown to be particularly abundant in ice algae samples from the marginal ice zone (MIZ) in the Barents Sea (Falk-Petersen *et al.*, 1998). Seasonal high production of these FAs underneath the sea-ice and within it closely correlates with high IP<sub>25</sub> concentrations, and the concentration of the FAs is much higher than that the IP<sub>25</sub> concentration (Brown *et al.*, 2011).

In a number of studies, <sup>13</sup>C enrichment of ice algal particulate organic matter (POM; Gibson *et al.*, 1999; Kennedy *et al.*, 2002), and of individual compounds produced by ice algae (Belt *et al.*, 2008; Budge *et al.*, 2008), has been observed, relative to POM and individual compounds produced by pelagic algae. This enrichment of the heavy isotope is likely due to a decreased supply of CO<sub>2</sub> within the ice, but other factors such as cell growth likely also impact the amount of <sup>13</sup>C enrichment (McMinn *et al.*, 1999).

7. Can the carbon isotopic signature of sedimentary fatty acids reconstruct palaeo-sea-ice cover? A case study for the north-western Fram Strait

The influence of the relatively heavy ( $^{13}\text{C}$  enriched) carbon isotopes of ice algal POM and individual compounds has been shown to propagate into marine sediments (Belt *et al.*, 2008; Gibson *et al.*, 1999).

### **7.1.1 Aim and hypothesis**

Because ice algae produce such high quantities of FAs, and their carbon isotopic signature is distinct from pelagic algae, it is hypothesised that the isotopic signature of FAs found in sediments may indicate the presence or absence of sea-ice. If the hypothesis holds true, then sea-ice extent can be determined, even in the absence of  $\text{IP}_{25}$ . This study aims to elucidate whether the  $\delta^{13}\text{C}$  signature of FAs in sediments can offer insights into the occurrence of sea-ice. The aim is to compare, whether isotopic variations in FAs correlate with the occurrence or absence of  $\text{IP}_{25}$  in sediments. To this end, the  $\text{IP}_{25}$  content is quantified in sea ice, ice algae, POM and sediment samples, and the results are compared with the  $\delta^{13}\text{C}$  signatures of the FAs from the different samples types.

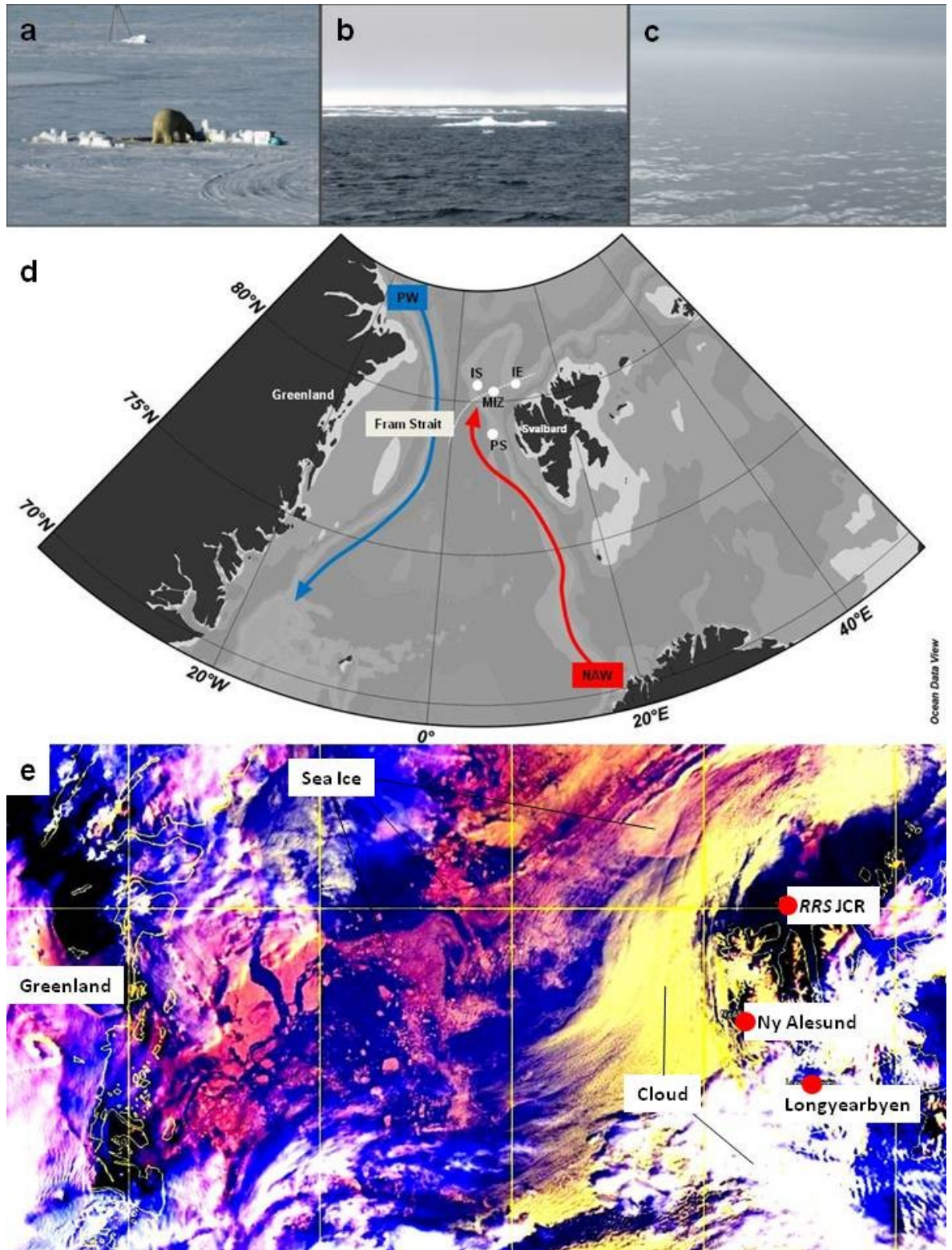
### **7.2 Materials and Methods**

During the ICE CHASER 2010 cruise aboard the *RRS James Clark Ross* (JCR) from the 13<sup>th</sup> of June 2010 to the 22<sup>nd</sup> of July 2010 through the North Sea and the Arctic Ocean, sediment, ice, POM, and ice algae samples were collected. The samples were collected in the Fram Strait at four different locations, the ice station (IS), the marginal ice zone (MIZ), the ice edge (IE) and at the pelagic station (PS; Figure 7.1).

The Fram Strait is one of the most important water connections between the Arctic and the Atlantic Ocean (Rudels *et al.*, 2000). Warm and saline North Atlantic water (NAW), which is the largest oceanic heat source to the Arctic Ocean (Spielhagen *et al.*, 2011) flows along the coast of Svalbard through the Fram Strait. The influx of NAW leads to a heat and sea-ice gradient, whereby the eastern Fram Strait is perennially ice free today, while the western Fram Strait covered by sea-ice under the influence of the east Greenland current (Hansen & Østerhus, 2000). The

7. Can the carbon isotopic signature of sedimentary fatty acids reconstruct palaeo-sea-ice cover? A case study for the north-western Fram Strait

extent and distribution of sea-ice in the Fram Strait is mainly controlled by the strengths of the influx of the NAW (Müller *et al.*, 2009; references therein).



## 7. Can the carbon isotopic signature of sedimentary fatty acids reconstruct palaeo-sea-ice cover? A case study for the north-western Fram Strait

Figure 7.1 ICE CHASER 2010 sampling locations (previous page). Ice algae-and POM-samples were collected at the ice station (IS, a); POM-samples were collected at the marginal ice zone (MIZ, b); POM-and sediment samples were collected at the ice edge (IE, b), and on the pelagic station (PS, c). (d) Sampling locations and surface water currents in the Fram Strait. Red arrow indicates warm, North Atlantic water (NAW), the blue arrow indicates polar water (PW, modified after Hansen & Østerhus, 2000; source of base map: Schlitzer, 2010), The white dashed line indicates the approximate ice extent during August 2010 as observed from satellite images. (e) Dartcom satellite image showing the sea-ice extent in the Fram Strait on the 17.07.2010, and the location of the *RRS James Clark Ross* north of Svalbard (Source: Crew of the *RRS JCR*).

### 7.2.1 Sampling strategy

All water column POM, ice algal and ice core samples were filtered using pre-cleaned (furnaced at 450°C/8 hours) Whatman 47 mm GF/F glass fibre filters (pore size 0.7 µm). The filters were dried at 50°C for 24 hours before being placed in furnaced (450°C/8 hours) Al-foil, packed in sample bags and stored at -20°C. Sediment samples were placed in 5 ml glass vials (furnaced at 450°C/8 hours) and sealed with furnaced Al-foil. Alternatively, some samples were placed in furnaced Al-foil which in turn was placed in sampling bags. All Sediment samples were stored at -20°C until sample workup commenced.

Sea water from CTD-casts and from the non-toxic underway sea water supply was sampled using Nalgene carboys. The sea water from the CTD-casts was taken from the deep chlorophyll maximum at each station, while the sea water from the non-toxic water supply was taken from a depth of 5 m below the sea surface. Depending on the POM content of the water at the sampling site between 10 and 100 litres of seawater were filtered per sample.

At the Ice Station (80° 16.47N, 003° 3.67E) six ice cores were retrieved (Figure 7.2). The ice at the time of sampling had a thickness of 80 to 100 cm. The cores were cut into three sections, bottom (30 cm), middle (30 cm) and top (rest of ice core) and placed in buckets to melt. Once the cores had melted, the water was filtered. Only the bottom 30 cm of the ice cores were analysed for biomarkers.

7. Can the carbon isotopic signature of sedimentary fatty acids reconstruct palaeo-sea-ice cover? A case study for the north-western Fram Strait

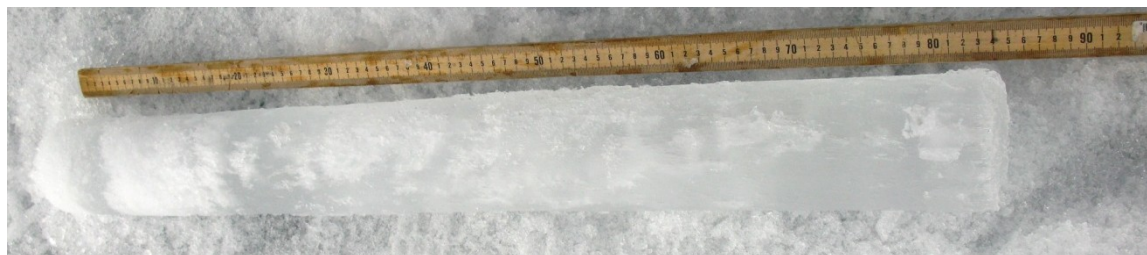


Figure 7.2: Ice core collected at the ice station

Ice algae samples were collected by divers (incl. the author) at the Ice Station (Leg 2; 80° 16.47'N, 003° 3.67'E; Figure 7.3) and subsequently filtered.

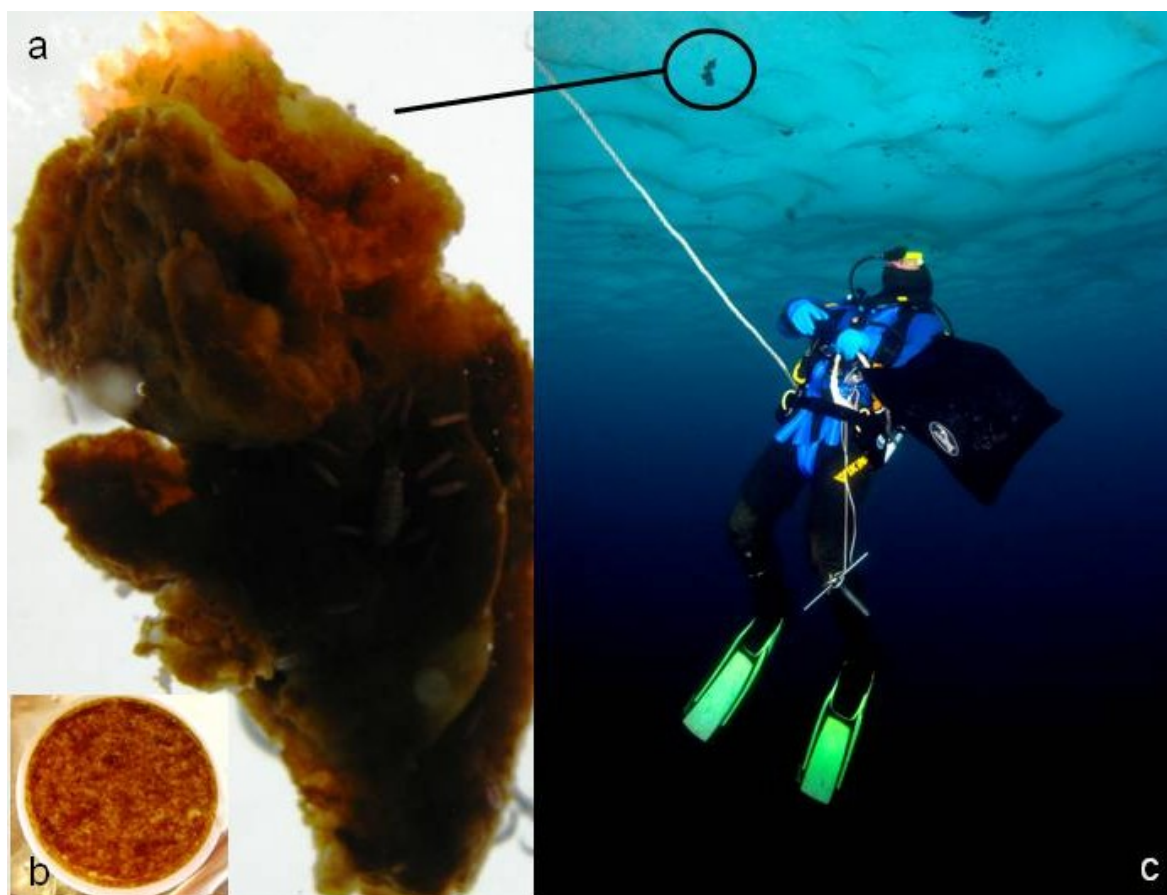


Figure 7.3: Collection of sea-ice algae; (a) buoyant ice algal mass beneath the sea-ice; (b) filtered ice algal organic matter; (c) diver (author) collecting ice algae.

Sediment samples were obtained with a multi corer at the pelagic station and at the ice edge station. The cores were between 20 and 40 cm in length. Each core

7. Can the carbon isotopic signature of sedimentary fatty acids reconstruct palaeo-sea-ice cover? A case study for the north-western Fram Strait

was sliced into one and two centimetre slices, whereby sediment from each slice represented one sample.

## **7.2.2 Lipid extraction and analysis**

For a detailed account of the sample extraction and lipid purification strategy consult the methods chapter. The filtered samples were extracted and purified analogous to the sediment samples.

### **7.2.2.1 Quantification of IP<sub>25</sub>**

The IP<sub>25</sub> peak was identified and quantified with the aid of an external standard sediment originating from the Lancaster Sound (IP<sub>25</sub> standard; Figure 7.4). The IP<sub>25</sub> peak was quantified by adding an internal standard (IntSTD; Squalane; 0.1 µg/ml) to the IP<sub>25</sub> standard and analysing it using a Shimadzu 2010 GC with a flame ionisation detector (FID). The GC-FID was equipped with an AOC-20i hot injection held at 350 °C. Hydrogen was used as a carrier gas (constant pressure; 190 KPa). The separation of the components was achieved using a TG-1MS (Thermo Scientific) column (60m, diameter: 0.25 mm, film thickness: 0.25 µm; coating: 100% Dimethyl-polysiloxane). The following temperature program was used: Initially the GC oven was held at 60 °C for two minutes, then the temperature was ramped up to 120 °C at 30 °C min<sup>-1</sup> and then to 350 °C at 3 °C min<sup>-1</sup> where the temperature was held for 5 minutes. The GC-MS analysis of the IP<sub>25</sub> standard was done using a Shimadzu OP2010-Plus Mass Spectrometer interfaced with a Shimadzu 2010 GC. Helium was used as a carrier gas (constant pressure; 230 KPa). The ion source temperature was 200 °C and the interface temperature was 300°C. The same GC column and the same temperature program as for the GC-FID analysis were used. The ionisation energy was 70 eV and the scan width was 50 to 800 mass units.

7. Can the carbon isotopic signature of sedimentary fatty acids reconstruct palaeo-sea-ice cover? A case study for the north-western Fram Strait

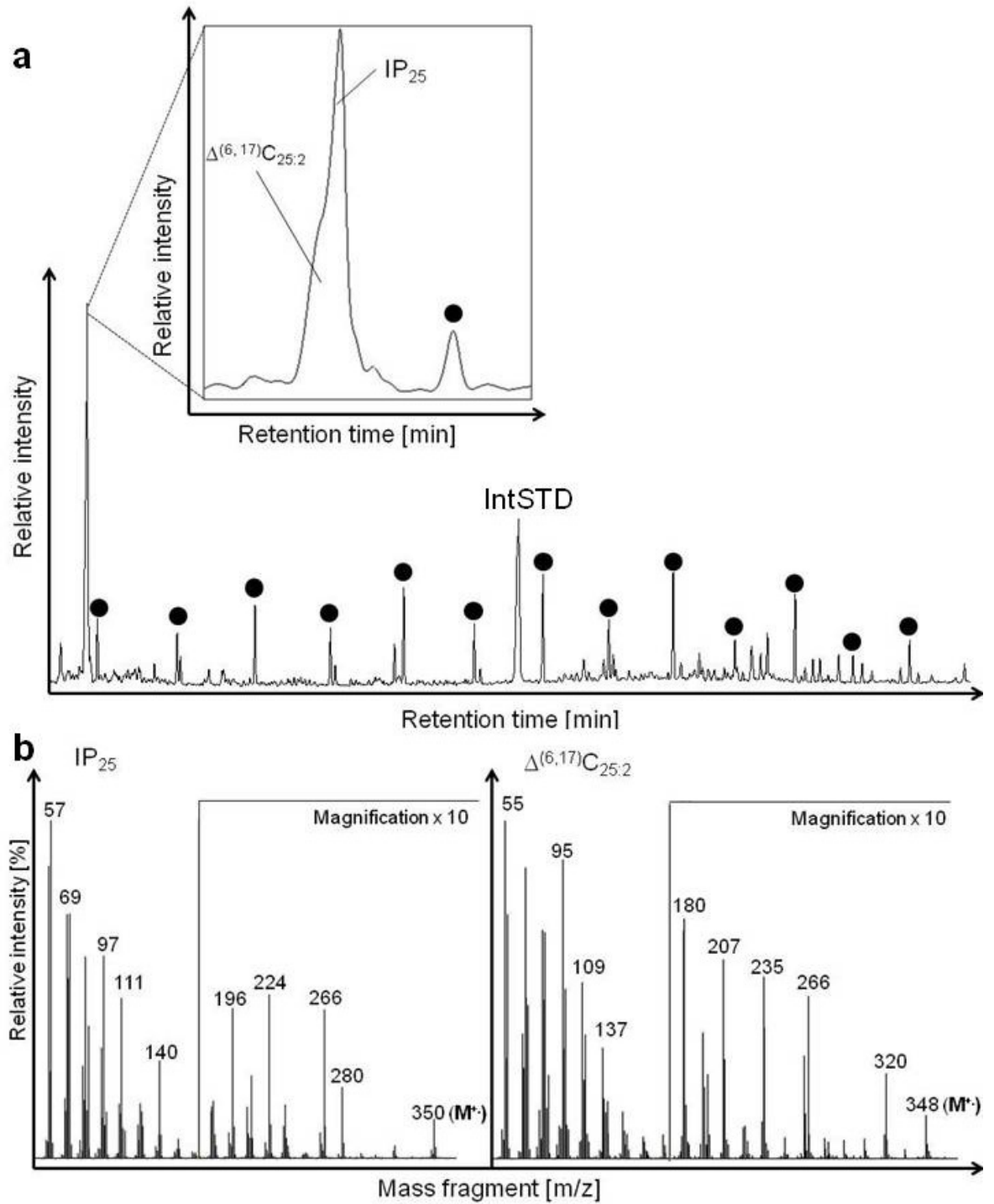
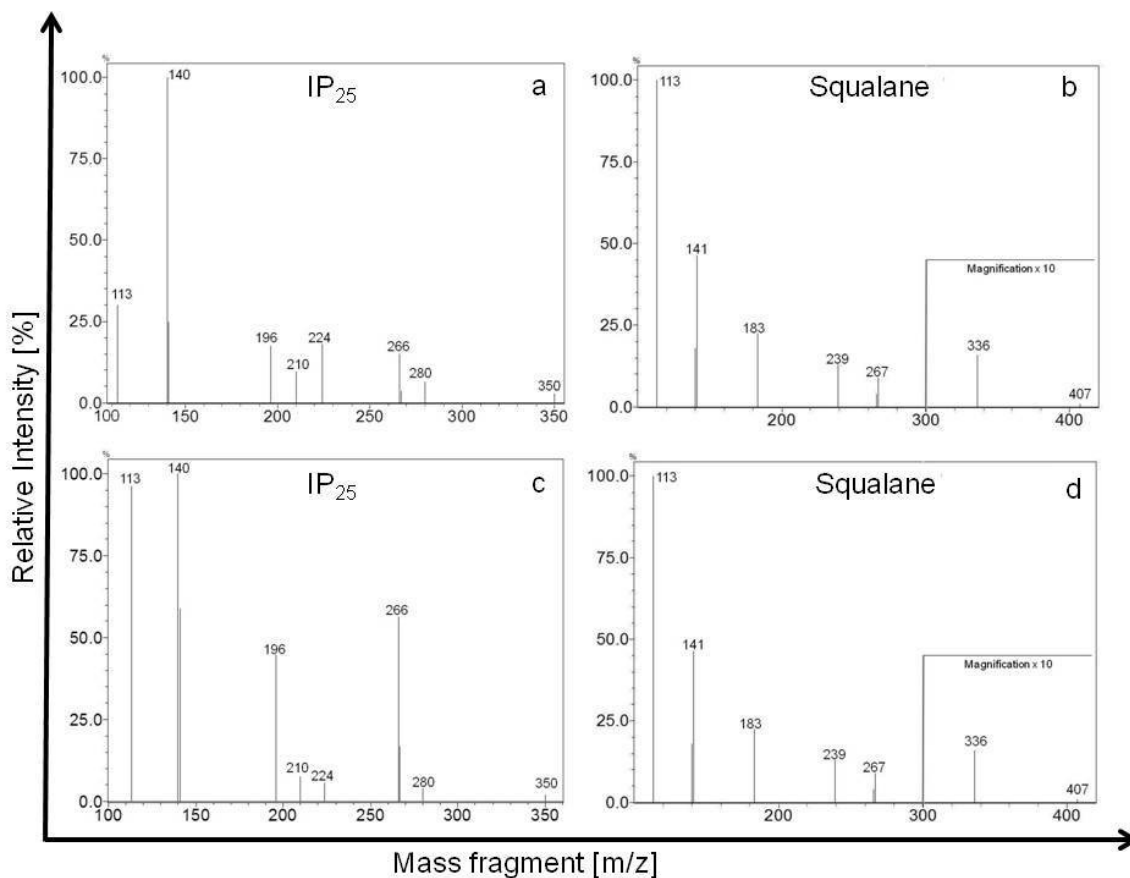


Figure 7.4: Qualitative analysis of IP<sub>25</sub> ice-proxy. (a) Gas chromatogram of the IP<sub>25</sub>-standard. Black dots indicate the homologous series of *n*-alkanes (C<sub>21</sub>-C<sub>33</sub>). The magnification shows the peak containing the co-eluting IP<sub>25</sub> and the IP<sub>25</sub>-diene (Δ<sup>(6,17)</sup>C<sub>25:2</sub>), and the C<sub>21</sub>-*n*-alkane. (b) Mass spectra of IP<sub>25</sub> and Δ<sup>(6,17)</sup>C<sub>25:2</sub>.

7. Can the carbon isotopic signature of sedimentary fatty acids reconstruct palaeo-sea-ice cover? A case study for the north-western Fram Strait

The IP<sub>25</sub> compound occurred in low concentrations in the ice algae samples. Hence, it was quantified using the single ion mode (SIM) rather than the scan mode on the GC-MS. The characteristic ions of IP<sub>25</sub> are published in Belt *et al.* (2007), and the ions used in SIM are shown in Figure 7.5. The GC temperature program used for the GC-MS SIM mode analysis was analogous to the temperature program used for the GC-FID analysis with the exception of not having a hold time after the final temperature ramp. The temperature parameters for the ion source and interface were the same as for the standard GC-MS analysis. For the first 37 minutes of the analysis the MS was run in scan mode. For the next 5 minutes, the MS was switched into SIM mode, only analysing mass fragments with weights characteristic to IP<sub>25</sub> (Figure 7.5). From 42 to 54 minutes, the MS was run in scan mode again. Throughout the subsequent three minutes, the MS was operated in SIM mode again, this time analysing only the mass fragments with weights which are characteristic to Squalane (Figure 7.5). The MS switched to scan mode throughout the rest of the analysis.



7. Can the carbon isotopic signature of sedimentary fatty acids reconstruct palaeo-sea-ice cover? A case study for the north-western Fram Strait

Figure 7.5: SIM-GC-MS analysis of the IP<sub>25</sub>-Standard and an ice algae sample(previous page). The mass fragments (m/z) used to qualitatively analyse IP<sub>25</sub> were: 350, 280, 267, 266, 224, 210, 196, 141, 140, 113. The mass fragments (m/z) used to qualitatively analyse Squalane were (IntSTD) were: 407, 336, 266, 267, 239, 183, 141, 140, 113. (a) SIM-spectrum of IP<sub>25</sub> in the IP<sub>25</sub>-Standard; (b) SIM-spectrum of Squalane in the IP<sub>25</sub>-Standard; (c) SIM-spectrum of the peak with the same retention time as IP<sub>25</sub> in the ice algae samples; (d) SIM-spectrum of Squalane in the ice algae samples.

Prior to the analysis of the collected samples, the IP<sub>25</sub> standard was analysed in a dilution series using the GC-MS in SIM. The IP<sub>25</sub> standard was run in the following concentrations: 0.023 µg/µl, 0.0115 µg/µl, 0.00575 µg/µl, 0.002875 µg/µl, 0.001437 µg/µl, 0.000144 µg/µl and 0.000014µg/µl, to determine the relationship between the concentration and the area of the total ion current (TIC) of the IP<sub>25</sub> peak (Figure 7.6). The TIC, which is comprised of the combined intensities of all mass fragments scanned during SIM, increased linearly with concentration. Subsequently, the apolar (N1) fraction of all samples was analysed. The concentration of IP<sub>25</sub> molecule in the samples was calculated using the linear relationship between the TIC intensity and the concentration as determined for the IP<sub>25</sub> standard.

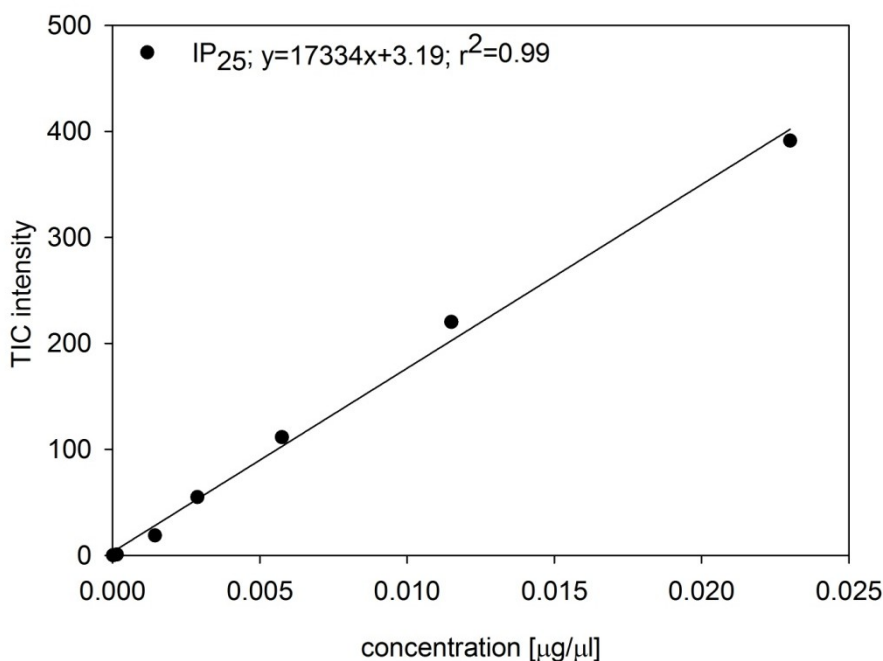


Figure 7.6: Response of the total ion current to the concentration of IP<sub>25</sub>. The total ion current is made up of the ions measured in SIM.

7. Can the carbon isotopic signature of sedimentary fatty acids reconstruct palaeo-sea-ice cover? A case study for the north-western Fram Strait

#### 7.2.2.2 Clean-up of the acid fraction of ICE CHASER 2010 samples

In order to separate the acids from the non-carboxylic compounds in the N4 fraction of the ICE CHASER 2010 samples, the acids were methylated using Methanol with a known isotopic signature ( $\delta^{13}\text{C}$ :  $-27.88 \pm 0.1$  ‰). 200  $\mu\text{l}$  of MeOH (12 %  $\text{BF}_3$ ) were added to the N4 fraction of each sample. The N4 fractions were placed in a heating cabinet for one hour at 70 °C. When the derivatisation was complete, the samples were dried down and separated using a silica gel column chromatographic procedure. The columns used were analogous to the ones used in the fractionation of the total lipid extract (see chapter 2). The whole derivatised N4 fraction, redissolved in 200 $\mu\text{l}$  of DCM, was placed on a column, which had previously been conditioned with 2 ml of DCM. The fatty acid methyl esters (FAMES) were eluted with 4 ml of DCM into the first fraction (A1), while the rest of the polar fraction (non-methylated polar compounds) was eluted with 5 ml of MeOH:DCM (95:5) into the second fraction (A2).

The methods used for the GC-FID and GC-MS analyses of the FAMES, were the same as those used for the N1 fraction of the samples. The FAMES were identified by GC-MS analysis and by comparing their retention times with a marine-oil FAME mix standard (RESTEK; Catalog No. 35066). The quantification of the methyl esters was done by comparing their area with that of the InjSTD Squalane (0.1  $\mu\text{g}/\text{ml}$ ). An external standard (see chapter 2) was analysed after every tenth sample of a batch to ensure analytical precision.

The carbon isotopic measurements of the fatty acid methyl esters of the ICE CHASER 2010 samples were conducted at the Institute of Low Temperature Science at the Hokkaido University, Japan. The carbon isotopic values are expressed as per mil (‰; Equation 16), vs. Vienna Pee Dee Belemnite (VPDB). An external standard consisting of an *n*-alkane mix ( $\text{C}_{16}$  -  $\text{C}_{30}$ ) with a known carbon isotopic composition was injected daily to evaluate the measurement drift of the machine and ensure analytical precision. The carbon isotopic signature of the FAMES was analysed using an HP6890 GC interfaced with a Finnigan MAT Delta Plus MS. The Finnigan MAT combustion furnace was held at 850 °C. The

7. Can the carbon isotopic signature of sedimentary fatty acids reconstruct palaeo-sea-ice cover? A case study for the north-western Fram Strait

chromatographic separation of the FAMES was accomplished using a HP5-MS column (Agilent J&W GC Columns; 60 m, 0.25 mm diameter; 0.25  $\mu\text{m}$  film thickness). The following GC oven temperature program was used: the temperature was ramped up from 50 to 120  $^{\circ}\text{C}$  at 30  $^{\circ}\text{Cmin}^{-1}$ , and then to 310  $^{\circ}\text{C}$  at 5  $^{\circ}\text{Cmin}^{-1}$ , where the temperature was held for 45 minutes. An InjSTD ( $\text{C}_{27}$ -*n*-alkane;  $-29.56 \pm 0.01$  ‰ vs. VPDB) with a known isotopic composition was added to each sample and the isotopic composition of all FAME peaks was calculated relative to the isotopic composition of that InjSTD. The isotopic composition of the FAs was corrected for the addition of the carbon due to the derivatisation using a bimodal mixing model (Equation 24).

$$\delta^{13}\text{C}_{\text{FAME}} = x \cdot \delta^{13}\text{C}_{\text{FA}} + (1-x) \cdot \delta^{13}\text{C}_{\text{MeOH}}$$

Equation 24: Correction of the FA isotopic value.  $\delta^{13}\text{C}_{\text{FA}}$  is the carbon isotopic signature of the free acid,  $\delta^{13}\text{C}_{\text{FAME}}$  that of the FAME, and  $\delta^{13}\text{C}_{\text{MeOH}}$  the isotopic signature of the derivatisation agent,  $x$  is the carbon number of the underivatized FA.

The analytical error of all measurements as determined by a second InjSTD (Squalane; 10  $\mu\text{g/ml}$ ) was within  $\pm 0.5$  ‰. 4 samples were run in triplicate and reproducibility of the carbon isotopic values of all but one sample is better than  $\pm 0.5$  ‰.

## 7.3 Results

### 7.3.1 IP<sub>25</sub>

Figure 7.5 shows the IP<sub>25</sub> and the Squalane (IntSTD) mass spectra of the IP<sub>25</sub> standard and an ice algae sample. Only the two ice algae samples exhibit a peak that has the same retention time (39.9 min) as the IP<sub>25</sub> peak in the IP<sub>25</sub> standard. The sediment and water column POM samples, as well as the POM extracted from the ice cores, do not exhibit a peak with the same retention time as the IP<sub>25</sub> peak in the IP<sub>25</sub> standard. The compound detected in the ice algae samples was tentatively identified as IP<sub>25</sub>, however, there are notable differences in the mass

7. Can the carbon isotopic signature of sedimentary fatty acids reconstruct palaeo-sea-ice cover? A case study for the north-western Fram Strait

spectral characteristics of the mass fragments, which are discussed below. The concentration of the IP<sub>25</sub> peak in the two ice algae samples was 111 and 201 ng/g dry algal POM (concentration corrected for the weight of the GF/F filters used to filter the ice algal POM).

### 7.3.2 Fatty acid composition of ice algae, ice core, particulate organic matter and sediment samples

In this study the focus lies on the analysis of free fatty acids, rather than acids bound in esters. Figure 7.7 and 7.8 show typical chromatograms of the free fatty acids found in the ice algae, ice core, water column POM and sediment samples. The C<sub>16</sub> FA was the most prominent FA in all analysed samples and the only FA on which the isotopic composition was measured in all samples. Therefore, the main focus in the results and subsequent discussion section are on C<sub>16</sub>.

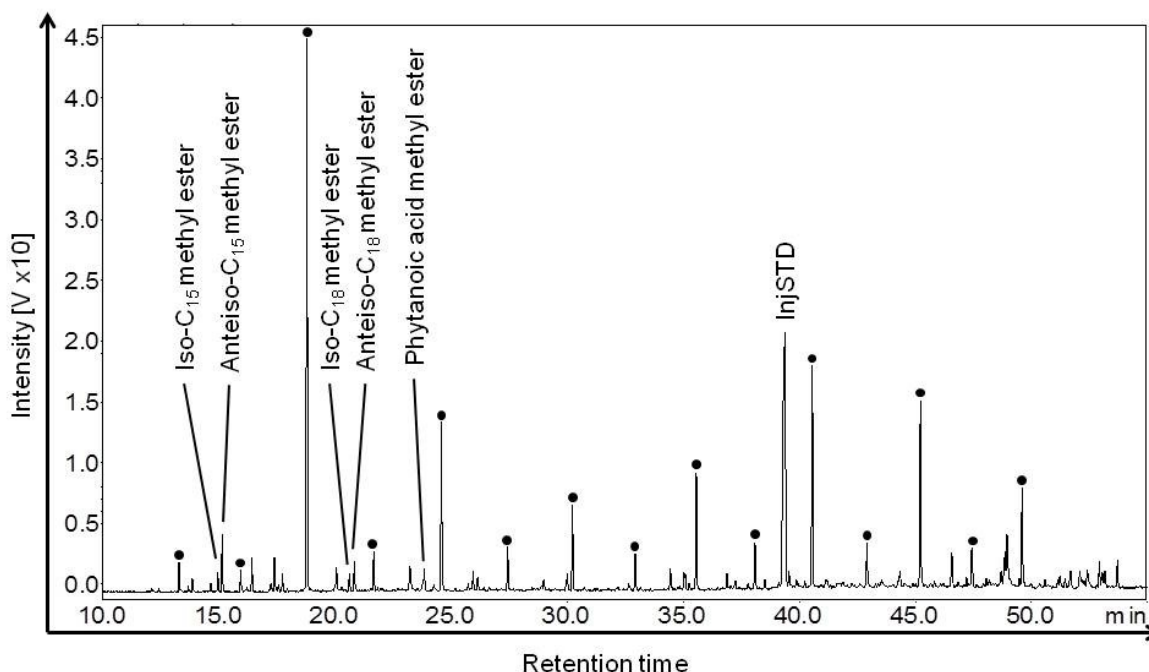


Figure 7.7: Chromatogram of the sedimentary fatty acid methyl esters from the pelagic station (10 cm bsf). The black dots denote the saturated, straight chained (C<sub>14</sub>-C<sub>28</sub>) fatty acids. The iso- and anteiso-fatty acids indicate the presence of bacteria (Viso & Marty, 1993). Phytanoic acid methyl ester is a degradation product of chlorophyll. The InjSTD is Squalane (10 µg/ml).

7. Can the carbon isotopic signature of sedimentary fatty acids reconstruct palaeo-sea-ice cover? A case study for the north-western Fram Strait

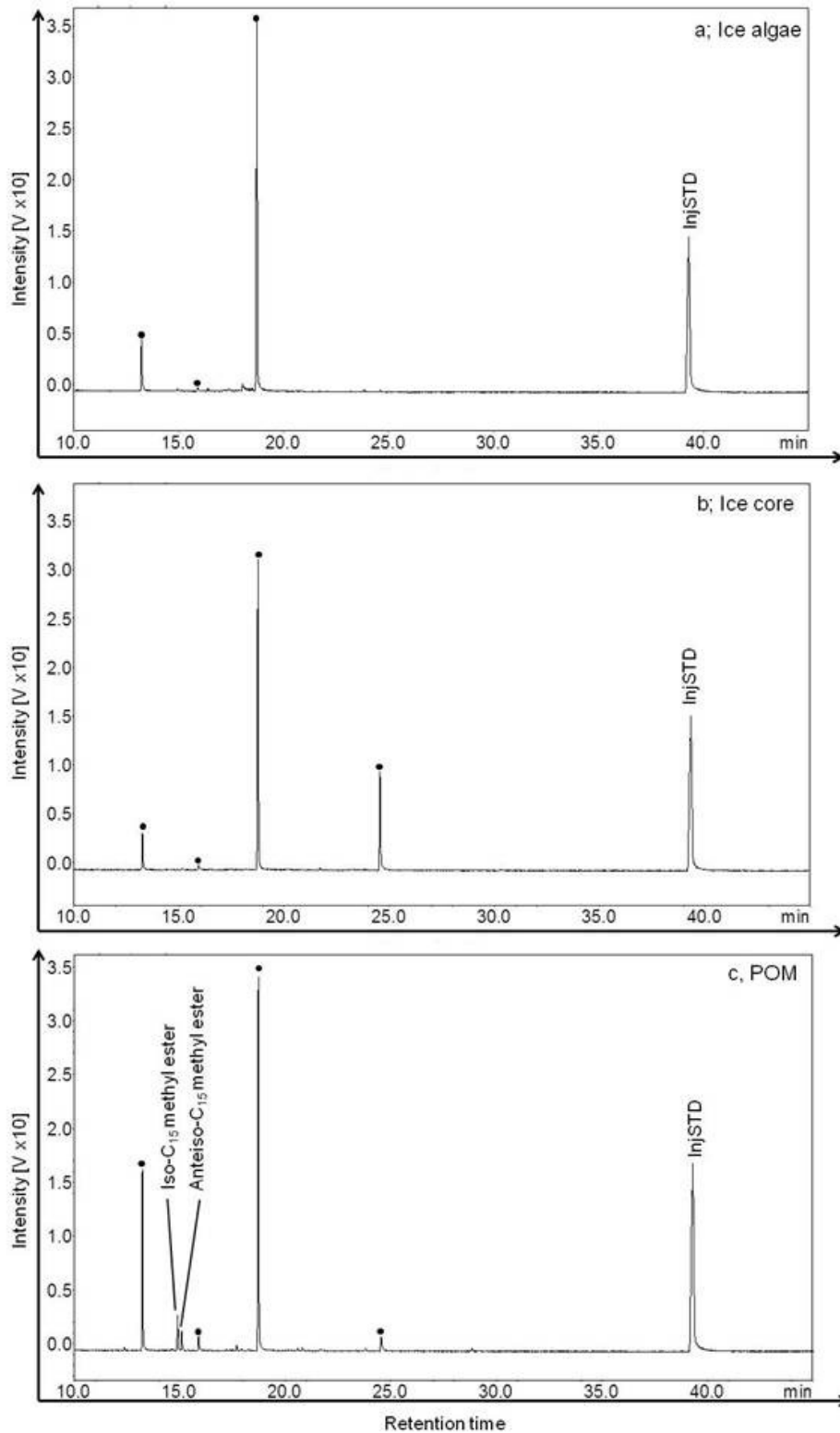


Figure 7.8: Free fatty acids in ice algae (a), ice core (b) and POM samples(c). Black dots indicate the saturated free fatty acids (C<sub>14</sub>-C<sub>18</sub>). The C<sub>17</sub>-FA is missing in all chromatograms and the C<sub>18</sub>-FA is missing in the ice algae chromatogram (a). The InjSTD is Squalane (10 µg/ml).

7. Can the carbon isotopic signature of sedimentary fatty acids reconstruct palaeo-sea-ice cover? A case study for the north-western Fram Strait

Table 3 shows the concentrations and the isotopic signature of the C<sub>16</sub> fatty acid of the POM samples. The concentrations of the C<sub>16</sub> FA of the POM samples range between 356 ng/g dry sample and 10,259 ng/g DS. The highest C<sub>16</sub> FA concentration was found in the ice core POM, and the lowest concentration was found in a water column POM sample from the ice station. Three water column POM samples were recovered from the IE, covering the whole water column. In the upper 500 m of the water column, the C<sub>16</sub> FA decreased from 972 to 950 ng/g DS. At a water depth of 934 m, just above the sediment/water column interface, the C<sub>16</sub> FA concentration was markedly lower at 488 ng/g DS.

Table 3: Concentrations and carbon isotopic signatures of the C<sub>16</sub> FA in the analysed POM from water column, ice algae and ice core samples.

Sample	type	depth [m]	Station	Sample weight* [g]	C <sub>16</sub> FA concentration ng/g dry sample	C <sub>16</sub> FA δ <sup>13</sup> C [‰]
1236	POM	5	MIZ	0.254	1697	-32.2 ± 0.2
1237	POM	5	MIZ	0.3376	2887	-29.6 ± 0.5
1238	POM	60	IS	0.234	856	-31.8
1239	POM	37	IS	0.857	356	-34.4
1240	POM	27	PS	0.2206	966	-32.2 ± 0.1
1241	POM	934	IE	0.107	488	-28.0
1242	POM	500	IE	0.107	950	-28.6 ± 1.2
1243	POM	57	IE	0.097	972	-34.0
1244	Ice algae	1	IS	0.9076	923	-19.5
1246	Ice algae	1	IS	0.3604	1745	-22.7
1247	Ice core		IS	0.0202	10259	-27.9

\*: sample weight was corrected for the weight of the filters used (0.13 ± 0.0007 g; n = 25)

The carbon isotopic signatures of the C<sub>16</sub> fatty acid of the POM samples vary between -19.5 and -34.4 ‰ (Figure 7.9). The C<sub>16</sub> FA of both ice algae samples exhibits the most <sup>13</sup>C enriched isotopic signature. The lightest carbon isotopic signatures found in water column samples were recorded at the IE and at the IS with values of -34 and -34.4 ‰ respectively. The C<sub>16</sub> FA along the water column depth gradient at the IE becomes more <sup>13</sup>C enriched with increasing depth.

7. Can the carbon isotopic signature of sedimentary fatty acids reconstruct palaeo-sea-ice cover? A case study for the north-western Fram Strait

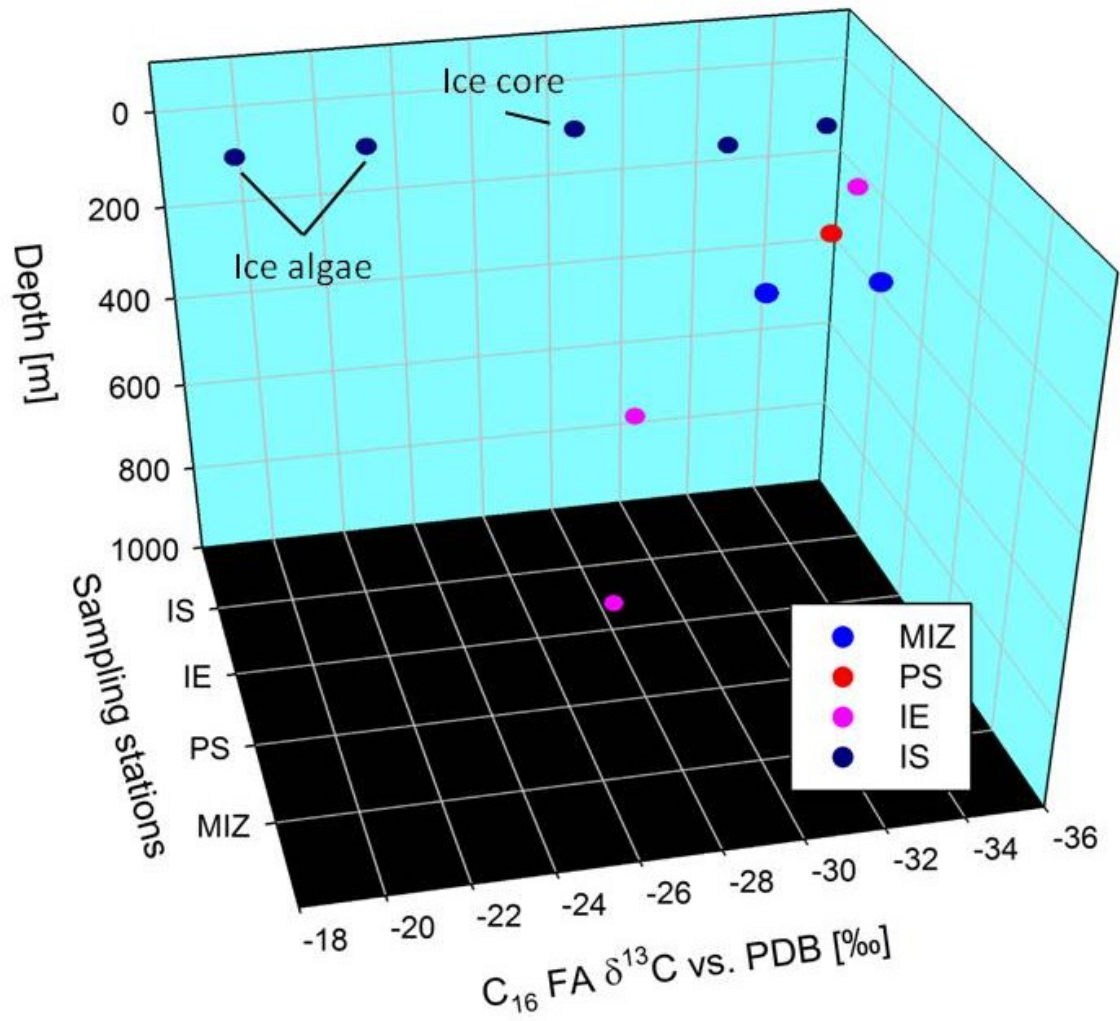


Figure 7.9: Carbon isotopic composition of the  $C_{16}$  FA in the POM samples.

Table 4 shows the concentrations and the isotopic signature of the  $C_{16}$  fatty acid of the POM samples. The  $C_{16}$  FA concentrations in the sediments at the PS and IE range between 132 and 2909 ng/g dry sediment. In the upper 15 cm of the sediment cores, the  $C_{16}$  FA concentration is higher at the IE than at the PS. Below 15 cm, the  $C_{16}$  FA concentration in the PS core is higher than in the IE core (Figure 7.10).

7. Can the carbon isotopic signature of sedimentary fatty acids reconstruct palaeo-sea-ice cover? A case study for the north-western Fram Strait

Table 4: Concentration and carbon isotopic signature of the C<sub>16</sub> FA found in sediments at the PS and IE. The sediment depth is given in cm below sea floor (bsf).

Sample	type	depth (cm bsf)	Station	Sample weight [g]	C <sub>16</sub> FA concentration ng/g dry sample	C <sub>16</sub> FA δ <sup>13</sup> C [‰]
1248	Sediment	2	PS	8.46	681	-26.4 ± 1.0
1249	Sediment	3	PS	7.45	365	-25.6 ± 0.1
1250	Sediment	4	PS	6.42	344	-25.7
1251	Sediment	5	PS	6.51	156	-25.5
1252	Sediment	6	PS	7.23	414	-26.2
1253	Sediment	10	PS	7.42	381	-27.6 ± 0.5
1254	Sediment	15	PS	10.39	143	-27.7
1255	Sediment	20	PS	7.98	647	-27.8 ± 0.1
1256	Sediment	25	PS	7.1	330	-27.8 ± 0.1
1257	Sediment	30	PS	9.05	369	-27.5
1258	Sediment	2	IE	7.5	1406	-30.5
1259	Sediment	3	IE	7.15	621	-24.1
1260	Sediment	4	IE	9.93	614	-24.4 ± 0.1
1261	Sediment	5	IE	6.24	360	-24.6 ± 0.4
1262	Sediment	6	IE	5.99	587	-24.7
1263	Sediment	7	IE	7.61	1966	-24.2
1264	Sediment	8	IE	7.57	2909	-24.3
1266	Sediment	10	IE	7.11	1217	-26.1 ± 0.8
1267	Sediment	15	IE	8.3	665	-24.8 ± 0.1
1268	Sediment	20	IE	8.22	133	-26.3 ± 0.7
1269	Sediment	25	IE	7.7	132	-27.71

The isotopic signatures of the C<sub>16</sub> FA in the IE core are more <sup>13</sup>C enriched than those of the PS core in the upper 20 cm below the sea floor (bsf). However, the C<sub>16</sub> FA isotopic signature becomes more <sup>13</sup>C depleted with depth in both cores, but more so in the ice edge sediment core (Figure 7.10). At 25 cm bsf the C<sub>16</sub> FA carbon isotopic signature in both cores the same within the analytical error.

7. Can the carbon isotopic signature of sedimentary fatty acids reconstruct palaeo-sea-ice cover? A case study for the north-western Fram Strait

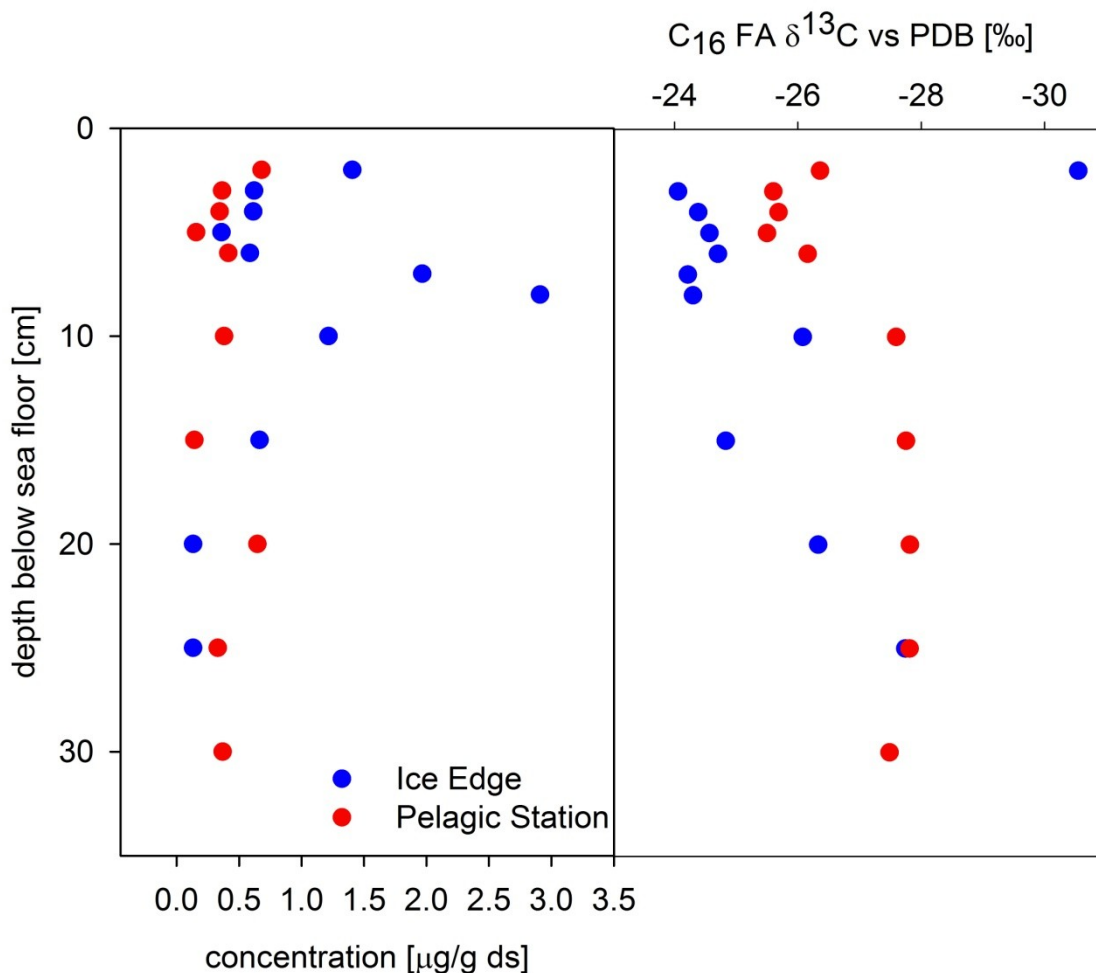


Figure 7.10: Concentrations and isotopic signatures of the C<sub>16</sub> FA of the PS and IE sediments

### 7.3.3 Amount of sea ice cover over the coring sites

A two end member model was used to evaluate the fraction of ice algal C<sub>16</sub> FA ( $f_{IA}$ ) to the sedimentary C<sub>16</sub> pool (**Error! Reference source not found.**)

$$f_{IA} = \frac{X_{\text{sample}} - X_{PA}}{X_{IA} - X_{PA}}$$

Equation 25: Two end-member model to calculate the contribution of ice algal C<sub>16</sub> FA to marine sediments.  $X_{\text{sample}}$ ,  $X_{PA}$  and  $X_{IA}$  represent the isotopic values of the C<sub>16</sub> FA representing the sample, the pelagic algae end member and the ice algae end-member, respectively.

7. Can the carbon isotopic signature of sedimentary fatty acids reconstruct palaeo-sea-ice cover? A case study for the north-western Fram Strait

The mean C<sub>16</sub> FA δ<sup>13</sup>C value of all sediment samples from the ice edge is -25.6 ± 1.9 ‰. The mean C<sub>16</sub> FA δ<sup>13</sup>C value of all sediment samples from the pelagic station is slightly more depleted with -26.8 ± 0.9 ‰. By using the end member C<sub>16</sub> FA δ<sup>13</sup>C values for ice and pelagic algae and the mean isotopic composition of the C<sub>16</sub> FA in the sediment samples from the IE and PS cores, the relative amount of ice algal C<sub>16</sub> FA contribution to the total C<sub>16</sub> FA pool is calculated. The mean contribution of ice algae to the C<sub>16</sub> FA pool in the ice edge sediment core is 60 %. The mean contribution of ice algae to the C<sub>16</sub> FA pool at the pelagic station is 49.7 %.

## **7.4 Discussion**

### **7.4.1 IP<sub>25</sub>**

A peak in the apolar fraction of the extract of the two ice algae samples was tentatively identified as IP<sub>25</sub>. The identification is based on the comparison of the retention time and SIM mass spectra (Figure 7.5) of the peak in the ice algae samples, with the IP<sub>25</sub> peak in the IP<sub>25</sub> standard. The identification of that peak remains tentative because of the different intensities of some of the mass fragments in the SIM mass spectrum of the samples, compared to the SIM mass spectrum of the relevant peak in the IP<sub>25</sub> standard. The difference in the relative intensities of some of the mass fragments of the IP<sub>25</sub> peak in the sample compared to the IP<sub>25</sub> peak in the IP<sub>25</sub> standard suggests that another compound maybe co-eluting. For example the diene was not completely separated from the IP<sub>25</sub> peak in the IP<sub>25</sub> standard. The increased influence of mass fragments common to both the diene and the IP<sub>25</sub> can account for the difference in the mass spectra, particularly, if the concentration of the diene is as high, or higher than that of the IP<sub>25</sub>. Another possible explanation is the occurrence of a regioisomer of IP<sub>25</sub>, where the double bond is located in a different position. Such constitutional isomers of IP<sub>25</sub>, which are of diatomaceous origin, have been reported in sediments of the Florida Bay (Xu *et al.*, 2006), and in hypersaline sediments in Australia (Dunlop & Jefferies, 1985).

## 7. Can the carbon isotopic signature of sedimentary fatty acids reconstruct palaeo-sea-ice cover? A case study for the north-western Fram Strait

The IP<sub>25</sub> molecule has previously been associated with diatoms of the genus *Haslea* (Belt *et al.*, 2007). The algal community of one ice algal clump from the studied area was microscopically analysed and contains diatoms of the genera *Navicula* (59 %), *Tropidoneis* (10 %), *Nitzschia* (~ 9%) and *Achnanthes* (6 %) (Leakey *et al.*, in prep). No diatoms of the genus *Haslea* were detected. Such diatoms were also not found in a previous study of ice algal assemblages southwest of Svalbard in the Barents sea (Falk-Petersen *et al.*, 1998; Syvertsen, 1991). The fact that *Haslea* spp. was not detected, may explain, why the IP<sub>25</sub> molecule was not found in large abundances in the ice algal samples, and not at all in the water column, ice core or sediment samples. Furthermore, if the tentatively identified peak is in fact IP<sub>25</sub>, then diatoms of other genera than *Haslea* are responsible for its production.

The lack of IP<sub>25</sub> in the sea-ice samples, even in the ice-algae colonies, calls the use of the IP<sub>25</sub> as a sea-ice proxy into question. IP<sub>25</sub> may only be a proxy for sea-ice in specific regions, where *Haslea* spp. are at least seasonally abundant.

### **7.4.2 Fatty acid composition of ice algae, ice core, particulate organic matter and sediment samples**

The C<sub>16</sub> FA is the most abundant fatty acid found in all samples. None of the samples analysed in this study contained FAs typical for ice algal diatoms such as the C<sub>16:4(n-1)</sub> and the C<sub>20:5(n-3)</sub> FAs (Dalsgaard *et al.*, 2003; Falk-Petersen *et al.*, 1998). High amounts of C<sub>16</sub> and C<sub>18</sub> FAs in the water column in the vicinity of sea-ice have previously been reported in the Arctic and Antarctic (Fahl & Kattner, 1993; Falk-Petersen *et al.*, 1998). Falk-Petersen *et al.* (1998) suggest that a shift towards higher amounts of saturated FAs may be a result of copious amounts of decaying or decomposed OM in the water column. Therefore, the results presented here may indicate that the sampled ice algae were dead or dying and that the biologically mediated diagenesis of algal OM was advanced in all sample types. Another explanation for the lack of unsaturated fatty acids may be found in the way the samples were treated. The esters in the samples were not hydrolysed. Therefore, any fatty acids bound in esters were not analysed. Thus the results

## 7. Can the carbon isotopic signature of sedimentary fatty acids reconstruct palaeo-sea-ice cover? A case study for the north-western Fram Strait

indicate: a) that most unsaturated FAs, which are typically found in ice and pelagic algae, are possibly bound as esters, or b) unsaturated FAs decay rapidly. In addition to the straight chained fatty acids associated with algae, branched fatty acids, which are of bacterial origin (Viso & Marty, 1993) were detected in all samples (Figure 7.7). However, the concentration of bacterial derived fatty acids was considerably lower than that of the C<sub>16</sub> FA. Long chain saturated fatty acids with a strong even over odd carbon chain lengths predominance were detected in the sediment samples. These FAs are typically found in the wax coating of higher land plants (Eglinton *et al.*, 1968) and are transported by aeolian, riverine and sea-ice to the location where they are deposited (Birgel *et al.*, 2004). However, long chain (C<sub>24</sub>) FAs are also produced by arctic phytoplankton (Henderson *et al.*, 1998), and even though no long chain FAs were detected in the water column or the algal samples, the possibility that a certain proportion of the long chain FAs in the sediments are not of terrestrial origin cannot be excluded.

### 7.4.2.1 Carbon isotopic composition of C<sub>16</sub> FA of POM

The ice algae samples exhibit the most <sup>13</sup>C enriched C<sub>16</sub> FA carbon isotopic signature of all the analysed samples. Similar isotopic signatures to the ones reported here have previously been reported. Tاملander *et al.* (2008) collected POM from beneath sea-ice with a δ<sup>13</sup>C value of -20 ± 3.8 ‰. The C<sub>16</sub> FA retrieved from ice cores from the Canadian Arctic has an isotopic signature of -14.7 ± 4.7 ‰ (Brown *et al.*, 2011). Budge *et al.* (2008) analysed two FAs originating from ice algae, and found that the C<sub>20:5(n-3)</sub> FA was significantly more <sup>13</sup>C enriched (-18.2 ± 2 ‰) than the C<sub>16:1(n-4)</sub> FA (-24 ± 2.4 ‰). The isotopic values of both FAs of pelagic phytoplankton were significantly more depleted compared to the δ<sup>13</sup>C isotopic signature of ice algal FAs. The isotopic signature of the C<sub>16</sub> FA derived from the ice cores was expected to be similarly enriched in <sup>13</sup>C compared to the ice algal samples. However, the isotopic signature of -27.9 ‰ suggests that diatoms may not be the only contributor to the C<sub>16</sub> FA pool within the sea-ice. Indeed, Riedel *et al.* (2008) have shown that other microorganisms such as bacteria can contribute up to 60 % of the total carbon found in sea-ice. Very small amounts of

7. Can the carbon isotopic signature of sedimentary fatty acids reconstruct palaeo-sea-ice cover? A case study for the north-western Fram Strait

branched FAs associated with bacteria were detected. Thus the  $^{13}\text{C}$  signature of the  $\text{C}_{16}$  FA isotopic signature in the ice cores may be affected by bacteria. Another explanation for the  $^{13}\text{C}$  depleted  $\text{C}_{16}$  FA isotopic signature in the ice cores comes from the structure of the sea-ice itself. Based on the distribution of the  $\text{IP}_{25}$  biomarker in ice cores and its association with diatoms, Brown *et al.* (2011) hypothesise that a brine volume fraction of at least 5 % is needed for diatoms to grow. The light  $\delta^{13}\text{C}$  values of the sea-ice suggest that ice algae may not have been prominent within the sea-ice, possibly because the sea-ice was not porous enough for diatoms to grow within its brine channels. However, the highly enriched  $^{13}\text{C}$  signature of the  $\text{C}_{16}$  FA of the ice algae found floating beneath the ice strongly suggests that these diatoms grew within the ice. The *RRS James Clark Ross* was moored to the ice floe at the ice station for a total of eight days. During that time the ice was melting fast, and finally the ship had to leave the ice station because the ice floe had become unstable. It is suggested that prior to the arrival at the ice station, the ice must already have melted significantly, releasing the ice algae that was subsequently found floating beneath the ice. Brown *et al.* (2011) show that the brine volume within the ice decreases with increasing distance from the water/ice boundary layer. The remaining ice which was sampled in the form of ice cores represents the upper portion of the ice floe, with brine volumes too small for a significant amount of diatoms to grow in.

The  $\delta^{13}\text{C}$  values of the ice algae samples are markedly enriched in  $^{13}\text{C}$  compared to the isotopic signature of the  $\text{C}_{16}$  FA from water column derived POM (Figure 7.9). During photosynthesis,  $\text{CO}_2$  molecules containing the  $^{12}\text{C}$  rather than the  $^{13}\text{C}$  isotope are preferentially utilised (Deuser *et al.*, 1968). When  $\text{CO}_2$  becomes depleted, the heavier  $\text{CO}_2$  species starts to get used, causing the  $\delta^{13}\text{C}$  signature of subsequently produced OM to be more  $^{13}\text{C}$  enriched (Deuser *et al.*, 1968; McMinn *et al.*, 1999). Diatoms utilise the  $\text{CO}_2$  which is dissolved in sea water and transported through the brine channels of the ice. With increasing distance from the ice/water interface, the amount of available  $\text{CO}_2$  decreases. The decrease in available  $\text{CO}_2$  can be caused by a decreased supply of  $\text{CO}_2$ , or increased demand. McMinn *et al.* (1999) suggest that a decreased supply of  $\text{CO}_2$  is more likely as very high algal growth rates are required to cause a decline of the

7. Can the carbon isotopic signature of sedimentary fatty acids reconstruct palaeo-sea-ice cover? A case study for the north-western Fram Strait

available CO<sub>2</sub>. However, increased growth rates can also drain the CO<sub>2</sub> supply and lead to decreased  $\delta^{13}\text{C}$  fractionation (Deuser *et al.*, 1968). Even though restricted CO<sub>2</sub> availability has marked effect on the carbon isotopic signature of ice algal organic matter, in this case on the C<sub>16</sub> FA, other factors such as cell growth and phenotype controls likely make the relationship between CO<sub>2</sub> availability and <sup>13</sup>C enrichment of ice algal OM more complicated (Belt *et al.*, 2008; Pancost *et al.*, 1997).

The carbon isotopic signature of the C<sub>16</sub> FA of the water column derived POM from the IS is significantly <sup>13</sup>C depleted. The same is true for the water column derived POM samples from the MIZ and IE stations (Figure 7.9, Table 3). Within the photic zone, the C<sub>16</sub> FA  $\delta^{13}\text{C}$  values vary around -32.4 ‰. This value is very close to that of the isotopic value of the C<sub>16</sub> FA from the POM sample taken at the pelagic station. It has previously been shown that POM and individual FAs, which are mainly derived from pelagic algae are <sup>13</sup>C depleted compared to ice algal POM (Budge *et al.*, 2008; Tamelander *et al.*, 2008). Even though the MIZ, the IS and the IE are influenced by sea-ice, the depleted isotopic values suggest that the main source of the POM are pelagic algae. Either OM from ice algae does not contribute to the water column POM, or the dominance of pelagic phytoplankton overprints any influence on the isotopic signal from ice algae. It seems unlikely that ice algae do not contribute to the POM samples from the stations which are influenced by sea-ice. It is however plausible, that pelagic phytoplankton dominates the water column POM directly underneath the ice. Large phytoplankton blooms are associated with melting sea-ice at the ice edge (Falk-Petersen *et al.*, 1998). These phytoplankton blooms which may initially be seeded by algae released from melting sea-ice, occur all along the ice edge during summer (Syvertsen, 1991). The melting ice causes stratification of the upper water column, keeping the phytoplankton in the euphotic zone (Engelsen *et al.*, 2002). Furthermore, Atlantic water transports nutrients to the eastern Fram Strait (Rudels *et al.*, 1991). The combination of these conditions cause the region around Svalbard to be one of the most productive marine areas in the northern hemisphere (Falk-Petersen *et al.*, 1998). Thus it is plausible that the water column

7. Can the carbon isotopic signature of sedimentary fatty acids reconstruct palaeo-sea-ice cover? A case study for the north-western Fram Strait

POM is dominated by pelagic algae, completely overprinting the ice algae isotopic signal.

Throughout the water column, the carbon isotopic signature of the C<sub>16</sub> FA is not stable. The isotopic signature of the C<sub>16</sub> FA from POM samples from three depths covering the whole water column at the ice edge becomes more enriched in <sup>13</sup>C in the deeper samples compared to the shallow sample (Figure 7.9). There are two possible reasons for this observation. Either there is a measurable ice algal contribution to the POM at depth, or organisms which feed on ice- and pelagic algae alter the isotopic composition of the C<sub>16</sub> FA.

It seems unlikely that metabolic effects on the isotopic composition of the C<sub>16</sub> FA pool cause the observed <sup>13</sup>C enrichment. The enzymes of the FA metabolism prefer to utilise the isotopically light precursor molecules (Budge *et al.*, 2008; references therein). Thus, decreasing  $\delta^{13}\text{C}$  values with depths are expected to be observed, if grazers of pelagic and ice algae significantly affect the C<sub>16</sub> FA isotopic composition by contributing to its pool. Even though metabolic processes in algal predators do not seem to significantly alter the isotopic composition of the C<sub>16</sub> pool, these predators may have a significant effect on the efficiency of OM export from the photic zone. For example, *Calanus* sp. copepods represent the prime herbivores in the food chain of the arctic and Nordic seas (Falk-Petersen *et al.*, 2009). As a specialised adaptation to the seasonality of the food availability *Calanus* sp. species synthesise wax esters as storage lipids. The acid moiety of these wax esters predominantly originates from the prey of the *Calanus* sp. zooplankton (Sargent & Falk-Petersen, 1988) and is incorporated into the wax esters largely unaltered (Dalsgaard *et al.*, 2003). Therefore, the isotopic composition of the C<sub>16</sub> FA incorporated by *Calanus* sp. is not significantly altered. *Calanus* sp. copepods migrate to deeper parts of the water column in response to predatory pressure (Falk-Petersen *et al.*, 2009). Thus *Calanus* sp. zooplankton may contribute to the export of isotopically unaltered FAs such as the C<sub>16</sub> FA from the photic zone to deeper parts of the water column and subsequently the sediment. The hydrolysis of such wax esters could free up FAs with an isotopic composition that directly

7. Can the carbon isotopic signature of sedimentary fatty acids reconstruct palaeo-sea-ice cover? A case study for the north-western Fram Strait

reflects the relative abundance of ice vs. pelagic algae fed upon by *Calanus* sp. zooplankton in the photic zone.

Seasonal pulses of POM produced via algal blooms at the edge of the melting sea-ice can lead to a large amount of vertical POM export (Tamelander *et al.*, 2008). Wassmann *et al.* (1996) have shown that high OM fluxes out of the photic zone coincide with algal blooms. During periods of high primary production, the abundance of POM in the water column can thus cause increased POM export with little or no alteration by zooplankton. Smith *et al.* (2002) have shown the the  $\delta^{13}\text{C}$  isotopic signature of POM collected in sediment traps becomes more  $^{13}\text{C}$  enriched with increased primary production both in space and time. This enrichment is thought to be due to high amounts of primary produced OM.

Consequently the  $^{13}\text{C}$  enrichment of the  $\text{C}_{16}$  FA with depth observed at the ice edge may reflect an increased proportion of  $\text{C}_{16}$  FA derived from ice algal production or increased primary production due to blooms which are associated with the proximity of sea-ice in the Arctic ocean, as discussed above.

#### 7.4.2.2 Carbon isotopic composition of $\text{C}_{16}$ FA of sediments

The  $\text{C}_{16}$  FA is found ubiquitously in lacustrine and marine environments and it is established that a wide range of phytoplankton species biosynthesise it (Viso & Marty, 1993; Volkman *et al.*, 1998). However, because it is very abundant in the ice algae and POM samples analysed, it is likely that the major source of the  $\text{C}_{16}$  FA in the sediments studied here originates from ice algae or pelagic phytoplankton. It is recognised, that bacteria also produce  $\text{C}_{16}$  FA, and the occurrence of iso- and anteiso fatty acids in the sediments shows the existence of such bacteria (Figure 7.7). However the concentration of these FAs is very low in all samples and similar low concentrations (5-10 %) of bacterially produced FAs in recent Fram Strait sediments have previously been reported (Birgel *et al.*, 2004). Therefore, it is suggested that the contribution of bacterially synthesised  $\text{C}_{16}$  to the total  $\text{C}_{16}$  pool is negligible.

7. Can the carbon isotopic signature of sedimentary fatty acids reconstruct palaeo-sea-ice cover? A case study for the north-western Fram Strait

Under the assumption that the sediment collected at the IE receives more input from ice algal OM than the sediments at the PS, it is expected that the isotopic signature of the C<sub>16</sub> FA in the sediments of the IE is more <sup>13</sup>C enriched, than the C<sub>16</sub> FA found in PS sediments. With the exception of the core top samples and the samples 25 cm bsf, the δ<sup>13</sup>C signatures of the C<sub>16</sub> FA from the IE sediments are more enriched than those from the PS (Figure 7.10). However, other factors such as lateral OM transport in the water column and biological degradation in the core top sediments may also affect the carbon isotopic signature of the C<sub>16</sub> FA. The C<sub>16</sub> FA concentration decreases rapidly in the first 25 cm of sediment, coinciding with a trend towards <sup>13</sup>C depleted carbon isotopic signatures. Both trends are more pronounced in the IE core, compared to the PS core. Culturing experiments with <sup>13</sup>C labelled ice algal OM have shown that benthic organisms readily respond to, and consume ice algal OM (McMahon *et al.*, 2006; Sun *et al.*, 2007). The ubiquitous occurrence of the C<sub>15</sub> and C<sub>17</sub> iso and anteiso FAs in the sediment samples indicates that bacteria are present (Viso & Marty, 1993). Sun *et al.* (2007) observed an increase in bacteria specific fatty acids immediately after adding ice algal and phytoplankton detritus to culturing sediments, indicating that benthic bacteria play a major role in the OM degradation. When ice algae are the primary food source of benthic bacteria, ice algal polyunsaturated FAs are preferentially utilised. In the absence of ice algal OM, saturated FAs from phytoplankton are rapidly used (Sun *et al.*, 2007). <sup>13</sup>C labelling experiments have shown, that surface sediment organic carbon isotopic signatures become more <sup>13</sup>C depleted as a consequence of benthic grazing (McMahon *et al.*, 2006; Middelburg *et al.*, 2000). Therefore, biologically mediated diagenesis of the C<sub>16</sub> FA pool can account for the down core <sup>13</sup>C depletion of the C<sub>16</sub> FA in the sediment samples.

The lateral transport of organic matter can also influence the isotopic composition of the C<sub>16</sub> FA in both studied sediment cores. The Fram Strait is occupied by a number of different water masses flowing in different directions (Rudels *et al.*, 2000). Schewe & Stoltwedel (2003) have shown that the lateral transport of OM in the eastern and central Fram Strait is affected by the northward flow of Atlantic water, while the southward flow of the east Greenland current affects the lateral

7. Can the carbon isotopic signature of sedimentary fatty acids reconstruct palaeo-sea-ice cover? A case study for the north-western Fram Strait

transport of OM in the western Fram Strait. Thus it is conceivable that C<sub>16</sub> FA originating from phytoplankton from the southern Fram Strait is contributing to the sedimentary C<sub>16</sub> pool of the ice edge sediments. Such a contribution would lead to overall lighter  $\delta^{13}\text{C}$  values of the C<sub>16</sub> FA in the ice edge sediments. Consequently the down core  $^{13}\text{C}$  depletion may indicate a strengthening of the Atlantic water current, transporting more pelagic algal material to the ice edge sediment.

The previous discussion shows that a number of different factors can affect the isotopic composition of the C<sub>16</sub> FA other than ice cover and subsequent contribution of ice algal OM. However, under the assumption, that the isotopic composition of the sedimentary C<sub>16</sub> FA pool is primarily affected by varying amounts of ice algal contribution, and that other influences on the carbon isotopic signature of sedimentary C<sub>16</sub> FA are similar in both sediment cores and in the overlying water column, and thus cancel each other out, then the data indicates, that the ocean above the ice edge sediments has been completely or partially ice covered more often than the ocean above the pelagic station sediments (Figure 7.10)

A two end member model was used to calculate the percentile contribution of ice algal C<sub>16</sub> FA. This approach requires a number of assumptions to be made. Firstly it is assumed that most of the C<sub>16</sub> FA reaching the sediments originates either from ice algal or pelagic phytoplankton. This assumption seems plausible due to the fact that the Fram Strait is characterised by extremely high primary production. However, as discussed earlier, the OM produced via primary production enters the food chain and is altered to some degree by biological degradation in the water column and sediments. The C<sub>16</sub> FAs produced via secondary production by pelagic and benthic herbivores likely has an altered isotopic composition compared to the C<sub>16</sub> FA isotopic composition of the food source. This constitutes an error source to the estimate of the contribution of ice algal C<sub>16</sub> FA to the sediments. The second assumption is, that the C<sub>16</sub> FA isotopic values of pelagic and ice algae represent the end member values. The mean ice algal C<sub>16</sub>  $\delta^{13}\text{C}$  value of both analysed ice algal samples is -21.1 ‰, and represents the ice algae end-member value in this study. The C<sub>16</sub> FA produced by ice algae in the

7. Can the carbon isotopic signature of sedimentary fatty acids reconstruct palaeo-sea-ice cover? A case study for the north-western Fram Strait

Canadian Arctic has been shown to be markedly more  $^{13}\text{C}$  enriched (Brown *et al.*, 2011), compared to the  $\text{C}_{16}$  FA from the ice algae studied here. This suggests that at least the end member value for ice algae used here can only be applied to the region of the Fram Strait. Furthermore, Budge *et al.* (2008) have shown, that FAs originating from ice algae have varying isotopic signatures. Therefore, the use of different FAs can give varying results. The mean isotopic value of water column POM derived  $\text{C}_{16}$  FA is  $-32.4\text{‰}$ , and is used here as the pelagic algae end-member value. The  $\text{C}_{16}$  FA in the POM samples has been mainly attributed to pelagic algae (see previous discussion). All carbon isotopic values of the  $\text{C}_{16}$  FA in sedimentary samples studied here range between the  $\delta^{13}\text{C}$  values of the ice and pelagic algal  $\text{C}_{16}$  FA validating those values as end member values. The third assumption that is made is that there is a linear relationship between the amount of sea-ice and ice algae and subsequently produced  $\text{C}_{16}$  FA. Brown *et al.* (2011) have shown that the FA concentration is positively correlated with ice algal blooms, suggesting that it is legitimate to assume, that the amount of isotopically heavy  $\text{C}_{16}$  FA reflects the amount of ice algae and thus sea-ice cover.

The mean contribution of ice algae to the  $\text{C}_{16}$  FA pool in the ice edge sediment core is  $60\%$ , while the mean contribution of ice algae to the  $\text{C}_{16}$  FA pool at the pelagic station is  $49.7\%$ . The result suggests that the water column above the IE sediments has been more strongly influenced by sea-ice than the water column above the pelagic station.

Even though a number of different biological and oceanographic factors, above and beyond their ice or pelagic algal source (Figure 7.11), affect the isotopic composition of the  $\text{C}_{16}$  FA, the above back of the envelope calculation suggests that the isotopic composition of the  $\text{C}_{16}$  FA in sediments can be used to estimate the amount of sea-ice cover in a certain area.

7. Can the carbon isotopic signature of sedimentary fatty acids reconstruct palaeo-sea-ice cover? A case study for the north-western Fram Strait

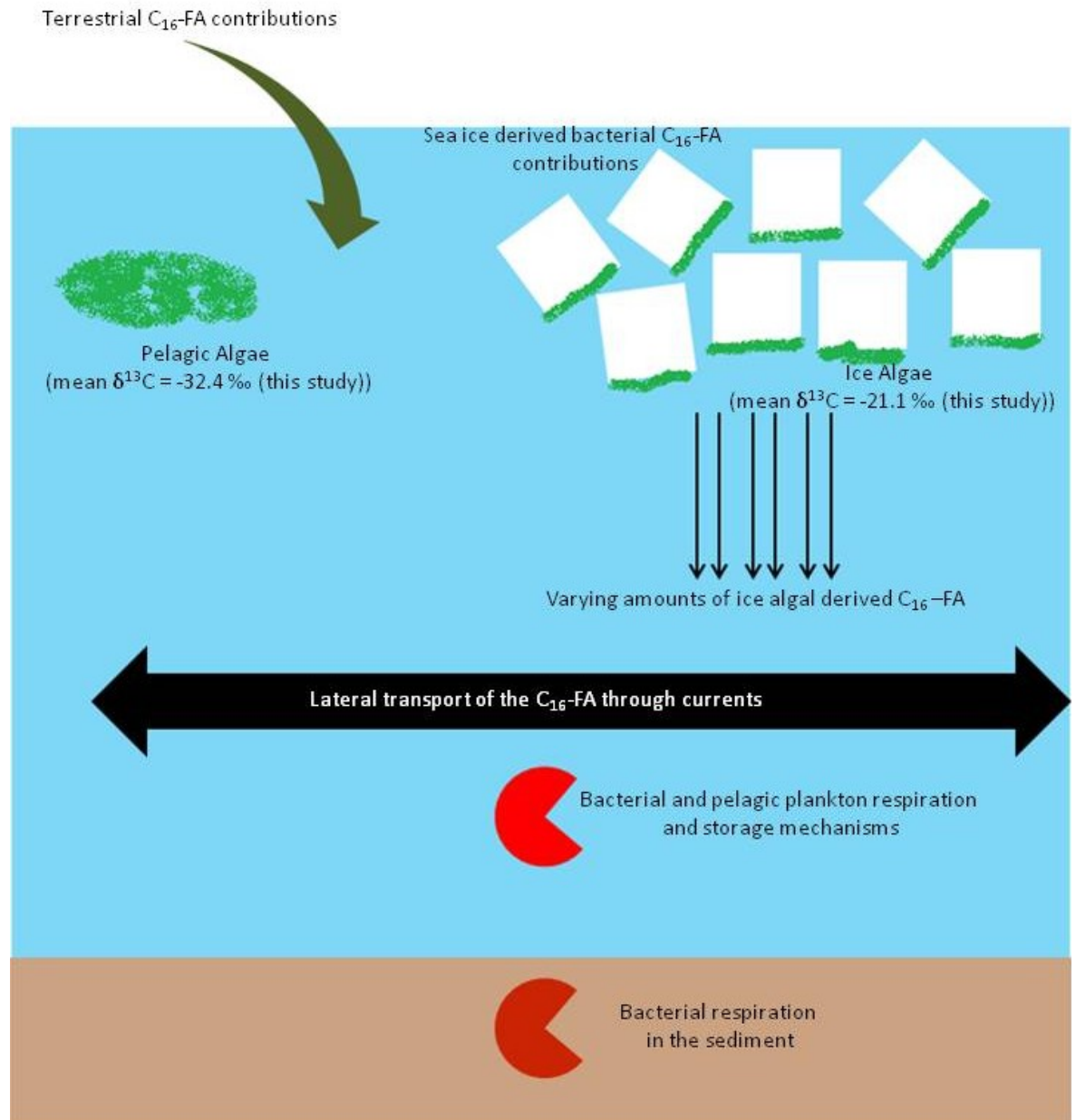


Figure 7.11: Summary of  $C_{16}$ -FA producers and the oceanographic and biological processes (as discussed in this thesis) affecting the carbon isotopic signature of the  $C_{16}$ -FA in the sediments studied in this thesis.

## 7.5 Conclusion

The aim of this study was to determine whether the carbon isotopic signature of fatty acids found in sediments can be used to evaluate the presence or absence of sea-ice cover. The intention was to compare the variations of the FA isotopic signature with the occurrence of the  $IP_{25}$ , a recently established biomarker for the

7. Can the carbon isotopic signature of sedimentary fatty acids reconstruct palaeo-sea-ice cover? A case study for the north-western Fram Strait

presence or absence of sea-ice. A compound found in the ice algae samples was tentatively identified as IP<sub>25</sub>. However, IP<sub>25</sub> was not detected in the sediment, ice core, or water column POM samples that were studied. The production of the IP<sub>25</sub> has been linked to diatoms of the genus *Haslea*. This type of diatom was not detected in the ice algal samples. If the peak that was identified is indeed IP<sub>25</sub>, then other diatoms which are part of the ice algal community are also responsible for its production, but these diatoms probably produce much lower quantities than *Haslea* spp.

IP<sub>25</sub> seems to only indicate sea-ice in areas, where diatoms of the genus *Haslea* are present in sea-ice. The fact, that IP<sub>25</sub> could not be detected in sediments, which underlie a water column covered at least periodically by sea-ice, emphasises the need for another approach to the evaluation of paleo-sea-ice cover. It is suggested that one such approach constitutes the study of the isotopic signatures of FAs, as the <sup>13</sup>C depletion of these compounds gives insight into whether ice or pelagic algae are their source.

The C<sub>16</sub> FA isotopic composition from pelagic and ice algae, and that of sediments affected by different levels of sea-ice cover, was studied. The ice algal C<sub>16</sub> FA is markedly <sup>13</sup>C enriched compared to that sourced from pelagic algae. However, the C<sub>16</sub> FA isotopic signature in ice cores was not distinctly <sup>13</sup>C enriched, which is likely due to microbial organisms populating the ice and due to the ice structure itself. The C<sub>16</sub> FA of the water column POM under the ice was found to have an isotopic signature indicative of pelagic algae. This is attributed to the occurrence of phytoplankton blooms close to the marginal ice zone. The sedimentary C<sub>16</sub> FA isotopic signature at the ice station was found to generally be more <sup>13</sup>C enriched than that of the pelagic sediments. The use of a binary mixing model revealed, that the mean contribution of ice algae to the ice edge sediment core is nearly 11% higher than than the ice algae contribution to the pelagic station core.

The C<sub>16</sub> FA is ubiquitous in the marine realm. By better constraining the source of the FAs through the study of diatom specific fatty acids such as C<sub>16:4(n-1)</sub> and

7. Can the carbon isotopic signature of sedimentary fatty acids reconstruct palaeo-sea-ice cover? A case study for the north-western Fram Strait

$C_{20:5(n-3)}$  for example, better estimates on the occurrence of sea-ice will likely be achieved.

The interpretation of the isotopic signature of FAs is by no means straight forward. For example lateral transport of fatty acids by current systems, particularly in the Fram Strait, likely introduces an error to the estimation of sea-ice cover. Furthermore, FAs are a high value food source for pelagic and benthic organisms, and by metabolising FAs and producing their own, they affect the isotopic signature of the FA pool. This is obvious in the down core variability of the  $C_{16}$  FA in both cores, and impacts the use of  $C_{16}$  FA isotopic signatures as a palaeo sea-ice proxy. However, under the assumption that these factors affect the isotopic signature of the  $C_{16}$  FA in the sediments of both stations in a similar way, the marked  $^{13}C$  enrichment of the sediments at the ice station compared to the pelagic station is attributed to increased amounts of ice cover at the ice station.

One more point will need to be considered if the isotopic signatures of FAs are to be utilised in assessing past sea-ice extent and that is the residence time of such compounds in sediments. In light of the fact that FAs are a preferred food source for microorganisms compared to, for example, aliphatic compounds, the residence time of FAs in sediments may be comparatively short compared to the  $IP_{25}$ . Indeed, Cranwell (1981) showed that the stability of organic compounds in lacustrine sediments increased from unsaturated FAs to saturated FAs, and that the most stable organic compounds in sediments are *n*-alkanes. The  $C_{16:1(n-7)}$  FA, sourced from marine phytoplankton, has been detected in Fram strait sediments as old as 17,000 years (Birgel & Hass, 2004), while the  $IP_{25}$  molecule has been detected in sediment in the same area which are ~ 30,000 years old (Müller *et al.*, 2009). Therefore, when the isotopic signature of FAs is implemented to study sea-ice extent, the use of this technique will likely be restricted to periods spanning the Holocene or possibly the late Pleistocene, while the  $IP_{25}$  can be utilised in older sediments.

## 8 Summary and Outlook

Organic geochemical biomarkers were developed and applied in this study, to a) better understand the mechanisms driving Holocene climate change and its impacts, and b) to improve the interpretation of geochemical palaeoclimate proxies. To this end, biomarkers from a sediment core from Northwest Iceland, and from samples collected during the ICE CHASER 2010 cruise aboard the *RRS James Clark Ross* were studied.

The multi-biomarker study, entailing the analysis of 326 samples from the 38.9 meter long MD99-2266 sediment core, is the most comprehensive and high-resolution, organic biomarker based study of North Atlantic Holocene climate change to date.

In order to study and develop the use of sea-ice biomarkers, surface sediments and particulate organic matter samples collected during the ICE CHASER 2010 research cruise aboard the *RRS James Clark Ross* were analysed.

In the following section the main results of this study are summarised and further work, which has arisen as a result of this study, is discussed.

### 8.1 Chapter 4: Assessing Holocene changes in marine productivity and terrestrial organic carbon inputs into Iceland fjords

The aim of this chapter was to determine terrestrial and marine organic carbon fluxes and to estimate the changing palaeoproductivity throughout the Holocene. The contribution of terrestrial and marine organic carbon to the sediment of Ísafjarðardjúp fjord was determined by utilising biomarker and bulk proxy data in binary mixing models. The palaeoproductivity was estimated using different primary productivity models.

The contribution of terrestrial organic matter is not controlled by the sedimentation rate, but rather by climatic changes. Soil and vegetation development, following the retreat of the last glacial remnants from the last glacial maximum mediated an increase in the erosion and deposition of terrestrial organic matter. Throughout the middle Holocene, soil erosion processes also contributed to an increased terrestrial organic carbon input into the fjordic sediments. Icelandic settlers and/or NAO-type fluctuations also influenced the terrestrial organic matter deposition in the late Holocene.

The estimate of variable Holocene terrestrial organic matter contribution to the fjordic sediment contains considerable uncertainty that arises from constraints intrinsic to the different biomarker and bulk proxies. For example, branched GDGTs used to calculate the BIT-Index are of terrestrial, but likely also of marine origin (Fietz *et al.*, 2012; accepted for publication). Therefore, one way to better constrain the error on the  $OC_{terr}$  contribution is to further study the source of branched GDGTs. Furthermore, using more biomarker proxies to evaluate the  $OC_{terr}$  contribution to the sediments of Ísafjarðardjúp fjord will also help to further constrain the error associated with the sedimentary  $OC_{terr}$  content. For example, Bacteriohopanepolyol (BHP) biomarkers and lignin phenols can be used to trace  $OC_{terr}$  fluxes into marine sediments (Cooke *et al.*, 2009; Tareq *et al.*, 2011). These biomarkers will be analysed in core MD99-2266 to reduce the uncertainty associated with the  $OC_{terr}$  flux. Constraining this uncertainty will also increase the precision of the marine organic carbon content and flux estimates throughout the Holocene.

The model by Knies and Mann (2002) is the most appropriate model to evaluate palaeoproductivity in Ísafjarðardjúp fjord. The Holocene  $OC_{mar}$  variability follows the palaeoproductivity closely, indicating that diagenetic processes affecting the marine organic carbon export from the surface to the sediments must have been relatively constant throughout the Holocene. Allochthonous and autochthonous nutrient supply has affected the palaeoproductivity and consequently the marine organic carbon content of the sediment core studied. Changes in the palaeoproductivity throughout the Holocene are indirectly influenced by changing

climate through the transport of nutrients to Ísafjarðardjúp fjord by varying current systems.

It appears that Norse settlers influenced the  $OC_{terr}$  contribution to the sediments of Ísafjarðardjúp fjord. To verify this idea, the presence of biomarkers such as poly aromatic hydrocarbons, but also levoglucosan, which is a specific marker for wood burning at temperature greater than 300 °C (Kehrwald *et al.*, 2010) will be studied in core MD99-2266. The burning of wood by the Norse settlers may have left biomarker traces in the sediment, which can help to identify anthropogenic influences in the late Holocene.

One major question has not been addressed in this study, that is, the age of different biomarkers. Age differences of different biomarker molecules are for example caused by different transport mechanisms of biomarkers from different sources (Zonneveld *et al.*, 2010). Terrestrially derived biomarkers are usually older than the marine derived biomarkers in the same sediment horizons (Drenzek *et al.*, 2007; Mollenhauer & Eglinton, 2007). Where a biomarker is derived from different sources, for example the  $C_{16}$ -FA, which is ubiquitous in marine and terrestrial environments, the faster degradation of the marine derived acid, compared to that of the terrestrially derived acid affects the age of the biomarker in the sediment (Zonneveld *et al.*, 2010). Furthermore, the mixing of old and new biomarkers from the same source can cause significant offsets between the ages within a biomarker class and the sediment horizons (Smittenberg *et al.*, 2006).

Age differences between different biomarkers can have a significant effect on the interpretation of biomarker proxies, particularly in this study, where terrestrial and marine biomarker records are directly compared. Due to the proximal location of the MD99-2266 coring site to Vestfirðir Peninsula, it is assumed that the relative age difference between terrestrial (e.g. *n*-alkane) and marine (e.g. alkenones) sourced biomarkers is smaller than the time interval encompassed by each sediment sample. However, this assumption can only be verified by compound specific  $^{14}C$ -Accelerate Mass spectrometric analysis of the terrestrial and marine biomarkers. Therefore, future work will entail the analysis of the  $^{14}C$ -ages of the different biomarkers in the sediment core, to study transport times of the terrestrial

biomarkers within Ísafjarðardjúp fjord, and to elucidate whether mixing of old and new organic carbon has taken place.

## **8.2 Chapter 5: New insights into Holocene climate evolution from high-resolution terrestrial and marine biomarker records from Northwest Iceland**

Four different biomarkers were used to reconstruct the climatic history of northwest Iceland throughout the Holocene at a very high temporal resolution (one sample every 32 years). Sea surface temperature and mean air temperature variations were reconstructed using the  $U^{K'}_{37}$  and the CBT/MBT proxy, respectively. The hydrogen isotopic composition and  $ACL_{25-35}$  variability of terrestrial *n*-alkanes, and the GDGT inferred soil pH variability were used to reconstruct Holocene precipitation changes. The  $U^{K'}_{37}$ -SSTs and the MATs reflect summer, rather than annual mean temperatures, and  $ACL_{25-35}$  variations are induced by variations in the amount of precipitation throughout the Holocene.

The combination of the four biomarker proxies revealed two periods during the Holocene, where major climatic changes occurred. The early and middle Holocene are separated by a climatic alteration at ~7700 cal. a BP, while the second climatic alteration separates the middle and late Holocene at ~2900 cal. a BP. High summer insolation and meltwater events governed the climate of the early Holocene. The middle Holocene was controlled by decreasing summer insolation. A slowdown of the Atlantic Meridional Overturning Circulation probably also affected decreasing SSTs during the middle Holocene. The heat transport from the central latitudes to the core site, mediated by the AMOC, but also by NAO-type fluctuations became more important than summer insolation in driving the SSTs and MATs in the late Holocene. This is apparent in the decoupling of the SST and MAT variability from summer insolation during the late Holocene. The late Holocene precipitation record and the SST variability are linked to NAO-type fluctuations. During periods characterised by a prevalent +NAO (e.g. MCA), SSTs and precipitation are higher compared to period, where the NAO is predominantly in its negative mode. The air temperature variability does not follow the expected

trend, when comparing the air temperature relationship with NAO fluctuations as observed today. This is likely due to the fact, that the organisms, on which the MAT-proxy is based, react to soil, rather than air temperature.

The  $U^{K'}_{37}$  and the MBT/CBT proxies used in this study use previously determined calibrations, comparing temperature estimates from core top sediments and soils, respectively, with contemporary SST and air temperature values (Conte *et al.*, 2006; Weijers *et al.*, 2007c). The high resolution record presented here, along with the fact, that comprehensive instrumental air temperature, sea surface temperature, and precipitation records exist for Iceland, ranging back into the mid 19<sup>th</sup> century (Hanna *et al.*, 2004; Hanna *et al.*, 2006), offers the possibility to improve the proxy calibrations, by comparing instrumental and proxy records. Such a study would contribute greatly to the reduction of the errors on proxy calibrations and it would better constrain proxy sensitivity. However, the youngest part of the sediment core, from ~ 300 cal. a BP to present times was not recovered. Therefore, the next logical step will be to retrieve surface sediments from Ísafjarðardjúp fjord that cover the last 300 years, and to correlate the biomarker proxies of those sediment cores with the instrumental record. Thus, a regional air and sea surface temperature calibrations can be produced. Furthermore, the variability of the hydrogen isotopic values and ACL<sub>25-35</sub> values of terrestrial leaf wax *n*-alkanes of those cores can be correlated with precipitation variability which may lead to a quantitative assessment of Holocene precipitation change.

This study has shown, that a number of different forcing mechanisms drive Holocene climate variability in northwest Iceland, however, where more than one forcing mechanism affects the climate it is difficult to assess which mechanism dominates. Therefore, following on from this study, model simulations will be conducted to elucidate the relative importance of different climatic drivers. For example, the relative importance of the NAO and the AMOC as climatic drivers in the late Holocene will be studied.

Finally, the question of whether the biomarker records studied here contain climatic cycles akin to for example 1500 year Bond cycles (Bond *et al.*, 2001) will be answered. In order to subject the data sets to power spectra analysis, the sample ages will have to be refined by applying a Bayesian approach to the age model (Ghil *et al.*, 2002; Quillmann *et al.*, 2010). Therefore, the existing age model will be refined and then the biomarker records will be subjected to time series analysis.

### **8.3 Chapter 6: Using the TEX<sub>86</sub> palaeothermometer in a fjordic environment: Unreasonable reconstructed sea surface temperatures indicate anaerobic oxidation of methane**

The TEX<sub>86</sub>-SST proxy was applied in Ísafjarðardjúp fjord, and it was predicted, that both the TEX<sub>86</sub>- and the U<sup>K</sup><sub>37</sub>-SST proxies should show similar absolute temperatures, and temperature trends, throughout the Holocene.

The TEX<sub>86</sub>-SST proxy does not work as a sea surface temperature proxy in Ísafjarðardjúp fjord, regardless of whether the TEX<sub>86</sub> or the TEX<sub>86</sub><sup>L</sup> calibration equations are used. The increased deviation of the TEX<sub>86</sub> derived SSTs from the U<sup>K</sup><sub>37</sub> derived SSTs correlates well with increasing methane indices. Therefore, GDGTs associated with AOM mediating archaea influence the TEX<sub>86</sub>-SST signal. The MI indicates changing redox conditions in Ísafjarðardjúp fjord throughout the Holocene that were likely forced by changing climatic conditions. An MI as low as 0.1 indicates AOM activity in Ísafjarðardjúp fjord. Therefore, the previously published threshold of 0.5 is likely too conservative in many marine settings. It is suggested, that the MI index is measured whenever TEX<sub>86</sub>-SSTs are reconstructed, and that careful interpretation of the SST variations is necessary, whenever the MI index is higher than 0.1.

This study has shown that the MI index is variable throughout the Holocene, indicating more or less AOM activity. The work done here, and the sediment core offer a unique opportunity to assess, whether the MI correlates with GDGT concentrations and archaeal cell concentrations. Therefore, the GDGT

concentrations and the archaeal cell abundances need to be analysed. This is partly already in progress. Dr. Jillian Couto, a research associate in molecular environmental genomic methods at the University of Glasgow, is currently quantifying archaeal cells in 6 pilot samples with different methane indices. This will offer new insights into whether the MI is correlated with cell concentrations.

#### **8.4 Chapter 7: Can the stable carbon isotopic signature of sedimentary fatty acids reconstruct palaeo-sea-ice cover? a case study for the north-western Fram Strait**

The aim of this chapter was to study, whether the stable carbon isotope signature of sedimentary fatty acids can be used to elucidate palaeo-sea-ice cover. Furthermore, a comparison between the variability of FA carbon isotopic signatures and changing concentrations of IP<sub>25</sub> was planned. To this end, sediment, ice algal, ice core and water column particulate organic matter samples were collected during the ICE CHASER 2010 cruise aboard the *RRS James Clark Ross*.

A compound, tentatively identified as IP<sub>25</sub> was detected in the ice algal samples. However, no IP<sub>25</sub> was detected in any other samples. The fact, that no IP<sub>25</sub> was detected in sediment samples which lie beneath a water column which is at least periodically ice covered, indicates, that alternative palaeo-sea-ice proxies need to be developed.

The C<sub>16</sub> FA of ice algae is significantly <sup>13</sup>C enriched, compared to the C<sub>16</sub> FA of particulate organic matter derived from pelagic algae. The C<sub>16</sub> FA in the sediment samples collected from the ice edge is generally more <sup>13</sup>C enriched than the C<sub>16</sub> FAs in sediments from the pelagic station. Using a binary mixing model with attached, intrinsic assumptions, it is suggested, that the influence of ice algal C<sub>16</sub> FAs is higher in the ice core, compared to the pelagic sediment core. Carbon isotopic signatures of C<sub>16</sub> FAs in sediments can offer insights into contemporary sea-ice cover and may be useful in studying palaeo-sea-ice cover.

The interpretation of the C<sub>16</sub> FA isotopic composition is very challenging. However, further study will help to better interpret the data. For example, biological degradation, which affects the carbon isotopic signature of the C<sub>16</sub> FA in surface sediments, is most pronounced in the upper centimetres of marine sediments (Zonneveld *et al.*, 2010). Furthermore, the Fram Strait has variable sea-ice cover from west to east, with more sea-ice cover closer to Greenland, and less sea-ice near Svalbard. Therefore, it is suggested, that the C<sub>16</sub> FA carbon isotopic composition of sediment cores from an east-west transect be analysed. Such a study will verify, whether the down core variability of the FA carbon isotopic signature persists deeper in the sediments, but also, whether the variable sea-ice conditions of the Fram Strait are recorded by the FA isotopic composition. Furthermore, it is suggested, that diatom specific FAs are analysed, rather than ubiquitously occurring FAs.

In order to further investigate whether  $\delta^{13}\text{C}$  values of sedimentary fatty acids can be used to elucidate past sea ice cover variability, a direct down-core comparison between the abundance of the IP<sub>25</sub> and the  $\delta^{13}\text{C}$  signature of diatom specific fatty acids should be undertaken. Where IP<sub>25</sub> has been found in sediments, it is interpreted to indicate sea ice cover fluctuations. If the  $\delta^{13}\text{C}$  signature of diatom specific fatty acids is an indicator for fluctuation sea ice cover, then it is expected, that the fatty acids exhibit heavier carbon isotopic signatures with increasing amounts of IP<sub>25</sub> in the sediments, which would indicate increased sea ice cover.

### **8.5 Concluding remarks**

This thesis represents a detailed study of the applicability of biomarker proxies in the central North Atlantic and the Arctic Ocean. This PhD shows that when tackling geochemical research questions, biomarkers complement each other and offer deeper insights to the problem when used in combination. A combined biomarker approach can reveal how organic carbon from different sources is deposited over time (Chapter 4). A multi-proxy approach affords the opportunity to study the interactions of the terrestrial and marine climate systems, and it offers insights into the response of these climate systems to changing climates (chapter 5). Furthermore, a multi-proxy approach can give insight into the usefulness and

## 8. Conclusion and further work

applicability of different biomarker proxies in certain geographical areas (chapter 6). It is suggested, that such an approach is taken when elucidating the usefulness of fatty acid carbon isotopic signature as indicators of sea ice cover.

Subsequently, researchers in the future should aim to use a host of biomarkers in combination, when addressing geochemical research questions such as the reconstruction of climate.

## 9 Literature

- Alley, R.B., Ágústsdóttir, A.M., (2005) The 8k event: cause and consequences of a major Holocene abrupt climate change. *Quaternary Science Reviews*, 24(10-11), 1123-1149.
- Alley, R.B., Mayewski, P.A., Sowers, T., Stuiver, M., Taylor, K.C., Clark, P.U., (1997) Holocene climatic instability: A prominent, widespread event 8200 yr ago. *Geology*, 25(6), 483-486.
- Andersen, C., Koc, N., Jennings, A., Andrews, J.T., (2004) Nonuniform response of the major surface currents in the Nordic Seas to insolation forcing: Implications for the Holocene climate variability. *Paleoceanography*, 19(2).
- Andrews, J.T., (2009) Seeking a Holocene drift ice proxy: non-clay mineral variations from the SW to N-central Iceland shelf: trends, regime shifts, and periodicities. *Journal of Quaternary Science*, 24(7), 664-676.
- Andrews, J.T., Belt, S.T., Olafsdottir, S., Massé, G., Vare, L.L., (2009a) Sea ice and marine climate variability for NW Iceland/Denmark Strait over the last 2000 cal. yr BP. *The Holocene*, 19(5), 775-784.
- Andrews, J.T., Caseldine, C., Russell, A., Harðardóttir, J., Knudsen, Ó., (2005) 2. Late Quaternary marine sediment studies of the iceland shelf--palaeocenography, land/ice sheet/ocean interactions, and deglaciation: a review, *Developments in Quaternary Sciences, Volume 5*, pp. 5-24. Elsevier.
- Andrews, J.T., Caseldine, C., Weiner, N.J., Hatton, J., (2001) Late Holocene (ca. 4 ka) marine and terrestrial environmental change in Reykjarfjordur, north Iceland: climate and/or settlement? *Journal of Quaternary Science*, 16(2), 133-143.
- Andrews, J.T., Darby, D., Eberle, D., Jennings, A.E., Moros, M., Ogilvie, A., (2009b) A robust, multisite Holocene history of drift ice off northern Iceland: implications for North Atlantic climate. *The Holocene*, 19(1), 71-77.
- Andrews, J.T., Harðardóttir, J., Stoner, J.S., Principato, S.M., (2008) Holocene sediment magnetic properties along a transect from Isafiardardiup to Djupall, Northwest Iceland. *Arctic Antarctic and Alpine Research*, 40(1), 1-14.
- Arnalds, O., (2008) Soils of Iceland. *Jokull*, 58, 409-421.

## 9. Literature

- Arnalds, O., Gretarsson, E., (2001) Soil map of Iceland. Agricultural University of Iceland, Reykjavik.
- Axford, Y., Andresen, C.S., Andrews, J.T., Belt, S.T., Geirsdóttir, Á., Massé, G., Miller, G.H., Ólafsdóttir, S., Vare, L.L., (2011) Do paleoclimate proxies agree? A test comparing 19 late Holocene climate and sea-ice reconstructions from Icelandic marine and lake sediments. *Journal of Quaternary Science*, 26(6), 645-656.
- Axford, Y., Geirsdóttir, Á., Miller, G., Langdon, P., (2009) Climate of the Little Ice Age and the past 2000 years in northeast Iceland inferred from chironomids and other lake sediment proxies. *Journal of Paleolimnology*, 41(1), 7-24.
- Bader, J., Mesquita, M.D.S., Hodges, K.I., Keenlyside, N., Østerhus, S., Miles, M., (2011) A review on Northern Hemisphere sea-ice, storminess and the North Atlantic Oscillation: Observations and projected changes. *Atmospheric Research*, 101(4), 809-834.
- Belicka, L.L., Harvey, H.R., (2009) The sequestration of terrestrial organic carbon in Arctic Ocean sediments: A comparison of methods and implications for regional carbon budgets. *Geochimica Et Cosmochimica Acta*, 73(20), 6231-6248.
- Belt, S.T., Allard, W.G., Massé, G., Robert, J.-M., Rowland, S.J., (2000) Highly branched isoprenoids (HBIs): identification of the most common and abundant sedimentary isomers. *Geochimica et Cosmochimica Acta*, 64(22), 3839.
- Belt, S.T., Massé, G., Allard, W.G., Robert, J.-M., Rowland, S.J., (2001) C<sub>25</sub> highly branched isoprenoid alkenes in planktonic diatoms of the *Pleurosigma* genus. *Organic Geochemistry*, 32(10), 1271.
- Belt, S.T., Massé, G., Rowland, S.J., Poulin, M., Michel, C., LeBlanc, B., (2007) A novel chemical fossil of palaeo sea ice: IP<sub>25</sub>. *Organic Geochemistry*, 38(1), 16.
- Belt, S.T., Masse, G., Vare, L.L., Rowland, S.J., Poulin, M., Sicre, M.-A., Sampei, M., Fortier, L., (2008) Distinctive <sup>13</sup>C isotopic signature distinguishes a novel sea ice biomarker in Arctic sediments and sediment traps. *Marine Chemistry*, 112(3-4), 158-167.
- Bendle, J., Kawamura, K., Yamazaki, K., Niwai, T., (2007) Latitudinal distribution of terrestrial lipid biomarkers and *n*-alkane compound-specific stable carbon isotope ratios in the atmosphere over the western Pacific and Southern Ocean. *Geochimica Et Cosmochimica Acta*, 71, 5934-5955.
- Bendle, J., Rosell-Melé, A., (2004) Distributions of U<sup>K</sup><sub>37</sub> and U<sup>K'</sup><sub>37</sub> in the surface waters and sediments of the Nordic Seas: Implications for paleoceanography. *Geochemistry Geophysics Geosystems*, 5.

## 9. Literature

- Bendle, J.A.P., Rosell-Melé, A., (2007) High-resolution alkenone sea surface temperature variability on the North Icelandic Shelf: implications for Nordic Seas palaeoclimatic development during the Holocene. *The Holocene*, 17(1), 9-24.
- Betts, J.N., Holland, H.D., (1991) The oxygen content of ocean bottom waters, the burial efficiency of organic carbon, and the regulation of atmospheric oxygen. *Palaeogeography, Palaeoclimatology, Palaeoecology*, 97(1-2), 5-18.
- Betzer, P.R., Showers, W.J., Laws, E.A., Winn, C.D., DiTullio, G.R., Kroopnick, P.M., (1984) Primary productivity and particle fluxes on a transect of the equator at 153° W in the Pacific Ocean. *Deep Sea Research Part A. Oceanographic Research Papers*, 31(1), 1-11.
- Bianchi, G., (1995) Plant Waxes. In: R.J. Hamilton (Ed.), *Waxes: Chemistry, Molecular Biology and Functions* (Ed. by R.J. Hamilton), pp. 175 - 222. The Oily Press, Dundee.
- Bianchi, G.G., McCave, I.N., (1999) Holocene periodicity in North Atlantic climate and deep-ocean flow south of Iceland. *Nature*, 397(6719), 515-517.
- Birgel, D., Hass, H.C., (2004) Oceanic and atmospheric variations during the last deglaciation in the Fram Strait (Arctic Ocean): a coupled high-resolution organic-geochemical and sedimentological study. *Quaternary Science Reviews*, 23, 29-47.
- Birgel, D., Himmler, T., Freiwald, A., Peckmann, J., (2008) A new constraint on the antiquity of anaerobic oxidation of methane: Late Pennsylvanian seep limestones from southern Namibia. *Geology*, 36(7), 543-546.
- Birgel, D., Stein, R., Hefter, J., (2004) Aliphatic lipids in recent sediments of the Fram Strait/Yermak Plateau (Arctic Ocean): composition, sources and transport processes (revised version February 19th, 2004). *Marine Chemistry*, 88(3-4), 127-160.
- Blindheim, J., Borovkov, V., Hansen, B., Malmberg, S.A., Turrell, W.R., Østerhus, S., (2000) Upper layer cooling and freshening in the Norwegian Sea in relation to atmospheric forcing. *Deep Sea Research Part I: Oceanographic Research Papers*, 47(4), 655-680.
- Blindheim, J., Malmberg, S.-A., (2002) The Mean Sea Level Pressure (MSLP) Gradient across the Denmark Strait as Index for the Oceanographic Conditions in North Icelandic Waters. In: *Annual Science Conference*, pp. 16. 2002 ICES Annual Science Conference and ICES CEntenary, Copenhagen.
- Blindheim, J., Malmberg, S.-A., (2005) The Mean Sea Level Pressure Gradient Across the Denmark Strait as an Indicator of Conditions in the North Icelandic Irminger Current. In: H. Drange, T. Dokkken, T. Furevik, R. Gerdes, W. Berger (Eds.), *The Nordic Seas: An*

## 9. Literature

*Integrated Perspective*, 158 (Ed. by H. Drange, T. Dokken, T. Furevik, R. Gerdes, W. Berger), pp. 65-71. AGU.

- Blumenberg, M., Seifert, R., Reitner, J., Pape, T., Michaelis, W., (2004) Membrane lipid patterns typify distinct anaerobic methanotrophic consortia. *Proceedings of the National Academy of Sciences of the United States of America*, 101(30), 11111-11116.
- Boe, J.L., Hall, A., Qu, X., (2009) September sea-ice cover in the Arctic Ocean projected to vanish by 2100. *Nature Geoscience*, 2(5), 341-343.
- Boetius, A., Ravenschlag, K., Schubert, C.J., Rickert, D., Widdel, F., Gieseke, A., Amann, R., Jorgensen, B.B., Witte, U., Pfannkuche, O., (2000) A marine microbial consortium apparently mediating anaerobic oxidation of methane. *Nature*, 407(6804), 623-626.
- Bond, G., Kromer, B., Beer, J., Muscheler, R., Evans, M.N., Showers, W., Hoffmann, S., Lottibond, R., Hajdas, I., Bonani, G., (2001) Persistent solar influence on North Atlantic climate during the Holocene. *Science*, 294(5549), 2130-2136.
- Boot, C.S., Ettwein, V.J., Maslin, M.A., Weyhenmeyer, C.E., Pancost, R.D., (2006) A 35,000 year record of terrigenous and marine lipids in Amazon Fan sediments. *Organic Geochemistry*, 37(2), 208-219.
- Bralower, T.J., Thierstein, H.R., (1984) Low productivity and slow deep-water circulation in mid-Cretaceous oceans. *Geology*, 12(10), 614-618.
- Brassell, S.C., Dumitrescu, M., (2004) Recognition of alkenones in a lower Aptian porcellanite from the west-central Pacific. *Organic Geochemistry*, 35(2), 181-188.
- Brassell, S.C., Eglinton, G., Marlowe, I.T., Pflaumann, U., Sarnthein, M., (1986) Molecular Stratigraphy - A new tool for climatic assessment. *Nature*, 320(6058), 129-133.
- Bray, E.E., Evans, E.D., (1961) Distribution of n-paraffins as a clue to recognition of source beds. *Geochimica Et Cosmochimica Acta*, 22(1), 2-15.
- Brochier-Armanet, C., Boussau, B., Gribaldo, S., Forterre, P., (2008) Mesophilic crenarchaeota: proposal for a third archaeal phylum, the Thaumarchaeota. *Nature Reviews Microbiology*, 6(3), 245-252.
- Bromwich, D.H., Bai, L., Bjarnason, G.G., (2005) High-Resolution Regional Climate Simulations over Iceland Using Polar MM5\*. *Monthly Weather Review*, 133(12), 3527-3547.
- Brown, T.A., Belt, S.T., (2012) Identification of the sea ice diatom biomarker IP<sub>25</sub> in Arctic benthic macrofauna: direct evidence for a sea ice diatom diet in Arctic heterotrophs. *Polar Biology*, 35(1), 131-137.

## 9. Literature

- Brown, T.A., Belt, S.T., Philippe, B., Mundy, C.J., Masse, G., Poulin, M., Gosselin, M., (2011) Temporal and vertical variations of lipid biomarkers during a bottom ice diatom bloom in the Canadian Beaufort Sea: further evidence for the use of the IP<sub>25</sub> biomarker as a proxy for spring Arctic sea ice. *Polar Biology*, 34(12), 1857-1868.
- Bryden, H.L., Longworth, H.R., Cunningham, S.A., (2005) Slowing of the Atlantic meridional overturning circulation at 25 degrees N. *Nature*, 438(7068), 655-657.
- Budge, S.M., Wooller, M.J., Springer, A.M., Iverson, S.J., McRoy, C.P., Divoky, G.J., (2008) Tracing carbon flow in an arctic marine food web using fatty acid-stable isotope analysis. *Oecologia*, 157(1), 117-129.
- Bukantis, A., Bartkeviciene, G., (2005) Thermal effects of the North Atlantic Oscillation on the cold period of the year in Lithuania. *Climate Research*, 28(3), 221-228.
- Buntgen, U., Tegel, W., Nicolussi, K., McCormick, M., Frank, D., Trouet, V., Kaplan, J.O., Herzig, F., Heussner, K.U., Wanner, H., Luterbacher, J., Esper, J., (2011) 2500 Years of European Climate Variability and Human Susceptibility. *Science*, 331(6017), 578-582.
- Calvo, E., Grimalt, J., Jansen, E., (2002) High resolution U<sup>K</sup><sub>37</sub> sea surface temperature reconstruction in the Norwegian Sea during the Holocene. *Quaternary Science Reviews*, 21(12-13), 1385-1394.
- Calvo, E., Pelejero, C., Logan, G.A., De Deckker, P., (2004) Dust-induced changes in phytoplankton composition in the Tasman Sea during the last four glacial cycles. *Paleoceanography*, 19(2), 10.
- Cameron, K.D., Teece, M.A., Smart, L.B., (2006) increased accumulation of cuticular wax and expression of lipid transfer protein in response to periodic drying events in leaves of tree tobacco. *Plant Physiology*, 140, 176-183.
- Caseldine, C., Geirsdottir, A., Langdon, P., (2003) Efstadalsvatn - a multi-proxy study of a Holocene lacustrine sequence from NW Iceland. *Journal of Paleolimnology*, 30(1), 55-73.
- Caseldine, C., Langdon, P., Holmes, N., (2006) Early Holocene climate variability and the timing and extent of the Holocene thermal maximum (HTM) in northern Iceland. *Quaternary Science Reviews*, 25(17-18), 2314-2331.
- Castañeda, I.S., Schouten, S., (2011) A review of molecular organic proxies for examining modern and ancient lacustrine environments. *Quaternary Science Reviews*, 30(21-22), 2851-2891.

## 9. Literature

- Castañeda, I.S., Smith, L.M., Kristjánsdóttir, G.B., Andrews, J.T., (2004) Temporal changes in Holocene  $\delta^{18}\text{O}$  records from the northwest and central North Iceland Shelf, *19*, pp. 321-334. John Wiley & Sons, Ltd.
- Chikaraishi, Y., Naraoka, H., (2003) Compound-specific  $\delta\text{D}-\delta^{13}\text{C}$  analysis of *n*-alkanes extracted from terrestrial and aquatic plants. *Phytochemistry*, *63*, 361 - 371.
- Clark, R.C., Jr., Blumer, M., (1967) Distribution of *n*-Paraffins in Marine Organisms and Sediment. *Limnology and Oceanography*, *12*(1), 79-87.
- Collister, J.W., Rieley, G., Stern, B., Eglinton, G., Fry, B., (1994) Compound-specific  $\delta^{13}\text{C}$  analyses of leaf lipids from plants with differing carbondioxide metabolisms. *Organic Geochemistry*, *21*(6/7), 619-627.
- Conte, M.H., Sicre, M.A., Rühlemann, C., Weber, J.C., Schulte, S., Schulz-Bull, D., Blanz, T., (2006) Global temperature calibration of the alkenone unsaturation index ( $U^K_{37}$ ) in surface waters and comparison with surface sediments. *Geochemistry Geophysics Geosystems*, *7*.
- Cook, M.S., Keigwin, L.D., Birgel, D., Hinrichs, K.-U., (2011) Repeated pulses of vertical methane flux recorded in glacial sediments from the southeast Bering Sea. *Paleoceanography*, *26*.
- Cooke, M.P., van Dongen, B.E., Talbot, H.M., Semiletov, I., Shakhova, N., Guo, L., Gustafsson, Ö., (2009) Bacteriohopanepolyol biomarker composition of organic matter exported to the Arctic Ocean by seven of the major Arctic rivers. *Organic Geochemistry*, *40*(11), 1151-1159.
- Cottier, F.R., Nilsen, F., Skogseth, R., Tverberg, V., Skardhamar, J., Svendsen, H., (2010) Arctic fjords: a review of the oceanographic environment and dominant physical processes. *Geological Society, London, Special Publications*, *344*(1), 35-50.
- Cranwell, P.A., (1973) Chain length distribution of *n*-alkanes from lake sediments in relation to postglacial environmental change. *Freshwater Biology*, *3*(3), 259-265.
- Cranwell, P.A., (1981) Diagenesis of free and bound lipids in terrestrial detritus deposited in a lacustrine sediment. *Organic Geochemistry*, *3*(3), 79-89.
- Cranwell, P.A., (1991) Paleolimnological studies using sequential lipid extraction from recent lacustrine sediment: recognition of source organisms from biomarkers. *Hydrobiologia*, *214*(1), 293-303.
- D'Andrea, W.J., Huang, Y., Fritz, S.C., Anderson, N.J., (2011) Abrupt Holocene climate change as an important factor for human migration in West Greenland. *Proceedings of the National Academy of Sciences of the United States of America*, *108*(24), 9765-9769.

## 9. Literature

- Dalsgaard, J., St John, M., Kattner, G., Muller-Navarra, D., Hagen, W., (2003) Fatty acid trophic markers in the pelagic marine environment. *Advances in Marine Biology*, Vol 46, 46, 225-340.
- Daly, G.T., (1964) Leaf-surface wax in *Poa colensoi*. *Journal of Experimental Botany*, 15(43), 160-165.
- Dansgaard, W., Johnsen, S.J., Clausen, H.B., Dahljensen, D., Gundestrup, N.S., Hammer, C.U., Hvidberg, C.S., Steffensen, J.P., Sveinbjornsdottir, A.E., Jouzel, J., Bond, G., (1993) Evidence for general instability of past climate from a 250 kyr ice-core record. *Nature*, 364(6434), 218-220.
- de Vernal, A., Hillaire-Marcel, C., Turon, J.L., Matthiessen, J., (2000) Reconstruction of sea-surface temperature, salinity, and sea-ice cover in the northern North Atlantic during the last glacial maximum based on dinocyst assemblages. *Canadian Journal of Earth Sciences*, 37(5), 725-750.
- DeLong, E.F., (1992) Archaea in coastal marine environments. *Proceedings of the National Academy of Sciences of the United States of America*, 89(12), 5685-5689.
- DeLong, E.F., (1998) Everything in moderation: Archaea as 'non-extremophiles'. *Current Opinion in Genetics & Development*, 8(6), 649-654.
- deMenocal, P.B., (2001) Cultural responses to climate change during the Late Holocene. *Science*, 292(5517), 667-673.
- Denton, G.H., Karlén, W., (1973) Holocene climatic variations-Their pattern and possible cause. *Quaternary Research*, 3(2), 155-174.
- Deuser, W.G., Degens, E.T., Guillard, R.R.L., (1968) Carbon isotope relationships between plankton and sea water. *Geochimica Et Cosmochimica Acta*, 32(6), 657-660.
- Dickson, R.R., Osborn, T.J., Hurrell, J.W., Meincke, J., Blindheim, J., Adlandsvik, B., Vinje, T., Alekseev, G., Maslowski, W., (2000) The Arctic Ocean Response to the North Atlantic Oscillation. *Journal of Climate*, 13(15), 2671-2696.
- Divine, D.V., Dick, C., (2006) Historical variability of sea ice edge position in the Nordic Seas. *J. Geophys. Res.*, 111(C1), C01001.
- Drenzek, N.J., Montlucon, D.B., Yunker, M.B., Macdonald, R.W., Eglinton, T.I., (2007) Constraints on the origin of sedimentary organic carbon in the Beaufort Sea from coupled molecular <sup>13</sup>C and <sup>14</sup>C measurements. *Marine Chemistry*, 103(1-2), 146-162.

## 9. Literature

- Dugmore, A., Newton, A., Larsen, G., Cook, G., (2000) Tephrochronology, Environmental Change and the Norse Settlement of Iceland. *Environmental Archaeology*, 5(1), 21-34.
- Dunlop, R.W., Jefferies, P.R., (1985) Hydrocarbons of the hypersaline basins of Shark Bay, Western Australia. *Organic Geochemistry*, 8(5), 313-320.
- Dyke, A.S., Andrews, J.T., Clark, P.U., England, J.H., Miller, G.H., Shaw, J., Veillette, J.J., (2002) The Laurentide and Innuitian ice sheets during the Last Glacial Maximum. *Quaternary Science Reviews*, 21, 9-31.
- Eglinton, G., Gonzalez, A.G., Hamilton, R.J., Raphael, R.A., (1962) Hydrocarbon constituents of the wax coatings of plant leaves: a taxonomic survey. *Phytochemistry*, 1, 89 - 102.
- Eglinton, G., Hamilton, R.J., (1967) Leaf epicuticular waxes. *Science*, 156, 1322-1334.
- Eglinton, G., Hunneman, D.H., Douraghi-Zadeh, K., (1968) Gas chromatographic-mass spectrometric studies of long chain hydroxy acids-II: The hydroxy acids and fatty acids of a 5000-year-old lacustrine sediment. *Tetrahedron*, 24(18), 5929-5941.
- Eglinton, T.I., Eglinton, G., (2008) Molecular proxies for paleoclimatology. *Earth and Planetary Science Letters*, 275(1-2), 1-16.
- Eiriksson, J., Knudsen, K.L., Hafliðason, H., Henriksen, P., (2000) Late-glacial and Holocene palaeoceanography of the North Icelandic shelf. *Journal of Quaternary Science*, 15(1), 23-42.
- Eltgroth, M.L., Watwood, R.L., Wolfe, G.V., (2005) Production and cellular localization of neutral long-chain lipids in the haptophyte algae *Isochrysis galbana* and *Emiliana huxleyi*. *Journal of Phycology*, 41(5), 1000-1009.
- Elvert, M., Hopmans, E.C., Treude, T., Boetius, A., Suess, E., (2005) Spatial variations of methanotrophic consortia at cold methane seeps: implications from a high-resolution molecular and isotopic approach. *Geobiology*, 3(3), 195-209.
- Emiliani, C., (1955) Pleistocene temperatures. *Journal of Geology*, 63(6), 538-578.
- Engelsen, O., Hegseth, E.N., Hop, H., Hansen, E., Falk-Petersen, S., (2002) Spatial variability of chlorophyll-a in the Marginal Ice Zone of the Barents Sea, with relations to sea ice and oceanographic conditions. *Journal of Marine Systems*, 35(1-2), 79-97.
- Fahl, K., Kattner, G., (1993) Lipid Content and fatty acid composition of algal communities in sea-ice and water from the Weddell Sea (Antarctica). *Polar Biology*, 13(6), 405-409.

## 9. Literature

- Falk-Petersen, S., Mayzaud, P., Kattner, G., Sargent, J., (2009) Lipids and life strategy of Arctic Calanus. *Marine Biology Research*, 5(1), 18-39.
- Falk-Petersen, S., Sargent, J.R., Henderson, J., Hegseth, E.N., Hop, H., Okolodkov, Y.B., (1998) Lipids and fatty acids in ice algae and phytoplankton from the Marginal Ice Zone in the Barents Sea. *Polar Biology*, 20(1), 41-47.
- Fawcett, P.J., Werne, J.P., Anderson, R.S., Heikoop, J.M., Brown, E.T., Berke, M.A., Smith, S.J., Goff, F., Donohoo-Hurley, L., Cisneros-Dozal, L.M., Schouten, S., Sinninghe Damste, J.S., Huang, Y., Toney, J., Fessenden, J., WoldeGabriel, G., Atudorei, V., Geissman, J.W., Allen, C.D., (2011) Extended megadroughts in the southwestern United States during Pleistocene interglacials. *Nature*, 470(7335), 518-521.
- Fietz, S., Huguët, C., Bendle, J., Escala, M., Gallacher, C., Herfort, L., Jamieson, R., Martínez-García, A., McClymont, E.L., Peck, V.L., Prah, F.G., Rossi, S., Rueda, G., Sanson-Barrera, A., Rosell-Melé, A., (2012) Co-variation of crenarchaeol and branched GDGTs in globally-distributed marine and freshwater sedimentary archives. *Global Biogeochemical Cycles*.
- Fietz, S., Martínez-García, A., Huguët, C., Rueda, G., Rosell-Melé, A., (2011) Constraints in the application of the Branched and Isoprenoid Tetraether index as a terrestrial input proxy. *J. Geophys. Res.*, 116(C10), C10032.
- Fisher, E., Oldfield, F., Wake, R., Boyle, J., Appleby, P., Wolff, G.A., (2003) Molecular marker records of land use change. *Organic Geochemistry*, 34(1), 105-119.
- Ford, J.D., (2009) Vulnerability of Inuit food systems to food insecurity as a consequence of climate change: a case study from Igloodik, Nunavut. *Regional Environmental Change*, 9(2), 83-100.
- France, R., Loret, J., Mathews, R., Springer, J., (1998) Longitudinal variation in zooplankton  $\delta^{13}\text{C}$  through the Northwest Passage: inference for incorporation of sea-ice POM into pelagic foodwebs. *Polar Biology*, 20(5), 335-341.
- Fraser, A.J., Sargent, J.R., Gamble, J.C., Seaton, D.D., (1989) Formation and transfer of fatty acids in an enclosed marine food chain comprising phytoplankton, zooplankton and herring (*Clupea harengus* L.) larvae. *Marine Chemistry*, 27(1-2), 1-18.
- Gabriel, J.L., Lee Gau Chong, P., (2000) Molecular modelling of archaeobacterial bipolar tetraether lipid membranes. *Chemistry and Physics of Lipids*, 105(2), 193-200.

## 9. Literature

- Geirsdottir, A., Miller, G.H., Axford, Y., Olafsdottir, S., (2009) Holocene and latest Pleistocene climate and glacier fluctuations in Iceland. *Quaternary Science Reviews*, 28(21-22), 2107-2118.
- Gersonde, R., Zielinski, U., (2000) The reconstruction of late Quaternary Antarctic sea-ice distribution - the use of diatoms as a proxy for sea-ice. *Palaeogeography Palaeoclimatology Palaeoecology*, 162(3-4), 263-286.
- Ghil, M., Allen, M.R., Dettinger, M.D., Ide, K., Kondrashov, D., Mann, M.E., Robertson, A.W., Saunders, A., Tian, Y., Varadi, F., Yiou, P., (2002) Advanced spectral methods for climatic time series. *Rev. Geophys.*, 40(1), 1003.
- Gibson, J.A.E., Trull, T., Nichols, P.D., Summons, R.E., McMinn, A., (1999) Sedimentation of <sup>13</sup>C-rich organic matter from Antarctic sea-ice algae: A potential indicator of past sea-ice extent. *Geology*, 27(4), 331-334.
- Gimeno, L., Ribera, P., Iglesias, R., de la Torre, L., Garcia, R., Hernandez, E., (2002) Identification of empirical relationships between indices of ENSO and NAO and agricultural yields in Spain. *Climate Research*, 21(2), 165-172.
- Giraudeau, J., Cremer, M., Manthé, S., Labeyrie, L., Bond, G., (2000) Coccolith evidence for instabilities in surface circulation south of Iceland during Holocene times. *Earth and Planetary Science Letters*, 179(2), 257-268.
- Giraudeau, J., Grelaud, M., Solignac, S., Andrews, J.T., Moros, M., Jansen, E., (2010) Millennial-scale variability in Atlantic water advection to the Nordic Seas derived from Holocene coccolith concentration records. *Quaternary Science Reviews*, 29(9-10), 1276-1287.
- Giraudeau, J., Jennings, A.E., Andrews, J.T., (2004) Timing and mechanisms of surface and intermediate water circulation changes in the Nordic Seas over the last 10,000 cal years: a view from the North Iceland shelf. *Quaternary Science Reviews*, 23(20-22), 2127-2139.
- Gliozzi, A., Paoli, G., De Rosa, M., Gambacorta, A., (1983) Effect of isoprenoid cyclization on the transition temperature of lipids in thermophilic archaeobacteria. *Biochimica et Biophysica Acta (BBA) - Biomembranes*, 735(2), 234-242.
- Graeve, M., Kattner, G., Hagen, W., (1994) Diet-induced changes in the fatty acid composition of Arctic herbivorous copepods: Experimental evidence of trophic markers. *Journal of Experimental Marine Biology and Ecology*, 182(1), 97-110.
- Graham, N.E., Ammann, C.M., Fleitmann, D., Cobb, K.M., Luterbacher, J., (2011) Support for global climate reorganization during the "Medieval Climate Anomaly". *Climate Dynamics*, 37(5-6), 1217-1245.

## 9. Literature

- Gronvold, K., Oskarsson, N., Johnsen, S.J., Clausen, H.B., Hammer, C.U., Bond, G., Bard, E., (1995) Ash layers from iceland in teh Greenland GRIP ice core correlated with oceanic and land sediments. *Earth and Planetary Science Letters*, 135(1-4), 149-155.
- Grootes, P.M., Stuiver, M., (1997) Oxygen 18/16 variability in Greenland snow and ice with  $10^{-3}$ - $10^{-5}$  year time resolution. *J. Geophys. Res.*, 102(C12), 26455-26470.
- Hall, I.R., Bianchi, G.G., Evans, J.R., (2004) Centennial to millennial scale Holocene climate-deep water linkage in the North Atlantic. *Quaternary Science Reviews*, 23(14-15), 1529-1536.
- Hallsdottir, M., (1995) On the pre-settlement history of Icelandic vegetation. *Buvisindi*, 9(0), 17-29.
- Hallsdóttir, M., Caseldine, C.J., C. Caseldine, A.R.J.H., Ó, K., (2005) 14. The Holocene vegetation history of Iceland, state-of-the-art and future research, *Developments in Quaternary Sciences, Volume 5*, pp. 319-334. Elsevier.
- Hanna, E., Jonsson, T., Box, J.E., (2004) An analysis of Icelandic climate since the nineteenth century. *International Journal of Climatology*, 24(10), 1193-1210.
- Hanna, E., Jonsson, T., Olafsson, J., Valdimarsson, H., (2006) Icelandic coastal sea surface temperature records constructed: Putting the pulse on air-sea-climate interactions in the northern North Atlantic. Part I: Comparison with HadISST1 open-ocean surface temperatures and preliminary analysis of long-term patterns and anomalies of SSTs around Iceland. *Journal of Climate*, 19(21), 5652-5666.
- Hansen, B., Østerhus, S., (2000) North Atlantic-Nordic Seas exchanges. *Progress In Oceanography*, 45(2), 109-208.
- Hansen, J., Sato, M., Ruedy, R., Kharecha, P., Lacis, A., Miller, R., Nazarenko, L., Lo, K., Schmidt, G.A., Russell, G., Aleinov, I., Bauer, S., Baum, E., Cairns, B., Canuto, V., Chandler, M., Cheng, Y., Cohen, A., Del Genio, A., Faluvegi, G., Fleming, E., Friend, A., Hall, T., Jackman, C., Jonas, J., Kelley, M., Kiang, N.Y., Koch, D., Labow, G., Lerner, J., Menon, S., Novakov, T., Oinas, V., Perlwitz, J., Perlwitz, J., Rind, D., Romanou, A., Schmunk, R., Shindell, D., Stone, P., Sun, S., Streets, D., Tausnev, N., Thresher, D., Unger, N., Yao, M., Zhang, S., (2007) Dangerous human-made interference with climate: a GISS modelE study. *Atmospheric Chemistry and Physics*, 7(9), 2287-2312.
- Harrison, S.P., Prentice, I.C., Bartlein, P.J., (1992) Influence of insolation and glaciation on atmospheric circulation in the North Atlantic sector: Implications of general circulation model experiments for the Late Quaternary climatology of Europe. *Quaternary Science Reviews*, 11(3), 283-299.

## 9. Literature

- Hedges, J.I., Oades, J.M., (1997) Comparative organic geochemistries of soils and marine sediments. *Organic Geochemistry*, 27(7-8), 319-361.
- Heegaard, E., Birks, H.J.B., Telford, R.J., (2005) Relationships between calibrated ages and depth in stratigraphical sequences: an estimation procedure by mixed-effect regression. *Holocene*, 15(4), 612-618.
- Henderson, R.J., Hegseth, E.N., Park, R.T., (1998) Seasonal variation in lipid and fatty acid composition of ice algae from the Barents Sea. *Polar Biology*, 20(1), 48-55.
- Hinrichs, K.-U., Hayes, J.M., Sylva, S.P., Brewer, P.G., DeLong, E.F., (1999) Methane-consuming archaeobacteria in marine sediments. *Nature*, 398(6730), 802-805.
- Hinrichs, K.-U., Summons, R.E., Orphan, V., Sylva, S.P., Hayes, J.M., (2000) Molecular and isotopic analysis of anaerobic methane-oxidizing communities in marine sediments. *Organic Geochemistry*, 31(12), 1685-1701.
- Hoefs, M.J.L., Rijpstra, W.I.C., Damste, J.S.S., (2002) The influence of oxic degradation on the sedimentary biomarker record I: Evidence from Madeira Abyssal Plain turbidites. *Geochimica Et Cosmochimica Acta*, 66(15), 2719-2735.
- Hofmann, P., Stusser, I., Wagner, T., Schouten, S., Damste, J.S.S., (2008) Climate-ocean coupling off North-West Africa during the Lower Albian: The Oceanic Anoxic Event 1b. *Palaeogeography Palaeoclimatology Palaeoecology*, 262(3-4), 157-165.
- Hönisch, B., Hemming, N.G., (2005) Surface ocean pH response to variations in pCO<sub>2</sub> through two full glacial cycles. *Earth and Planetary Science Letters*, 236, 305-314.
- Hoogakker, B.A.A., Chapman, M.R., McCave, I.N., Hillaire-Marcel, C., Ellison, C.R.W., Hall, I.R., Telford, R.J., (2011) Dynamics of North Atlantic Deep Water masses during the Holocene. *Paleoceanography*, 26(4), PA4214.
- Hopmans, E.C., Weijers, J.W.H., Schefuss, E., Herfort, L., Damste, J.S.S., Schouten, S., (2004) A novel proxy for terrestrial organic matter in sediments based on branched and isoprenoid tetraether lipids. *Earth and Planetary Science Letters*, 224(1-2), 107-116.
- Howe, J.A., Austin, W.E.N., Forwick, M., Paetzel, M., Harland, R., Cage, A.G., (2010) Fjord systems and archives: a review. *Geological Society, London, Special Publications*, 344(1), 5-15.
- Huang, Q., Dong, C.Z., Dong, R.M., Jiang, H., Wang, S., Wang, G., Fang, B., Ding, X., Niu, L., Li, X., Zhang, C., Dong, H., (2011) Archaeal and bacterial diversity in hot springs on the Tibetan Plateau, China. *Extremophiles*, 15(5), 549-563.

## 9. Literature

- Hughes, M.K., Diaz, H.F., (1994) Was there a medieval warm period, and if so, where and when? . *Climatic Change*, 26(2-3), 109-142.
- Huguet, C., Kim, J.-H., Sinninghe Damsté, J.S., Schouten, S., (2006) Reconstruction of sea surface temperature variations in the Arabian Sea over the last 23 kyr using organic proxies (TEX<sub>86</sub> and U<sup>K</sup><sub>37</sub>). *Paleoceanography*, 21(3), PA3003.
- Huguet, C., Smittenberg, R.H., Boer, W., Damste, J.S.S., Schouten, S., (2007) Twentieth century proxy records of temperature and soil organic matter input in the Drammensfjord, southern Norway. *Organic Geochemistry*, 38(11), 1838-1849.
- Hurrell, J.W., (1995) Decadal trends in the North Atlantic Oscillation - Regional temperatures and precipitation. *Science*, 269(5224), 676-679.
- Hurrell, J.W., Deser, C., (2009) North Atlantic climate variability: The role of the North Atlantic Oscillation. *Journal of Marine Systems*, 78(1), 28-41.
- Hurrell, J.W., Kushiner, Y., Ottersen, G., Visbeck, M., (2003) An overview of the North Atlantic Oscillation. American Geophysical Union, Washington, DC, ETATS-UNIS.
- Hurrell, J.W., VanLoon, H., (1997) Decadal variations in climate associated with the north Atlantic oscillation. *Climatic Change*, 36(3-4), 301-326.
- Imbrie, J., Boyle, E.A., Clemens, S.C., Duffy, A., Howard, W.R., Kukla, G., Kutzbach, J., Martinson, D.G., McIntyre, A., Mix, A.C., Molfino, B., Morley, J.J., Peterson, L.C., Pisias, N.G., Prell, W.L., Raymo, M.E., Shackleton, N.J., Toggweiler, J.R., (1992) On the Structure and Origin of Major Glaciation Cycles 1. Linear Responses to Milankovitch Forcing. *Paleoceanography*, 7(6), 701-738.
- Inall, M.E., Gillibrand, P.A., (2010) The physics of mid-latitude fjords: a review. *Geological Society, London, Special Publications*, 344(1), 17-33.
- IPCC, (2007) Climate Change 2007 Synthesis Report.
- Jackson, M.G., Oskarsson, N., Trønnnes, R.G., McManus, J.F., Oppo, D.W., Grönvold, K., Hart, S.R., Sachs, J.P., (2005) Holocene loess deposition in Iceland: Evidence for millennial-scale atmosphere-ocean coupling in the North Atlantic. *Geology*, 33(6), 509-512.
- Jansen, E., Overpeck, J., Briffa, K.R., Duplessy, J.C., Joos, F., Masson-Delmotte, V., Olago, D., Otto-Bliesner, B.L., Peltier, W.R., Rahmstorf, S., Ramesh, R., Raynaud, D., Rind, D., Solomina, O., Villalba, R., Zhang, D., (2007) Palaeoclimate. In: S. Solomon, D. Qin, M. Manning, Z. Chen, M. Marquis, K.B. Averyt, M. Tignor, H.L. Miller (Eds.), *Climate Change 2007: The Physical Science Basis. Contribution of Working Group I to the Fourth*

## 9. Literature

*Assessment Report of the Intergovernmental Panel on Climate Change* (Ed. by S. Solomon, D. Qin, M. Manning, Z. Chen, M. Marquis, K.B. Averyt, M. Tignor, H.L. Miller). Cambridge University Press, Cambridge.

- Jennings, A., Andrews, J., Wilson, L., (2011) Holocene environmental evolution of the SE Greenland Shelf North and South of the Denmark Strait: Irminger and East Greenland current interactions. *Quaternary Science Reviews*, 30(7-8), 980-998.
- Jennings, A.E., Knudsen, K.L., Hald, M., Hansen, C.V., Andrews, J.T., (2002) A mid-Holocene shift in Arctic sea-ice variability on the East Greenland Shelf. *Holocene*, 12(1), 49-58.
- Jiang, H., Seidenkrantz, M.S., Knudsen, K.L., Eiriksson, J., (2002) Late-Holocene summer sea-surface temperatures based on a diatom record from the north Icelandic shelf. *Holocene*, 12(2), 137-147.
- Johnson-Ibach, L.E., (1982) Relationship between sedimentation rate and total organic carbon content in ancient marine sediments. *AAPG Bulletin*, 66(2), 170-188.
- Johnson, D.W., Hanson, P.J., Todd, D.E., Susfalk, R.B., Trettin, C.F., (1998) Precipitation Change and Soil Leaching: Field Results and Simulations from Walker Branch Watershed, Tennessee. *Water, Air, & Soil Pollution*, 105(1), 251-262.
- Jónsson, S., Valdimarsson, H., (2010) Water mass transport variability to the North Icelandic shelf, 1994-2010. *ICES Journal of Marine Science: Journal du Conseil*.
- Justwan, A., Koç, N., Jennings, A.E., (2008) Evolution of the Irminger and East Icelandic Current systems through the Holocene, revealed by diatom-based sea surface temperature reconstructions. *Quaternary Science Reviews*, 27(15-16), 1571-1582.
- Kan, J., Clingenpeel, S., Macur, R.E., Inskeep, W.P., Lovalvo, D., Varley, J., Gorby, Y., McDermott, T.R., Neelson, K., (2011) Archaea in Yellowstone Lake. *Isme Journal*, 5(11), 1784-1795.
- Kates, M., (1978) The phytanyl ether linked polar lipids and isoprenoid neutral lipids of extremely halophilic bacteria. *Progress in the Chemistry of Fats and Other Lipids*, 15(4), 301-342.
- Kaufman, D.S., Ager, T.A., Anderson, N.J., Anderson, P.M., Andrews, J.T., Bartlein, P.J., Brubaker, L.B., Coats, L.L., Cwynar, L.C., Duvall, M.L., Dyke, A.S., Edwards, M.E., Eisner, W.R., Gajewski, K., Geirsdóttir, A., Hu, F.S., Jennings, A.E., Kaplan, M.R., Kerwin, M.W., Lozhkin, A.V., MacDonald, G.M., Miller, G.H., Mock, C.J., Oswald, W.W., Otto-Bliesner, B.L., Porinchu, D.F., Rühland, K., Smol, J.P., Steig, E.J., Wolfe, B.B., (2004) Holocene thermal maximum in the western Arctic (0-180°W). *Quaternary Science Reviews*, 23(5-6), 529-560.

## 9. Literature

- Kawamura, K., Ishimura, Y., (2003) Four years' observations of terrestrial lipid class compounds in marine aerosols from the western North Pacific. *Global Biogeochemical Cycles*, 17(1), 1003.
- Kawamura, K., Ishimura, Y., Yamazaki, K., (2003) Four years' observations of terrestrial lipid class compounds in marine aerosols from the western North Pacific. *Global Biogeochem. Cycles*, 17(1), 1003.
- Kehrwald, N., Zangrando, R., Gambaro, A., Barbante, C., (2010) Fire and climate: Biomass burning recorded in ice and lake cores. *EPJ Web of Conferences*, 9, 105-114.
- Kennedy, H., Thomas, D.N., Kattner, G., Haas, C., Dieckmann, G.S., (2002) Particulate organic matter in Antarctic summer sea ice: concentration and stable isotopic composition. *Marine Ecology-Progress Series*, 238, 1-13.
- Killops, S., Killops, V., (2005) Introduction to Organic Geochemistry. Blackwell Science Ltd.
- Kim, J.H., Schouten, S., Hopmans, E.C., Donner, B., Damste, J.S.S., (2008) Global sediment core-top calibration of the TEX<sub>86</sub> paleothermometer in the ocean. *Geochimica Et Cosmochimica Acta*, 72, 1154-1173.
- Kim, J.H., van der Meer, J., Schouten, S., Helmke, P., Willmott, V., Sangiorgi, F., Koc, N., Hopmans, E.C., Damste, J.S.S., (2010) New indices and calibrations derived from the distribution of crenarchaeal isoprenoid tetraether lipids: Implications for past sea surface temperature reconstructions. *Geochimica Et Cosmochimica Acta*, 74(16), 4639-4654.
- Knies, J., (2005) Climate-induced changes in sedimentary regimes for organic matter supply on the continental shelf off northern Norway. *Geochimica Et Cosmochimica Acta*, 69(19), 4631-4647.
- Knies, J., Hald, M., Ebbesen, H., Mann, U., Vogt, C., (2003) A deglacial-middle Holocene record of biogenic sedimentation and paleoproductivity changes from the northern Norwegian continental shelf. *Paleoceanography*, 18(4).
- Knies, J., Mann, U., (2002) Depositional environment and source rock potential of Miocene strata from the central Fram Strait: introduction of a new computing tool for simulating organic facies variations. *Marine and Petroleum Geology*, 19(7), 811-828.
- Knittel, K., Losekann, T., Boetius, A., Kort, R., Amann, R., (2005) Diversity and distribution of methanotrophic archaea at cold seeps. *Applied and Environmental Microbiology*, 71(1), 467-479.

## 9. Literature

- Knudsen, K.L., Jiang, H., Jansen, E., Eiriksson, J., Heinemeier, J., Seidenkrantz, M.S., (2004) Environmental changes off North Iceland during the deglaciation and the Holocene: foraminifera, diatoms and stable isotopes. *Marine Micropaleontology*, 50(3-4), 273-305.
- Knudsen, K.L., Søndergaard, M.K.B., Eiriksson, J., Jiang, H., (2008) Holocene thermal maximum off North Iceland: Evidence from benthic and planktonic foraminifera in the 8600-5200 cal year BP time slice. *Marine Micropaleontology*, 67(1-2), 120-142.
- Koc, N., Jansen, E., (1994) Response to the high-latitude northern-hemisphere to orbital climate forcing - Evidence from the Nordic Seas. *Geology*, 22(6), 523-526.
- Koc, N., Jansen, E., Hafliðason, H., (1993) Paleoclimatographic reconstructions of surface ocean conditions in the Greenland, Iceland and Norwegian Seas throughout the last 14-ka based on Diatoms. *Quaternary Science Reviews*, 12(2), 115-140.
- Koga, Y., Morii, H., Akagawa-Matsushita, M., Ohga, I., (1998) Correlation of polar lipid composition with 16S rRNA phylogeny in methanogens. Further analysis of lipid component parts. *Bioscience Biotechnology and Biochemistry*, 62(2), 230-236.
- Kornilova, O., Rosell-Melé, A., (2003) Application of microwave-assisted extraction to the analysis of biomarker climate proxies in marine sediments. *Organic Geochemistry*, 34(11), 1517-1523.
- Labeyrie, L., Jansen, E., Cortijo, E., (2003) Les rapports des campagnes à la mer MD114/IMAGES V. *Institut Polaire Français Paul-Emile Victor, Brest*.
- Lamb, A.L., Wilson, G.P., Leng, M.J., (2006) A review of coastal palaeoclimate and relative sea-level reconstructions using  $\delta^{13}\text{C}$  and C/N ratios in organic material. *Earth-Science Reviews*, 75(1-4), 29-57.
- Lamb, H.H., (1995) *Climate, History and the Modern World*. Routledge.
- Langdon, P.G., Leng, M.J., Holmes, N., Caseldine, C.J., (2010) Lacustrine evidence of early-Holocene environmental change in northern Iceland: a multiproxy palaeoecology and stable isotope study. *Holocene*, 20(2), 205-214.
- Laskar, J., Robutel, P., Joutel, F., Gastineau, M., Correia, A.C.M., Levrard, B., (2004) A long-term numerical solution for the insolation quantities of the Earth. *Astronomy & Astrophysics*, 428(1), 261-285.
- Lee, K.E., Schneider, R., (2005) Alkenone production in the upper 200 m of the Pacific Ocean. *Deep Sea Research Part I: Oceanographic Research Papers*, 52(3), 443-456.

## 9. Literature

- Lee, R.F., Nevenzel, J.C., Paffenhofer, G., (1971) Importance of wax esters and other lipids in the marine food chain: phytoplankton and copepods. *Marine Biology*, 9(2), 99-8.
- Leu, E., Søreide, J.E., Hessen, D.O., Falk-Petersen, S., Berge, J., (2011) Consequences of changing sea-ice cover for primary and secondary producers in the European Arctic shelf seas: Timing, quantity, and quality. *Progress In Oceanography*, 90(1-4), 18-32.
- Liu, Z., Brady, E., Lynch-Stieglitz, J., (2003) Global ocean response to orbital forcing in the Holocene. *Paleoceanography*, 18(2).
- Longhurst, A., Sathyendranath, S., Platt, T., Caverhill, C., (1995) An estimate of global primary production in the ocean from satellite radiometer data. *Journal of Plankton Research*, 17(6), 1245-1271.
- Madigan, M.T., Martinko, J.M., Dunlap, P.V., Clark, D.P., (2009) Brock Biology of Microorganisms. Pearson Education, Inc.
- Mangelsdorf, K., (2000) Rekonstruktion der klimatischen und ozeanographischen Bedingungen am kalifornischen Kontinentalrand während des Spätquartärs anhand organisch-geochemischer Indikatoren. In: *Institute of pure and applied chemistry, PhD*, pp. 177. University of Oldenburg, Oldenburg.
- Marchal, O., Cacho, I., Stocker, T.F., Grimalt, J.O., Calvo, E., Martrat, B., Shackleton, N., Vautravers, M., Cortijo, E., van Krevelend, S., Andersson, C., Koc, N., Chapman, M., Saffi, L., Duplessy, J.C., Sarnthein, M., Turon, J.L., Duprat, J., Jansen, E., (2002) Apparent long-term cooling of the sea surface in the northeast Atlantic and Mediterranean during the Holocene. *Quaternary Science Reviews*, 21(4-6), 455-483.
- Marret, F., Scourse, J.D., Versteegh, G., Jansen, J.H.F., Schneider, R., (2001) Integrated marine and terrestrial evidence for abrupt Congo River palaeodischarge fluctuations during the last deglaciation. *Journal of Quaternary Science*, 16(8), 761-766.
- Massana, R., DeLong, E.F., Pedros-Alio, C., (2000) A few cosmopolitan phylotypes dominate planktonic archaeal assemblages in widely different oceanic provinces. *Applied and Environmental Microbiology*, 66(5), 1777-1787.
- Massé, G., Belt, S.T., Rowland, S.J., Rohmer, M., (2004) Isoprenoid biosynthesis in the diatoms *Rhizosolenia setigera* (Brightwell) and *Haslea ostrearia* (Simonsen). *Proceedings of the National Academy of Sciences of the United States of America*, 101(13), 4413-4418.
- Massé, G., Rowland, S.J., Sicre, M.A., Jacob, J., Jansen, E., Belt, S.T., (2008) Abrupt climate changes for Iceland during the last millennium: Evidence from high resolution sea ice reconstructions. *Earth and Planetary Science Letters*, 269(3-4), 564-568.

## 9. Literature

- Mayewski, P., White, F., (2002) *The Ice Chronicles - The Quest to Understand Global Climate Change*. University Press of New England Hanover and London.
- Mayewski, P.A., Rohling, E.E., Stager, J.C., Karlen, W., Maasch, K.A., Meeker, L.D., Meyerson, E.A., Gasse, F., van Kreveld, S., Holmgren, K., Lee-Thorp, J., Rosqvist, G., Rack, F., Staubwasser, M., Schneider, R.R., Steig, E.J., (2004) Holocene climate variability. *Quaternary Research*, 62(3), 243-255.
- McMahon, K.W., Jr., W.G.A., Johnson, B.J., Sun, M.-Y., Lopez, G.R., Clough, L.M., Carroll, M.L., (2006) Benthic community response to ice algae and phytoplankton in Ny-Ålesund, Svalbard. *Marine Ecology Progress Series*, 310, 1-14.
- McMinn, A., Skerratt, J., Trull, T., Ashworth, C., Lizotte, M., (1999) Nutrient stress gradient in the bottom 5 cm of fast ice, McMurdo Sound, Antarctica. *Polar Biology*, 21(4), 220-227.
- Medina-Elizalde, M., Rohling, E.J., (2012) Collapse of Classic Maya Civilization Related to Modest Reduction in Precipitation. *Science*, 335(6071), 956-959.
- Meyers, P.A., (1994) Preservation of elemental and isotopic source identification of sedimentary organic matter. *Chemical Geology*, 114(3-4), 289-302.
- Meyers, P.A., (1997) Organic geochemical proxies of paleoceanographic, paleolimnologic, and paleoclimatic processes. *Organic Geochemistry*, 27(5-6), 213-250.
- Middelburg, J.J., Barranguet, C., Boschker, H.T.S., Herman, P.M.J., Moens, T., Heip, C.H.R., (2000) The Fate of Intertidal Microphytobenthos Carbon: An In situ <sup>13</sup>C-Labeling Study. *Limnology and Oceanography*, 45(6), 1224-1234.
- Mollenhauer, G., Eglinton, T.I., (2007) Diagenetic and Sedimentological Controls on the Composition of Organic Matter Preserved in California Borderland Basin Sediments. *Limnology and Oceanography*, 52(2), 558-576.
- Moros, M., Emeis, K., Risebrobakken, B., Snowball, I., Kuijpers, A., McManus, J., Jansen, E., (2004) Sea surface temperatures and ice rafting in the Holocene North Atlantic: climate influences on Northern Europe and Greenland. *Quaternary Science Reviews*, 23(20-22), 2113-2126.
- Müller, J., Masse, G., Stein, R., Belt, S.T., (2009) Variability of sea-ice conditions in the Fram Strait over the past 30,000 years. *Nature Geosci*, 2(11), 772-776.
- Müller, P.J., Kirst, G., Ruhland, G., von Storch, I., Rosell-Mele, A., (1998) Calibration of the alkenone paleotemperature index  $U^{K}_{37}$  based on core-tops from the eastern South Atlantic

## 9. Literature

- and the global ocean (60° N-60° S). *Geochimica Et Cosmochimica Acta*, 62(10), 1757-1772.
- Müller, P.J., Suess, E., (1979) Productivity, sedimentation rate, and sedimentary organic matter in the oceans-I. Organic carbon preservation. *Deep Sea Research Part A. Oceanographic Research Papers*, 26(12), 1347-1362.
- Murray, J., King, D., (2012) Climate policy: Oil's tipping point has passed. *Nature*, 481(7382), 433-435.
- Mutterlose, J., Malkoc, M., Schouten, S., Sinninghe Damsté, J.S., Forster, A., (2010) TEX<sub>86</sub> and stable  $\delta^{18}\text{O}$  paleothermometry of early Cretaceous sediments: Implications for belemnite ecology and paleotemperature proxy application. *Earth and Planetary Science Letters*, 298, 286-298.
- Nauhaus, K., Boetius, A., Kruger, M., Widdel, F., (2002) In vitro demonstration of anaerobic oxidation of methane coupled to sulphate reduction in sediment from a marine gas hydrate area. *Environmental Microbiology*, 4(5), 296-305.
- Nauhaus, K., Treude, T., Boetius, A., Kruger, M., (2005) Environmental regulation of the anaerobic oxidation of methane: a comparison of ANME-I and ANME-II communities. *Environmental Microbiology*, 7(1), 98-106.
- Niemann, H., Elvert, M., (2008) Diagnostic lipid biomarker and stable carbon isotope signatures of microbial communities mediating the anaerobic oxidation of methane with sulphate. *Organic Geochemistry*, 39(12), 1668-1677.
- Niemann, H., Losekann, T., de Beer, D., Elvert, M., Nadalig, T., Knittel, K., Amann, R., Sauter, E.J., Schluter, M., Klages, M., Foucher, J.P., Boetius, A., (2006) Novel microbial communities of the Haakon Mosby mud volcano and their role as a methane sink. *Nature*, 443(7113), 854-858.
- Nuwer, J.M., Keil, R.G., (2005) Sedimentary Organic Matter Geochemistry of Clayoquot Sound, Vancouver Island, British Columbia. *Limnology and Oceanography*, 50(4), 1119-1128.
- Ogilvie, A.E.J., Caseldine, C., Russell, A., Harðardóttir, J., Knudsen, Ó., (2005) 11. Local knowledge and travellers' tales: a selection of climatic observations in Iceland, *Developments in Quaternary Sciences, Volume 5*, pp. 257-287. Elsevier.
- Ogilvie, A.E.J., Jonsdottir, I., (2000) Sea ice, climate, and Icelandic fisheries in the eighteenth and nineteenth centuries. *Arctic*, 53(4), 383-394.

## 9. Literature

- Ogilvie, A.E.J., Jonsson, T., (2001) "Little Ice Age" research: A perspective from Iceland. *Climatic Change*, 48(1), 9-52.
- Okada, H., Honjo, S., (1973) The distribution of oceanic coccolithophorids in the Pacific. *Deep Sea Research and Oceanographic Abstracts*, 20(4), 355-364, IN3-IN4, 365-374.
- Ólafsdóttir, R., Gudmundsson, H.J., (2002) Holocene land degradation and climatic change in northeastern Iceland. *The Holocene*, 12(2), 159-167.
- Ólafsdóttir, R., Schlyter, P., Haraldsson, H.V., (2001) Simulating Icelandic Vegetation Cover during the Holocene Implications for Long-Term Land Degradation. *Geografiska Annaler. Series A, Physical Geography*, 83(4), 203-215.
- Ólafsdóttir, S., Jennings, A.E., Geirsdóttir, Á., Andrews, J., Miller, G.H., (2010) Holocene variability of the North Atlantic Irminger current on the south- and northwest shelf of Iceland. *Marine Micropaleontology*, 77(3-4), 101-118.
- Orphan, V.J., House, C.H., Hinrichs, K.-U., McKeegan, K.D., DeLong, E.F., (2002) Multiple archaeal groups mediate methane oxidation in anoxic cold seep sediments. *Proceedings of the National Academy of Sciences*, 99(11), 7663-7668.
- Ottersen, G., Planque, B., Belgrano, A., Post, E., Reid, P.C., Stenseth, N.C., (2001) Ecological effects of the North Atlantic Oscillation. *Oecologia*, 128(1), 1-14.
- Paetzel, M., Schrader, H., (1992) Recent environmental changes recorded in anoxic Barsnesfjord sediments: Western Norway. *Marine Geology*, 105(1-4), 23-36.
- Pagani, M., Pedentchouk, N., Huber, M., Sluijs, A., Schouten, S., Brinkhuis, H., Sinninghe Damste, J.S., Dickens, G.R., Expedition, S., (2006) Arctic hydrology during global warming at the Palaeocene/Eocene thermal maximum. *Nature*, 442(7103), 671-675.
- Pancost, R.D., Boot, C.S., (2004) The palaeoclimatic utility of terrestrial biomarkers in marine sediments. *Marine Chemistry*, 92(1-4), 239-261.
- Pancost, R.D., Freeman, K.H., Wakeham, S.G., Robertson, C.Y., (1997) Controls on carbon isotope fractionation by diatoms in the Peru upwelling region. *Geochimica Et Cosmochimica Acta*, 61(23), 4983-4991.
- Pancost, R.D., Hopmans, E.C., Sinninghe Damsté, J.S., (2001) Archaeal lipids in Mediterranean cold seeps: molecular proxies for anaerobic methane oxidation. *Geochimica Et Cosmochimica Acta*, 65(10), 1611-1627.
- Pancost, R.D., Sinninghe Damsté, J.S., de Lint, S., van der Maarel, M.J.E.C., Gottschal, J.C., Party, T.M.S.S., (2000) Biomarker Evidence for Widespread Anaerobic Methane Oxidation

## 9. Literature

- in Mediterranean Sediments by a Consortium of Methanogenic Archaea and Bacteria. *Applied and Environmental Microbiology*, 66(3), 1126-1132.
- Pardue, J.W., Scalan, R.S., Van Baalen, C., Parker, P.L., (1976) Maximum carbon isotope fractionation in photosynthesis by blue-green algae and a green alga. *Geochimica Et Cosmochimica Acta*, 40(3), 309-312.
- Patterson, W.P., Dietrich, K.A., Holmden, C., Andrews, J.T., (2010) Two millennia of North Atlantic seasonality and implications for Norse colonies. *Proceedings of the National Academy of Sciences of the United States of America*, 107(12), 5306-5310.
- Peckmann, J., Birgel, D., Kiel, S., (2009) Molecular fossils reveal fluid composition and flow intensity at a Cretaceous seep. *Geology*, 37(9), 847-850.
- Perdue, E.M., Koprivnjak, J.-F., (2007) Using the C/N ratio to estimate terrigenous inputs of organic matter to aquatic environments. *Estuarine, Coastal and Shelf Science*, 73(1-2), 65-72.
- Perrette, M., Yool, A., Quartly, G.D., Popova, E.E., (2011) Near-ubiquity of ice-edge blooms in the Arctic. *Biogeosciences*, 8(2), 515-524.
- Peters, K.E., Walters, C.C., Moldowan, J.M., (2005) *The Biomarker Guide - Biomarkers and Isotopes in the Environment and Human History*. Cambridge University Press.
- Peterse, F., Kim, J.-H., Schouten, S., Kristensen, D.K., Koç, N., Sinninghe Damsté, J.S., (2009a) Constraints on the application of the MBT/CBT palaeothermometer at high latitude environments (Svalbard, Norway). *Organic Geochemistry*, 40(6), 692-699.
- Peterse, F., Nicol, G.W., Schouten, S., Sinninghe Damsté, J.S., (2010) Influence of soil pH on the abundance and distribution of core and intact polar lipid-derived branched GDGTs in soil. *Organic Geochemistry*, 41(10), 1171-1175.
- Peterse, F., Schouten, S., van der Meer, J., van der Meer, M.T.J., Sinninghe Damsté, J.S., (2009b) Distribution of branched tetraether lipids in geothermally heated soils: Implications for the MBT/CBT temperature proxy. *Organic Geochemistry*, 40(2), 201-205.
- Pithey, A.F., (1979) *Geography and soil properties*. Methuen & Co Ltd.
- Poynter, J.G., Farrimond, P., Robinson, N., Eglinton, G., (1989) Aeolian derived higher plant lipids in the marine sedimentary record - Links with paleoclimate. In: *Paleoclimatology and Paleometeorology : Modern and Past Patterns of Global Atmospheric Transport*, 282 (Ed. by M.S.M. Leinen), pp. 435-462.

## 9. Literature

- Prahl, F.G., Rontani, J.F., Zabeti, N., Walinsky, S.E., Sparrow, M.A., (2010) Systematic pattern in  $U^{K}_{37}$  Temperature residuals for surface sediments from high latitude and other oceanographic settings. *Geochimica Et Cosmochimica Acta*, 74(1), 131-143.
- Prahl, F.G., Wakeham, S.G., (1987) Calibration of unsaturation patterns in long-chain ketone compositions for paleotemperature assessment. *Nature*, 330(6146), 367-369.
- Principato, S.M., (2008) Geomorphic evidence for Holocene glacial advances and sea level fluctuations on eastern Vestfirir, northwest Iceland. *Boreas*, 37(1), 132-145.
- Quillmann, U., Jennings, A., Andrews, J., (2010) Reconstructing Holocene palaeoclimate and palaeoceanography in Isafjaroardjup, northwest Iceland, from two fjord records overprinted by relative sea-level and local hydrographic changes. *Journal of Quaternary Science*, 25(7), 1144-1159.
- Reid, F.M.H., (1980) Coccolithophorids of the north pacific central gyre with notes on their vertical and seasonal distribution. *Micropaleontology (New York)*, 26(2), 151-176.
- Renssen, H., Goosse, H., Fichefet, T., Brovkin, V., Driesschaert, E., Wolk, F., (2005) Simulating the Holocene climate evolution at northern high latitudes using a coupled atmosphere-sea ice-ocean-vegetation model. *Climate Dynamics*, 24(1), 23-43.
- Riedel, A., Michel, C., Gosselin, M., LeBlanc, B., (2008) Winter-spring dynamics in sea-ice carbon cycling in the coastal Arctic Ocean. *Journal of Marine Systems*, 74, 918-932.
- Rommerskirchen, F., Eglinton, G., Dupont, L., Guntner, U., Wenzel, C., Rullkötter, J., (2003) A north to south transect of Holocene southeast Atlantic continental margin sediments: Relationship between aerosol transport and compound-specific  $\delta^{13}C$  land plant biomarker and pollen records. *Geochemistry Geophysics Geosystems*, 4.
- Rommerskirchen, F., Plader, A., Eglinton, G., Chikaraishi, Y., Rullkötter, J., (2006) Chemotaxonomic significance of distribution and stable carbon isotopic composition of long-chain alkanes and alkan-1-ols in C4 grass waxes. *Organic Geochemistry*, 37(10), 1303-1332.
- Rosell-Melé, A., Eglinton, G., Pflaumann, U., Sarnthein, M., (1995) Atlantic core-top calibration of the  $U^{K}_{37}$  index as a sea-surface palaeotemperature indicator. *Geochimica Et Cosmochimica Acta*, 59(15), 3099-3107.
- Rowland, S.J., Belt, S.T., Wraige, E.J., Masse, G., Roussakis, C., Robert, J.M., (2001) Effects of temperature on polyunsaturation in cytosolic lipids of *Haslea ostrearia*. *Phytochemistry*, 56(6), 597-602.

## 9. Literature

- Rowland, S.J., Robson, J.N., (1990) The widespread occurrence of highly branched acyclic C<sub>20</sub>, C<sub>25</sub> and C<sub>30</sub> hydrocarbons in recent sediments and biota--A review. *Marine Environmental Research*, 30(3), 191-216.
- Rudels, B., Larsson, A.M., Sehlstedt, P.I., (1991) Stratification and water mass formation in the Arctic Ocean - some implications for the nutrient distribution. *Polar Research*, 10(1), 19-31.
- Rudels, B., Meyer, R., Fahrbach, E., Ivanov, V.V., Osterhus, S., Quadfasel, D., Schauer, U., Tverberg, V., Woodgate, R.A., (2000) Water mass distribution in Fram Strait and over the Yermak Plateau in summer 1997. *Annales Geophysicae-Atmospheres Hydrospheres and Space Sciences*, 18(6), 687-705.
- Rueda, G., Rosell-Melé, A., Escala, M., Gyllencreutz, R., Backman, J., (2009) Comparison of instrumental and GDGT-based estimates of sea surface and air temperatures from the Skagerrak. *Organic Geochemistry*, 40(2), 287-291.
- Sachse, D., Radke, J., Gleixner, G., (2004) Hydrogen isotope ratios of recent lacustrine sedimentary n-alkanes record modern climate variability. *Geochimica Et Cosmochimica Acta*, 68(23), 4877-4889.
- Sachse, D., Radke, J., Gleixner, G., (2006)  $\delta D$  values of individual n-alkanes from terrestrial plants along a climatic gradient - Implications for the sedimentary biomarker record. *Organic Geochemistry*, 37(4), 469-483.
- Sargent, J.R., Falk-Petersen, S., (1988) The lipid biochemistry of Calanoid copepods. *Hydrobiologia*, 167, 101-114.
- Sathyendranath, S., Longhurst, A., Caverhill, C.M., Platt, T., (1995) Regionally and seasonally differentiated primary production in the North Atlantic. *Deep Sea Research Part I: Oceanographic Research Papers*, 42(10), 1773-1802.
- Sauer, P.E., Eglinton, T.I., Hayes, J.M., Schimmelmann, A., Sessions, A.L., (2001) Compound-specific D/H ratios of lipid biomarkers from sediments as a proxy for environmental and climatic conditions. *Geochimica et Cosmochimica Acta*, 65(2), 213.
- Schefuss, E., Ratmeyer, V., Stuut, J.-B.W., Jansen, J.H.F., Sinninghe Damsté, J.S., (2003a) Carbon isotope analyses of n-alkanes in dust from the lower atmosphere over the central eastern Atlantic. *Geochimica Et Cosmochimica Acta*, 67(10), 1757-1767.
- Schefuss, E., Schouten, S., Jansen, J.H.F., Damste, J.S.S., (2003b) African vegetation controlled by tropical sea surface temperatures in the mid-Pleistocene period. *Nature*, 422(6930), 418-421.

## 9. Literature

- Schefuss, E., Schouten, S., Schneider, R.R., (2005) Climatic controls on central African hydrology during the past 20,000 years. *Nature*, 437(7061), 1003-1006.
- Schewe, I., Soltwedel, T., (2003) Benthic response to ice-edge-induced particle flux in the Arctic Ocean. *Polar Biology*, 26(9), 610-620.
- Schidlowski, M., (1987) Application of stable isotopes to early biochemical evolution on earth. *Ann. Rev. Earth Planet. Sci.*, 15, 47-72.
- Schlitzer, R., (2010) Ocean Data View, <http://odv.awi.de>.
- Schlüter, M., Sauter, E.J., Schäfer, A., Ritzrau, W., (2000) Spatial budget of organic carbon flux to the seafloor of the northern North Atlantic (60°N-80°N). *Global Biogeochem. Cycles*, 14(1), 329-340.
- Schouten, S., Forster, A., Panoto, F.E., Sinninghe Damsté, J.S., (2007) Towards calibration of the TEX86 palaeothermometer for tropical sea surface temperatures in ancient greenhouse worlds. *Organic Geochemistry*, 38, 1537-1546.
- Schouten, S., Hopmans, E.C., Schefuss, E., Sinninghe Damsté, J.S., (2002) Distributional variations in marine crenarchaeotal membrane lipids: a new tool for reconstructing ancient sea water temperatures? *Earth and Planetary Science Letters*, 204(1-2), 265-274.
- Sharp, Z., (2007) Principles of Stable Isotope Geochemistry. Pearson, Prentice Hall, Upper Saddle River, NJ 07458.
- Shuman, B., Huang, Y., Newby, P., Wang, Y., (2006) Compound-specific isotopic analyses track changes in seasonal precipitation regimes in the Northeastern United States at ca 8200 cal yr BP. *Quaternary Science Reviews*, 25(21-22), 2992.
- Sicre, M.A., Jacob, J., Ezat, U., Rouse, S., Kissel, C., Yiou, P., Eiriksson, J., Knudsen, K.L., Jansen, E., Turon, J.L., (2008a) Decadal variability of sea surface temperatures off North Iceland over the last 2000 years. *Earth and Planetary Science Letters*, 268(1-2), 137-142.
- Sicre, M.A., Yiou, P., Eiriksson, J., Ezat, U., Guimbaut, E., Dahhaoui, I., Knudsen, K.L., Jansen, E., Turon, J.L., (2008b) A 4500-year reconstruction of sea surface temperature variability at decadal time-scales off North Iceland. *Quaternary Science Reviews*, 27(21-22), 2041-2047.
- Sikes, E.L., Volkman, J.K., Robertson, L.G., Pichon, J.-J., (1997) Alkenones and alkenes in surface waters and sediments of the Southern Ocean: Implications for paleotemperature estimation in polar regions. *Geochimica Et Cosmochimica Acta*, 61(7), 1495-1505.

## 9. Literature

- Simoneit, B.R.T., Sheng, G., Chen, X., Fu, J., Zhang, J., Xu, Y., (1991) Molecular marker study of extractable organic matter in aerosols from urban areas of China. *Atmospheric Environment. Part A. General Topics*, 25(10), 2111-2129.
- Sinninghe Damsté, J.S., Hopmans, E.C., Pancost, R.D., Schouten, S., Geenevasen, J.A.J., (2000) Newly discovered non-isoprenoid glycerol dialkyl glycerol tetraether lipids in sediments. *Chemical Communications*(17), 1683-1684.
- Sinninghe Damsté, J.S., Rijpstra, W.I.C., Hopmans, E.C., Weijers, J.W.H., Foesel, B.U., Overmann, J., Dedysh, S.N., (2011) 13,16-Dimethyl Octacosanedioic Acid (iso-Diabolic Acid), a Common Membrane-Spanning Lipid of Acidobacteria Subdivisions 1 and 3. *Applied and Environmental Microbiology*, 77(12), 4147-4154.
- Sinninghe Damsté, J.S., Rijpstra, W.I.C., Reichart, G.J., (2002a) The influence of oxic degradation on the sedimentary biomarker record II. Evidence from Arabian Sea sediments. *Geochimica Et Cosmochimica Acta*, 66(15), 2737-2754.
- Sinninghe Damsté, J.S., Schouten, S., Hopmans, E.C., van Duin, A.C.T., Geenevasen, J.A.J., (2002b) Crenarchaeol: the characteristic core glycerol dibiphytanyl glycerol tetraether membrane lipid of cosmopolitan pelagic crenarchaeota. *Journal of Lipid Research*, 43(10), 1641-1651.
- Sinninghe Damsté, J.S., Schouten, S., Rijpstra, W.I.C., Hopmans, E.C., Peletier, H., Gieskes, W.W.C., Geenevasen, J.A.J., (1999) Structural identification of the C<sub>25</sub> highly branched isoprenoid pentaene in the marine diatom *Rhizosolenia setigera*. *Organic Geochemistry*, 30(12), 1581-1583.
- Skei, J., (1983) Why sedimentologists are interested in fjords. *Sedimentary Geology*, 36(2-4), 75-80.
- Skrzypek, G., Paul, D., Wojtun, B., (2008) Stable isotope composition of plants and peat from Arctic mire and geothermal area in Iceland. *Polish Polar Research*, 29(4), 365-376.
- Sluijs, A., Schouten, S., Pagani, M., Woltering, M., Brinkhuis, H., Damsté, J.S.S., Dickens, G.R., Huber, M., Reichart, G.-J., Stein, R., Matthiessen, J., Lourens, L.J., Pedentchouk, N., Backman, J., Moran, K., the Expedition, S., (2006) Subtropical Arctic Ocean temperatures during the Palaeocene/Eocene thermal maximum. *Nature*, 441(7093), 610-613.
- Smith, F.A., Freeman, K.H., (2006) Influence of physiology and climate on  $\delta D$  of leaf wax n-alkanes from C<sub>3</sub> and C<sub>4</sub> grasses. *Geochimica et Cosmochimica Acta*, 70(5), 1172.
- Smith, K., (2011) We are seven billion. *Nature Climate Change*, 1(7), 331-335.

## 9. Literature

- Smith, S.L., Henrichs, S.M., Rho, T., (2002) Stable C and N isotopic composition of sinking particles and zooplankton over the southeastern Bering Sea shelf. *Deep Sea Research Part II: Topical Studies in Oceanography*, 49(26), 6031-6050.
- Smittenberg, R.H., Eglinton, T.I., Schouten, S., Sinninghe Damsté, J.S., (2006) Ongoing Buildup of Refractory Organic Carbon in Boreal Soils During the Holocene. *Science*, 314(5803), 1283-1286.
- Smittenberg, R.H., Pancost, R.D., Hopmans, E.C., Paetzel, M., Sinninghe Damsté, J.S., (2004) A 400-year record of environmental change in an euxinic fjord as revealed by the sedimentary biomarker record. *Palaeogeography, Palaeoclimatology, Palaeoecology*, 202(3-4), 331-351.
- Spielhagen, R.F., Werner, K., Sorensen, S.A., Zamelczyk, K., Kandiano, E., Budeus, G., Husum, K., Marchitto, T.M., Hald, M., (2011) Enhanced modern heat transfer to the Arctic by warm atlantic water. *Science*, 331(6016), 450-453.
- St. John, M.A., Lund, T., (1996) Lipid biomarkers: Linking the utilization of frontal plankton biomass to enhanced condition of juvenile North Sea cod. *Marine Ecology-Progress Series*, 131(1-3), 75-85.
- Stefansson, U., Gudmundsson, G., (1969) Hydrographic conditions off the northeast coast of Iceland in relation to meteorological factors. *Tellus*, 21(2), 245-258.
- Steig, E.J., Morse, D.L., Waddington, E.D., Stuiver, M., Grootes, P.M., Mayewski, P.A., Twickler, M.S., Whitlow, S.I., (2000) Wisconsinan and Holocene climate history from an ice core at Taylor Dome, western Ross Embayment, Antarctica. *Geografiska Annaler Series a-Physical Geography*, 82A(2-3), 213-235.
- Stein, R., (1986) Surface-water paleo-productivity as inferred from sediments deposited in oxic and anoxic deep-ater environments of the Mesozoic Atlantic Ocean. *Mitt. Geol.-Paläont. Inst. University Hamburg*, 60, 55-70.
- Stein, R., (1990) Organic carbon content/sedimentation rate relationship and its paleoenvironmental significance for marine sediments. *Geo-Marine Letters*, 10(1), 37-44.
- Stein, R., Rullkötter, J., Welte, D.H., (1986) Accumulation of organic-carbon-rich sediments in the Late Jurassic and Cretaceous Atlantic Ocean - A synthesis. *Chemical Geology*, 56(1-2), 1-32.
- Stenseth, N.C., Mysterud, A., Ottersen, G., Hurrell, J.W., Chan, K.-S., Lima, M., (2002) Ecological Effects of Climate Fluctuations. *Science*, 297(5585), 1292-1296.

## 9. Literature

- Stroeve, J., Holland, M.M., Meier, W., Scambos, T., Serreze, M., (2007) Arctic sea ice decline: Faster than forecast. *Geophysical Research Letters*, 34(9).
- Stuiver, M., Reimer, P.J., Braziunas, T.F., (1998) High-precision radiocarbon age calibration for terrestrial and marine samples. *Radiocarbon*, 40(3), 1127-1151.
- Sun, M.Y., Carroll, M.L., Ambrose, W.G., Clough, L.M., Zou, L., Lopez, G.R., (2007) Rapid consumption of phytoplankton and ice algae by Arctic soft-sediment benthic communities: Evidence using natural and C-13-labeled food materials. *Journal of Marine Research*, 65(4), 561-588.
- Syvertsen, E.E., (1991) Ice algae in the Barents Sea: types of assemblages, origin, fate and role in the ice-edge phytoplankton bloom. *Polar Research*, 10(1), 277-288.
- Tamelander, T., Reigstad, M., Hop, H., Carroll, M.L., Wassmann, P., (2008) Pelagic and sympagic contribution of organic matter to zooplankton and vertical export in the Barents Sea marginal ice zone. *Deep Sea Research Part II: Topical Studies in Oceanography*, 55(20-21), 2330-2339.
- Tamelander, T., Renaud, P.E., Hop, H., Carroll, M.L., Ambrose, W.G., Hobson, K.A., (2006) Trophic relationships and pelagic-benthic coupling during summer in the Barents Sea Marginal Ice Zone, revealed by stable carbon and nitrogen isotope measurements. *Marine Ecology-Progress Series*, 310, 33-46.
- Tareq, S.M., Kitagawa, H., Ohta, K., (2011) Lignin biomarker and isotopic records of paleovegetation and climate changes from Lake Erhai, southwest China, since 18.5 ka BP. *Quaternary International*, 229(1-2), 47-56.
- Teixidor, P., Grimalt, J.O., (1992) Gas chromatographic determination of isoprenoid alkylglycerol diethers in archaeobacterial cultures and environmental samples. *Journal of Chromatography A*, 607(2), 253-259.
- Ternois, Y., Sicre, M.A., Boireau, A., Beaufort, L., Miquel, J.C., Jeandel, C., (1998) Hydrocarbons, sterols and alkenones in sinking particles in the Indian Ocean sector of the Southern Ocean. *Organic Geochemistry*, 28(7-8), 489-501.
- Trouet, V., Esper, J., Graham, N.E., Baker, A., Scourse, J.D., Frank, D.C., (2009) Persistent Positive North Atlantic Oscillation Mode Dominated the Medieval Climate Anomaly. *Science*, 324(5923), 78-80.
- Uda, I., Sugai, A., Itoh, Y.H., Itoh, T., (2001) Variation in molecular species of polar lipids from *Thermoplasma acidophilum* depends on growth temperature. *Lipids*, 36(1), 103-105.

## 9. Literature

- Valentine, D.L., (2002) Biogeochemistry and microbial ecology of methane oxidation in anoxic environments: a review. *Antonie Van Leeuwenhoek International Journal of General and Molecular Microbiology*, 81(1-4), 271-282.
- van de Vossenberg, J., Driessen, A.J.M., Konings, W.N., (1998a) The essence of being extremophilic: the role of the unique archaeal membrane lipids. *Extremophiles*, 2(3), 163-170.
- van de Vossenberg, J., Driessen, A.J.M., Zillig, W., Konings, W.N., (1998b) Bioenergetics and cytoplasmic membrane stability of the extremely acidophilic, thermophilic archaeon *Picrophilus oshimae*. *Extremophiles*, 2(2), 67-74.
- Vare, L.L., Massé, G., Belt, S.T., (2010) A biomarker-based reconstruction of sea ice conditions for the Barents Sea in recent centuries. *The Holocene*, 20(4), 637-643.
- Vare, L.L., Massé, G., Gregory, T.R., Smart, C.W., Belt, S.T., (2009) Sea ice variations in the central Canadian Arctic Archipelago during the Holocene. *Quaternary Science Reviews*, 28, 1354-1366.
- Viso, A.-C., Marty, J.-C., (1993) Fatty acids from 28 marine microalgae. *Phytochemistry*, 34(6), 1521-1533.
- Vogts, A., Moossen, H., Rommerskirchen, F., Rullkotter, J., (2009) Distribution patterns and stable carbon isotopic composition of alkanes and alkan-1-ols from plant waxes of African rain forest and savanna C3 species. *Organic Geochemistry*, 40(10), 1037-1054.
- Volkman, J.K., Barrerr, S.M., Blackburn, S.I., Sikes, E.L., (1995) Alkenones in *Gephyrocapsa oceanica*: Implications for studies of paleoclimate. *Geochimica et Cosmochimica Acta*, 59(3), 513-520.
- Volkman, J.K., Barrett, S.M., Blackburn, S.I., Mansour, M.P., Sikes, E.L., Gelin, F., (1998) Microalgal biomarkers: A review of recent research developments. *Organic Geochemistry*, 29(5-7), 1163-1179.
- Volkman, J.K., Barrett, S.M., Dunstan, G.A., (1994) C<sub>25</sub> and C<sub>30</sub> highly branched isoprenoid alkenes in laboratory cultures of two marine diatoms. *Organic Geochemistry*, 21(3-4), 407-413.
- Volkman, J.K., Eglinton, G., Corner, E.D.S., Forsberg, T.E.V., (1980) Long-chain alkenes and alkenones in the marine coccolithophorid *Emiliana huxleyi*. *Phytochemistry*, 19(12), 2619-2622.

## 9. Literature

- Walsh, E.M., Ingalls, A.E., Keil, R.G., (2008) Sources and transport of terrestrial organic matter in Vancouver Island fjords and the Vancouver-Washington Margin: A multiproxy approach using  $\delta^{13}\text{C}_{\text{org}}$ , lignin phenols, and the ether lipid BIT index. *Limnology and Oceanography*, 53(3), 1054-1063.
- Wang, G., Dolman, A.J., Alessandri, A., (2011) A summer climate regime over Europe modulated by the North Atlantic Oscillation. *Hydrology and Earth System Sciences*, 15(1), 57-64.
- Wassmann, P., Andreassen, I., Reigstad, M., Slagstad, D., (1996) Pelagic-benthic coupling in the Nordic Seas: The role of episodic events. *Marine Ecology-Pubblicazioni Della Stazione Zoologica Di Napoli I*, 17(1-3), 447-471.
- Wastl, M., Stötter, J., Caseldine, C., (2001) Reconstruction of Holocene Variations of the Upper Limit of Tree or Shrub Birch Growth in Northern Iceland Based on Evidence from Vesturardalur-Skidadalur, Trölaskagi. *Arctic, Antarctic, and Alpine Research*, 33(2), 191-203.
- Weijers, J.W.H., Bernhardt, B., Peterse, F., Werne, J.P., Dungait, J.A.J., Schouten, S., Sinninghe Damsté, J.S., (2011a) Absence of seasonal patterns in MBT-CBT indices in mid-latitude soils. *Geochimica Et Cosmochimica Acta*, 75(11), 3179-3190.
- Weijers, J.W.H., Schefuss, E., Schouten, S., Sinninghe Damsté, J.S., (2007a) Coupled thermal and hydrological evolution of tropical Africa over the last deglaciation. *Science*, 315(5819), 1701-1704.
- Weijers, J.W.H., Schouten, S., Hopmans, E.C., Geenevasen, J.A.J., David, O.R.P., Coleman, J.M., Pancost, R.D., Sinninghe Damsté, J.S., (2006a) Membrane lipids of mesophilic anaerobic bacteria thriving in peats have typical archaeal traits. *Environmental Microbiology*, 8, 648-657.
- Weijers, J.W.H., Schouten, S., Schefuss, E., Schneider, R.R., Sinninghe Damsté, J.S., (2009) Disentangling marine, soil and plant organic carbon contributions to continental margin sediments: A multi-proxy approach in a 20,000 year sediment record from the Congo deep-sea fan. *Geochimica Et Cosmochimica Acta*, 73(1), 119-132.
- Weijers, J.W.H., Schouten, S., Sluijs, A., Brinkhuis, H., Sinninghe Damsté, J.S., (2007b) Warm arctic continents during the Palaeocene-Eocene thermal maximum. *Earth and Planetary Science Letters*, 261(1-2), 230-238.
- Weijers, J.W.H., Schouten, S., Spaargaren, O.C., Sinninghe Damsté, J.S., (2006b) Occurrence and distribution of tetraether membrane lipids in soils: Implications for the use of the TEX<sub>86</sub> proxy and the BIT index. *Organic Geochemistry*, 37(12), 1680-1693.

## 9. Literature

- Weijers, J.W.H., Schouten, S., van den Donker, J.C., Hopmans, E.C., Sinninghe Damsté, J.S., (2007c) Environmental controls on bacterial tetraether membrane lipid distribution in soils. *Geochimica Et Cosmochimica Acta*, 71(3), 703-713.
- Weijers, J.W.H., Steinmann, P., Hopmans, E.C., Schouten, S., Sinninghe Damsté, J.S., (2011b) Bacterial tetraether membrane lipids in peat and coal: Testing the MBT/CBT temperature proxy for climate reconstruction. *Organic Geochemistry*, 42(5), 477-486.
- Wollenburg, J.E., Knies, J., Mackensen, A., (2004) High-resolution paleoproductivity fluctuations during the past 24 kyr as indicated by benthic foraminifera in the marginal Arctic Ocean. *Palaeogeography, Palaeoclimatology, Palaeoecology*, 204(3-4), 209-238.
- Wu, S.H., Jansson, P.E., Zhang, X.Y., (2011) Modelling temperature, moisture and surface heat balance in bare soil under seasonal frost conditions in China. *European Journal of Soil Science*, 62(6), 780-796.
- Wuchter, C., Schouten, S., Coolen, M.J.L., Damsté, J.S.S., (2004) Temperature-dependent variation in the distribution of tetraether membrane lipids of marine Crenarchaeota: Implications for TEX<sub>86</sub> paleothermometry. *Paleoceanography*, 19(4).
- Xu, Y., Jaffé, R., Wachnicka, A., Gaiser, E.E., (2006) Occurrence of C<sub>25</sub> highly branched isoprenoids (HBIs) in Florida Bay: Paleoenvironmental indicators of diatom-derived organic matter inputs. *Organic Geochemistry*, 37(7), 847-859.
- Zhang, Y.G., Zhang, C.L., Liu, X.-L., Li, L., Hinrichs, K.-U., Noakes, J.E., (2011) Methane Index: A tetraether archaeal lipid biomarker indicator for detecting the instability of marine gas hydrates. *Earth and Planetary Science Letters*, 307(3-4), 525-534.
- Zhou, W.J., Xie, S.C., Meyers, P.A., Zheng, Y.H., (2005) Reconstruction of late glacial and Holocene climate evolution in southern China from geolipids and pollen in the Dingnan peat sequence. *Organic Geochemistry*, 36(9), 1272-1284.
- Zonneveld, K.A.F., Versteegh, G.J.M., Kasten, S., Eglinton, T.I., Emeis, K.C., Huguet, C., Koch, B.P., de Lange, G.J., de Leeuw, J.W., Middelburg, J.J., Mollenhauer, G., Prahl, F.G., Rethemeyer, J., Wakeham, S.G., (2010) Selective preservation of organic matter in marine environments; processes and impact on the sedimentary record. *Biogeosciences*, 7(2), 483-511.